

**INVESTIGATION ON SOME  
ANTIFERROELECTRIC LIQUID CRYSTALS  
AND THEIR MIXTURES**

**THESIS SUBMITTED TO THE UNIVERSITY OF NORTH BENGAL  
FOR THE AWARD OF THE DEGREE OF DOCTOR OF  
PHILOSOPHY (SCIENCE) IN PHYSICS**

**BY  
KARTICK CH. DEY**

**SUPERVISOR  
PROF. PRADIP KUMAR MANDAL**

**DEPARTMENT OF PHYSICS  
UNIVERSITY OF NORTH BENGAL  
RAJA RAMMOHUNPUR, DIST: DARJEELING, PIN: 734013  
WEST BENGAL, INDIA**

**FEBRUARY, 2020**

*DEDICATED TO MY PARENTS,  
MY WIFE AND MY  
DAUGHTER*

# DECLARATION

I declare that the thesis entitled “**INVESTIGATION ON SOME ANTIFERROELECTRIC LIQUID CRYSTALS AND THEIR MIXTURES**” has been prepared by me under the guidance and supervision of Prof. Pradip Kumar Mandal, Department of Physics, University of North Bengal. No part of the thesis has formed the basis for the award of any degree or any fellowship previously.

Date: 07.02.2020  
Place: NBU



KARTICK CH. DEY  
Department of Physics  
University of North Bengal  
Dist– Darjeeling, Pin–734013  
West Bengal, India

# UNIVERSITY OF NORTH BENGAL

Accredited by NAAC with Grade A

## DEPARTMENT OF PHYSICS

P.O. NORTH BENGAL UNIVERSITY  
RAJA RAMMOHUNPUR, DIST. DARJEELING,  
WEST BENGAL, PIN 734013,  
INDIA



ENLIGHTENMENT TO PERFECTION

Railway Station: New Jalpaiguri  
Nearest Airport: Bagdogra  
Phone: +91-(0) 353-2776338  
Fax: +91-(0) 353-2699001  
Website: www.nbu.ac.in

Ref. No. ....

Date : .....

## CERTIFICATE

I certify that Mr. Kartick Ch. Dey has prepared the thesis entitled  
“**INVESTIGATION ON SOME ANTIFERROELECTRIC LIQUID  
CRYSTALS AND THEIR MIXTURES**” for the award of Ph. D. degree (Science)  
in Physics of the University of North Bengal under my guidance and supervision. He  
has carried out the work in the Department of Physics, University of North Bengal.

Date: 07.02.2020

Place: NBU

PROF. PRADIP KUMAR MANDAL

Department of Physics  
University of North Bengal  
Raja Rammohunpur  
P.O. – North Bengal University  
Dist– Darjeeling, Pin–734013, West Bengal

## Urkund Analysis Result

Analysed Document: Kartick Ch. Dey\_Physics.pdf (D61941573)  
Submitted: 1/7/2020 9:36:00 AM  
Submitted By: nbuplg@nbu.ac.in  
Significance: 2 %

### Sources included in the report:

[https://autodocbox.com/69174506-Auto\\_Parts/Atlas-copco-torque-arms.html](https://autodocbox.com/69174506-Auto_Parts/Atlas-copco-torque-arms.html)  
[https://www.researchgate.net/figure/Frequency-dependence-of-the-transverse-component-of-the-dielectric-permittivity-and-loss\\_fig4\\_262905738](https://www.researchgate.net/figure/Frequency-dependence-of-the-transverse-component-of-the-dielectric-permittivity-and-loss_fig4_262905738)  
ff306de3-3b41-4b6a-ae56-18864dd66a36  
de53e032-cdba-4cb7-b03e-ef54d00cf547  
3fcd601c-fad9-44c0-acd7-7cc6bf300d13  
e276ac72-d0bc-4d96-a1da-9b4d71600dff  
[https://www.researchgate.net/figure/Temperature-dependence-of-relaxation-frequencies-f-r-in-SmA-SmC-and-SmC-A-phases\\_fig6\\_233304629](https://www.researchgate.net/figure/Temperature-dependence-of-relaxation-frequencies-f-r-in-SmA-SmC-and-SmC-A-phases_fig6_233304629)

### Instances where selected sources appear:

32

Kartick Ch. Dey  
07.02.2020

Anand  
07.02.2020

# ABSTRACT

Liquid crystals are fascinating self-assembled soft materials in which the molecules are orientationally ordered and partially positionally ordered. Liquid crystals easily response to small perturbations like the electric field, magnetic field, surface effect, etc. for which they find applications in diversified fields along with display technology.

At present high definition displays (AMLCDs) with a viewing angle of  $\sim 178$  degrees are available in the market. Twisted nematic liquid crystals are generally used in such displays. The high value of response time ( $\sim$ ms) governing the frame rate, ghost effect and contrast ratio is still a matter for further improvement. As a result, ferroelectric liquid crystal (FLC) and antiferroelectric liquid crystal (AFLC) draw a special interest from the last decades of the 20<sup>th</sup> century due to their low response time ( $\mu$ s). But manifold problems were faced in the development of displays based on FLCs. Some of them are small cell spacing ( $1\text{--}2\text{ }\mu\text{m}$ ) to unwind the helix, the problem of mechanical shock due to unstable molecular anchoring at the surface, contrast ratio, etc. The AFLCs are promising materials to solve the issues because of their fascinating properties – tristable switching behavior, micro-second order response time, intrinsic analog gray-scale capability, hemispherical viewing angle (in-plane switching geometry) high contrast ratio and no-ghost effect, etc. AFLCs are also interesting for the basic studies in soft condensed matter field as these materials show various sub-phases with distinct macroscopic properties. So enough scope is here for the improvement of the display industry in the coming years with fascinating properties of antiferroelectric liquid crystals.

Physical properties of six antiferroelectric liquid crystals and their three mixtures have been studied in this dissertation using different experimental techniques viz. polarizing optical microscopy, differential scanning calorimetry, synchrotron X-ray diffraction, dielectric spectroscopy, electro-optic study. The first four compounds (**DM0**, **DM1**, **DM2**, and **DM3**) are biphenyl benzoate core-based, in which the number and position of lateral fluorination in the core differ. The first compound DM0 is a core protonated compound but in DM1 one fluorine atom is introduced at ortho position of the benzoate core, while it is introduced at position meta in DM2,

but in DM3 fluorine atoms are introduced both at ortho and meta positions of the benzoate core structure. In chapter 3, the effect of lateral fluorination on the mesogenic behaviour of these four compounds is discussed. All the four compounds exhibit Cr–SmC<sub>A</sub>\*–SmC\*–SmA\*–Iso phase sequence but in different temperature ranges. Due to lateral fluorination, the clearing point decreases in all the fluorinated compounds but the melting point and the stability of SmC<sub>A</sub>\* phase decrease or increase depending upon the position of lateral fluorination. Layer spacings increase in DM1 and DM2 whereas it is found to decrease in DM3. All the compounds show a tricritical nature of SmC\*–SmA\* transition and orthoconic nature of tilt. They also exhibit very large dielectric increments in SmC\* phase but in singly fluorinated DM1 and DM2 its value is less and in doubly fluorinated DM3 it is more than the core protonated compound. Four relaxation modes (P<sub>L</sub>, P<sub>H</sub>, GM, and SM) are observed and their critical frequencies are found to decrease in all fluorinated compounds. Domain mode is also observed. Fluorination results in the slower response under a square pulse, of the order of a few hundred microseconds.

Properties of a binary eutectic antiferroelectric mixture, formed mixing 50 wt.% of two pure compounds DM0 and DM3 are discussed in chapter 4. The behaviour of the mixture is not always found to be proportional to the concentration of the protonated and the fluorinated components although it shows the same phase sequence as in the pure compounds but with an increased range of SmC<sub>A</sub>\* phase. In this eutectic mixture also four collective relaxation modes (P<sub>L</sub>, P<sub>H</sub>, GM, and SM) are observed and their critical frequencies are found to lie in between the pure compounds. However, P<sub>L</sub> and SM critical frequencies are not proportional to the concentration of the pure compounds but for P<sub>H</sub> and GM they are almost proportional. The critical field for the suppression of the P<sub>L</sub> and Goldstone modes is found to increase significantly. The GM mode dielectric increment decreased substantially. SmC\*–SmA\* transition temperature ( $T_c$ ) is found to increase linearly with a bias field and the phenomenon has been explained using the Landau model. Spontaneous polarization is found to be in between those of the pure compounds. Switching time also exhibits similar behaviour and observed to be about a few hundred microseconds.

Motivated by the formulation of the binary eutectic mixture, a room temperature multi-component high tilt antiferroelectric mixture is prepared by mixing DM0, DM1, DM2, and DM3 in equal wt.% and is discussed in chapter 5. The range of SmC<sub>A</sub>\* phase is increased significantly and extended far below room temperature

( $\sim -8^{\circ}\text{C}$  to  $65^{\circ}\text{C}$ ), keeping the phase sequence the same as the pure compounds. Some properties of the mixture are found to be equal to the average of the pure compounds. The mixture is of orthoconic nature and  $\text{SmC}^*-\text{SmA}^*$  transition shows tricritical nature like the pure compounds. Correlation lengths across and within the layers are found to increase from paraelectric to ferroelectric to antiferroelectric phases. Four collective modes *viz.*  $P_L$ ,  $P_H$ , GM and SM and the domain mode are observed.  $f_{SM}$  and  $\Delta\varepsilon_{SM}$  were found to follow the Curie–Weiss law.  $T_c$  is found to increase with bias which was explained using the Landau model. The mixture also exhibits sub-millisecond switching, near the onset of  $\text{SmC}_A^*$  phase.

The key feature behind the compatibility of LCs and CNTs is the highly anisotropic nature of both. In the recent past, few groups studied the CNT composite of ferroelectric liquid crystals (FLCs). But studies on nanocomposites of antiferroelectric liquid crystals are very less. In chapter 6 we have made a comparative study of the dynamic behaviour and electro-optic response of the pure AFLC (DM1) and its MWCNT composite (0.12 wt.%). The phase boundaries are lowered and the stability of the  $\text{SmA}^*$  and the  $\text{SmC}^*$  phases are found to increase but that of  $\text{SmC}_A^*$  phase is decreased. Distinct textural changes are observed in different phases in the nanocomposite. Pitch of the helicoidal structure is found to increase with decreasing temperature in the pure compound in both the tilted phases, the opposite trend is observed in the composite in the  $\text{SmC}^*$  phase. The absolute values and the ranges of the anti-phase antiferroelectric mode critical frequency ( $f_{PH}$ ) and the absorption strength ( $\varepsilon_{PH}''$ ) are found to decrease in the doped system. In the composite, the dielectric increment ( $\Delta\varepsilon_{GM}$ ) of GM decreases and the critical frequency ( $f_{GM}$ ) increases and has been explained using generalized Landau theory. The critical field for suppression of the Goldstone mode is increased by 2 times in the composite, signifying the helical structure in the nanocomposite is more stable than in the pure compound. A significant reduction of spontaneous polarization and switching time is observed in the composite. A lower value of conductivity in the composite signifies trapping of impurity ions by the CNTs.

To probe the structure-property relationship further, we have investigated the effect of fluorination in the achiral chain in chapter 7. For this, we have selected two partially fluorinated terphenyl based pure antiferroelectric liquid crystals 4F6T and 6F6T. While the first compound has 4 fluorinated carbon atoms and 6 oligomethelene

spacers, the second one has 6 fluorinated carbon atoms and the same 6 oligomethelene spacers in the achiral chain. Another compound 5F6T, having 5 fluorinated carbon atoms and 6 oligomethelene spacers in the achiral chain, belonging to the above homologous series, was studied and published by our group before, its results are compared with the present compounds for the sake of better understanding of structure-property relations. The molecules of this series structurally differ from the DM series, discussed in Chapter 3, by the number of fluorinated carbon atoms at achiral chain, instead of alkoxy group in the chain carbonyl group is attached here, the core is doubly fluorinated terphenyl based instead of biphenyl benzoate in DM series. Here we discuss the change of properties of these three compounds due to the major change with respect to the biphenyl benzoate core-based series as well as the change of properties of compounds within the series due to the change of the number of fluorinated carbon atom at achiral chain.

Although all of them exhibited Cr-SmC<sub>A</sub>\*- SmC\*-SmA\*-Iso phase sequence, the melting point is observed to decrease with increasing achiral chain length but the clearing point shows the opposite trend, range of SmC<sub>A</sub>\* and SmC\* phases showed odd-even effect like the molecular dipole moments and spontaneous polarization. Layer spacings, average intermolecular distances and correlation lengths across the smectic planes are also observed to increase with achiral chain length. Like DM series, SmC\*-SmA\* transition shows tricritical nature. Dielectric increments are found to decrease with increased achiral chain. Both soft mode and Goldstone mode critical frequencies are found to decrease with decreasing temperature in the lower derivative but opposite behaviour is observed in the higher derivative. Both the compounds, however, show Curie–Weiss behaviour in soft mode near  $T_c$ . Goldstone mode critical frequency is much higher in 6F6T. Both P<sub>L</sub> and P<sub>H</sub> modes are observed in SmC<sub>A</sub>\* phase in 6F6T but in 4F6T only P<sub>H</sub> is observed and in 5F6T both modes are absent. Optical tilts exhibited orthoconic nature of the SmC<sub>A</sub>\* phase in both the compounds. However, X-ray tilt is much less and the discrepancy has been explained. Both the compounds show sub-millisecond order switching time which is also found to increase with achiral chain length. Antiferroelectric-ferroelectric transition temperature ( $T_{AF}$ ) is observed to decrease with increasing ac field, effect is more in the higher derivative compared to the lower one. There is an indication of the presence of a *sub-phase* (SmC <sub>$\alpha$</sub> \*) between SmA\* and SmC\* phases in 6F6T. These

two compounds are expected to be suitable for the preparation of mixtures suitable for display and non-display applications because of their orthoconic nature, sub-millisecond switching time and moderate spontaneous polarization. Thus the number of fluorinated carbon in the achiral part is found to influence the mesogenic properties of various liquid crystalline systems.

Conclusions of all the experimental results have been summarized in Chapter 8.



# PREFACE

The present dissertation entitled **“INVESTIGATION ON SOME ANTIFERROELECTRIC LIQUID CRYSTALS AND THEIR MIXTURES”** is submitted to fulfill the requirements for the degree of Doctor of Philosophy (Science) in Physics of the University of North Bengal. This dissertation explores various fruitful results of different physical properties of a few fluorinated antiferroelectric liquid crystalline compounds and their mixtures investigated by different experimental techniques. The analysis presented in this dissertation evaluates the benefits of choosing such compounds for the successful application of liquid crystals in many areas of science and technology. All the studies have been carried out in Liquid Crystal Research Laboratory, Department of Physics, University of North Bengal under the supervision of Prof. Pradip Kumar Mandal, Department of Physics, University of North Bengal, Siliguri-734013. Some part of the research work has been performed in Deutsches Elektronen-Synchrotron (DESY), Hamburg, Germany. The thesis consists of eight chapters.

The first chapter of this thesis contains a brief introduction to the liquid crystal (LC) physics and the list of investigated compounds and mixtures. The basic theory and experimental procedures followed for studying different properties of liquid crystalline materials are described in chapter 2. In chapter 3, results of four biphenyl benzoate core-based high tilt antiferroelectric liquid crystal compounds (DM0, DM1, DM2, and DM3) investigated by polarizing optical microscopy, differential scanning calorimetry, synchrotron X-ray diffraction, dielectric and electro-optical methods have been presented. Chapter 4 describes mesogenic behavior of a binary eutectic antiferroelectric mixture formulated by mixing compounds DM0 and DM3. In chapter 5, mesogenic behavior of a multi-component high tilt antiferroelectric liquid crystal mixture prepared by mixing all the compounds DM0, DM1, DM2 and DM3 in equal wt.% have been discussed. CNT doped antiferroelectric liquid crystal (DM1) is investigated by polarizing optical microscopy, dielectric relaxation spectroscopy

and electro-optic techniques and various properties are compared with those of pure compound in chapter 6 to see the effect of nanoparticles. The phase behaviour, structure and molecular dynamics of two high tilt terphenyl core based antiferroelectric liquid crystalline compounds have been discussed in chapter 7. A summary of all the experimental results is given in chapter 8.

Date: 07.02.2020.  
Place: NBU



KARTICK CH. DEY  
Department of Physics  
University of North Bengal  
Dist- Darjeeling, Pin-734013  
West Bengal, India

# ACKNOWLEDGEMENTS

I would like to express my sincere thanks and deep gratitude to my supervisor Prof. Pradip Kumar Mandal for his encouragement, constant support and guidance. His expertise, keen physical insight, clear conception and clear vision in the field of liquid crystals have always been the inspiration and motivation during my research. At every stage of my research, Prof. Mandal showed great patience and good faith in me which enriched my capability. It was a great privilege to work with him.

I express my deep gratitude to Prof. Roman Dabrowski and Przemysław Kula, Military University of Technology, Warsaw, Poland, for supplying good quality pure liquid crystal samples. I would also like to thank Department of Science and Technology, Government of India, for providing financial assistance to perform experiments at Deutsches Elektronen-Synchrotron (DESY), Hamburg, Germany. I also acknowledge the technical assistance of Martin V. Zimmermann and Olof Gutowski, Abhisakh Sarma, DESY Photon Science during the experiment with the synchrotron beam at DESY. I also like to thank Dr. Sripada Haldar, Head, Department of Physics, University of North Bengal and Dr. Suman Chattopadhyay, Department of Physics, University of North Bengal for their help during experiments and data analysis. I also like to thank Mr. Gautam Sarkar, Head, USIC, University of North Bengal, Dr. Tamal Sarkar, Scientific Research Officer-II, High Energy & Cosmic Ray Research Center, University of North Bengal, and Mr. Subrata Hazra, Senior technical assistant, Department of physics, University of North Bengal for their technical support.

I also like to thank and acknowledge my coworkers Mr. Debarghya Goswami, Dr. Debasish Sinha, and Dr. Asim Debnath, Department of physics, University of North Bengal, for their valuable discussion, cooperation and continuous support during experiment and data analysis. I also like to acknowledge research scholars Mr. Rajat Biswas, Smt. Aparna Ghosh, Mr. Manabindu Das, Mr. Biplab Singh, Mr. Tanmay Basak, Department of physics, University of North Bengal, for their cooperation and helpful assistance.

Last but not least I would love to thank my father Late Kalachand Dey and mother Late Jharna Dey, for unconditional support and inspiration. I would love to thank my dear wife Smt. Lovely Paul and daughter Miss Kairabi Dey for their unconditional love, patience, and faith in me. Without their support and encouragement, I would not have been able to accomplish this task.

Date: 07.02.2020  
Place: NBU

  
KARTICK CH. DEY

# TABLE OF CONTENTS

<b>Table of Contents</b>	<b>I-IV</b>
<b>List of Tables</b>	<b>V-VI</b>
<b>List of Figures</b>	<b>VII-XIV</b>
<b>List of Appendices</b>	<b>XIV</b>

## CHAPTERS

<b>Chapter 1:</b>	<b><i>Introduction</i></b>	<b>1-32</b>
1.1	INTRODUCTION TO LIQUID CRYSTAL	3
1.2	CLASSIFICATION OF LIQUID CRYSTAL	3
1.2.1	NEMATIC LIQUID CRYSTAL	4
1.2.2	CHOLESTERIC LIQUID CRYSTAL	4
1.2.3	SMECTIC LIQUID CRYSTAL	5
1.2.4	CHIRALITY	6
1.2.5	FERROELECTRIC LIQUID CRYSTAL	7
1.2.6	SURFACE STABILIZED FERROELECTRIC LIQUID CRYSTAL	9
1.2.7	ANTIFERROELECTRIC LIQUID CRYSTAL	12
1.2.8	ORTHOCONIC ANTIFERROELECTRIC LIQUID CRYSTAL	14
1.3	EFFECT OF FLUORO-SUBSTITUTION IN FERROELECTRIC AND ANTIFERROELECTRIC LIQUID CRYSTALS	16
1.3.1	EFFECT OF LONGITUDINAL FLUORO-SUBSTITUTION	16
1.3.2	EFFECT OF LATERAL FLUORO-SUBSTITUTION	17
1.4	LIQUID CRYSTAL MIXTURES	18
1.5	MOTIVATION OF THE PRESENT WORK	19
1.6	LIQUID CRYSTAL COMPOUNDS STUDIED IN THE DISSERTATION	21
1.7	REFERENCES	25
<b>Chapter 2:</b>	<b><i>Experimental techniques and theory</i></b>	<b>33-66</b>
2.1	INTRODUCTION	35
2.2	IDENTIFICATION OF MESOPHASES AND DETERMINATION OF TRANSITION TEMPERATURES	35
2.2.1	POLARIZING OPTICAL MICROSCOPY	36
2.2.2	DIFFERENTIAL SCANNING CALORIMETRY	37
2.3	DETERMINATION OF STRUCTURAL PARAMETERS USING	

THE X-RAY DIFFRACTION TECHNIQUE	39
2.4 DIELECTRIC SPECTROSCOPY	43
2.4.1 DEBYE MODEL	44
2.4.2 COLE-COLE MODEL	46
2.4.3 DIELECTRIC RELAXATIONS IN FERROELECTRIC AND ANTIFERROELECTRIC LIQUID CRYSTALS	47
2.4.4 DIELECTRIC MEASUREMENT TECHNIQUE	52
2.5 MEASUREMENTS OF ELECTRO-OPTIC PARAMETERS – TILT ANGLE ( $\Theta$ ), SPONTANEOUS POLARIZATION ( $P_s$ ), SWITCHING TIME ( $\tau$ ), VISCOSITY ( $\gamma$ ) AND ROTATIONAL VISCOSITY ( $\gamma_\phi$ )	53
2.5.1 TILT ANGLE ( $\Theta$ )	54
2.5.2 SPONTANEOUS POLARIZATION ( $P_s$ )	55
2.5.3 SWITCHING TIME ( $\tau$ )	57
2.5.4 ROTATIONAL VISCOSITY ( $\gamma_\phi$ )	58
2.6 REFERENCES	59
 <b>Chapter 3: <i>Effect of lateral fluorination on the                     properties of four antiferroelectric                     liquid crystal</i></b>	 <b>67-98</b>
3.1 INTRODUCTION	69
3.2 EXPERIMENTAL TECHNIQUES	71
3.3 RESULTS AND DISCUSSION	71
3.3.1 POLARIZING OPTICAL MICROSCOPY (POM) AND DSC STUDY	71
3.3.2 OPTIMIZATION OF GEOMETRY	73
3.3.3 X-RAY DIFFRACTION STUDY	74
3.3.4 DIELECTRIC STUDY	79
3.3.4.1 SmC <sub>A</sub> * PHASE	80
3.3.4.2 SmC* AND SmA* PHASE	83
3.3.5 SPONTANEOUS POLARIZATION ( $P_s$ ) MEASUREMENTS	85
3.3.6 OPTICAL TILT ( $\theta_{opt}$ )	86
3.3.7 SWITCHING TIME ( $\tau$ ) AND VISCOSITY ( $\gamma$ ) MEASUREMENTS	88
3.4 CONCLUSION	90
3.5 REFERENCES	92

## **Chapter 4: *Formulation of a binary eutectic antiferroelectric liquid crystal mixture*** **99-124**

4.1	INTRODUCTION	101
4.2	EXPERIMENTAL TECHNIQUES	102
4.3	RESULTS AND DISCUSSION	104
4.3.1	POLARIZING OPTICAL MICROSCOPY AND DSC STUDY	104
4.3.2	DIELECTRIC STUDY	106
4.3.2.1	SmC <sub>A</sub> * PHASE	106
4.3.2.2	SmC* PHASE	110
4.3.2.3	SmA* PHASE	113
4.3.3	ELECTRO-OPTIC STUDY	117
4.4	CONCLUSION	119
4.5	REFERENCES	120

## **Chapter 5: *Formulation of a room temperature multi-component high tilt anti-ferroelectric liquid crystal mixture*** **125-150**

5.1	INTRODUCTION	127
5.2	EXPERIMENTAL TECHNIQUES	128
5.3	RESULTS AND DISCUSSION	129
5.3.1	POLARIZING OPTICAL MICROSCOPY (POM)	129
5.3.2	DSC STUDY	131
5.3.3	SYNCHROTRON RADIATION STUDY	131
5.3.4	DIELECTRIC STUDY	134
5.3.5	ELECTRO-OPTIC STUDY	140
5.4	CONCLUSION	143
5.5	REFERENCES	145

## **Chapter 6: *Effect of multi-walled carbon nanotubes on dielectric and electro-optic properties of a high tilt antiferroelectric liquid crystal*** **151-174**

6.1	INTRODUCTION	153
6.2	EXPERIMENTAL TECHNIQUES	154
6.3	RESULTS AND DISCUSSION	155
6.3.1	POLARIZING OPTICAL MICROSCOPY	155

6.3.2	DIELECTRIC STUDY	158
6.3.3	ELECTRO-OPTIC STUDY	164
6.4	CONCLUSION	168
6.5	REFERENCES	169

**Chapter 7: *Effect of fluorinated achiral chain length on structural, dielectric and electro-optic properties of a laterally fluorinated terphenyl based high tilt antiferroelectric liquid crystals*** **175-202**

7.1	INTRODUCTION	177
7.2	EXPERIMENTS	179
7.3	RESULTS AND DISCUSSIONS	180
7.3.1	POLARIZING OPTICAL MICROSCOPY	180
7.3.2	DIFFERENTIAL SCANNING CALORIMETRY	180
7.3.3	OPTIMIZED GEOMETRY	181
7.3.4	SYNCHROTRON RADIATION DIFFRACTION STUDY	183
7.3.5	DIELECTRIC STUDY	186
7.3.6	ELECTRO-OPTIC STUDY	188
7.3.6.1	SPONTANEOUS POLARIZATION	188
7.3.6.2	OPTICAL AND X-RAY TILT	190
7.3.6.3	SWITCHING TIME	191
7.3.6.4	EFFECT OF FIELD ON FERROELECTRIC- ANTIFERROELECTRIC TRANSITION TEMPERATURE	192
7.4	CONCLUSION	193
7.5	REFERENCES	195

**Chapter 8: *Summary and Conclusions*** **203-210**

# LIST OF TABLES

## Chapter 1:

<b>Table 1.1:</b>	<i>The symmetry elements of the N, SmA, SmC, and SmC* phases</i>	8
<b>Table 1.2:</b>	<i>Values of the 'spontaneous polarization <math>P_s</math>' (<math>\text{nC/cm}^{-2}</math>) at temperature <math>T_c - 10^\circ\text{C}</math> and temperature range of the SmC* mesophase as they influenced by the substitution on the central core near an asymmetric carbon in an ortho position to the linkage group Z (<math>-\text{O}-</math>)</i>	18
<b>Table 1.3:</b>	<i>Molecular structures, phase sequences and transition temperatures of the investigated pure compounds</i>	23
<b>Table 1.4:</b>	<i>Molecular structures, phase sequences and transition temperatures of the investigated mixtures</i>	24

## Chapter 3:

<b>Table 3.1:</b>	<i>Molecular structures and transition temperatures (<math>^\circ\text{C}</math>) of the compounds</i>	70
<b>Table 3.2:</b>	<i>Few important parameters of the molecules in optimized geometry</i>	74
<b>Table 3.3:</b>	<i>Comparison of a few important parameters of the molecules obtained from Synchrotron X-ray study</i>	78
<b>Table 3.4:</b>	<i>A selected list of parameters of DM0, DM1, DM2, and DM3 and related compounds</i>	89

## Chapter 4:

<b>Table 4.1:</b>	<i>Formulae structures of DM0 and DM3, their transition temperatures and transition temperatures of the eutectic mixture M3</i>	103
<b>Table 4.2:</b>	<i>Transition temperatures of mixtures as obtained by texture study during heating</i>	105
<b>Table 4.3:</b>	<i>Comparison of <math>E_c</math>, <math>\Delta\epsilon_{GM}</math>, and <math>f_{GM}</math> of the eutectic M3 with DM0 and DM3 at <math>T_c - 10</math></i>	112
<b>Table 4.4:</b>	<i>Field dependence of <math>T_c</math>, <math>f_{SMm}</math> and <math>\Delta\epsilon_{SMm}^{-1}</math></i>	117

**Chapter 5:**

<b>Table 5.1:</b>	<i>Phase sequence and transition temperatures (°C) of the mixture as obtained from POM study during heating. Figures within parentheses are transition temperatures during cooling.</i>	128
<b>Table 5.2:</b>	<i>A Selected list of parameters of mixture M6 and pure compounds DM0, DM1, DM2 and DM3</i>	143

**Chapter 6:**

<b>Table 6.1:</b>	<i>Comparison of phase stability of pure and CNT doped systems</i>	156
<b>Table 6.2:</b>	<i>Comparison of different critical frequencies of the pure and the CNT composite</i>	162

**Chapter 7:**

<b>Table 7.1:</b>	<i>Comparison of various thermal parameters obtained from POM study during heating</i>	181
<b>Table 7.2:</b>	<i>Molecular lengths, energy, principal moments of inertia and dipole moments of the molecules</i>	183
<b>Table 7.3:</b>	<i>Selected list of parameters of 4F6T, 5F6T, 6F6T</i>	193

# LIST OF FIGURES

## Chapter 1:

<b>Figure 1.1:</b>	<i>(a) Nematic, (b) Cholesteric (c) Smectic–A and (b) Smectic–C liquid crystals. (Adapted from internet documents)</i>	5
<b>Figure 1.2:</b>	<i>Symmetry elements of (a) SmC phase (b) SmC* phase</i>	7
<b>Figure 1.3:</b>	<i>Structure of DOBAMBC, first FLC compound</i>	7
<b>Figure 1.4:</b>	<i>(a) The helicoidal structure of chiral smectic C (SmC*) liquid crystal, polarization is tangential to the circle of intersection of the cone with the boundary plane of the layer. (b) The molecular polarization <math>P</math> is always perpendicular to the director <math>\mathbf{n}</math>, the angle between <math>\mathbf{n}</math> and <math>\mathbf{z}</math> is the tilt angle (<math>\theta</math>), and the azimuthal angle (<math>\varphi</math>) differs from layer to layer and is a function of the coordinate <math>z</math> parallel to the layer normal</i>	9
<b>Figure 1.5:</b>	<i>Schematic surface stabilized ferroelectric SmC* liquid crystal (SSFLC) geometry with tilt angle <math>\theta</math> (T) and spontaneous polarization <math>P_s</math> (T)</i>	10
<b>Figure 1.6:</b>	<i>The potential curve along a phase variable</i>	11
<b>Figure 1.7:</b>	<i>(a) Structure and transition temperature of MHPOBC, first AFLC compound [32], (b) Herringbone pattern in the hypothetical structure of antiferroelectric liquid crystal, (c) Molecules, on average, have alternating tilt in alternating layers, corresponding to dipole moments pointing in opposite direction in alternate layers form double helix</i>	13
<b>Figure 1.8:</b>	<i>Double hysteresis loop of antiferroelectric liquid crystal under applied AC field (<math>E</math>). At <math>E=0</math>, the antiferroelectric state is stable. For a field <math>E &gt; E_{th}</math> or <math>E &lt; -E_{th}</math>, the ferroelectric states are obtained from antiferroelectric states as shown to right and left and corresponding to the two saturated states at the ends of the double hysteresis loop beyond the threshold fields <math>\pm E_{th}</math></i>	14
<b>Figure 1.9:</b>	<i>Electro-optical properties of orthoconic AFLCs in compared to ferroelectrics. (Adapted from [41])</i>	15

## Chapter 2:

<b>Figure 2.1:</b>	<i>(a) Texture of (a) <math>SmC_A^*</math> phase, (b) <math>SmC^*</math> phase, and (c) <math>SmA^*</math> phase</i>	36
<b>Figure 2.2:</b>	<i>Block diagram of polarizing optical microscopy</i>	37
<b>Figure 2.3:</b>	<i>(a) The Experimental set up of DSC experiment</i>	38
<b>Figure 2.4:</b>	<i>A typical DSC thermogram</i>	39
<b>Figure 2.5:</b>	<i>Schematic representation of typical X-ray diffraction pattern of an aligned (a) nematic phase and (b) Smectic-A phase and (c) Smectic-C phase (X-ray beam is perpendicular to the paper)</i>	40
<b>Figure 2.6:</b>	<i>Schematic diagram of experimental arrangement of X-ray diffraction study (not to scale)</i>	41
<b>Figure 2.7:</b>	<i>(a) Synchrotron X-ray diffraction set up unit (b) Perkin Elmer 2D detector of size 400x400 mm, at DESY, Hamburg, Germany</i>	41
<b>Figure 2.8:</b>	<i>Intensity profile of the diffraction features showing FWHM (<math>\Delta Q = Q_{max} - Q_{min}</math>)</i>	42
<b>Figure 2.9:</b>	<i>Frequency dependence of <math>\epsilon'(\omega)</math> and <math>\epsilon''(\omega)</math> for a relaxation process</i>	45
<b>Figure 2.10:</b>	<i>Cole-Cole plot of a spectrum showing Debye type relaxation</i>	46
<b>Figure 2.11:</b>	<i>(a) Homogeneous arrangement of molecules and transverse component of the permittivity (<math>\epsilon_{\perp}</math>) (b) homeotropic arrangement of molecules and parallel component of the permittivity (<math>\epsilon_{\parallel}</math>)</i>	48
<b>Figure 2.12:</b>	<i>Schematic representation of director fluctuation in (a) the Goldstone mode relaxation, originates from the phase fluctuation (<math>\delta\phi</math>) of the director in chiral <math>SmC^*</math> phase, (b) the soft mode relaxation, arises due to the tilt (<math>\delta\theta</math>) fluctuation of the molecular director</i>	49
<b>Figure 2.13:</b>	<i>Goldstone mode and soft mode in a frequency window, the soft mode becomes prominent after the Goldstone mode is suppressed under DC bias (inset)</i>	50
<b>Figure 2.14:</b>	<i>The absorption spectrum in <math>SmC_A^*</math> phase showing <math>P_L</math> and <math>P_H</math> mode</i>	51
<b>Figure 2.15:</b>	<i>Schematic representation of molecular rotations in successive layers in the in-phase <math>P_L</math> and the anti-phase <math>P_H</math> mode</i>	51
<b>Figure 2.16:</b>	<i>Experimental set up for dielectric spectroscopy</i>	53
<b>Figure 2.17:</b>	<i>The molecular tilt <math>\theta</math> as a function of temperature near the <math>SmA^*</math>–<math>SmC^*</math> transition</i>	54

<b>Figure 2.18:</b>	<i>Block diagram of the experimental set up for the measurement for electro-optic parameters (<math>P_s</math>, <math>\tau</math>, <math>\theta</math>, etc.)</i>	55
<b>Figure 2.19:</b>	<i>The voltage waveform across resistor R, obtained from oscilloscope Tektronics TDS 2012 B</i>	56
<b>Figure 2.20:</b>	<i>The voltage waveform of the response of the ferroelectric liquid crystal to the square pulse wave</i>	58

### Chapter 3:

<b>Figure 3.1:</b>	<i>Exemplary characteristic textures of DM0 in (a) <math>SmC_A^*</math>, (b) <math>SmC^*</math> and (c) <math>SmA^*</math> phases and of DM1 in (e) <math>SmC_A^*</math>, (f) <math>SmC^*</math> and (g) <math>SmA^*</math> phases during cooling cycle</i>	72
<b>Figure 3.2:</b>	<i>DSC thermograms of compounds DM0, DM1, DM2 and DM3 during heating cycle</i>	72
<b>Figure 3.3:</b>	<i>Optimized structures of the (a) DM0, (b) DM1, (c) DM2 and (d) DM3</i>	73
<b>Figure 3.4:</b>	<i>Intensity profile of the (a) low and (b) high angle diffraction features.</i>	75
<b>Figure 3.5:</b>	<i>Temperature dependence of (a) intermolecular distance and (b) smectic layer spacing of the compounds, (c) anomalous change of layer spacing at <math>T_{AF}</math> is seen, (d) fitted data near <math>T_c</math> as discussed in the text</i>	76
<b>Figure 3.6:</b>	<i>Temperature variation of (a) tilt angle (<math>\theta</math>) of the compounds (b) correlation lengths across the smectic layers [<math>\xi_{  }</math>] (c) magnified view of (b) near <math>T_{AF}</math> showing a discontinuity and (d) correlation lengths within the smectic layers (<math>\xi_{\perp}</math>)</i>	77
<b>Figure 3.7:</b>	<i>(a) Fitted absorption spectra in <math>SmC_A^*</math> phase of DM0 at 33°C showing clearly the <math>P_L</math> and <math>P_H</math> modes, (b) Temperature dependence of dielectric increment (<math>\Delta\epsilon</math>).</i>	79
<b>Figure 3.8:</b>	<i>Temperature dependence of critical frequencies of all the modes observed in (a) DM0, (b) DM1, (c) DM2 and (d) DM3</i>	80
<b>Figure 3.9:</b>	<i>(a) Clear evidence of <math>P_L</math> in DM3 on application of small bias field (0.6V/<math>\mu m</math>) voltage, (b) Temperature dependence of <math>f_{PL}</math> of DM3</i>	81
<b>Figure 3.10:</b>	<i>Bias field dependence of (a) <math>\epsilon_{PL}''</math> and <math>\epsilon_{HM}''</math> and (b) <math>f_{PL}</math> and <math>f_{HM}</math></i>	83
<b>Figure 3.11:</b>	<i>Bias field dependence of (a) <math>\epsilon_{PH}''</math> and (b) <math>f_{PL}</math></i>	83

<b>Figure 3.12:</b>	<i>Bias field dependence of (a) dielectric increment (<math>\Delta\epsilon_{GM}</math>) of Goldstone mode and (b) critical frequencies of domain mode (<math>f_{DM}</math>)</i>	85
<b>Figure 3.13:</b>	<i>Field dependence of spontaneous polarization (<math>P_s</math>) at <math>T_c - 28^\circ C</math></i>	86
<b>Figure 3.14:</b>	<i>Temperature dependence of <math>P_s</math> at saturation field of (a) DM0, (b) DM1, (c) DM2, and (d) DM3. Fitted curves near <math>T_c</math> are also shown</i>	86
<b>Figure 3.15:</b>	<i>(a) Variation of optical tilts with reduced temperature of DM0, DM1, DM2, and DM3, (b) Fitted X-ray tilt and Optical Tilt of DM0.</i>	88
<b>Figure 3.16:</b>	<i>Comparison of (a) switching times (<math>\tau</math>) and (b) viscosities (<math>\gamma</math>) of the compounds.</i>	89

## Chapter 4:

<b>Figure 4.1:</b>	<i>Diagram of state showing melting points of the binary mixtures of DM0 and DM3, (b) Phase diagram (c) bar diagram of different phases of the mixtures (heating cycle)</i>	105
<b>Figure 4.2:</b>	<i>Observed textures of M3 in (a) <math>SmC_A^*</math>, (b) <math>SmC^*</math> and (c) <math>SmA^*</math> phases</i>	106
<b>Figure 4.3:</b>	<i>Fitted absorption spectra of the mixture M3 (a) in <math>SmC_A^*</math> phase at <math>30^\circ C</math> showing two modes <math>P_L</math> and <math>P_H</math>, (b) in <math>SmC^*</math> phase at <math>110^\circ C</math> and showing GM and (c) in <math>SmA^*</math> phase at <math>114^\circ C</math> showing soft mode. Fitted parameters are also shown</i>	107
<b>Figure 4.4:</b>	<i>(a) Critical frequencies of all the observed collective modes of relaxations – soft mode in <math>SmA^*</math>, Goldstone mode in <math>SmC^*</math>, in-phase (<math>P_L</math>) and anti-phase (<math>P_H</math>) modes in <math>SmC_A^*</math> (b) their absorption strengths</i>	108
<b>Figure 4.5:</b>	<i>Bias field dependence of (a) <math>\epsilon_{PL}''</math> and (b) <math>f_{PL}</math> of M3 at different temperatures in <math>SmC_A^*</math> phase</i>	108
<b>Figure 4.6:</b>	<i>Bias field dependence of (a) <math>\epsilon_{PH}''</math> and (b) <math>f_{PH}</math> of M3 at different temperatures in <math>SmC_A^*</math> phase</i>	109
<b>Figure 4.7:</b>	<i>Comparison of dielectric increment (<math>\Delta\epsilon</math>) of M3 with those of its constituents</i>	111
<b>Figure 4.8:</b>	<i>Bias dependence of (a) absorption strength <math>\epsilon_{GM}''</math> and (b) critical frequency <math>f_{GM}</math> of the mixture M3 compared at two temperatures <math>T_c - 10</math> and <math>T_c - 20</math></i>	113
<b>Figure 4.9:</b>	<i>Temperature variation of (a) <math>f_{SM}</math> and (b) <math>\Delta\epsilon_{SM}^{-1}</math> of DM0, DM3 and M3 without bias</i>	114
<b>Figure 4.10:</b>	<i>Critical temperature (<math>T_c</math>) as a function of bias electric field</i>	115

<b>Figure 4.11:</b>	<i>(a) Inverse of dielectric increment of soft mode (<math>\Delta\epsilon_{SM}^{-1}</math>) as a function of reduced temperature at different bias field, (b) Minimum value of inverse of dielectric increment of soft mode (<math>\Delta\epsilon_{SMm}^{-1}</math>) as a function of <math>(T-T_c)</math></i>	116
<b>Figure 4.12:</b>	<i>(a) Relaxation frequency of the soft mode (<math>f_{SM}</math>) as a function of reduced temperature at different bias field, (b) Minimum value of relaxation frequency of the soft mode (<math>f_{SMm}</math>) as a function <math>(T-T_c)</math></i>	116
<b>Figure 4.13:</b>	<i>(a) <math>P_s</math> as a function of applied field in DM0, DM3 and M3 at <math>T_c-28</math>, (b) Comparison of <math>P_s</math> as a function of temperature of M3, DM0 and DM3</i>	118
<b>Figure 4.14:</b>	<i>Comparison of (a) switching time (<math>\tau</math>) and (b) rotational viscosity (<math>\gamma</math>) as a function of the temperature of M3, DM0 and DM3</i>	118
<b>Figure 4.15:</b>	<i><math>\ln\gamma</math> vs <math>1000/T</math> plot for the mixture M3</i>	119

## Chapter 5:

<b>Figure 5.1:</b>	<i>Phase diagram of the pure compounds and the mixture during heating</i>	129
<b>Figure 5.2:</b>	<i>Observed textures of the mixture in different phases (a) <math>SmA^*</math> (<math>110.5^\circ C</math>), (b) <math>SmC^*</math> (<math>105^\circ C</math>), (c) <math>SmC^*-SmC_A^*</math> transition, (d) <math>SmC_A^*</math> (<math>20^\circ C</math>), (e) monodomain texture under electric field (<math>5.0 V/\mu m</math>) in <math>SmC^*</math> phase</i>	130
<b>Figure 5.3:</b>	<i>DSC thermograms of M6 during heating and cooling</i>	130
<b>Figure 5.4:</b>	<i>Synchrotron x-ray diffraction photographs at (a) <math>70^\circ C</math> (<math>SmC_A^*</math>), (b) <math>100^\circ C</math> (<math>SmC^*</math>) and (c) <math>112^\circ C</math> (<math>SmA^*</math>)</i>	131
<b>Figure 5.5:</b>	<i>X-ray diffraction profiles at <math>70^\circ C</math> (<math>SmC_A^*</math>), <math>100^\circ C</math> (<math>SmC^*</math>) and <math>112^\circ C</math> (<math>SmA^*</math>) of the (a) low angle and (b) high angle diffraction features</i>	132
<b>Figure 5.6:</b>	<i>Temperature dependence of layer spacing of the (a) mixture and (b) pure compounds, (c) layer shrinkage of the mixture and (d) fitted layer spacing near <math>T_c</math> as discussed in the text.</i>	132
<b>Figure 5.7:</b>	<i>Temperature dependence of intermolecular distance (<math>D</math>) of the mixture</i>	133
<b>Figure 5.8:</b>	<i>Temperature dependence of correlation lengths across the layers (<math>\xi_{  }</math>) in the (a) mixture and (b) pure compounds and that of within the layers (<math>\xi_{\perp}</math>) in the (c) mixture and (d) pure compounds</i>	134

<b>Figure 5.9:</b>	<i>Fitted absorption spectrum (a) in SmC<sub>A</sub>* phase at 27°C showing P<sub>L</sub> and P<sub>H</sub>, (b) in SmC* and SmA* phases at 105°C and at 111°C showing GM and SM, and (c) in SmC* phase under bias 0.7 V/μm at 108°C showing DM and SM</i>	135
<b>Figure 5.10:</b>	<i>Temperature dependence of (a) the critical frequencies of soft mode, Goldstone mode, P<sub>L</sub> mode and P<sub>H</sub> mode and (b) the maximum dielectric absorptions (<math>\epsilon''_{\max}</math>) at critical frequencies of the corresponding modes</i>	136
<b>Figure 5.11:</b>	<i>Bias field dependence of (a) f<sub>PL</sub> and (b) <math>\epsilon''_{PL}</math> of M6</i>	137
<b>Figure 5.12:</b>	<i>Dielectric increment (<math>\Delta\epsilon_{GM}</math>) of Goldstone mode of the mixture in comparison to pure compounds</i>	138
<b>Figure 5.13:</b>	<i>(a) Effect of bias on Goldstone mode, (b) Appearance of domain mode with bias, (c) Linear dependence of E<sub>c</sub> and f<sub>DM</sub> with reduced temperature (T-T<sub>c</sub>), (d) Bias dependence of f<sub>GM</sub> and f<sub>DM</sub> at different temperatures</i>	139
<b>Figure 5.14:</b>	<i>Temperature dependence of (a) f<sub>SM</sub> at selected bias field near T<sub>c</sub> and (b) Bias field dependence of T<sub>c</sub></i>	140
<b>Figure 5.15:</b>	<i>(a) Temperature variation of P<sub>s</sub> of M6, the fitted line is also shown. (b) Comparison of P<sub>s</sub> of the mixture with the pure compounds</i>	141
<b>Figure 5.16:</b>	<i>Temperature dependence of optical tilt (<math>\theta_{\text{opt.}}</math>) and X-ray tilt (<math>\theta_{X\text{-ray}}</math>) of M6. Power law fitted lines near T<sub>c</sub> are also shown as discussed in text</i>	141
<b>Figure 5.17:</b>	<i>Temperature dependence of switching time (<math>\tau</math>) of M6 (b) comparison of <math>\tau</math> of M6 with the pure compounds</i>	142

## Chapter 6:

<b>Figure 6.1:</b>	<i>Molecular structure of the antiferroelectric liquid crystal (DM1)</i>	155
<b>Figure 6.2:</b>	<i>Textures of SmA*, SmC* and SmC<sub>A</sub>* phases of the pure compound in (a)-(c) and those of the composite in (d)-(f)</i>	157
<b>Figure 6.3:</b>	<i>Temperature variation of pitch in SmC* and SmC<sub>A</sub>* phases of (a) pure and (b) MWCNT composite</i>	158
<b>Figure 6.4:</b>	<i>Temperature dependence of critical frequencies (f<sub>c</sub>) of all modes of (a) pure AFLC, (b) nanocomposite, (c) fitted absorption (<math>\epsilon''</math>) curve in SmC<sub>A</sub>* phase of pure AFLC and (d) its CNT composite. Soft mode in the SmC* phase seen under bias field</i>	159

<b>Figure 6.5:</b>	<i>Comparison of the fitted (a) dispersion (<math>\epsilon'</math>) and (b) absorption (<math>\epsilon''</math>) curves in the SmC* phase at 86°C</i>	160
<b>Figure 6.6:</b>	<i>Temperature dependence of dielectric increment (<math>\Delta\epsilon_{GM}</math>) of the pure AFLC and its CNT composite</i>	161
<b>Figure 6.7:</b>	<i>(a) Dielectric increments and (b) critical frequencies as a function of dc bias field of the pure AFLC and its composite at Tc–12.5</i>	163
<b>Figure 6.8:</b>	<i>Frequency dependent dielectric dispersion (<math>\epsilon'</math>) curves in SmC* phase under the bias field of 0V (curve 1), 30V (curve 2) and again 0V (curve 3) of the (a) pure AFLC and (b) its nanocomposite</i>	163
<b>Figure 6.9:</b>	<i>(a) The delay of polarization bump of pure AFLC and its CNT composite occurring in time axis at Tc–12.5 (b) Variation of switching time with temperature</i>	165
<b>Figure 6.10:</b>	<i>Temperature dependence of spontaneous polarization of (a) Pure AFLC and (b) Nanocomposite, fitted curves near Tc is also shown, (c) Temperature dependence of rotational viscosity of the pure and the CNT composite</i>	165
<b>Figure 6.11:</b>	<i>Variation of optical tilt as a function of reduced temperature (T–Tc)</i>	167
<b>Figure 6.12:</b>	<i>(a) Variation of conductivity as a function of frequency, (b) Magnified view is shown in the low frequency region</i>	167
<b>Figure 6.13:</b>	<i>Variation of conductivity as a function of dc bias field</i>	168

## Chapter 7:

<b>Figure 7.1:</b>	<i>Molecular structures and transition temperatures (°C) of the molecules obtained from texture studies during heating; cooling data are shown within parentheses</i>	179
<b>Figure 7.2:</b>	<i>Textures of 6F6T in different phases (a) SmC<sub>A</sub>* (40°C), (b) SmC* (71°C), (c) SmA* (95°C), magnification 200x</i>	180
<b>Figure 7.3:</b>	<i>Typical DSC thermogram obtained for the compounds (a) 4F6T and (b) 6F6T on heating</i>	181
<b>Figure 7.4:</b>	<i>Optimized structures along with the directions of dipole moments (red line) and principal moments of inertia (black line) of (a) 4F6T, (b) 5F6T and (c) 6F6T</i>	182

<b>Figure 7.5:</b>	<i>X-ray diffraction profiles at 44 °C (SmC<sub>A</sub>*), 72 °C (SmC*) and 84 °C (SmA*) of the (a) low angle and (b) high angle diffraction features of 6F6T</i>	184
<b>Figure 7.6:</b>	<i>Temperature evolution of (a) layer spacing, (b) intermolecular distance of 4F6T and 6F6T; fitted layer spacings in SmC* phase of (c) 4F6T and (d) 6F6T</i>	185
<b>Figure 7.7:</b>	<i>Temperature evolution of correlation lengths (a) across the smectic layers (<math>\xi_{  }</math>), (b) within the smectic layers (<math>\xi_{\perp}</math>) and (c) intensity of the low angle Bragg peak (arbitrary unit) of 4F6T and 6F6T</i>	186
<b>Figure 7.8:</b>	<i>Dielectric increment <math>\Delta\epsilon</math> (a) of 4F6T and 6F6T during cooling, (b) of 6F6T during heating and cooling showing anomaly</i>	188
<b>Figure 7.9:</b>	<i>Temperature dependence of critical frequencies (<math>f_c</math>) of various modes in (a) 4F6T and (b) 6F6T</i>	188
<b>Figure 7.10:</b>	<i>(a) Polarization versus field in 6F6T at different temperatures and (b) linear increase of saturation field (<math>E_{sat}</math>) with decreasing temperature</i>	189
<b>Figure 7.11:</b>	<i>Temperature variation of spontaneous polarization of (a) 4F6T and (b) 6F6T, fitted curves near <math>T_c</math> is also shown</i>	190
<b>Figure 7.12:</b>	<i>Temperature variation of optical tilt of (a) 4F6T and (b) 6F6T, fitted curves near <math>T_c</math> is also shown</i>	190
<b>Figure 7.13:</b>	<i>Temperature variation of x-ray tilt of (a) 4F6T, (b) 6F6T, fitted curves near <math>T_c</math> is also shown</i>	191
<b>Figure 7.14:</b>	<i>Comparison of temperature dependence of switching time</i>	192
<b>Figure 7.15:</b>	<i>AC field dependence of SmC*–SmC<sub>A</sub>* transition temperature (<math>T_{AF}</math>) of 4F6T and 6F6T</i>	192

## LIST OF APPENDICES

<b>APPENDIX A:</b>	<i>List of selected books and monographs on liquid crystals</i>	211
<b>APPENDIX B:</b>	<i>(I) List of papers published in journals and (II) List of papers presented in the seminars and conferences</i>	213
<b>INDEX:</b>		217

# CHAPTER 1

---

## Introduction

1.1	INTRODUCTION TO LIQUID CRYSTAL	3
1.2	CLASSIFICATION OF LIQUID CRYSTAL	3
1.2.1	NEMATIC LIQUID CRYSTAL	4
1.2.2	CHOLESTERIC LIQUID CRYSTAL	4
1.2.3	SMECTIC LIQUID CRYSTAL	5
1.2.4	CHIRALITY	6
1.2.5	FERROELECTRIC LIQUID CRYSTAL	7
1.2.6	SURFACE STABILIZED FERROELECTRIC LIQUID CRYSTAL	9
1.2.7	ANTIFERROELECTRIC LIQUID CRYSTAL	12
1.2.8	ORTHOCONIC ANTIFERROELECTRIC LIQUID CRYSTAL	14
1.3	EFFECT OF FLUORO-SUBSTITUTION IN FERROELECTRIC AND ANTIFERROELECTRIC LIQUID CRYSTALS	16
1.3.1	EFFECT OF LONGITUDINAL FLUORO-SUBSTITUTION	16
1.3.2	EFFECT OF LATERAL FLUORO-SUBSTITUTION	17
1.4	LIQUID CRYSTAL MIXTURES	18
1.5	MOTIVATION OF THE PRESENT WORK	19
1.6	LIQUID CRYSTAL COMPOUNDS AND MIXTURES STUDIED IN THE DISSERTATION	21
1.7	REFERENCES	25



## 1.1 INTRODUCTION TO THE LIQUID CRYSTAL

Liquid Crystal is a delicate phase of matter intermediate between the crystalline solid and the amorphous liquid. In 1888 Friedrich Reinitzer, an Austrian botanist, was performing investigations about cholesterol at Charles University in Prague [1]. He synthesized the benzoates and found that cholesteryl benzoate does not melt in the same manner as other compounds, but has two melting points. At 145.5 °C it melts into a cloudy liquid, and at 178.5 °C it melts again and the cloudy liquid becomes clear [2]. Reinitzer send his sample to German physicist Otto Lehmann, who was an expert in optics, for better examination. Lehmann examined the intermediate cloudy fluid and reported it as crystalline state and he named the new state as “Liquid Crystal”. Reinitzer presented his results, with due credits to Lehmann at a meeting of the Vienna Chemical Society on May 3, 1888 [3]. Thus Reinitzer discovered the novel state of matter by chance. The notion ‘Liquid Crystal’ suggests that it is an intermediate state of a matter, in between the liquid and the crystal. It possesses some typical properties of a liquid (e. g. fluidity, inability to support shear, formation and coalescence of droplets) as well as some crystalline properties (anisotropy in optical, electrical, and magnetic properties, periodic arrangement of molecules in one spatial direction, etc.). The important characteristics of liquid crystals (LC) are that it is affected by electric and magnetic fields and can rotate plane of polarization of light. For their electro-optic properties, they find applications in display industries. The Liquid crystal display (LCD) is more energy-efficient and can be disposed of more safely than a CRT. Its low electrical power consumption enables it to be used in battery-powered electronic equipments. LCDs are used in a wide range of applications including computer monitors, televisions, cameras, instrument panels, aircraft cockpit displays, medical appliances, clocks, watches, calculators, etc.

## 1.2 CLASSIFICATION OF LIQUID CRYSTAL

Liquid crystal is divided into two categories – lyotropic and thermotropic. Lyotropic liquid crystalline phases show mesomorphic behaviour by the change in the concentration of the solute in a solution. On the other hand, the term “thermotropic” arises because transitions involving these mesophases are effected by changing temperature. These liquid crystals are divided into main two categories – calamatic

and discotic. Calamatic liquid crystals are composed of rod-like molecules and discotic liquid crystals are composed of disc-like molecules [3]. George Friedel, a French scientist, proposed in 1922 a classification scheme based on the molecular arrangement of thermotropic liquid crystals. These are named as nematic, cholesteric and smectic [4].

### 1.2.1 NEMATIC LIQUID CRYSTAL

The nematic phase is a one dimensional ordered elastic fluid. In this type of liquid crystals, there is only long-range orientational orders, i.e., molecules tend to align parallel to each other, shown schematically in **Figure 1.1(a)** but there is no positional order. The orientational order is defined by an average direction of molecules called the director and is denoted by the vector **n**. In practice, the orientations of individual molecules are not exactly parallel to the director, therefore the nematic phase can be characterized by an orientation order parameter *S*. This order parameter *S*, based on the average of the second order Legendre polynomial is defined as:

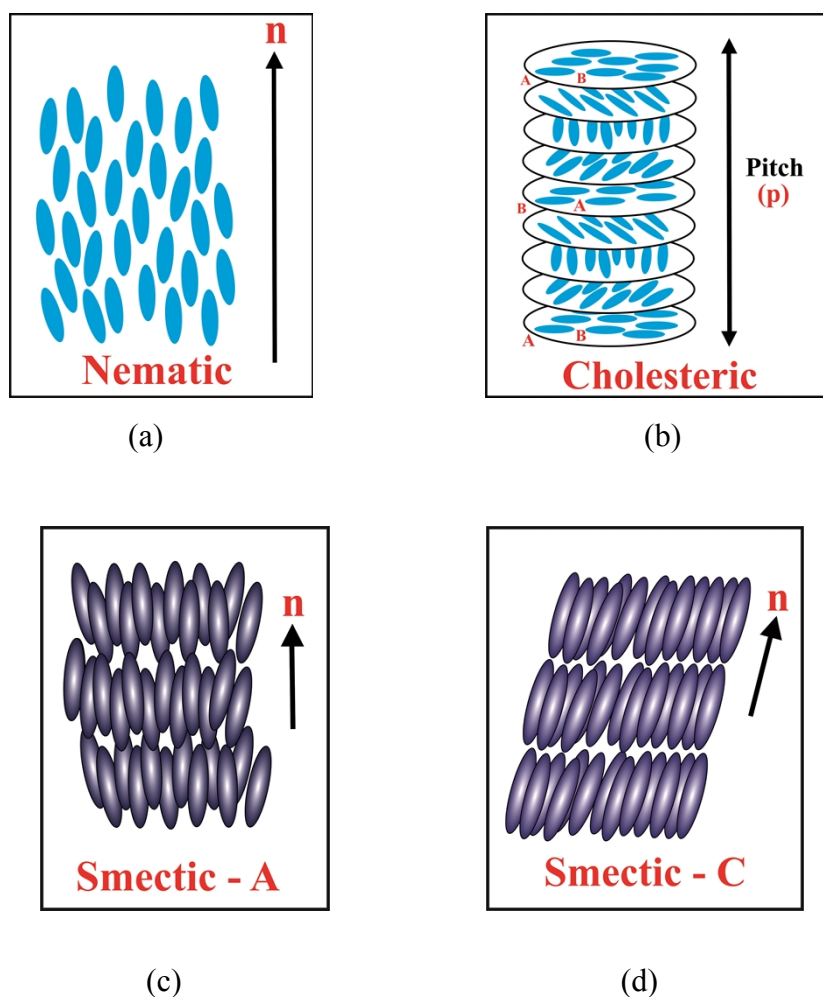
$$S = \langle P_2(\cos\theta_i) \rangle = \frac{1}{2}(3 \langle \cos^2\theta_i \rangle - 1) \quad (1.1)$$

Where  $\theta_i$  is the angle between the long axis of the  $i^{\text{th}}$  molecule and the director **n**, the statistical average is taken over all  $\theta_i$ . In a perfectly ordered state (crystalline state)  $\theta_i$ s are zero giving  $S=1$ , whereas in perfectly random state (isotropic liquid) average of  $\cos^2\theta_i$  is  $1/3$  so that  $S=0$ . So, higher is the order parameter, the more ordered is the nematic liquid crystal. The typical value of the order parameter in the nematic phase lies between 0.3 and 0.9. Strictly speaking the order parameter is real, symmetric and zero trace tensor. The nematic phase is sensitive to external electric and magnetic field and mechanical stresses, and it modifies the optical path of visible rays, for which they find wide application in display devices [5], most of the commercial LC displays are based on nematics.

### 1.2.2 CHOLESTERIC LIQUID CRYSTAL

When a nematic liquid crystal mixed with chiral molecules, the structure undergoes a helical distortion about an axis normal to the preferred molecular

direction  $\mathbf{n}$ . Thus the structure of a cholesteric liquid crystal is periodic and the director varies its direction. The period of this is known as the pitch  $p$  (**Figure 1.1(b)**).



**Figure 1.1.** (a) Nematic, (b) Cholesteric (c) Smectic–A and (d) Smectic–C liquid crystals.

### 1.2.3 SMECTIC LIQUID CRYSTAL

Upon cooling from the nematic phase (in some cases directly from the isotropic phase), LC molecules often self-assemble into layers (**Figure 1.1(c) and (d)**). These layered phases are called smectic liquid crystals. In the smectic phase, the molecules maintain the general orientational order of nematics, but also tend to align themselves in layers; with a well-defined interlayer spacing, which can be measured by X-ray diffraction [6]. Thus molecules in this phase show additional degrees of translational order not present in the nematic phase. The interlayer attractions are weak compared to the lateral forces between the molecules, and the layers can slide over one another

relatively easily. This gives rise to fluidity to the system but with higher viscosity than nematics.

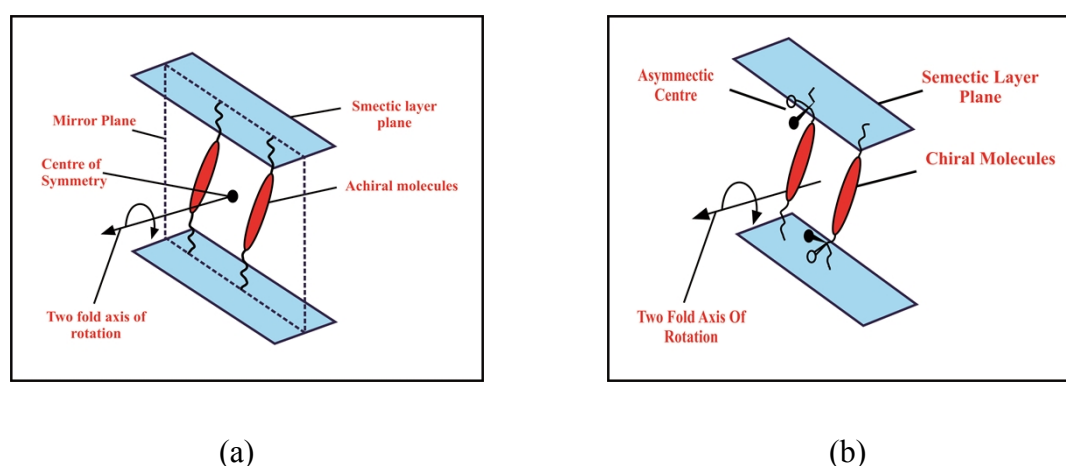
Smectic liquid crystals have stratified structure but a variety of molecular arrangements are possible within stratification with a difference in the way of layer formation and exhibiting difference in order inside the layers [7-9]. The simplest is the smectic A (SmA) phase where the director (**n**) is perpendicular to the smectic layers and thus parallel to the layer normal. In this phase, within the layers, molecules are randomly distributed. Thus, the structure may be defined as an orientationally ordered fluid on which a 1-D density wave is superimposed. On decreasing temperature, the SmA phase may transform into a phase possessing lower symmetry. The breaking of symmetry may lead to tilting of the molecules relative to the smectic layers normal. The phase thus formed is called the smectic C (SmC) phase. In this phase also no positional correlation is observed within the layer plane. There are many other types of smectic phases which, if exist, appear with increasing temperature according to a sequence rule, which may be in generalized form written as **Solid crystal - SmH - SmK - SmE - SmG - SmJ - SmF - SmB (cryst.) - SmI - SmB (hex.) - SmC - SmA - N - blue - isotropic** [10]. In general, most of the compounds show only a small part of the numerous phases, so that the generalized sequence rule is a combination of many compounds and is a hypothetical one. Ferroelectric and antiferroelectric liquid crystals are important smectic C type liquid crystal and their structures are discussed in sections 1.2.5 to 1.2.7.

#### 1.2.4 CHIRALITY

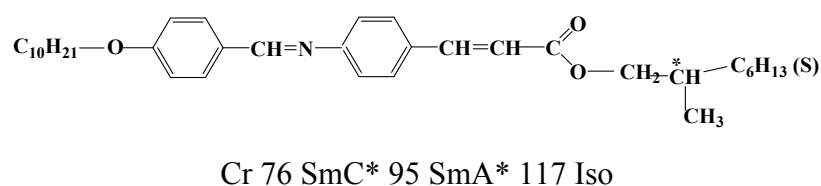
Before the discussion of ferroelectric and antiferroelectric liquid crystals, we introduce the term ‘chirality’ which is essential characteristics of these liquid crystals. An object or a molecule that is not superimposable on its mirror image is termed as chiral. Chirality is generated by four different structural moieties attached to a tetrahedral,  $sp^3$  carbon atom (often described as a chiral center). Molecular chirality leads to a wonderful variety of equilibrium structures. All of the chiral smectic mesophases takes the form of a helical structure.

### 1.2.5. FERROELECTRIC LIQUID CRYSTAL

Idea of the ferroelectric mesophase was first presented by R.B. Meyer at the 5<sup>th</sup> International Liquid Crystal Conference in 1974. From symmetry considerations, he deduced that all tilted smectic phases composed of rod-like chiral molecules have to exhibit a (local) spontaneous polarization if the molecules contain a permanent transverse dipole moment. In this phase molecules are arranged in fluid layers. On average the molecules are tilted from the layer normal by an angle. The angle made between the layer normal (**k**) and the director (**n**) is termed the tilt angle ( $\theta$ ). The tilt defines a plane containing **n** and **z**, called the tilt plane. The phase is optically biaxial [11].



**Figure 1.2.** Symmetry elements of (a) SmC and (b) SmC\* phase after reference [12]


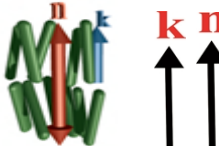
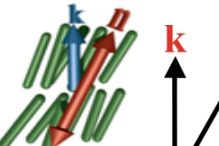
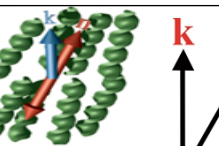


**Figure 1.3.** Structure of DOBAMBC, first FLC compound

The maximum symmetry that an achiral SmC phase can possess is (i)  $C_2$  axis normal to the tilt plane, and (ii)  $\sigma$  plane congruent with the tilt plane. Meyer first realized the simple fact that a chiral phase can possess no reflection symmetry, and therefore the maximum possible symmetry for a chiral C phase is  $C_2$  (**Figure 1.2**). Any medium with  $C_2$  symmetry must possess polar order, and therefore Meyer

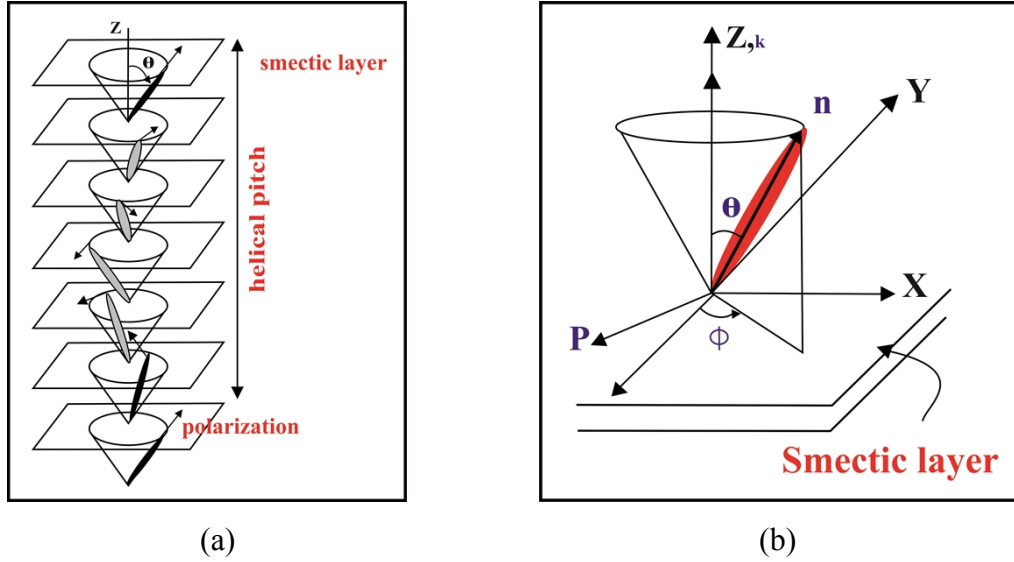
predicted that the chiral SmC phase (SmC\*) would be ferroelectric, i.e. the direction of the polarization in the polar LC phase would be switchable [13]. The molecular organization and symmetry elements of different phases Nematic, SmA, SmC and SmC\* are mentioned in **Table 1.1**.

**Table 1.1.** The symmetry elements of the N, SmA, SmC, and SmC\* phases [14, 15]

Phase	Molecular Organization	Symmetry
Nematic (N)		$D_{\infty h}$
Smectic A (SmA)		$D_{\infty}$
Smectic C (SmC)		$C_{2h}$
Chiral Smectic C (SmC*)		$C_2$

The first synthesized compound fulfilling Meyer's specification is known by an acronym DOBAMBC, standing for (S)-(-)-p'-decyloxybenzylidene p'-amino 2-methylbutyl cinnamate [16] (**Figure 1.3**). The molecule of DOBAMBC contains an asymmetric carbon atom C rendering molecular chirality, while a lateral C=O group provides a transverse permanent dipole moment. The aliphatic chain attached to the other end of the molecule by an oxygen atom is relatively long, favouring the SmC mesophase. The other aspect of chirality is the rotation of the director and hence the rotation of the direction of dipole moment about the smectic layer normal (**Figure 1.4**). Due to the formation of the helical superstructure, the spontaneous polarization is compensated to zero within one pitch of the helix,  $p$ , and the material appears to be non-polarized. With the synthesis and evaluation of DOBAMBC, the experimental study of the phenomenon of ferroelectricity in liquid crystals began. Since then, an

explosion of research and invention aimed at using and improving these novel materials has occurred.

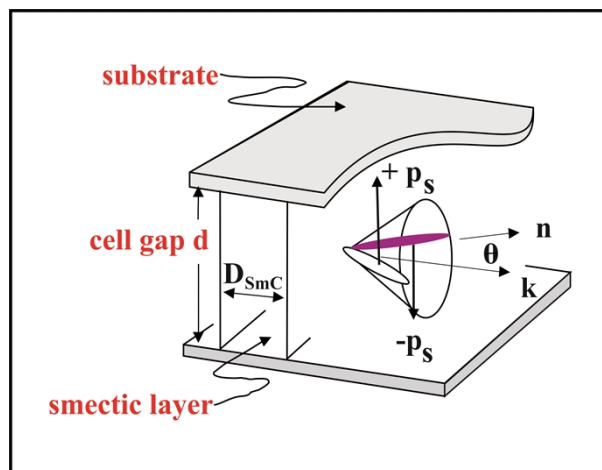


**Figure 1.4.** (a) The helicoidal structure of chiral smectic C (SmC\*) liquid crystal, polarization is tangential to the circle of intersection of the cone with the boundary plane of the layer. (b) The molecular polarization  $\mathbf{P}$  is always perpendicular to the director  $\mathbf{n}$ , the angle between  $\mathbf{n}$  and  $\mathbf{k}$  is the tilt angle ( $\theta$ ), and the azimuthal angle ( $\phi$ ) differs from layer to layer and is a function of the coordinate  $\mathbf{Z}$  parallel to the layer normal. [17]

### 1.2.6 SURFACE STABILIZED FERROELECTRIC LIQUID CRYSTAL

Although the individual molecules in SmC\* phase possess spontaneous polarization, the whole ferroelectric sample in a bulk do not have any macroscopic polarization because the molecules in layers form a helix and the net polarization is zero via helix. The stable structure of the SmC\* phase is characterized by the helicoidal structure in which the polarization is hidden and externally canceled. So it will not be possible to get macroscopic polarization in SmC\* phase in the absence of an electric field unless the helix is unwound. Thus the smectic C\* phase is not ferroelectric per se. The SmC\* phase in bulk more correctly is called helielectric [9]. In his review in 1977, Meyer addressed by pointing out that it is always possible to obtain helix-free materials by mixing (and this can be done in several ways), and thus achieving a permanent non-zero polarization that may be homogeneous in space [18].

This was demonstrated in 1980 by Clark and Lagerwall and they showed that the SmC\* phase could be rendered helix-free and bistable in a surface-stabilized structure [19].



**Figure 1.5.** Schematic surface stabilized ferroelectric SmC\* liquid crystal (SSFLC) geometry with tilt angle  $\theta$  (T) and spontaneous polarization  $P_s$  (T). [20]

In the surface-stabilized structure the helix is inherently unwound by the elastic interaction with the surrounding surfaces. The surface interaction is equivalent to a permanently applied external field, but of different nature and this interaction is non-interacting with the electric field which is to be applied. In the helix-free sample the SmC\* structure has a uniform polarization and is of special electro-optic interest. The ideal bookshelf geometry of SSFLC layers sandwiched between the glass plates of a capacitive cell, as suggested by Clark and Lagerwall is shown in the **Figure 1.5**. They illustrated that in a surface-stabilized ferroelectric liquid crystal (SSFLC) structure, the uniform polarization points in either of two ways, and this giving rise some unusual properties. These are:

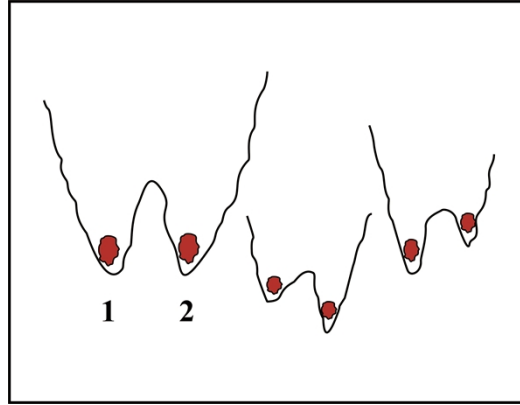
- (i) A change of sign in the electric field applied across the sample switches the optic axis of the molecule symmetrically between two equivalent ‘off’ and ‘on’ states. After application of a pulse the optic axis stays in its position until a pulse of opposite sign switches it back to the other position. This means that the device is bistable (symmetrically).
- (ii) The SSFLC device extends the switching speed from milliseconds regime in nematics to below microseconds.

- (iii) In contrast to other liquid crystal electro-optic mechanisms, in the SSFLC the optic axis (that switches by  $2\theta$ , twice the tilt angle, around the cone) is essentially perpendicular to glass plates and switched around an axis parallel to the transmitted/reflected light. This gives rise to a large optic effect with an excellent viewing angle.

SSFLC is a concept by which the energy degeneracy of  $\text{SmC}^*$  phase can be broken. If we rotate the polarisation  $P_s$  around the cone to the opposite position, corresponding to a change of sign in tilt  $\theta$ , then we see that  $P_s$  has reversed its direction. Thus a change of sign in  $\theta$  corresponds to a sign reversal of  $P_s$ , and from this, it follows that, at least for small  $\theta$ ,  $P_s$  and  $\theta$  must be linearly related i.e.,

$$P_s \sim \theta \quad (1.2)$$

The discovery of SSFLC saw great interest from the liquid crystal community due to its submicron response time, bistability and novel electro-optic effects. The bistability is a consequence of the broken symmetry in the phase variable. The potential curves along this variable, whether symmetric or slightly non-symmetric (**Figure 1.6**), illustrate that the bistability is an inherent property of the chosen geometry. It will be there as long as there are energy maxima between the states 1 and 2 that correspond to the two tilt directions.



**Figure 1.6.** The potential curve along a phase variable

### 1.2.7 ANTIFERROELECTRIC LIQUID CRYSTAL

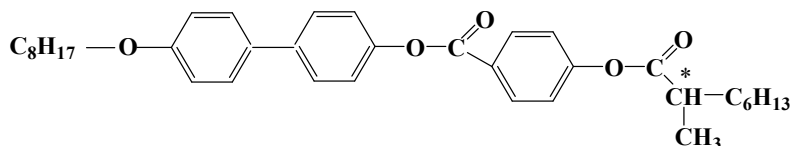
During the studies of ferroelectric liquid crystals a few groups [21-23] noticed some peculiar behaviors in their ferroelectric materials (still then they thought the materials to be ferroelectric). Hiji *et al.* [24] reported a third stable state exhibiting a dark view between crossed polarizers when one of the polarizers was parallel to the smectic layer. Furukawa *et al.* [25] reported a very small dielectric constant and a threshold behavior in the electro-optic response in the lower-temperature region of SmC\*, suggesting a new phase SmY\*. Finally, Chandani *et al.* [26] in 1989 discovered the novel antiferroelectric phase (SmC<sub>A</sub>\*) which exhibits tri-stable switching in a compound named as MHPOBC (**Figure 1.7(a)**). In the antiferroelectric phase, the direction of the molecular tilt, and hence the direction of the spontaneous polarization of the adjacent layers, are in the approximately opposite directions ( $\sim 180^\circ$ ) [13, 27-29] as shown in **Figure 1.7(b)** and **(c)**.

This type of molecular conformation is known as anticlinic conformation [25, 33-34]. Due to chirality in the SmC<sub>A</sub>\* phase, the direction of molecular tilt and hence the electric polarization precess from layer to layer along the layer normal and develops helix and leads to the formation of a double helicoidal structure with axis parallel to the layer normal.

“Antiferroelectric liquid crystal” is the common name for smectic liquid crystals that exhibit a number of smectic (Sm) tilted structures with variation of the tilt, azimuthal direction from layer to layer in non-synclinic structures in which the periodicity of crystallographic unit varies. The crystallographic unit periodicity may vary from a few (SmC <sub>$\alpha$</sub> \*), four (SmC<sub>FI2</sub>\*), three (SmC<sub>FI1</sub>\* or SmC <sub>$\gamma$</sub> \*), to two (SmC<sub>A</sub>\*) smectic layers and all of the phases arising in such a variation, possess liquid-like order inside the layer [27]. Nature of SmC<sub>FI1</sub>\* and SmC<sub>FI2</sub>\* is ferrielectric.

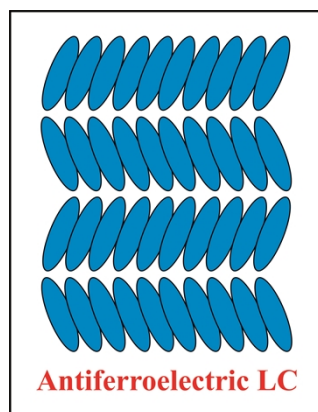
In AFLC materials sandwiched between two glass plates in homogeneous orientation (in surface stabilized structure), the smectic layers are arranged perpendicular to the glass plates giving rise to a bookshelf geometry. If an electric field  $E$  is applied parallel to smectic layers of AFLC material (i.e. perpendicular to the glass plates), placed under the cross polarizers, the material switches from the

antiferroelectric state at  $E=0$  (dark) to one of two symmetric ferroelectric states (bright) depending on the polarity of the field and show double hysteresis loops (**Figure 1.8**). This phenomenon in AFLC materials is known as tristable switching and is of great interest [35-36].

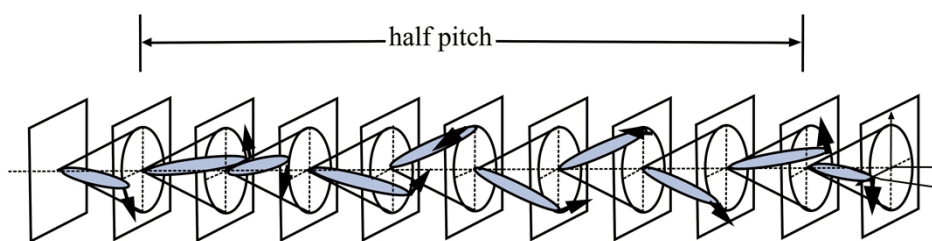


Cr 84 SmC<sub>A</sub>\* 118.4 SmC<sub>γ</sub>\* 119.2 SmC\* 120.9 SmC\*α 122 SmA\*148 Iso [30]

(a)

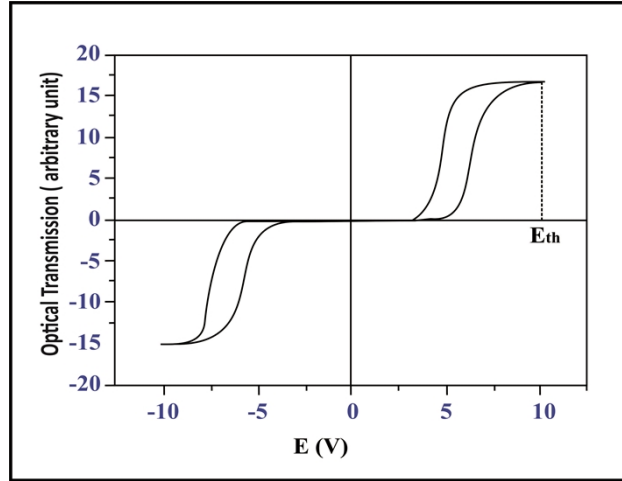


(b)



(c)

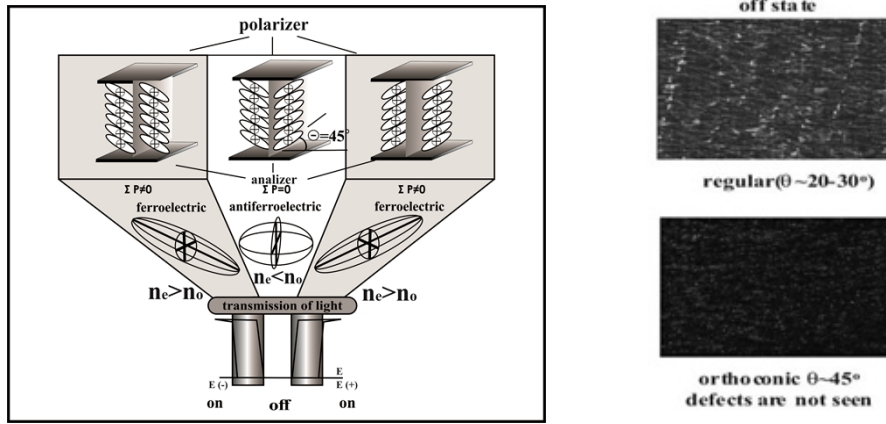
**Figure 1.7.** (a) Structure and transition temperature of MHPOBC, first AFLC compound [31], (b) Herring-bone pattern in the hypothetical structure of antiferroelectric liquid crystal, (c) Molecules, on average, have alternating tilt in alternating layers, corresponding to dipole moments pointing in opposite direction in alternate layers form double helix [32]



**Figure 1.8.** Double hysteresis loop of antiferroelectric liquid crystal under applied AC field ( $E$ ). At  $E=0$ , the antiferroelectric state is stable. For a field  $E > E_{th}$  or  $E < -E_{th}$ , the ferroelectric states are obtained from antiferroelectric states as shown to right and left and corresponding to the two saturated states at the ends of the double hysteresis loop beyond the threshold fields  $\pm E_{th}$  [20]

### 1.2.8 ORTHOCONIC ANTIFERROELECTRIC LIQUID CRYSTAL

Conventional AFLC materials are usually tilted between  $20^\circ$  and  $35^\circ$ . AFLCs with extremely high molecular tilt (equal or nearly equal to  $45^\circ$ ) are the most promising for special display and photonic applications due to their unusual optical properties which resulted from the high tilt angle of the molecular director in smectic layers [37-39]. In this phase, the conic angle between the directors of adjacent layers is nearly  $90^\circ$ . Therefore such antiferroelectrics were termed as orthoconic antiferroelectric liquid crystals (OAFLC). Typical structural defects within the surface stabilized structure of smectic phases of conventional AFLCs, corresponding to local disorientation of the smectic layers normal, deteriorates the optical contrast of such structures. Such materials in surface stabilized structures are usually optically biaxial positive liquid crystal and the effective optic axis is along the smectic layer normal i.e., parallel to cell plates. Whereas orthoconic antiferroelectric liquid crystals are a uniaxial negative liquid crystal with optic axis perpendicular to the glass plates of the cell at normal incidence (**Figure 1.9**).



**Figure 1.9.** Electro-optical properties of orthoconic AFLCs in compared to ferroelectrics. (Adapted from [42])

OAFLCs placed between crossed polarizers behaves as an isotropic medium at zero fields [39-41] for the incident light beam orthogonal to the sample plane and surface defects are not observed, which generates the excellent true dark state even the sample is rotated under crossed polarizers [42]. Abdulhalim *et al.* [43] calculated that orthoconic antiferroelectric LCs with dielectric constants fulfilling the condition:

$$\varepsilon_1 = \frac{\varepsilon_2 + \varepsilon_3}{2} \quad (1.3)$$

behave as an isotropic medium for all incidence angles of light. Such unusual optical properties of orthoconic antiferroelectrics open up new areas of applications. A partially fluorinated terminal chain promotes the high tilt of molecules in smectic layers. The Military University Group, Warsaw synthesized different families of such compounds with partially fluorinated chains having a biphenyl, naphthyl or terphenyl unit in the rigid core of molecules, un-substituted or laterally substituted with one or a few fluorine atoms [42, 44-45]. These compounds are proposed as the basis for liquid crystal displays and photonic devices with attractive advantages over existing nematic and ferroelectric technologies [39, 41].

### 1.3 EFFECT OF FLUORO-SUBSTITUTION IN FERROELECTRIC AND ANTIFERROELECTRIC LIQUID CRYSTALS

From the earlier discussions, it is clear that for the appearance of ferroelectric SmC\* phase the molecule should have chirality i.e. there should exist a terminal chiral center and transverse dipole moment. Considering these factors an FLC (or AFLC) molecule can be divided in several parts as R–A–X–A–Y–A–Z–R\*. Central linear rigid core is formed by two or three aromatic or heteroaromatic rings denoted as ‘A’ which are connected by linkage groups X and Y. As a rule, X and Y represent a simple bond e.g. –COO–, –CN=N–, –N=N– etc. R is a non-chiral terminal chain (as a rule an unbranched alkyl– or alkoxy group). R\* is a chiral terminal chain with one or more asymmetric carbon, as a rule, it is –C\*H(CH<sub>3</sub>)(CH<sub>2</sub>)<sub>m</sub>CH<sub>3</sub>, m=1-6. Sometimes chiral terminal chain is attached at both ends [46]. The linkage group Z between the core and the terminal chain formed either by a single bond or combination of more groups, some of them bringing the molecule transverse dipole moment (e.g. –CH<sub>2</sub>–, –CH=CH–, –COO–, –CO–) [47].

In the majority of FLCs, the linkage Z is the source of the transverse dipole moment and frequently it is carbonyl group (–CO–) is employed. The additional increase of spontaneous polarization can be achieved by lateral substitution of electronegative atoms or functional groups that behave as an acceptor of electrons. The location of the substitution is very important for the increase of Ps. Especially by the fluoro-substitution in different positions of ferroelectric and antiferroelectric liquid crystals the properties of parent system can be manipulated and improved predictably by changing melting point, mesophase types, transition temperatures and other physical properties [48].

#### 1.3.1 EFFECT OF LONGITUDINAL FLUORO-SUBSTITUTION

Fluoro-substitution at the hydrocarbon chain of compound favours smectic chiral phases, enhances the dielectric anisotropy and elastic constants by introducing high polarity of the C – F bond. The Compounds having terminal fluoro substitution posses a high resistivity, high photochemical stability and low viscosity which is suitable for active matrix (thin-flim transistor, TFT) displays [49]. The possibility of

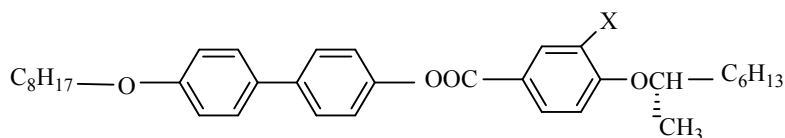
the appearance of a new phase and the modified temperature span of new mesophase are achieved by changing the degree of association between the molecules by introducing some substituent at the terminal chain [50]. R. Dabrowski *et al.* [51] reported that the fluorination at the terminal chain part of a chiral molecule is the key factor for the appearance of  $\text{SmC}_A^*$  phase. A large temperature difference in phase transitions between the hydrogenous and fluorinated structure is observed as a typical feature of fluorinated compounds by Janulis *et al.* [52]. Liquid crystals with fluorinated chains are very promising materials. Their physical and electro-optical properties in many aspects are quite different from their hydrogenous analogues, which creates new possibilities for their applications. As for example, stability of  $\text{SmC}^*$  phase observed to increase in 4'-(2-fluoro-octyloxy) phenyl4-[(perfluoroalkyl) alkyloxy] benzoates for the increasing number of fluorinated in achiral chain [49]. The influence of the perfluorinated part in the alkoxy  $[-(\text{CF})_n-(\text{CH}_2)_m-\text{O}-]$  terminal chain on the existence of the  $\text{SmC}_A^*$  phase was studied by Nugyen *et al.* [53]. For the fixed length of the methylene spacer  $m = 5$  the increase of the fluorinated part eliminates the  $\text{SmC}_A^*$  phase. The same appears for the smaller odd number  $m = 5$  of the fluorinated carbon atoms in the chain. In homologous series of perfluoroalkanoyloxy biphenylates, the antiferroelectric  $\text{SmC}_A^*$  phase was observed for members with a short as well as with a long fluorinated part of the tail. For a highly fluorinated compound a big temperature difference in phase transitions between the fluorinated and Hydrogenous structure was observed [53].

### 1.3.2 EFFECT OF LATERAL FLUORO-SUBSTITUTION

The lateral substitution of electronegative atom or functional groups (electron acceptor) is effective in the vicinity of the asymmetric carbon as well as on distant parts of the central skeleton. It not only brings additional transverse dipole moment but also influences the steric hindrance of both rotations of molecules (i) about the long axis and (ii) intra-molecular rotations. These rotations decrease the bulk spontaneous polarization. The chiral center which is depicted as an uneven tripod with unequally long arms plays an important role to influence steric hindrance to restrict the molecular rotations also. Methyl group ( $-\text{CH}_3$ ), nitril group ( $-\text{C} \equiv \text{N}$ ) and halogens (F, Cl, Br) are mostly used for a lateral substituent. These substituents (at the

vicinity of chiral center) generally influence the temperature stability of any mesophase [Table 1.2]. The increase of lateral dipole moment in FLCs is due to the dipole moment of C-X (X= F, Cl, Br) bond and when –O– group of the linkage Z is nearly parallel with this C-X bond, the dipole moment is thus added up. The increase of dipole moment and hence spontaneous polarization (Ps) occurs in the following sequence of substituents  $H < F < Cl < Br < CN$ .

**Table 1.2.** Values of the ‘spontaneous polarization Ps’ (nC/cm<sup>2</sup>) at temperature  $T_c$ -10 °C and temperature range of the SmC\* mesophase as they influenced by the substitution on the central core near an asymmetric carbon in an ortho position to the linkage group Z (–O–) [55].



X	Ps (nC/cm <sup>2</sup> )	Range of SmC*
H	45	78-99
F	78	64-97
Cl	123	72-95
Br	131	42-87
CN	160	67-90

Similarly when the lateral substitution is made at the opposite end of asymmetric carbon the value of polarization is also observed to increase [54]. With the increasing volume of the substituent thermal stability of the mesophase decreases and its temperature range becomes narrower. Considering the view that the span of a mesophase should be broad, only F is suitable for lateral substitution.

## 1.4 LIQUID CRYSTAL MIXTURES

For the application of ferroelectric and antiferroelectric materials in display technology, broad temperature range, low melting point, high switching speed, low viscosity, etc. are the essential properties which need to be optimized. Optimization of these properties can be achieved by (i) engineering of liquid crystalline molecular

structures i.e. by synthesis of new liquid crystalline compounds, (ii) formulation of mixtures. Generally, it is observed that no single FLC/AFLC compound can satisfy the above requirements. Therefore the formulation of a mixture (binary, multi-component, and host-dopant, nanocomposite) is a useful technique [56]. However, the nature and concentration of the host and dopant influence the phase behavior and properties of the resulting mixture enormously.

A binary mixture of one protonated oligomethylene spacer based chiral compound and one achiral biphenyl pyrimidine compound exhibits room temperature ferroelectric mixture with moderate spontaneous polarization and sub-millisecond switching time [57]. A partially fluorinated mesogenic chiral dopant homologue of the pure components when mixed with an achiral host mixture, results in an electroclinic mixture with large field-induced tilt and very small layer contraction at lower concentrations [58], however, at higher concentrations, wide range ferroelectric mixtures with a few hundred micro-second switching time are observed [59]. But a different fluorinated chiral dopant, with oligomethylene spacer, produces ferroelectric mixture with much faster (99  $\mu$ s) response time [60]. Intermolecular attractive forces, like Van der Waals forces, hydrogen bonds and electron donor-acceptor interaction influence the configurations of molecular arrangements in the mesophases of a mixture. Each of these forces, collectively or separately, may be responsible for increasing or decreasing the stability of the liquid crystalline phases and appearance of new intermediate phases in some cases.

As a general strategy multi-component mixtures are formulated by doping appropriate chiral dopant in achiral host mixture matrix. Host mixture is usually a mixture of several achiral compounds with wide range of SmC phase which controls the overall temperature range and tilt of the final mixture. The chiral dopant controls the spontaneous polarization, viscosity, helical pitch and switching speed of the final mixture [61-65].

## 1.5 MOTIVATION OF THE PRESENT WORK

Twisted nematic liquid crystals based displays are presently available in the market with a high viewing angle. The high value of response time ( $\sim$ ms) governing the frame rate, ghost effect and contrast ratio are still a matter for further improvement. The ferroelectric (FLCs) and antiferroelectric liquid crystal (AFLCs)

based display may be the option to solve the problem with their micro-second switching time and that is why these two materials gathered a special interest during last three decades. FLC based displays also encountered several problems - small cell spacing (1-2  $\mu\text{m}$ ) to unwind the helix, the problem of mechanical shock due to unstable molecular anchoring at the surface and desired gray scale capability which can only be achieved by indirect methods such as spatial and temporal dithering [66]. The surface stabilized antiferroelectric liquid crystals (SSAFLCs) are the smarter options to build fast response electro-optic devices and displays [67]. These materials have several advantages over the surface stabilized ferroelectric liquid crystals (SSFLCs) such as - inherent DC compensation, gray scale capability, relatively wide viewing angle, driving voltages acceptable for integrated drivers, and no ghost effect, etc. [68]. Due to the tristable switching of these materials, a simple passive matrix driving scheme can be utilized. Using these technologies even big flat panels with video-rate was demonstrated [36, 42]. But still, two major problems encountered in the development of SSAFLC based displays, due to which such displays did not find production commercially. The first one is so-called pre-transitional effect [40, 69]. It is of the dynamic nature and seems to be more important. The second one is poor optical uniformity in off state caused by the existence of microscopic defects and the existence of two preferred orientations of normal to the smectic layer which differ by few degrees from each other. Here surface stabilized orthoconic antiferroelectrics (SSOAFLCs) are appropriate stuff and they can solve the problem of SSAFLCs by their unusual optical properties.

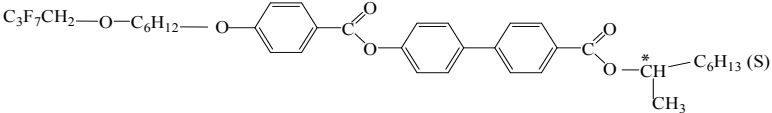
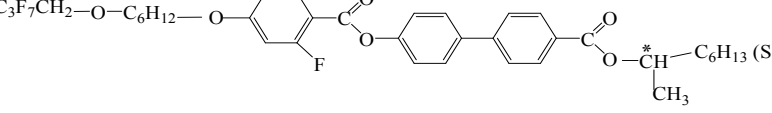
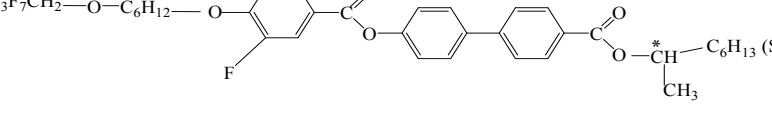
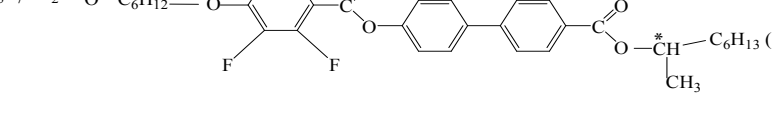
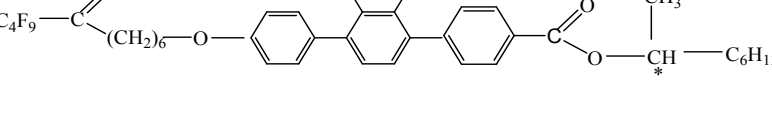
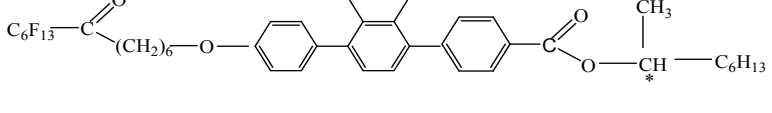
AFLCs are also interesting for the basic studies in soft condensed matter field as these materials have special molecular packing in them and are showing numerous sub-phases ( $\text{SmC}_\alpha^*$ ,  $\text{SmC}_\beta^*$ ,  $\text{SmC}_\gamma^*$ , etc.) with distinct macroscopic properties. So enough scope is here in the study of the fluorinated antiferroelectric liquid crystals for understanding the basic structure-property relations aiming at the improvement of the knowledge domain in the field.

## 1.6 LIQUID CRYSTAL COMPOUNDS AND MIXTURES STUDIED IN THE DISSERTATION

In the above background, we have selected six fluorinated antiferroelectric compounds for detailed investigation. We have also formulated three mixtures. Out of these six compounds, four are chosen from a homologous series of antiferroelectric compounds with partially fluorinated alkoxy terminal chain and biphenyl benzoate core [70]. The compounds have antiferroelectric phase in a broad temperature range similar to the compounds with partially fluorinated alkanoyloxyalkoxy chain but longer methylene spacer promotes the presence of ferroelectric phase (SmC\*) also. Four members of this series (named as DM0, DM1, DM2, and DM3) structurally differ only by the position and number of lateral fluoro-substitution on the benzoate core. In DM0 there is no fluorination, in DM1 one fluoro-substitution is made at ortho position, in DM2 one fluoro-substitution is made at meta position, and in DM3 two fluoro-substitutions are made at both ortho and meta position positions. We have probed how the properties of the homologues change due to the change of number and position of lateral fluorination at the benzoate core. In order to investigate how the properties of the biphenyl benzoate core-based compounds change when mixed with one another, a few binary mixtures of DM0 and DM3 (having no lateral fluorination and maximum fluorination in core) have also been investigated. It has been observed that the equal weight percent mixture is a eutectic mixture (M3) and this mixture has been studied in detail and the results are compared with those of the pure compounds. After observing the eutectic behaviour in the binary mixture we decided to formulate a mixture of all the compounds DM0, DM1, DM2, and DM3 which resulted in a room temperature AFLC mixture (M6). We have investigated various properties of this mixture in comparison to the pure compounds. Finally, in order to investigate the change of properties of one of the above biphenyl benzoate core-based compounds (DM1) in presence of tiny external particles (nanoscale), a small amount of (–COOH functionalized) multi-walled carbon nanotubes were doped in it and properties of this nanocomposite have also been studied in detail. We also selected another two antiferroelectric compounds (4F6T and 6F6T) for investigation which structurally differ from the DM series compounds by (i) the number of fluorinated carbon atom in the achiral chain, (ii) instead of alkoxy group in the chain, carbonyl group is attached and (iii) the core is doubly fluorinated terphenyl based instead of biphenyl benzoate.

The compound 4F6T differs from 6F6T only in the number of fluorinated carbon at the achiral chain. 4F6T has 4 fluorinated carbons at achiral chain and 6F6T has 6 fluorinated carbons. We discuss the change of properties of these two compounds due to the major change with respect to the biphenyl benzoate core-based series as well as the change of properties of compounds within the series due to the change of the number of fluorinated carbon atom at the achiral chain. Polarizing optical microscopy, differential scanning calorimetry, X-ray diffraction, frequency domain dielectric spectroscopy and electro-optic techniques have been used to investigate the pure as well as the mixtures. The molecular formulae, phase sequence and transition temperatures of the pure compounds, as well as of the mixtures, are shown in **Table 1.3 and Table 1.4**.

**Table 1.3.** Molecular structures, phase sequences and transition temperatures of the investigated pure compounds

Name	Molecular formula and transition temperatures of the compounds
<b>DM0</b>	 <p>Cr 61.0 SmC<sub>A</sub>* 94.0 SmC* 123.0 SmA* 125.0 I (Heating)</p>
<b>DM1</b>	 <p>Cr 41.0 SmC<sub>A</sub>* 75.2 SmC* 103.0 SmA* 103.6 I (Heating)</p>
<b>DM2</b>	 <p>Cr 57.3 SmC<sub>A</sub>* 80.5 SmC* 108.0 SmA* 112.2 I (Heating)</p>
<b>DM3</b>	 <p>Cr 63.2 SmC<sub>A</sub>* 85.2 SmC* 109.3 SmA* 111.6 I (Heating)</p>
<b>4F6T</b>	 <p>Cr 44.6 SmC<sub>A</sub>* 55.8 SmC* 68.7 SmA* 85.8 I (Heating)</p>
<b>6F6T</b>	 <p>Cr 36.0 SmC<sub>A</sub>* 64.0 SmC* 72.0 SmC<sub>α</sub>* 76.5 SmA* 99.2 (Heating)</p>

**Table 1.4.** Composition, phase sequences and transition temperatures of the investigated mixtures

<b>M3</b>	DM0 + DM3 (each 50%) Cr 39.8 SmC <sub>A</sub> * 86.1 SmC*112.8 SmA* 117.8 I (Heating)
<b>M6</b>	DM0 + DM1+ DM2+ DM3 (each 25%) SmC <sub>A</sub> * 81.5 SmC*110.0 SmA* 112.5 I (Heating) <RT SmC <sub>A</sub> * 65.0 SmC* 110.0 SmA* 112.0 I (Cooling)
<b>DM1+CNT</b>	DM1 (99.88%) + MWCNT (0.12%) Cr 39.05 SmC <sub>A</sub> * 70.0 SmC*102.5 SmA* 103.3 I (Heating) <RT SmC <sub>A</sub> * 48.0 SmC* 101.0 SmA* 102.2 I (Cooling)

## 1.7 REFERENCES

- [1] F. Reinitzer, *Monatsh, Chem.* 9 (1988) 421-441; English translation of this paper: *Contributions to the knowledge of cholesterol*, *Liq. Cryst.* 5 (1989) 7-18.
- [2] P. J. Collings, *Liquid Crystals: Nature's Delicate Phase of Matter* (Eds.), Princeton Press, Princeton, (1990).
- [3] S. Chandrasekhar, *Discotic liquid crystals. A brief review*, S. Chandrasekhar, *Liq. Cryst.* 14 (1993) 3-14.
- [4] G. Freidel, *Ann. Physique.* 18 (1922) 273.
- [5] E. P. Raynes. *Nematic Liquid Crystals: Applications*. *Encyclopedia of Materials: Science and Technology* (Second Edition), Elsevier, (2001) pp.6059–6065.
- [6] Vertogen and W. H. De Jeu, *Thermotropic Liquid Crystals, Fundamentals*, Springer-Verlag, Berlin, (1987).
- [7] P. S. Pershan, *Structure of Liquid Crystal phases*, World Scientific, Singapore, (1988).
- [8] S. Chandrasekhar, *Liquid Crystals* 2<sup>nd</sup> Edn., Cambridge University Press, Cambridge, (1992).
- [9] “Textures of Liquid Crystals”- Ingo Dierking. Wiley-VCH Verlag GmbH & Co. KGaA, Weinheim, (2003).
- [10] D. Demus, J. Goodby, G.W. Gray, “*Handbook of Liquid Crystals*”. Vols. 1, 2A, 2B, 3, Wiley-VCH, Verlag GmbH, Weinheim, FRG, (1998).
- [11] J. W. Goodby (Ed.), *Ferroelectric Liquid Crystals. Principles, Properties and Applications*. Gordon and Breach Science Publishers S.A., ISBN 2-88124-282-0, London, United Kingdom (1991).
- [12] M. Hird, *Ferroelectricity in liquid crystals—materials, properties, and applications*. *Liq. Cryst.* 38(11) (2011) 1467–1493.

- [13] R. B. Meyer, "Structural Problems in Liquid Crystal Physics," in *Molecular Fluids*, Balian, R. Weill, G. (Eds.); Gordon and Breach, London, 1976; p 272. This paper presents a written account of work presented at the "Summer School of Theoretical Physics," held in Les Houches, France, August, 1973. Meyer also presented this idea, along with preliminary experimental results, in a famous talk at the Vth International Liquid Crystal Conference in Stockholm, in 1974.
- [14] P. G. de Gennes, *The physics of liquid crystals*, Clarendon Press, Oxford, (1975).
- [15] S.T. Lagerwall, B. Otterholm, and K. Skarp. Material Properties of Ferroelectric Liquid Crystals and Their Relevance for Applications and Devices. *Mol. Cryst. Liq. Cryst.* 152 (1987) 503-587.
- [16] R. B. Meyer, L. Liebert, L. Strzelecki, P. Keller, *Ferroelectric Liquid Crystals*, *J. Phys. Lett. (Orsay, Fr.)* 36(3) (1975) L69-L71.
- [17] S. T. Lagerwall, B. Otterholm, K. Skarp, Material properties of ferroelectric liquid crystals and their relevance for applications and devices, *Mol. Cryst. Liq. Cryst.* 150 (1987) 503-587.
- [18] S.T. Lagerwall and I. Dahl, *Ferroelectric liquid crystal*, *Mol. Cryst. Liq. Cryst.* 114 (1984) 151-187.
- [19] N. A. Clark and S. T. Lagerwall, Sub-micro second bistable electrooptic switching in liquid crystals, *App. Phys. Lett.* 36 (1980) 899-901
- [20] S.T. Lagerwall, *Ferroelectric and Antiferroelectric Liquid Crystals*, *Ferroelectrics*. 301 (2004) 15–45.
- [21] T. Inukai, K. Furukawa, K. Terashima, S. Saito, M. Isogai, T. Kitamura, and A. Mukoh, 1985, in *Abstract Book of Japan Domestic Liquid Crystal Meeting*, Kanazawa, edited by K. Kawarabayashi and A. Ukawa, p. 172 (in Japanese).
- [22] A. M. Levelut, C. Germain, P. Keller, L. Liebert, and J. Billard, Two new mesophases in a chiral compound, *J. Phys. (France)*. 44(5) (1983) 623.

- [23] J. Goodby and E. Chin, A chiral induced ferroelectric liquid crystal phase transition with a vanishingly small enthalpy, *Liq. Cryst.* 3(9) (1988) 1245-1254.
- [24] N. Hiji, A. D. L. Chandani, S. Nishiyama, Y. Ouchi, H. Takezoe, and A. Fukuda, Layer structure and electro-optic properties in surface stabilized ferroelectric liquid crystal cells, *Ferroelectrics*. 85 (1988) 99-109.
- [25] K. Furukawa, K. Terashima, M. Ichihashi, S. Saitoh, K. Miyazawa, and T. Inukai, Chiral smectic C liquid crystals having an electronegative substituent ortho to the chiral tail group - a study of a factor determining the magnitude of spontaneous polarization, *Ferroelectrics*. 85 (1988) 451-459.
- [26] A. D. L. Chandani, Y. Ouchi, H. Takezoe, Novel Phases exhibiting tristable switching, *Jpn. J Appl Phys.* 28(1989) L1261- L1264.
- [27] A. Fukuda, Y. Takanishi, T. Isozaki, K. Ishikawa and H. Takezoe, Antiferroelectric chiral smectic liquid crystals, *J. Mater. Chem.* 4(7) (1994) 997.
- [28] J. P. F. Lagerwall and F. Giesselmann, Current Topics in Smectic Liquid Crystal Research, *Chem. Phys. Chem.* 7 (2006) 20-45.
- [29] H. Takezoe, E. Gorecka, and M. Cepic, Antiferroelectric liquid crystals: Interplay of simplicity and complexity, *Reviews of Modern Physics*. 82 (2010) 897-936.
- [30] K. Hiraoka, A. Taguchi, Y. Ouchi, H. Takezoe and A. Fukuda, Observation of Three Subphases in Smectic C\* of MHPOBC by Dielectric Measurements, *Jpn. J. Appl. Phys.* 29 (1990) L103-L106.
- [31] A. D.L. Chandani, E. Gorecka, Y. Ouchi, H. Takezoe, A. Fukuda. Antiferroelectric Chiral Smectic Phases Responsible for the Tristable Switching in MHPOBC. *Jpn. J. Appl. Phys.* 28 (1989) L1265-L1268.
- [32] H. Takezoe, Historical Overview of Polar Liquid Crystals, *Ferroelectrics*. 468 (2014) 1-17.
- [33] A. D. L. Chandani, T. Hagiwara, Y. Suzuki, Y. Ouchi, H. Takezoe, and A. Fukuda, Tristable Switching in Surface Stabilized Ferroelectric Liquid

- Crystals with a Large Spontaneous Polarization, *Jpn. J. Appl. Phys. (Part 2)*. 27 (1988) L729-L732.
- [34] A. D. L. Chandani, Y. Ouchi, H. Takezoe, A. Fukuda, K. Terashima, K. Furukawa, A. Kishi, Novel Phases Exhibiting Tristable Switching, *Jpn. J. Appl. Phys.* 28 (1989) L1261-L1264.
- [35] X. Quintana, P. L. Castillo, J. M. Oton, N. Bennis, A. Lara, V. Urruchi, R. Dabrowski, Novel addressing scheme for passive antiferroelectric liquid crystal display, *Proc. SPIE (XV Conference on Liquid Crystals)*. 5565 (2004) 290-296.
- [36] N. Yamamoto, N. Koshoubu, K. Mori, K. Nakamura, Y. Hamada, Full-color antiferroelectric liquid crystal display, *Ferroelectrics*. 149 (1993) 295-304.
- [37] R. Dabrowski, P. Kula, Z. Raszewski, W. Piecek, J. M. Otton, and A. Spadlo, New Orthoconic Antiferroelectrics: Useful for Applications, *Ferroelectrics*. 395 (2010) 116–132.
- [38] K. D’have, P. Rudquist, S. T. Lagerwall, H. Pauwels, W. Drzewinski, and R. Dabrowski, Solution of the dark state problem in antiferroelectric liquid crystal displays, *Appl. Phys. Lett.* 76 (2000) 3528–3530.
- [39] S. T. Lagerwall, A. Dahlgren, P. Jagemal, P. Rudquist, K. D’have, H. Pauwels, R. Dabrowski, and W. Drzewinski, Unique electro-optical properties of liquid crystals designed for molecular optics, *Adv. Funct. Mater.* 11(2001) 87–94.
- [40] K. D’have, P. Rudquist, M. Matuszczyk, S.T. Lagerwall, H. Pauwels, R. Dabrowski, Antiferroelectric liquid crystals with 45° tilt: new electro-optic effects in liquid crystals, *SPIE* 3955 (2000) 33–44.
- [41] K. D’have, A. Dahlgren, P. Rudquist, J.P.F. Lagerwall, G. Anderson, M. Matuszczyk, S.T. Lagerwall, R. Dabrowski, W. Drzewinski, Antiferroelectric liquid crystals with 45° tilt a new class of promising electro-optic materials, *Ferroelectrics* 244 (2000) 115–128.

- [42] R. Dabrowski, J. Gasowska, J. Oton, W. Piecek, J. Przedmojski, M. Tykarska, High tilted antiferroelectric liquid crystalline materials, *Displays*. 25 (2004) 9–19.
- [43] I. Abdulhalim, Optimization of antiferroelectric liquid crystal devices at the degeneration point. *Journal of Applied Physics* 93 (8) (2003) 4930–4932.
- [44] P. Kula, R. Dabrowski, K. Kenig and D. Chyczewska, New ferroelectric compounds from chiral terphenyls, *Ferroelectrics*. 343 (2006) 19–26.
- [45] M. Zurowska, R. Dabrowski, J. Dziaduszek, K. Czuprynski, K. Skrzypek, M. Filipowicz, N. Bennis, and J. M. Oton, Synthesis and properties of high tilted antiferroelectric esters with partially fluorinated alkoxyalkoxy terminal chains, *Opto-Electronics Review*. 16 (3) (2008) 251–256.
- [46] P. K. Mandal, S. Haldar, A. Lapanik, and W. Haase, Induction and Enhancement of Ferroelectric Smectic C Phase in Multi-Component Room Temperature Mixtures, *Jpn. J. Appl. Phys.* 48 (2009) 011501(1-6).
- [47] S. Pirkel and M. Glogarova. Ferroelectric Liquid Crystals with High Spontaneous Polarization (2011). 17<sup>th</sup> Chapter, *Ferroelectrics - Physical Effects*. Edited by Mickael Lallart (Ed), Intech, 407-428.
- [48] M. Hird and K. J. Toyne. Fluoro Substitution in Thermotropic Liquid Crystals. *Mol. Cryst. Liq. Cryst.* 323 (1998) 1– 67.
- [49] H. Liu and H. Nohira, Synthesis and mesomorphic properties of fluorinated liquid crystals obtained from optically active 2- fluoro-octanol, *Liq. Cryst.* 20(5) (1996) 581-586.
- [50] W. Drzewinski, K. Czuprynski, R. Dabrowski and M. Neubert. New Antiferroelectric Compounds Containing Partially Fluorinated Terminal Chains. Synthesis and Mesomorphic Properties, *Mol. Cryst. Liq. Cryst.* Vol. 328, (1999) 401-410.
- [51] Roman Dabrowski, Liquid Crystals with Fluorinated Terminal Chains and Antiferroelectric Properties, *Ferroelectrics*. 243 (2000) 1-18.

- [52] E. P. Janulis, J. C. Novack, G. A. Papapolymerou, M. Trislan-Kendra, W.A. Huffman, Fluorinated ferroelectric liquid crystals, *Ferroelectrics*. 85(1988) 375-.
- [53] H. T. Nguyen, J. C. Rouillon, A. Babeau, J. P. Marcerou, G. Sigaud, Synthesis, properties and crystal structure of chiral semiperfluorinated liquid crystals with ferro and antiferro anticlinic smectic phases, *Liq. Cryst.* 26(7) (1999) 1007-1019.
- [54] S. Pachomov. Syntheses and studies of ferroelectric liquid crystals. Ph.D. thesis. Institute of Chemical Technology, Prague, Czech Republic, April 1997, p1-142.
- [55] K. Furukawa, K. Terashima, M. Ichihashi, S. Saitoh, K. Miyazawa, & T. Inukai, Chiral smectic C liquid crystals having an electronegative substituent ortho to the chiral tail group – a study of a factor determining the magnitude of spontaneous polarization, *Ferroelectrics*.85. (1988) 451-459.
- [56] T. Geelhaar, Ferroelectric mixtures and their physico-chemical properties, *Ferroelectrics*. 85 (1988) 329–349.
- [57] A. Debnath, P. K. Mandal, D. Weglowska and R. Dabrowski, Induction of a room temperature ferroelectricSmC\* phase in binary mixtures with moderate spontaneous polarization and sub-milliseconds witching time, *RSC Adv.* 6 (2016) 84369-.
- [58] A. Debnath, D. Sinha, and P. K. Mandal, Wide range room temperature electroclinic liquid crystal mixture with large induced tilt and very small layer contraction, *J. App. Phys.*, 119 (2016) 124103.
- [59] A. Debnath, D. Sinha, P. K. Mandal, and R. Dabrowski, Formulation of a room temperature ferroelectric liquid crystal mixture with sub-millisecond switching time, *AIP Conf. Proc.* 1665 (2015) 040004-.
- [60] A. Debnath and P. K. Mandal, Wide range room temperature ferroelectric liquid crystal mixture with microsecond order switching, *J. Mol. Liq.* 221 (2016) 287-

- [61] W. Kuczyunski and H. Stegemeyer. Ferroelectric properties of smectic C liquid crystals with induced helical structure. *Chem. Phys. Lett.*, 1980; 70: 123-126.
- [62] M. Wand, R. Vobra, W. Thurmes, et al. New ferroelectric liquid crystal host materials for use in optoelectronic applications. *Proc SPIE*, 1994; 2175: 1-6.
- [63] W. Thurmes, M. Wand, R. Vohra, et al. FLC materials form microdisplay applications. *Proc SPIE*, 1997; 3015: 1-6.
- [64] M. Wand, W. Thurmes, M. Meadows, et al. FLC displays for high resolution magnified view and projection applications. *Proc SPIE*, 1999; 3635: 1-6.
- [65] N. Bennis, A. Spadlo, R. dabrowski, et al. Non-conventional alignment surfaces for antiferroelectric liquid crystals. *Mol. Cryst. Liq. Cryst.*, 2004; 422:37-45.
- [66] M. B. Pandey, R. Dabrowski and R. Dhar. Antiferroelectric Liquid Crystals: Smart Materials for Future Displays, Ashutosh Tiwari and Sergiy Valyukh (eds.) *Advanced Energy Materials*, Scrivener Publishing LLC, 2014 (389–432).
- [67] D. H. You, J.H. Lee, S.S. Park, S.D. Lee, Antiferroelectric liquid crystal display with one polarizer in a reflective configuration, *Ferroelectrics* 246 (2000) 2003.
- [68] J.M. Otton, X. Quintana, P.L. Castillo, *Optoelectron. Rev.*, Vol 12, p.263, 2004.
- [69] R. Beccherelli, S.J. Elston, Evaluation of optical anisotropy in the pre-transitional regime in antiferroelectric liquid crystals, *Liq. Cryst.* 25 (5) (1998) 573 – 577.
- [70] M. Zurowska, R. Dabrowski, J. Dziaduszek, K. Czuprynski, K. Skrzypek, and M. Filipowicz, Synthesis and Mesomorphic Properties of Chiral Esters Comprising Partially Fluorinated Alkoxyalkoxy Terminal Chains and a 1-methylheptyl Chiral Moiety, *Mol. Cryst. Liq. Cryst.* 495 (2008) 145[497]–157[509].



# CHAPTER 2

---

## Experimental techniques:

2.1	INTRODUCTION	35
2.2	IDENTIFICATION OF MESOPHASES AND DETERMINATION OF TRANSITION TEMPERATURES	35
2.2.1	POLARIZING OPTICAL MICROSCOPY	36
2.2.2	DIFFERENTIAL SCANNING CALORIMETRY	37
2.3	DETERMINATION OF STRUCTURAL PARAMETERS USING X-RAY DIFFRACTION TECHNIQUE	39
2.4	DIELECTRIC SPECTROSCOPY	43
2.4.1	DEBYE MODEL	44
2.4.2	COLE-COLE MODEL	46
2.4.3	DIELECTRIC RELAXATIONS IN FERROELECTRIC AND ANTIFERROELECTRIC LIQUID CRYSTALS	47
2.4.4	DIELECTRIC MEASUREMENT TECHNIQUE	52
2.5	MEASUREMENTS OF ELECTRO-OPTIC PARAMETERS – TILT ANGLE ( $\theta$ ), SPONTANEOUS POLARIZATION ( $P_s$ ), SWITCHING TIME ( $\tau$ ) AND ROTATIONAL VISCOSITY ( $\gamma_\varphi$ )	53
2.5.1	TILT ANGLE ( $\theta$ )	54
2.5.2	SPONTANEOUS POLARIZATION ( $P_s$ )	55
2.5.3	SWITCHING TIME ( $\tau$ )	57
2.5.4	ROTATIONAL VISCOSITY ( $\gamma_\varphi$ )	58
2.6	REFERENCES	59



## 2.1 INTRODUCTION

Liquid crystals have fascinating physical and electro-optical properties and have been explored by different group of scientists throughout the globe since their importance was understood from the application point of view. In order to apply them in the display and other devices, it is very much essential to characterize their properties by measuring some parameters which are defined and expressed in terms of some other measurable parameters based on well established models. The measurements of these parameters are accomplished with some instruments with some special techniques. In this chapter we present the techniques used in the preparation of sample cells, instruments involved and the methodology in different experimental measurements such as – the identification of phases, methods used for the determination of material constants, dielectric measurements, determination of electro-optic parameters, etc.

The following experimental techniques are employed in this dissertation:

- (i) Polarizing Optical Microscopy (POM)
- (ii) Differential Scanning Calorimetry (DSC)
- (iii) Molecular modeling.
- (iv) Synchrotron X-ray diffraction Technique
- (v) Frequency Domain Dielectric Spectroscopy (FDDS).
- (vi) Electro-optic measurements which include – the measurement of tilt angle ( $\theta$ ), spontaneous polarization ( $P_s$ ), switching Time ( $\tau$ ), rotational viscosity ( $\gamma$ ), etc.

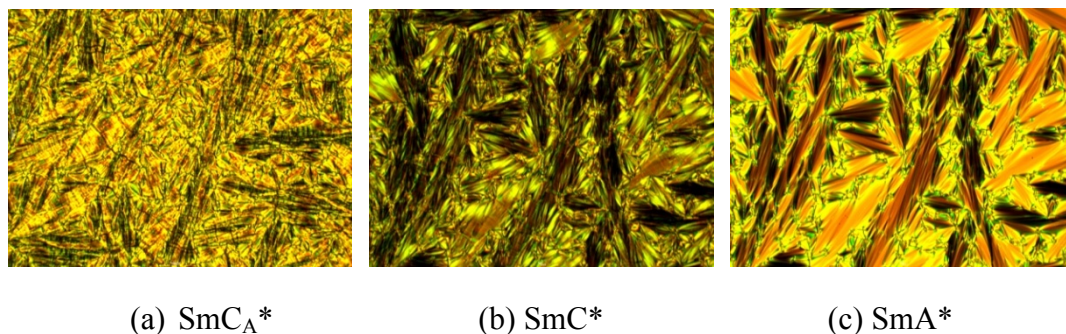
## 2.2 IDENTIFICATION OF MESOPHASES AND DETERMINATION OF TRANSITION TEMPERATURES

The primary and key task to characterize a liquid crystalline sample is to identify its mesophases and to determine the phase transition temperatures. Liquid crystalline materials may have different mesophases in between the crystalline solid and isotropic phase. There are several techniques to identify these mesophases and to determine the phase transition temperatures. These are – (i) Polarization optical microscopy (POM) [1], (ii) Differential scanning calorimetry (DSC) [2], (iii) X-ray diffraction [3-4], (iv) Frequency domain dielectric spectroscopy (FDDS) [5], (v) Neutron scattering techniques [6], (vi) Nuclear magnetic resonance (NMR) [6-8],

(vii) Raman Scattering [9], (viii) UV–visible spectroscopic studies [10], (ix) Fabry-Perot Etalon method [11], etc. Often these techniques give complementary information. We have employed only the first four techniques in this dissertation.

### 2.2.1 POLARIZING OPTICAL MICROSCOPY

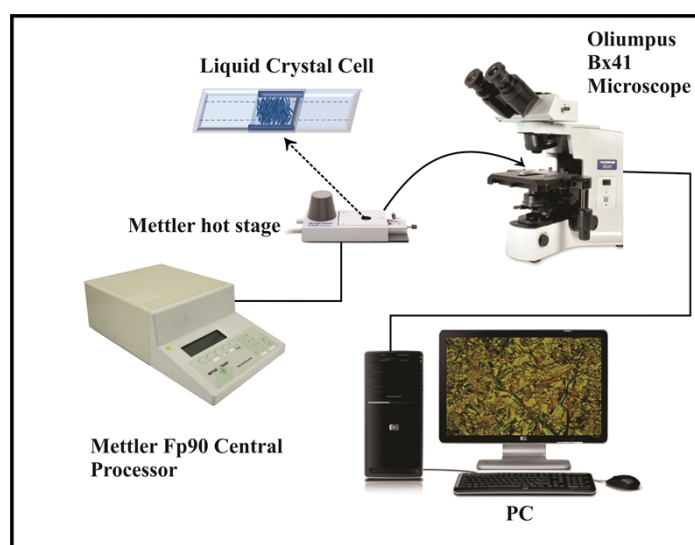
Polarizing optical microscopy is a very useful tool to identify mesophases and to determine the transition temperatures. In this method, the liquid crystalline samples are sandwiched between a microscope glass slide and a glass cover slip and set in a hot stage, the temperature of which is controlled using a Mettler Toledo FP90 central processor with accuracy  $\pm 0.1^\circ\text{C}$  within range of room temperature to  $300^\circ\text{C}$ . The hot stage (Mettler FP82) is placed under the microscope and the polarizer is set at crossed position ( $90^\circ$ ) with the analyzer. The temperature of the hot stage can be increased or decreased in a regulated manner and the textures are observed through the eyepiece of the microscope. There is also an arrangement to observe the textures on the monitor of a computer (PC) by fitting a Moticam 2500 digital camera on the top of the microscope and interfacing it with the PC using Moticam 2.0 software. The textures of the sample can be saved in photo or video mode using this software.



**Figure 2.1.** (a) Texture of (a)  $\text{SmC}_A^*$  phase, (b)  $\text{SmC}^*$  phase, and (c)  $\text{SmA}^*$  phase

When a liquid crystalline sample is observed under a polarizing microscope, colourful gorgeous visual pattern is observed and this pattern is nothing but the defect structure of molecules in the long-range order. This visual pattern is called texture. A particular mesophase has its characteristics texture; however, a particular phase may exhibit more than one type of textures depending on the surface treatment of the glasses, thickness of the samples and thermal history. When the sample is heated or cooled the molecules of the sample change their conformation and hence change the defect structures. This change of defect structure in the long-range molecular order

takes place at specific temperatures and is manifested in the visual pattern of the polarizing microscope is called the change of phase and the corresponding temperature is recorded as phase transition temperature. Many books with standard photographs of typical textures of a huge variety of mesophases with their origins have been published by Demus and Richter (1978) [12], Bouligand *et al.* [13], Slaney *et al.* [14], I. Dierking [1]. The identification of mesophases is done by comparing the observed textures with those given in these standard books. The block diagram of the polarizing optical microscopy is shown in **Figure 2.2**.

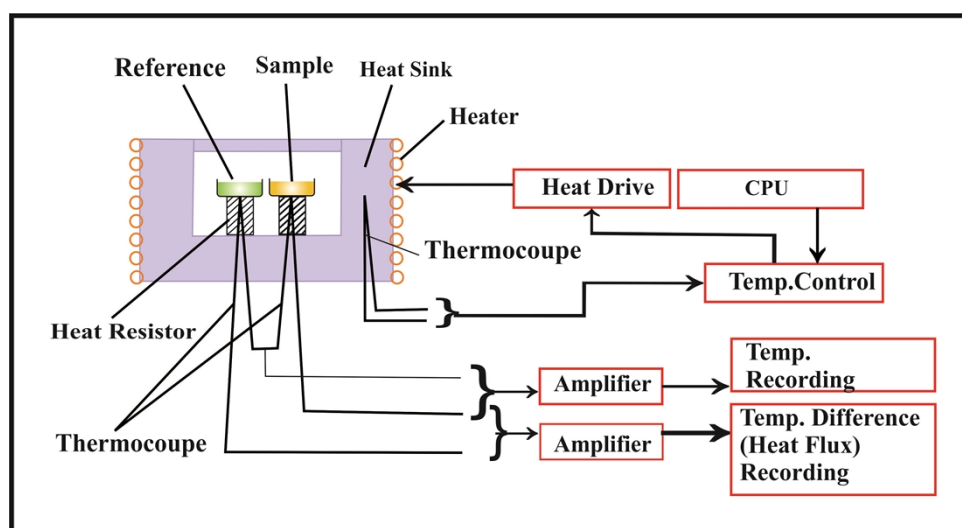


**Figure 2.2.** Block diagram of polarizing optical microscopy.

### 2.2.2 DIFFERENTIAL SCANNING CALORIMETRY

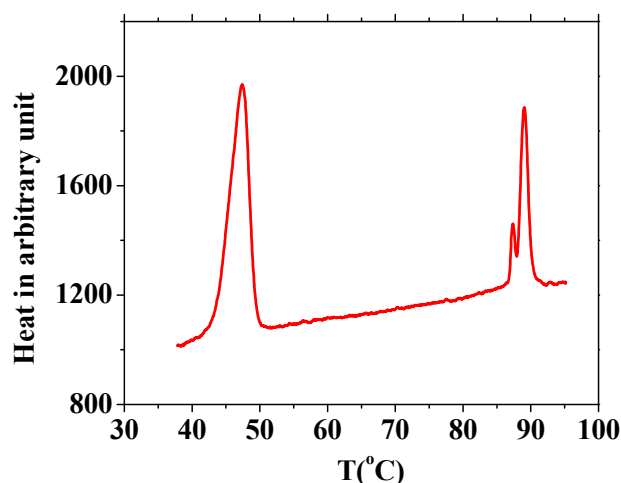
Differential Scanning Calorimetry (DSC), is a thermal analysis technique, that looks at how a material's enthalpy ( $\Delta H$ ) is changed at the transition temperature. This analysis measures the amount of energy absorbed or released by a sample when it is heated or cooled, providing quantitative and qualitative data on endothermic (heat absorption) and exothermic (heat evolution) processes. A sample of known mass is heated or cooled and the changes in its heat capacity are tracked as changes in the heat flow. In this technique the sample is placed in a suitable pan (of Al, Cu, Au, Pt, etc., we have used Al pan) and sits upon a constantan disc on a platform in the DSC analysis cell with chromel wafer immediately underneath. A chromel-alumel thermocouple under the constantan disc measures the sample temperature. An empty reference pan sits on a symmetric platform with its underlying chromel wafer and

chromel-alumel thermocouple. Heat flow is measured by comparing the difference in temperature across the sample and the reference chromel wafers. Mettler FP84 hot stage and Mettler FP90 central processor interfaced with a PC through FP99A software were used for DSC studies in our laboratory. The temperature run was given during heating and cooling at a specific scan rate (mostly 3°C per minute) and the thermogram was recorded in a PC automatically. The block diagram of the experimental arrangement is shown in **Figure 2.3**. When a phase transition of a material takes place, change of enthalpy also takes place and this change of enthalpy is qualitatively and quantitatively represented in the thermogram by an anomaly. The level of enthalpy change provides some indication about the nature of the phase transition.



**Figure 2.3.** The Experimental set up of DSC experiment [15].

Crystal to liquid crystal transition involves high energy of transition. It means that the large changes in transition enthalpies are related to structural changes at phase transition [16]. Usually, crystal to N or SmA transitions, N or SmA to isotropic transitions are first order and they are prominent although liquid crystal to isotropic liquid transition is less prominent than crystal to liquid crystal phase transition. But crystal to higher-order smectics (like SmG) and phase changes within them are weakly first order or second order in nature and not always detectable by DSC techniques or sometimes maybe better observed by choosing proper heating and cooling rate [17]. The typical DSC plot is shown in **Figure 2.4**.



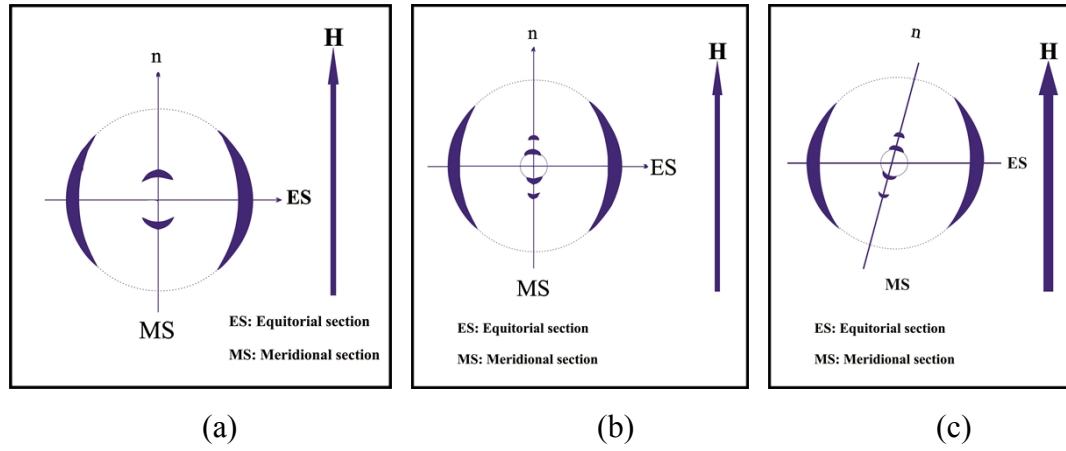
**Figure 2.4.** A typical DSC thermogram

### 2.3 DETERMINATION OF STRUCTURAL PARAMETERS USING THE X-RAY DIFFRACTION TECHNIQUE.

X-ray diffraction is the most reliable technique for investigation of the microscopic structure of liquid crystals. Details of this technique have been reviewed by many authors [18-21]. It maps the positions of the molecules in a particular phase and produces a typical diffraction pattern. From the knowledge of the structure of diffraction patterns over the temperature range, the phases present in the mesophase can be identified [22-31]. The alignment of the sample is done by applying a magnetic or an electric field in nematic LCs and by slow cooling in smectic LCs. The remarkable features of the x-ray diffraction pattern of nematic or smectic phases, which are obtained on normal incidence of the X-ray beam to the director  $\mathbf{n}$  are one outer halo and one inner halo (**Figure 2.5**).

For unaligned samples the halos are uniform but in aligned samples the outer halo is split into two crescents showing maxima along equatorial direction perpendicular to  $\mathbf{n}$  (or  $\mathbf{H}$ , aligning magnetic field) (**Figure 2.5**), which are formed due to intermolecular scattering [32] and the corresponding angle gives a measure of average intermolecular distance between elongated molecules ( $D$ ) (**Figure 2.5 (a)**). Similarly, the inner halo splits into two crescents with maxima at much lower angle in the meridional direction parallel to  $\mathbf{n}$  (or  $\mathbf{H}$ ). These crescents are formed due to the molecular layer arrangement along  $\mathbf{n}$  [32]. In smectic phases the inner pattern appears

as sharp spots, sometimes second order spots are also observed (**Figure 2.5 (b and c)**).



**Figure 2.5.** Schematic representation of typical X-ray diffraction pattern of an aligned (a) nematic phase and (b) Smectic–A phase and (c) Smectic–C phase (X-ray beam is perpendicular to the paper)

The low and high angle diffraction peaks were fitted to a Lorentzian and measuring the corresponding angle of diffraction from the fitted the apparent molecular length ( $l$ ) (in nematics) or layer spacing ( $d$ ) (in smectics) can be determined using Bragg equation

$$2d \sin\theta = \lambda \quad (2.1)$$

where  $\lambda$  is the wavelength of the X-ray beam. But the average intermolecular distance ( $D$ ) is determined using the modified Bragg formula [32],

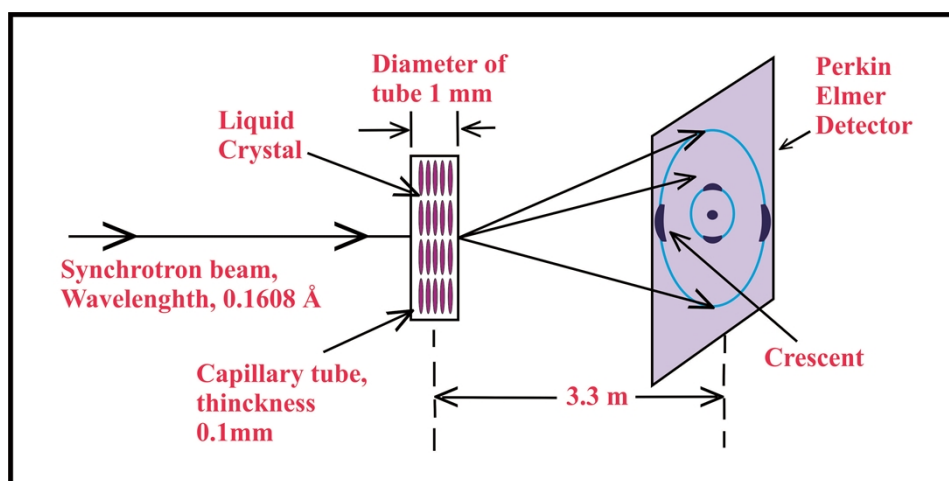
$$2D \sin\theta = 1.117\lambda \quad (2.2)$$

Estimated measurement error in  $d$  and  $D$  are  $0.02 \text{ \AA}$  and  $0.002 \text{ \AA}$  respectively.

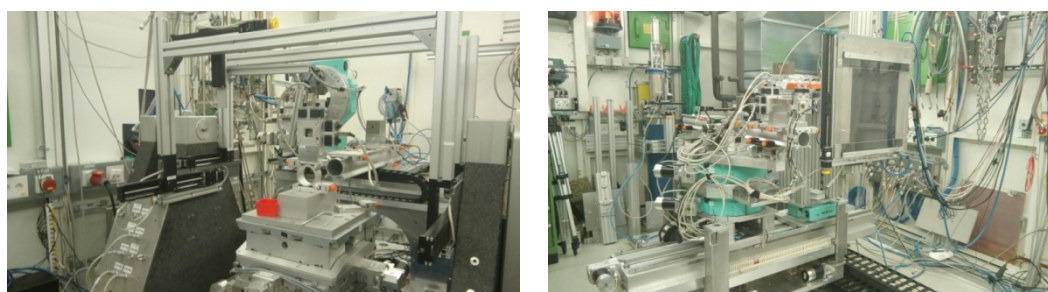
Chiral smectic phases give rise to a similar diffraction pattern. It is worth to mention here in conventional X-ray scattering experiment it is not possible to distinguish smectic liquid crystal phases that differ with respect to the orientation (but not packing) of the molecules in successive layers like in  $\text{SmC}_A^*$  and  $\text{SmC}^*$  phases (possible by resonant X-ray scattering experiment, not done in this dissertation) [33]

In order to explore the structure of the pure antiferroelectric samples, the diffraction experiments were performed using a synchrotron radiation facility (PETRA III beamline at P07 Physics Hutch station) at Deutsches Elektronen Synchrotron, Hamburg, Germany. The samples were taken in the Lindeman glass tube

of 1.0 mm diameter by capillary action. The synchrotron radiation beam was passed normal geometry. The temperature of the sample was decreased very slowly to the desired temperature to get better alignment. A Perkin Elmer 2D detector of pixel size  $200 \times 200 \mu\text{m}^2$  and total size  $400 \times 400 \text{ mm}^2$  was used for image grabbing which was placed at 3.3m away from the sample (**Figure 2.6**). 50 images of exposure time 0.2s were grabbed and averaged to get one diffraction image and two such images were collected at a particular temperature. All the physical parameters were averaged over these two image data. QXRD program for PE Area Detector (G. Jennings, version 9.8, 64 bit) was used for data acquisition and also for analyzing the image. Images were integrated using a step size of 0.002 to get the intensity versus scattering wave vector (Q) distribution. Experiments were also done by taking LC samples in dielectric cells and the electric field was applied but not presented in this dissertation.



**Figure 2.6.** Schematic diagram of experimental arrangement of X-ray diffraction study (not to scale)

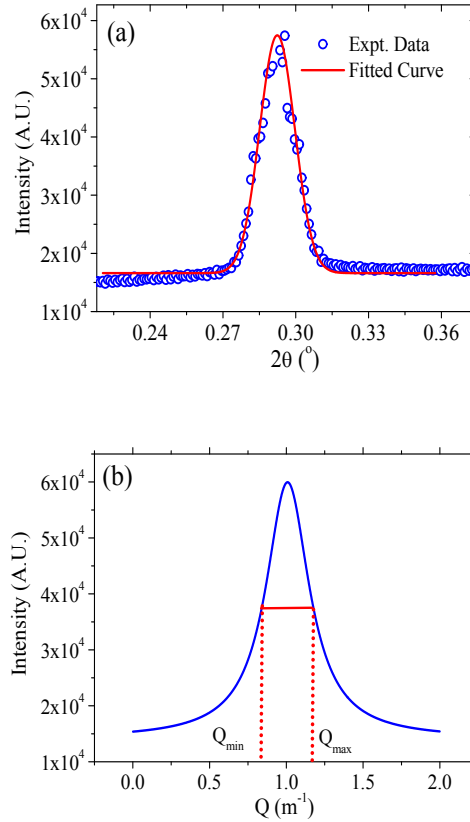


**Figure 2.7.**(a) Synchrotron X-ray diffraction set up unit (b) Perkin Elmer 2D detector of size  $400 \times 400 \text{ mm}^2$ , at DESY, Hamburg, Germany

Under rigid rod approximation tilt ( $\theta_{X-ray}$ ) of the molecules in smectic planes was determined using the formula,

$$\theta_{X-ray} = \cos^{-1}(d/l) \quad (2.3)$$

where  $l$  is the maximum layer spacing in SmA\* phase and  $d$  is the layer spacing in the tilted phases. Estimated error in this case is  $0.04^\circ$ .



**Figure 2.8.** (a) Fitted low angle intensity profile, (b) Intensity profile showing FWHM ( $\Delta Q = Q_{\max} - Q_{\min}$ )

To probe the extent of correlation of the molecules, correlation lengths ( $\xi$ ) were calculated both across ( $\xi_{\parallel}$ ) and within ( $\xi_{\perp}$ ) the smectic layers using the following formula.

$$\xi = \frac{2\pi}{\text{FWHM}} = \frac{2\pi}{\Delta Q} \quad (2.4)$$

here  $\text{FWHM} = \Delta Q = Q_{\max} - Q_{\min}$ , is the full width at half maxima in the scattering vector ( $Q$ ) of the relevant Bragg peak and was determined from the fitted intensity profile diffraction features (**Figure 2.8**) using Lorentzian fit function of the Origin software.

## 2.4 DIELECTRIC SPECTROSCOPY

When dielectric materials are placed in an electric field, the electric charges of the molecules shift slightly from their equilibrium position and generate electrical polarization in the material which is called dielectric polarization. Eventually, an internal electric field is produced which reduces the overall electric field within the dielectric. If the dielectric consists of polar molecules, under electric field the molecules orient themselves along the field. The ability of polarization of material in the presence of electric field is different for different materials. Dielectric constant or relative permittivity of a dielectric material is defined as the ratio of the capacitance of a capacitor filled with the material to the capacitance of the same capacitor in vacuum, to measure the ability of polarization of the material. The response of a medium to static electric fields is described by the low-frequency limit of permittivity, also called the static permittivity  $\varepsilon(0)$ .

$$\varepsilon(0) = \lim_{\omega \rightarrow 0} \varepsilon(\omega) \quad (2.5)$$

At the high-frequency limit, the complex permittivity is commonly referred to as  $\varepsilon(\infty)$ . It is worth pointing out here that for an anisotropic system  $\varepsilon$  is a tensor with different values in different directions.

The static dielectric permittivity in the uniaxial nematic and smectic-A phases have a tensorial property characterized by two principal components; one component being parallel to director  $\mathbf{n}$  ( $\varepsilon_{\parallel}$ ) and the other being perpendicular to the director  $\mathbf{n}$  ( $\varepsilon_{\perp}$ ). The dielectric anisotropy  $\Delta\varepsilon$  in the uniaxial phases is defined as [34]

$$\Delta\varepsilon = \varepsilon_{\parallel} - \varepsilon_{\perp} \quad (2.6)$$

When in a dielectric medium an applied field is reversed or withdrawn the polarization of the medium takes a finite time for reorientation. This phenomenon is known as dielectric relaxation. In an alternating field, this leads to a time lag between the field and the reorientation of the polar molecules. As a result, the dielectric permittivity becomes complex and usually expressed as [35]

$$\varepsilon^*(\omega) = \varepsilon'(\omega) - i\varepsilon''(\omega) \quad (2.7)$$

here  $\varepsilon'$  and  $\varepsilon''$  are real and imaginary part of  $\varepsilon^*$ . As long as the molecular reorientation follows the instantaneous field, the induced polarization is constant and the mode is fully contributing to the dielectric permittivity. This constant quantity is

called low frequency permittivity,  $\varepsilon'(0)$ . At higher frequencies the dipolar reorientations is no longer in phase with the field and the contribution of the mode decreases more and more until it becomes very small. This very small quantity is called high frequency permittivity,  $\varepsilon'(\infty)$ . The difference of these low and high frequency permittivities are defined as dielectric increment or dielectric strength and expressed as

$$\Delta\varepsilon' = \varepsilon'(0) - \varepsilon'(\infty) \quad (2.8)$$

Due to the phase difference between the field (stimulus) and induced polarization (response), a part of the electric energy is dissipated in the form of heat. Thus there is an energy loss ( $\varepsilon''$ ) which is absorbed by the dielectric medium. The energy loss happens to be maximum at a particular frequency, called critical frequency ( $f_c$ ). It is the reciprocal of the characteristic time of the relaxation. There are different dielectric relaxation mechanisms in a dielectric medium, each of which has different origins and are characterized by typical frequency ranges.

#### 2.4.1 DEBYE MODEL

The dielectric permittivity in terms of a single time constant polar substance was described by Debye and is known as Debye model [36]. According to this model, the complex dielectric permittivity can be described as

$$\varepsilon^*(\omega) = \varepsilon'(\omega) - i\varepsilon''(\omega) = \varepsilon'(\infty) + \frac{\varepsilon'(0) - \varepsilon'(\infty)}{1 + i\omega\tau} = \varepsilon'(\infty) + \frac{\Delta\varepsilon'}{1 + i\omega\tau} \quad (2.9)$$

This is known as the Debye equation. Relaxation time  $\tau$  is related to the relaxation frequency ( $f_c$ ) by the relation

$$\tau = \frac{1}{2\pi f_c} \quad (2.10)$$

The real part ( $\varepsilon'$ ) and imaginary part ( $\varepsilon''$ ) of the dielectric permittivity are expressed as

$$\varepsilon'(\omega) = \varepsilon'(\infty) + \frac{\Delta\varepsilon'}{1 + \omega^2\tau^2} \quad (2.11)$$

$$\varepsilon''(\omega) = \frac{\omega\tau\Delta\varepsilon'}{1 + \omega^2\tau^2} \quad (2.12)$$

$\varepsilon''$  reaches its maximum value at critical frequency given by  $\omega_c\tau = 1$ , and the maximum value is

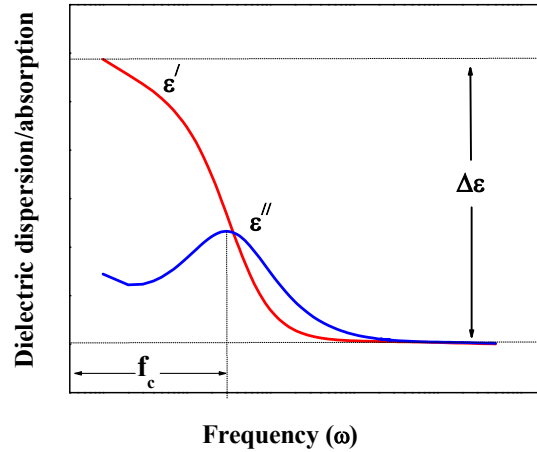
$$\varepsilon''_{max} = \frac{\Delta\varepsilon'}{2} \quad (2.13)$$

So the maximum value of absorption is just half of the dielectric increment.

The frequency dependence (in logarithmic scale) of  $\varepsilon'$  and  $\varepsilon''$  are shown in **Figure 2.9**. The frequency dependence of  $\varepsilon'$  is known as dielectric dispersion and the frequency dependence of  $\varepsilon''$  is known as dielectric absorption [37].

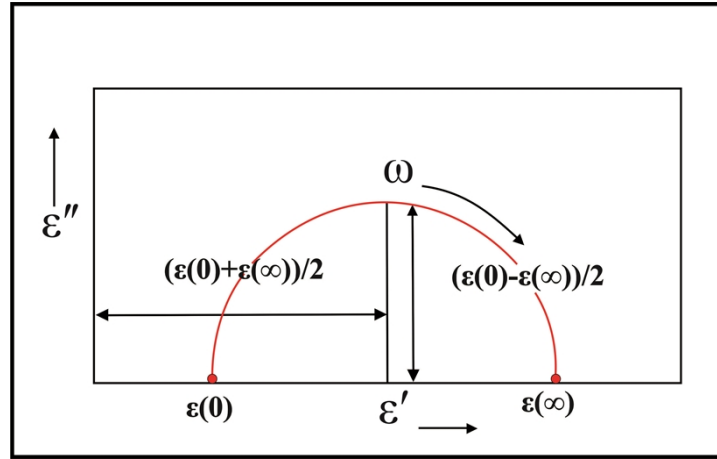
Cole and Cole [38-39] showed that in a material exhibiting Debye relaxation the dielectric spectra can also be represented by plotting  $\varepsilon'$  versus  $\varepsilon''$  in a complex plane and the curve obtained is a semicircle with its center lying on  $\varepsilon'$  axis at  $(\varepsilon'(0) + \varepsilon'(\infty))/2$  with radius  $(\varepsilon'(0) - \varepsilon'(\infty))/2$ . Each point on the semicircle corresponds to the complex dielectric permittivity of the material for a particular frequency (**Figure 2.10**). The Debye equation can be represented as

$$\left(\varepsilon' - \frac{\varepsilon'(0) + \varepsilon'(\infty)}{2}\right)^2 + (\varepsilon'')^2 = \left(\frac{\varepsilon'(0) - \varepsilon'(\infty)}{2}\right)^2 \quad (2.14)$$



**Figure 2.9.** Frequency dependence of  $\varepsilon'(\omega)$  and  $\varepsilon''(\omega)$  for a relaxation process.

This graphical representation of **equation 2.14** is called the Cole-Cole plot. The plot is very useful for checking whether the values of  $\varepsilon'$  and  $\varepsilon''$  are described by a single relaxation time or not, i.e., the plot is showing single semi-circle or multiple semi-circle. Each semi-circle represents a relaxation process.



**Figure 2.10.** Cole-Cole plot of a spectrum showing Debye type relaxation.

### 2.4.2 COLE-COLE MODEL

For liquid and solid rotator phases of organic polar compounds, the dielectric spectrum is Debye type [40-41]. However, in order to describe the dielectric behaviour in some system composed of flexible molecules [41-44] and some disordered solid phases [45-46] which exhibit broad dielectric spectra, Cole and Cole [38] extended the Debye equation by assuming a symmetrical distribution of relaxation times characterized by the symmetry parameter  $\alpha$  as follows.

$$\varepsilon^*(\omega) = \varepsilon'(\omega) - i\varepsilon''(\omega) = \varepsilon(\infty) + \sum_k \frac{\Delta\varepsilon'_k}{1 + (i\omega\tau_k)^{1-\alpha_k}} - i\frac{\sigma}{\omega\epsilon_0} \quad (2.15)$$

symmetry parameter  $\alpha$  varies from 0 to 1, here  $\Delta\varepsilon'_k = \varepsilon'(0) - \varepsilon'(\infty)$  is dielectric increment,  $\tau_k$  is relaxation time, and  $\alpha_k$  is symmetry parameter signifying deviation from Debye type behaviour of  $k$ -th mode relaxation process,  $\tau_k$  is the most probable relaxation time related to critical frequency  $\omega_c$  and  $\epsilon_0 (= 8.85 \text{ pF/m})$  is the permittivity of the free space. We added the conductivity term in the original Cole-Cole equation in order to consider the effect of conductivity of the cell that arises due to charge impurities and contributes mainly to the low frequency region [47]. The real  $\varepsilon'$  and imaginary  $\varepsilon''$  parts can be expressed as

$$\varepsilon'(\omega) = \varepsilon(\infty) + \Delta\varepsilon' \frac{1 + (\omega\tau_k)^{1-\alpha_k} \sin\left(\frac{1}{2}\pi\alpha\right)}{1 + 2(\omega\tau_k)^{1-\alpha_k} \sin\left(\frac{1}{2}\pi\alpha\right) + (\omega\tau_k)^{2(1-\alpha_k)}} \quad (2.16)$$

$$\varepsilon''(\omega) = \Delta\varepsilon' \frac{(\omega\tau_k)^{1-\alpha_k} \cos\left(\frac{1}{2}\pi\alpha\right)}{1 + 2(\omega\tau_k)^{1-\alpha_k} \sin\left(\frac{1}{2}\pi\alpha\right) + (\omega\tau_k)^{2(1-\alpha_k)}} + \frac{\sigma}{\omega\epsilon_0} \quad (2.17)$$

The maximum value of absorption  $\varepsilon''_{max}(\omega_c)$  corresponds to a particular frequency; called critical frequency  $\omega_c (= 2\pi f_c)$  and depends on the parameter  $\alpha$  according to the formula:

$$\varepsilon''(\omega_c) = \varepsilon''_{max} = \frac{\Delta\varepsilon' \cos\left(\frac{1}{2}\pi\alpha\right)}{2 + \sin\left(\frac{1}{2}\pi\alpha\right)} \quad (2.18)$$

For small values of  $\alpha$  ( $\alpha < 0.1$ ) the above expression for maximum absorption reduces to

$$\varepsilon''_{max} = \frac{\Delta\varepsilon'}{2 + \alpha\pi} \quad (2.19)$$

Obviously, for dielectric medium which does not obey the Debye type spectrum, the maximum absorption peak in the Cole-Cole plot is lowered and the broadened.

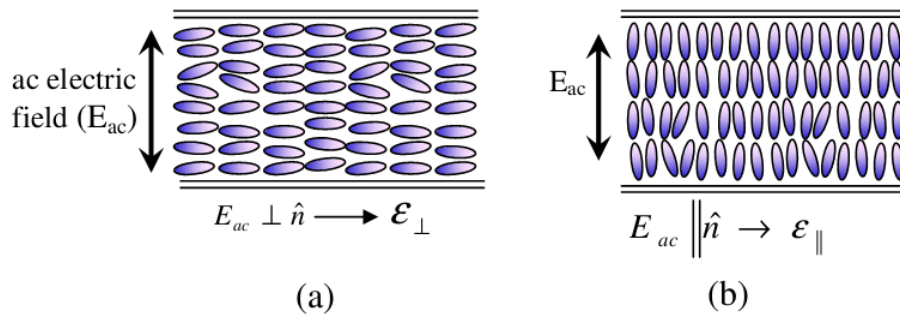
Another general function was proposed by Havriliak and Negami which was an empirical modification of the Debye relaxation model, accounting for the asymmetry and broadness of the dielectric dispersion curve [48-49]. The model was first used to describe the dielectric relaxation of some polymers, some disordered solids and also FLCs and AFLCs [50-52].

### 2.4.3 DIELECTRIC RELAXATIONS IN FERROELECTRIC AND ANTIFERROELECTRIC LIQUID CRYSTALS

Before we discuss the relaxation mechanisms in chiral smectic systems, we want to mention here that the time-dependent measuring electric fields are applied to the molecules of smectic layers in two geometries. If the electric field is applied in a direction parallel to the smectic layers i.e., in a direction perpendicular to the molecular director, then transverse component of the permittivity ( $\varepsilon_{\perp}$ ) is measured and the geometry is known as homogeneous or planar geometry and when the electric field is applied perpendicular to the smectic layers, i.e., in a direction parallel to the

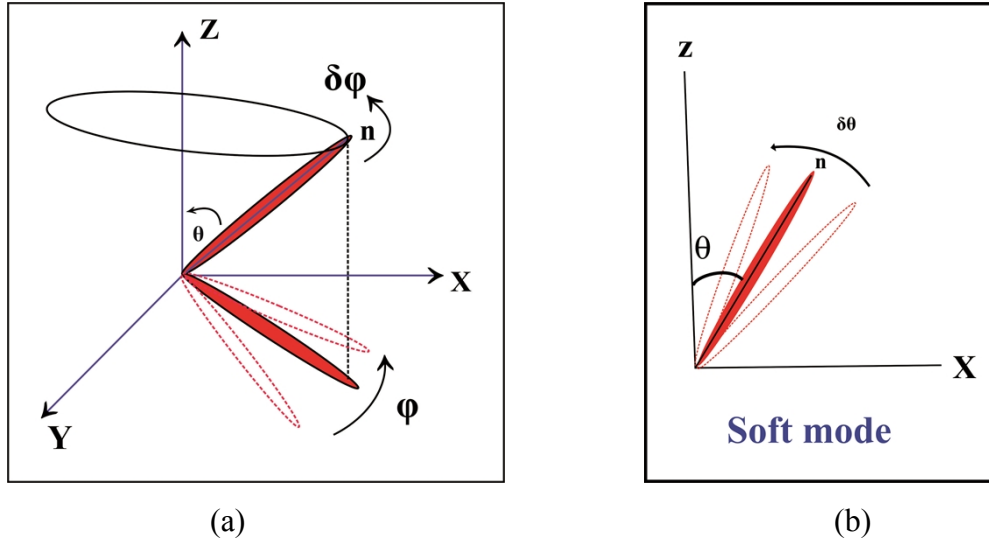
molecular director, then parallel component of the permittivity ( $\epsilon_{\parallel}$ ) is measured and the geometry is known as homeotropic geometry as shown in **Figure 2.11**. By proper surface treatment of the inner surfaces of the ITO coated glass plates, used to construct the dielectric cell, one may get the homogeneous or homeotropic alignment of the molecules. As in the present dissertation, the dielectric measurements are made in a planar geometry, hence by the term ‘dielectric permittivity’ we shall mean the transverse component.

The relaxations of dielectric materials are categorized as (i) non-collective relaxations (single molecular), arise from molecular rotation around the short axis, rotation around long axis, intramolecular rotations around single bond and motions of electrons relative to their nuclei and (ii) collective relaxations, arise from the collective reorientations of molecular directors.



**Figure 2.11.** (a) Homogeneous arrangement of molecules and transverse component of the permittivity ( $\epsilon_{\perp}$ ) (b) homeotropic arrangement of molecules and parallel component of the permittivity ( $\epsilon_{\parallel}$ ).

The dielectric response of ferroelectric system exhibiting SmC\* and SmA\* phase consists of four modes of relaxations two of which are (i) Goldstone mode (GM) and (ii) soft mode, related to the collective director fluctuations, lie in a few tens Hz to a few hundred kHz ranges. The other two modes are non-collective (molecular), related to the fluctuation of polarization and observed in the frequency range of several hundred kHz to a few GHz. It is not usually visible by dielectric spectroscopy when the planar orientation of the molecules exists in the measuring cell. We have investigated the collective relaxations only.



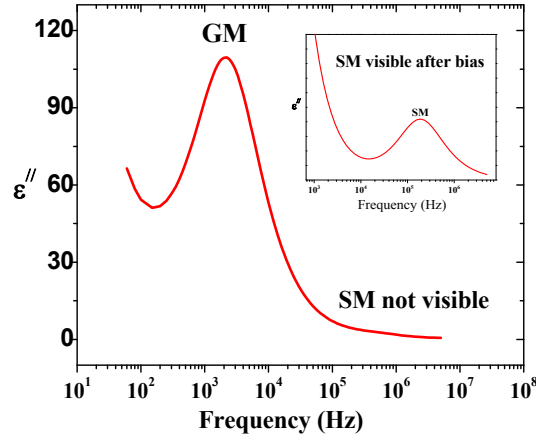
**Figure 2.12.** Schematic representation of director fluctuation in (a) the Goldstone mode relaxation, originates from the phase fluctuation ( $\delta\phi$ ) of the director in chiral SmC\* phase, (b) the soft mode relaxation, arises due to the tilt ( $\delta\theta$ ) fluctuation of the molecular director.

Goldstone mode is observed in SmC\* phase and arises from the phase fluctuation of azimuthal orientation of the director [35, 53-55] and hence also called as a phason mode. Its amplitude is high and hence the dielectric increment is also high and corresponding relaxation frequency is low. The Goldstone mode relaxation frequency and dielectric increment have only weak temperature dependence [35, 56].

The soft mode arises from the tilt fluctuation of the director in SmA\* phase and within SmC\* phase but near the SmA\*-SmC\* transition [35, 55, 57]. This is also called amplitude mode. Although the dielectric increment of soft mode is much lower than the Goldstone mode, the soft mode critical frequency is at least two orders higher than that of GM. In SmC\* phase, the weak SM dielectric spectra are usually masked by the strong Goldstone dielectric spectra hence it creates difficulty to explore the SM unless the GM is suppressed applying DC bias field.

From Landau model the concept of soft mode was first introduced to the SmA\*-SmC\* phase transition by Blinc and Zeks [57] for the case of a modulated structure and later modified by Carlsson *et al.* [56] where phase transition is described in terms of two order parameters – two-component tilt vector as primary order parameter and two-component in-plane polarization as the secondary order parameter. Two characteristic modes are observed in SmA\*-SmC\* second order phase transition

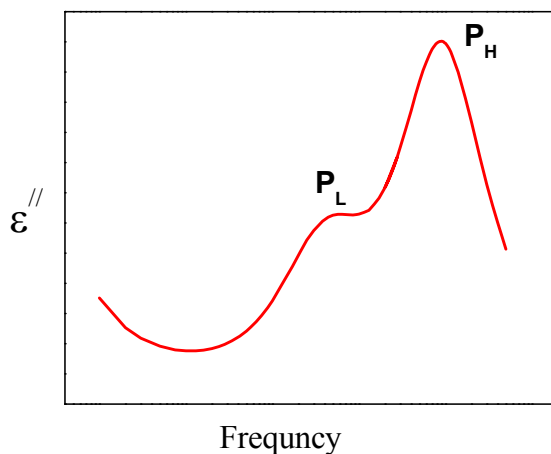
where the continuous symmetry group of SmA\* ( $D_{\infty}$ ) is spontaneously broken in SmC\* ( $C_2$ ). The soft mode is a symmetry breaking mode, which critically slows down (softens) on approaching the phase transition from above, the Goldstone mode is zero frequency mode that tries to restore the broken symmetry. Thus soft mode splits into the phason (GM) and amplitude (SM) modes in SmC\* near the transition.



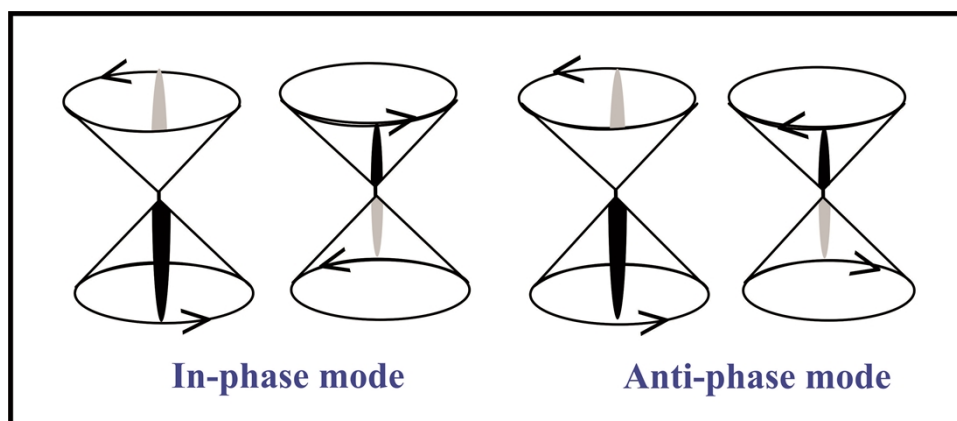
**Figure 2.13.** Goldstone mode and soft mode in a frequency window, the soft mode becomes prominent after the Goldstone mode is suppressed under DC bias (inset).

Under a strong bias field in SmC\* phase a residual mode, with dielectric spectrum different from that of GM, is observed, this mode is known as domain mode (DM) [58-60]. Beresnev *et al.* [61] discovered that ferroelectric liquid crystals with high spontaneous polarization can form solid ferroelectric like domain after suppression of GM; the relaxation mode arising out of such domain is termed as domain mode. Haase *et al.* [62] gave the same argument regarding the arising of the domain mode.

In the antiferroelectric phase two collective relaxation processes are usually observed – one in low frequency region (few hundred Hz to few kHz), called in-phase antiferroelectric ( $P_L$ ) mode and the other, comparatively in higher frequency region (few kHz to few hundred kHz ranges), is called anti-phase antiferroelectric ( $P_H$ ) mode [63-68]. Typical absorption spectra are shown in **Fig. 2.14**.



**Figure 2.14.** The absorption spectrum in  $\text{SmC}_A^*$  phase showing  $P_L$  and  $P_H$  mode.



**Figure 2.15.** Schematic representation of molecular rotations in successive layers in the in-phase  $P_L$  and the anti-phase  $P_H$  mode [69].

Diverse reports on range and temperature dependence of critical frequencies of both the modes are found in literature. J. Hou *et al.* [63] first reported that the modes  $P_L$  and  $P_H$  might arise due to in-phase and anti-phase fluctuation of molecules in the adjacent smectic layers (**Fig. 2.15**). Although there is ambiguity regarding the origin of the two modes, a strong correlation of bias dependence of absorption strengths of  $P_L$  and  $P_H$  modes indicates that their origin should be correlated.

#### 2.4.4 DIELECTRIC MEASUREMENT TECHNIQUE

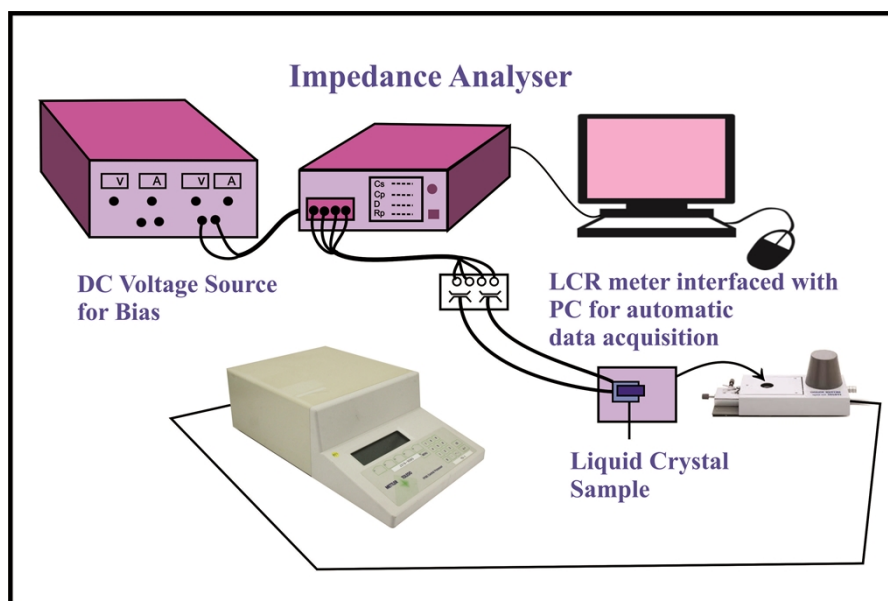
The dielectric behavior of liquid crystalline material is studied by measuring the complex dielectric permittivity at constant temperature and ambient pressure within a frequency domain and is commonly known as frequency domain dielectric spectroscopy (FDDS). The FDDS may be performed at varying temperatures during heating as well as cooling. The peaks in the absorption spectrum represent a dielectric relaxation. Examining the range of critical frequencies, absorption peak heights, and its behavior under bias one may decide about the relaxation mode and may decide about the phase in which it is arising. To find the dielectric increment, relaxation frequency and symmetry parameter of a particular mode, dielectric absorption spectra were fitted by non-linear least squares method to **equations 2.16** and **2.17**. In most cases, we had to fit two relaxation processes.

In the present work dielectric studies were performed using Indium-Tin oxide (ITO) coated homogeneously (HG) aligned EHC cells of thickness 10  $\mu\text{m}$  (5  $\mu\text{m}$  was used to study the nanocomposite). The sheet resistance of the ITO coated glass was low (20  $\Omega$  per sheet is used). This is because, at high frequencies, the effect of ITO resistance is seen as an increase in dielectric absorption and a decrease in dielectric permittivity, which mimics a relaxation process in the dielectric spectrum. The overlapping active area of the cell is 1.0  $\text{cm}^2$ . Dielectric measurements were made using HIOKI 3532-50 impedance analyzer (40 Hz – 5 MHz), cell temperature was controlled within  $\pm 0.1^\circ\text{C}$  placing the cell inside the Mettler FP82 hot stage. An automatic data acquisition arrangement was made using RS 232 interface with a PC. The experimental set up is shown in **Figure 2.16**.

The real and imaginary parts of the dielectric permittivity at a frequency were obtained as follows

$$\varepsilon'(\omega) = \frac{C}{C_o} \text{ and } \varepsilon''(\omega) = \varepsilon'(\omega) \tan\delta \quad (2.20)$$

where  $C$  is the capacitance of the cell filled with LC and  $C_o$  is that of the empty cell and  $\tan\delta$  is the dielectric loss. The effect of stray capacitances was eliminated by standard process.



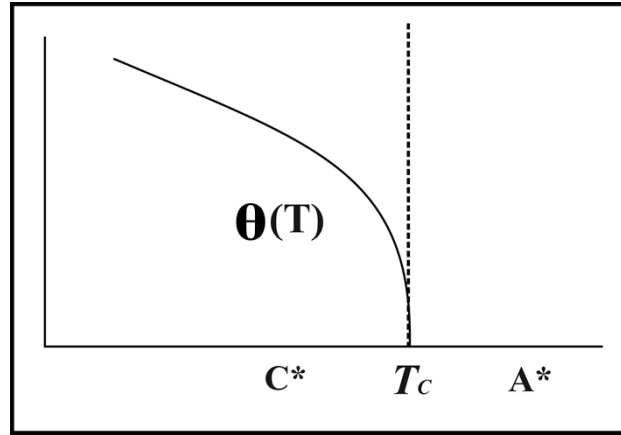
**Figure 2.16.** Experimental set up for dielectric spectroscopy.

There are two main sources of symmetric errors in the quantitative evaluation of the dielectric permittivity. One source is in the high frequency region due to the resistance of the ITO conducting layer. The ITO resistances were kept below  $20\Omega$  in order to reduce the high frequency effect. Moreover, our dielectric measurements are within the frequency window of 5MHz, hence there is a little possibility of arising error due to high frequency effect. The other source of error is in the low frequency region due to the freely moving ions and contribution from the dipolar reorientation. The measured data were fitted to suitable functions and the correct results were extracted. The accuracy in the measurement of capacitance (C) and  $\tan\delta$  (G) in the frequency range is  $<0.2\%$  and hence maximum uncertainty in the measurement of dielectric permittivity ( $\epsilon'$ ) and dielectric loss ( $\epsilon''$ ) within entire frequency regime is less than  $\pm 1\%$ .

## 2.5 MEASUREMENTS OF ELECTRO-OPTIC PARAMETERS – TILT ANGLE ( $\theta$ ), SPONTANEOUS POLARIZATION ( $P_s$ ), THE SWITCHING TIME ( $\tau$ ) AND ROTATIONAL VISCOSITY ( $\gamma_\phi$ )

The spontaneous polarization in SmC\* phase would feel a torque ( $\mathbf{P} \times \mathbf{E}$ ) in an electric field and it is a linear effect, although the other liquid crystals show an electrooptic effect with a response quadratic in the field, i.e. not sensitive to the sign

of E. The linear effect was verified by R. B. Meyer [70]. The transition from SmA\*-SmC\* is typically 2nd order, which implies that the tilt angle  $\theta$  increases with temperature as  $\theta \sim (T_c - T)^{1/2}$  [71], where  $T_c$  is transition temperature and  $T$  is any temperature below  $T_c$  (**Figure 2.17**). As the  $P_s$  ought to be essentially proportional to the tilt, it could be expected to increase in the same way, which was also proved in subsequent measurements.



**Figure 2.17.** The molecular tilt  $\theta$  as a function of temperature near the SmA\*-SmC\* transition [71].

By applying an electric field ( $E$ ) across a thin transparent cell one can induce a rotation of the molecular axis in the plane of the cell. On reversing the field the molecules rotate by twice the conic angle  $\theta$  ( $2\theta$ ). This molecular motion is called electrooptic switching which occurs in a viscous medium with a characteristic time  $\tau$ ,

$$\tau = \frac{\gamma_\phi}{P_s E} \quad (2.21)$$

here  $\gamma_\phi$  is rotational viscosity,  $P_s$  is spontaneous polarization [72]. With a moderate value of  $P_s$ , the low-viscous compounds will help to achieve sub-microsecond switching.

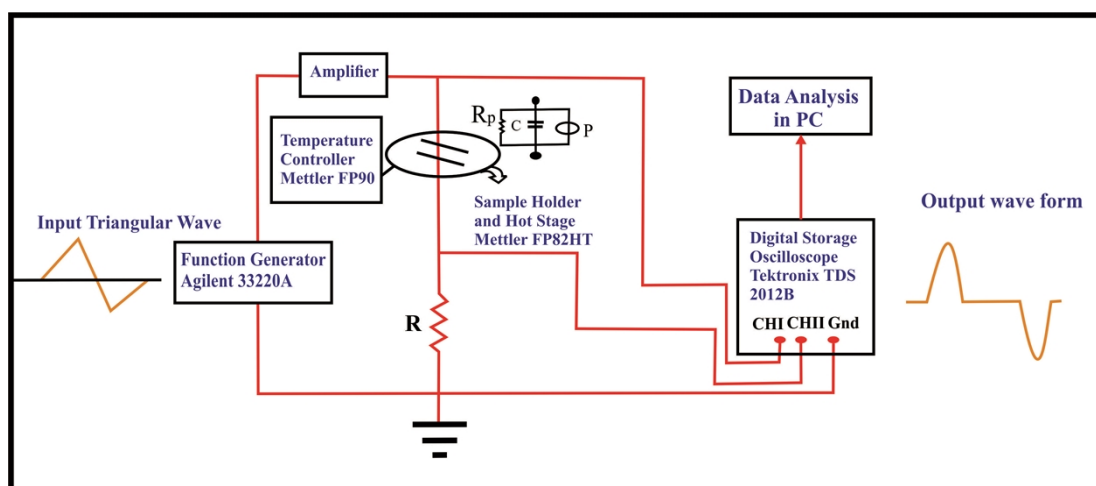
### 2.5.1 TILT ANGLE ( $\theta$ )

The molecular tilt angle  $\theta$ , the angle made by the molecular long axis with the layer normal, is considered as the primary order parameter of ferroelectric and antiferroelectric liquid crystals. To measure the molecular tilt ( $\theta$ ), a pulse electro-optical technique was proposed by Baikalov *et al.* [73] based on the linear electro-optical effect. In an ac field, the chiral molecules switch around an imaginary cone

through twice the tilt angle  $\theta$  ( $2\theta$ ) thereby reversing the sign of spontaneous polarization. The ferroelectric or antiferroelectric sample is taken in a capacitive cell in planar arrangement (same cell as in dielectric measurements). The cell is taken on the turntable of the polarizing microscope with crossed polarizers and polarized light is passed normally through glass plates of the cell. An electric field of sufficiently high magnitude is applied so that the helix is unwound and the molecules are aligned uniformly with a tilt  $\theta$  away from the layer normal. The sample cell is rotated to get the minimum optical transmission. Then the field is reversed and the sample cell is rotated in the opposite direction to achieve again the minimum transmission. The difference in angular readings on the microscope turntable for two nearby transmission minima gives twice the tilt angle ( $2\theta$ ) [73-74]. In our experiments about 20V (Vpp) square wave pulses of low frequency (about 50 mHz) were used. Estimated error in the tilt measurement was  $0.2^\circ$ .

### 2.5.2 SPONTANEOUS POLARIZATION ( $P_s$ )

Chiral smectic liquid crystals in surface stabilized geometry possess permanent dipoles normal to their molecular axis which gives rise to existence of polarization even in absence of an external field and is called spontaneous polarization ( $P_s$ ).  $P_s$  is the result of tilt ( $\theta$ ) of the molecules, and is essentially proportional to the  $\theta$ , and is considered as secondary order parameter.



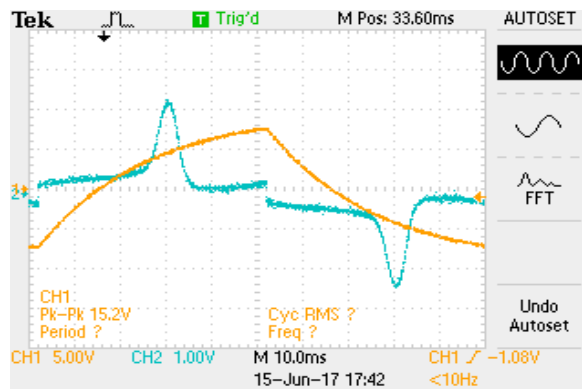
**Figure 2.18.** Block diagram of the experimental set up for the measurement for electro-optic parameters ( $P_s$ ,  $\tau$ ,  $\theta$ , etc.).

There are several methods to measure the  $P_s$  of ferroelectric materials. But a comparison of  $P_s$  values of DOBAMBC at a particular temperature shows a scattering over one decade and one of the main reason of which, according to K. Miyasto *et al.* [75], is the use of different methods.

The standard Sawyer-Tower method [76] for the determination of  $P_s$  of solid ferroelectric samples was used by several groups for the determination of  $P_s$  of ferroelectric liquid crystal [77-79]. The electric field dependent dielectric constant method has also been employed [80]. The other method is based on the measurement of current induced by rapidly reversing square wave field [81-82] in which the main problem was to separate the polarization bump from the baseline of the total current. The most useful technique was introduced by K. Miyasato *et al.* [75] utilizing triangular wave, in which the polarization bump can easily be separated from the base line of total current. Assuming the filled LC cell is equivalent to a parallel RC combination, the current induced in the cell due to passing of a triangular wave are composed of three components, namely, the capacitive term  $i_c = C(dV/dt)$ , the resistive term  $i_R = V/R$ , ( $R$ , the effective resistance of the cell), and the polarization current  $i_p = dP/dt$ .

$$I = i_c + i_R + i_p = C \frac{dV}{dt} + \frac{V}{R} + \frac{dP}{dt} \quad (2.22)$$

The first two terms exist at all the voltages but  $i_p$  appears as hump only when the applied voltage is high enough to unwind the helix and leads to the polarization reversal in the sample.



**Figure 2.19.** The voltage waveform across resistor  $R$ , obtained from oscilloscope Tektronics TDS 2012 B in response to the triangular wave.

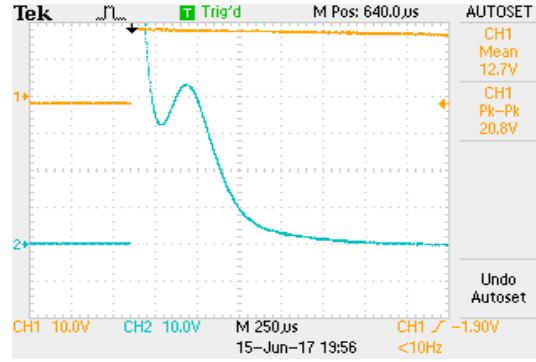
The voltage drop across a resistance  $R$ , connected in series with cell, is stored in a digital oscilloscope (**Fig. 2.19**).  $R$  is usually chosen less than the cell resistance  $R_p$  so that the time constant for the exponential decay is considerably shorter than the polarization reversal [83]. Subtracting the ionic and capacitive current, by drawing an appropriate baseline, from the overall voltage profile, the area under the polarization peak is found out which is  $\int V(t)dt$ . The  $P_s$  is calculated from the following formula.

$$P_s = \frac{1}{2AR} \int V(t)dt \quad (2.23)$$

here  $A$  is the effective area of the cell. In our experiments, we recorded the voltage waveform across  $R$  using a digital storage oscilloscope (Tektronix 2012B). A triangular wave pulse of frequency 10 Hz and varying amplitude from Agilent 33220A LXI function generator was amplified 20 times (F20 Amplifier, FLC, Sweden) and applied across the combination of a standard resistor ( $R = 100 \text{ k}\Omega$ ) and the cell containing the sample. The voltage wave across  $R$  and the input voltage wave at a fixed temperature were recorded using a digital storage oscilloscope Tektronix 2012 B in separate channels. The area of the polarization hump was calculated after using an appropriate baseline in Origin 8.5 software. The process of estimation of  $P_s$  was done at regular temperature intervals both during heating as well as cooling cycle. Estimated error in  $P_s$  measurement is less than 1%.

### 2.5.3 SWITCHING TIME ( $\tau$ )

The response of a ferroelectric material to a triangular wave is discussed above. The response of the same material to the square wave is shown in **Figure 2.20**. The response of the ions to the field is instantaneous and the current wave (or voltage wave) due to ions follows the applied field instantaneously. But the response of the ferroelectric polarizations are not instantaneous to the applied field thus the peak due to their reversal occurs over the exponential decay curve of the current wave (or voltage wave) away on the time scale from the square-pulse edge. This delay in time corresponds to the response time of switching between the stable states of polarization and represents the time in which the average number of molecules reorients after applying the pulse [83]. Incidentally, this representation of response time from the current signal coincides with the electro-optical transmission from 10% to 90% [84]. Estimated error in the measurement of response time is less than 4%.



**Figure 2.20.** The voltage waveform of the response of the ferroelectric liquid crystal to the square pulse wave.

### 2.5.4 ROTATIONAL VISCOSITY ( $\gamma_\varphi$ )

Rotational viscosity ( $\gamma_\varphi$ ) is the viscosity associated with the rotation of the molecules about the smectic-C cone and it strongly influences the switching of the molecules between two field-induced states. Measuring  $P_s$  and  $\tau$ , the value of  $\gamma_\varphi$  was calculated using the relation [72]

$$\gamma_\varphi = \tau_s \cdot P \cdot E \quad (2.24)$$

where  $E$  is the applied electric field.

### DETERMINATION ACTIVATION ENERGY ( $E_a$ )

If we consider the reorientation of director of molecules of a ferroelectric or antiferroelectric material is a thermally activated process of Arrhenius type [72, 85] then the viscosity can be represented as

$$\gamma_\varphi = \gamma_0 e^{\frac{E_a}{k_\beta T}} \quad (2.25)$$

where  $k_\beta$  is Boltzmann constant,  $\gamma_0$  is pre-exponential term and  $E_a$  is the activation energy which according to Arrhenius, the energy for any thermally activated process to start. The above equation signifies that the viscosity will decrease with increasing temperature. Taking the logarithm of both sides,

$$\ln \gamma_\varphi = \left( \frac{E_a}{k_\beta} \right) \frac{1}{T} + \ln \gamma_0 \quad (2.26)$$

Thus from a plot  $\ln \gamma_\varphi$  against  $(1/T)$ , the activation energy can be determined.

## 2.6 REFERENCES

- [1] I. Dierking, Textures of liquid crystals WILEY-VCH, GmbH & Co. KGaA p-16 (2003).
- [2] A. Wiegeleben, and D. Demus, Calorimetric Investigations in Liquid Crystalline Terephthalylidene-bis- [ 4-n-alkylanilines], Crystal Res. & Technol. 17(1982) 161-165.
- [3] C. R. Safinya, M. Kaplan, J. Als-Nielsen, R. J. Birgeneau, D. Davidov, J. D. Litster, D.L. Johnson, and M.E. Neubert, High-resolution x-ray study of a smectic-A-smectic-C phase transition, Phys. Rev. B. 21(9) (1980) 4149-4153.
- [4] P. S. Clegg, X-ray studies of the phases and phase transitions of liquid crystals, Acta Cryst. A61 (2005)112-121.
- [5] S. Wrobel, Dielectric Relaxation Spectroscopy, in W. Haase, S. Wrobel (Ed.), Relaxation phenomena – Liquid crystals, magnetic systems, polymers, high- $T_C$  superconductors, metallic glasses, Springer-Verlag, Berlin-Heidelberg, 2003, pp. 13.
- [6] G. Vertogen, and W. H. de Jeu (Eds.), Thermotropic Liquid Crystals Fundamentals, Springer-Verlag, (1988), p-207.
- [7] G. R. Luckhurst in Liquid Crystals & Plastic Crystals (G. W. Gray and P. A. Winsor, Eds.), Ellis Horwood Limited, 1974, Vol 2, p-144.
- [8] C. L. Khetrapal and A. C. Kunwar in Advances in Liquid Crystals, Vol. 1-6, Ed. G. H. Brown, pp-173, Academic Press (1983).
- [9] W. J. Borer, S. S. Mitra, and C. W. Brown, Crystal to Liquid-Crystal Transition Studied by Raman Scattering, Phys Rev. Lett. 27(7) (1971) 379-380.
- [10] V. D. Neff in Liquid Crystals & Plastic Crystals (Ed. G. W. Gray and P. A. Winsor), Ellis Horwood Limited, Vol 2, p-231 (1974).
- [11] S. J. Gupta, R. A. Gharde and A. R. Tripathi, Phase Transition Temperatures of LCs using Fabry-Perot Etalon, Mol. Cryst. Liq. Cryst. 364 (2001) 461- 468.

- [12] D. Demus, Textures of liquid crystals, Verlag Chemie Weinheim, New York (1978).
- [13] Bouligand in Handbook of Liquid Crystals. Vol. 1 (Fundamentals), Ed. D. Demus, J. Goodby, G. W. Gray, H.-W. Spiess and V. Vill, WILEY-VCH, Verlag GmbH, Weinheim, FRG (1998), Defects and textures.
- [14] A. J. Slaney, K. Takatohi and J. W. Goodby in The Optics of Thermotropic Liquid Crystals, Ed. S. Elston and R. Sambles, Taylor & Francis (1998), Defect textures in liquid crystals.
- [15] G.W.H. Hohne, W. Hemminger, H. J. Flammersheim, Differential Scanning Calorimetry, An Introduction for Practitioners, Springer (1994).
- [16] D. Mazotko and D. Demus, Advances in Liquid Crystals, Pramana Suppl. 1 (1976) 189.
- [17] A. Wiegeleben and D. Demus, Calorimetric Investigations in Liquid Crystalline Terephthalylidene-bis- [ 4-n-alkylanilines], Crystal Res. & Technol. 17 (1982) 161-165 (TBAA).
- [18] B. K. Vainstein, Diffraction of X-rays by Chain Molecules, Elsevier, Amsterdam (1966).
- [19] H. Kelkar and R. Hatz, Handbook of Liquid Crystals, Verlag Chemie, Ch.5 (1980).
- [20] P. S. Pershan, Structure of Liquid Crystalline Phases, World Scientific, Singapore (1988).
- [21] G. Ungar in Physical properties of liquid crystals, D. A. Dunmur, A. Fukuda and G. R. Luckhurst (Eds.), INSPEC, London, Ch. 4.1 (2001).
- [22] B. Jha, S. Paul, R. Paul and P. Mandal, Order parameters of some homologue cybotactic nematics from X-ray diffraction measurements, Phase Transit. 15 (1989) 39-48.
- [23] S. Diele, P. Brand and H. Sackmann, X-ray Diffraction and Polymorphism of Smectic Liquid Crystals 1. A-, B- and C-modifications, Mol. Cryst. Liq. Cryst. 16 (1972) 105-116.

- [24] A. de Vries, X-Ray Studies of Liquid Crystals: V, Classification of Thermotropic Liquid Crystals and Discussion of Intermolecular Distances, *Pramana Suppl.* No.1 (1975) 93.
- [25] A. de Vries, A. Ekachai and N. Spielberg, X-Ray Studies of Liquid Crystals VI The Structure of the Smectic A, C, Bn and Bt Phases of Trans-1, 4-Cyclohexane-DI-N-Octyloxybenzoate. *J. de Phys. Collques.* 40(C3) (1979) C3-147-C3-152.
- [26] A. J. Lead better, J. Prost, J. P. Gaughan and M. A. Mazid, The structure of the crystal, SmE and SmB forms of IBPBAC. *J. de Phys. Colloques.* 40 (1979) C3-185 – C3-193.
- [27] A. J. Leadbetter and P. G. Wrighton, Order parameters in  $S_A$ ,  $S_C$  and N phases by X-ray diffraction, *J. de Phys.* 40 (1979) C3-234 – C3-242.
- [28] V. M. Sethna, A. de Vries and N. Spielberg, X-Ray Studies of Liquid Crystals VIII: A Study of the Temperature Dependence of the Directly Observed Parameters of the Skewed Cybotactic Nematic Phase of Some Bis-(4'-n-Alkoxybenzal) -2-Chloro-1,4-Phenylenediamines, *Mol. Cryst. Liq. Cryst.* 62 (1980)141-153.
- [29] L. V. Azaroff and C. A. Schuman, X-Ray Diffraction by Cybotactic Nematics, *Mol. Cryst. Liq. Cryst.* 122 (1985) 309-319.
- [30] A. de Vries, The Use of X-Ray Diffraction in the Study of Thermotropic Liquid Crystals with Rod-Like Molecules, *Mol. Cryst. Liq. Cryst.* 131(1985) 125-145.
- [31] P. Mandal, M. Mitra, S. Paul and R. Paul, X-Ray Diffraction and Optical Studies of an Oriented Schiff's Base Liquid Crystal, *Liq. Cryst.* 2 (1987) 183-193.
- [32] A. de Vries, X-ray Photographic Studies of Liquid Crystals I. A Cybotactic Nematic Phase, *Mol. Cryst. Liq. Cryst.* 10(1970) 219-236
- [33] H. F. Gleeson and L. S. Hirst, Resonant X-ray Scattering: A Tool for Structure Elucidation in Liquid Crystals, *Chem. Phys. Chem.* 7 (2006) 321 – 328.

- [34] F. M. Gouda, Dielectric relaxation spectroscopy of chiral smectic liquid crystals, Ph. D. thesis, Department of Physics, Chalmers University of Technology, Goteborg, Sweden (1992).
- [35] F. Gouda, K. Skarp, and S.T. Lagerwall, Dielectric studies of the soft mode and goldstone mode in ferroelectric liquid crystals, *Ferroelectrics*. 113 (1991) 165-206.
- [36] P. Debye, *Polar Molecules*. Dover publications, New York, USA (1929).
- [37] S. Halder, Investigation on some achiral and chiral mesogenic systems by different experimental techniques. Ph. D. Thesis (2013), University of North Bengal, Siliguri, India.
- [38] K. S. Cole and R. H. Cole, Dispersion and Absorption in Dielectrics I. Alternating Current Characteristics, *J. Chem. Phys.* 9 (1941) 341.
- [39] K. S. Cole and R. H. Cole, Dispersion and Absorption in Dielectrics II. Direct Current Characteristics, *J. Chem. Phys.* 10 (1942) 98.
- [40] C. J. F. Bottcher, and P. Bordewijk, Ed., *Theory of Electric Polarization*, Vol II. Dielectric in time-dependent fields, Elsevier, Scientific Publishing Co. (1973).
- [41] N. Hill, W. E. Vaughan, A. H. Price, and M. Davies, *Dielectric Properties and Molecular Behavior*, Van Nostrand, London (1969).
- [42] W. Haase, H. Pranoto, F. J. Bormnuth, B. Bunsenges, Dielectric Properties of Some Side Chain Liquid Crystalline Polymers, *Phys. Chem.*, 89 (1985) 1229-1234.
- [43] C. P. Smyth, *Dielectric Behavior and Structure*, pp. 441. McGraw-Hill, N.Y. (1955).
- [44] V. I. Minkin, O. A. Osipov, and Y. A. Zhdanov, W.E. Vaughan, Dipole Moments and the Electronic Structure of Organic Compounds. In: Vaughan W.E.(eds) *Dipole Moments in Organic Chemistry*, Springer Link, New York-London (1970).
- [45] A. K. Jonscher, *Dielectric Relaxation in Solids*, Chelsea Dielectric Press, London (1983).

- [46] S. Wrobel, B. T. Gowda, and W. Haase, Dielectric study of phase transitions in 3-nitro-4-chloro-aniline, *J. Chem. Phys* 106 (10) (1997) 5904-5409.
- [47] W. Haase, S. Wrobel (Ed.), *Relaxation phenomena – Liquid crystals, magnetic systems, polymers, high- $T_C$  superconductors, metallic glasses*, Springer-Verlag, Berlin-Heidelberg, 2003, pp. 20.
- [48] S. Havriliak, and A. Negami, Complex plane analysis of  $\alpha$ -dispersions in some polymer systems, *S. J. Polimer Sci. C* 14 (1966) 99-117.
- [49] S. Havriliak, and A. Negami, complex plane representation of dielectric and mechanical relaxation processes in some polymers, *S. J. Polimer Sci.* 8 (1967) 161-210.
- [50] D. Ganzke, S. Wrobel, and W. Haase, Dielectric studies of bicyclohexylcarbonitrile nematogens with large negative dielectric anisotropy, *Mol. Cryst. Liq. Cryst.* 409 (2004) 323-333.
- [51] H. Uehara, Y. Hanakai, J. Hatano, S. Saito, and K. Murashiro, Dielectric Relaxation Modes in the Phases of Antiferroelectric Liquid Crystals, *Jpn. J. Appl. Phys.* 34 (1995) 5424-5428.
- [52] A. Fafara, B. Gestblom, S. Wrobel, R. Dabrowski, W. Drzewinski, D. Kilian, and W. Haase, Dielectric spectroscopy and electrooptic studies of new MHPOBC analogues, *Ferroelectrics* 212 (1998) 79-90.
- [53] A. M. Biradar, S. Wrobel and W. Haase, Dielectric relaxation in the smectic- $A^*$  and smectic- $C^*$  phases of a ferroelectric liquid crystal, *Phys. Rev. A* 39 (1989) 2693-2702.
- [54] J. K. Ahuja, and K. K. Raina, Polarization Switching and Dielectric Relaxations in Ferroelectric Liquid Crystals, *Jpn. J. Appl. Phys.* 39 (2000) 4076-4081.
- [55] Y. P. Panarin, O. Kalinovskaya, J. K. Vij, and J. W. Goodby, Observation and investigation of the ferrielectric subphase with high  $q_T$  parameter, *Phys. Rev.E* 55 (1997) 4345-4353.
- [56] T. Carlsson, B. Zeks, C. Filipic and A. Levstik, Theoretical model of the frequency and temperature dependence of the complex dielectric constant of

- ferroelectric liquid crystals near the smectic-C\*- smectic- A\* phase transition, *Phys. Rev.A.* 42 (1990) 877-889.
- [57] R. Blinc and B. Zeks, Dynamics of helicoidal ferroelectric smectic-C\* liquid crystals, *Phys. Rev. A.* 18 (1978) 740-745.
- [58] J. M. Czerwiec, R. Dabrowski, K. Garbat, M. Marzec, M. Tykarska, A. Wawrzyniak, S. Wrobel, Dielectric and electro-optic behaviour of two chiral compounds and their antiferroelectric mixtures, *Liq. Cryst.* 39(12) (2012) 1503-1511.
- [59] M. Marzec, W. Haase, E. Jacob, M. Pfeiffer, S. Wrobel, The existence of four dielectric modes in the planar oriented  $S^*_c$  phase of a fluorinated substance, *Liq. Cryst.* 14 (2) (1993) 1967-1976.
- [60] S. Wrobel, G. Cohen, D. Davidov, W. Hasse, M. Marzec, M. Pfeiffer, Dielectric, electro optic and X-ray studies of a room temperature ferroelectric mixture, *Ferroelectrics.* 166 (1995) 211-222.
- [61] L. A. Beresnev, M. V. Loseva, N. I. Chernova, S. G. Kononov, P. V. Adomenas, E. P. Pozhidayev, *Pis'ma Zh. Eksp. Teor. Fiz.* 51 (1990) 457.
- [62] W. Haase, S. Hiller, M. Pfeiffer, L. A. Beresnev, The domain mode in ferroelectric liquid crystals; electrooptical and dielectric investigations, *Ferroelectrics.* 140 (1993) 37-44.
- [63] J. Hou, J. Schacht, F. Giebelmann and P. Zugenmaier, Temperature and bias-field dependences of dielectric behaviour in the antiferroelectric liquid crystal, (R)-MHPOBC, *Liq. Cryst.* 22(4) (1997) 409-417.
- [64] M. Buivydas, F. Gouda, G. Andersson, S.T. Lagerwall, B. Stebler, Collective and non-collective excitations in antiferroelectric and ferroelectric liquid crystals studied by dielectric relaxation spectroscopy and electro-optic measurements, *Liq. Cryst.* 23(5) (1997) 723-739.
- [65] Yu. Panarin, O. Kalinovskaya, and J. K. Vij, The investigation of the relaxation processes in antiferroelectric liquid crystals by broad band dielectric and electro-optic spectroscopy, *Liq. Cryst.* 25 (2) (1998) 241-252.

- [66] Y. P. Panarin, O. Kalinovskaya, J. K. Vij, The relaxation processes in helical antiferroelectric liquid crystals, *Ferroelectrics*. 213 (1998) 101-108.
- [67] P. Perkowski, K. Ogrodnik, W. Piecek, M. Zurowska, Z. Raszewski, R. Dabrowski, L. Jaroszewicz, Influence of the bias field on dielectric properties of the  $\text{SmC}_A^*$  in the vicinity of the  $\text{SmC}^*-\text{SmC}_A^*$  phase transition, *Liq. Cryst.* 38(16) (2011) 1159-1167.
- [68] Yu. Panarin, O. Kalinovskaya, and J. K. Vij, Observation and investigation of the ferroelectric subphases with high  $q_T$  parameter, *Phy. Rev. E*. 55(4) (1997) 4345-4353.
- [69] M. Baral, A. P. Ranjitha and S. Krishna Prasad, Confinement of an antiferroelectric liquid crystal in a polymer nanonetwork: thermal and dielectric behavior, *Bull. Mater. Sci.* 41 (2018) 135 (1-7).
- [70] R. B. Meyer, L. Liebert, L. Strzelecki, P. Keller, Ferroelectric liquid crystals, *Journal de Physique Lettres*, Edp sciences, 1975 36 (3) 69-71.
- [71] S. T. Lagerwall, Ferroelectric and Antiferroelectric Liquid Crystals. *Ferroelectrics*. 301 (2004) 15–45.
- [72] S. T. Lagerwall, B. Otterholm and K. Skarp, Material properties of ferroelectric liquid crystals and their relevance for applications and devices, *Mol. Cryst. Liq. Cryst.* 150 (1987) 503-587.
- [73] V. A. Baikalov, L. A. Beresnev and L. M. Blinov, Measures of the Molecular Tilt Angle and Optical Anisotropy in Ferroelectric Liquid Crystals, *Mol. Cryst. Liq. Cryst.* 127 (1985) 397-406.
- [74] M. Buivydas, P. Adomenas, S. T. Lagerwall and B. Stebler, The Spontaneous Polarisation and Rotational viscosity in Host-dopant Mixtures, *Ferroelectrics*. 166 (1995) 165-174.
- [75] K. Miyasato, S. Abe, H. Takezoe, A. Fukuda and E. Kuze, Direct Method with Triangular Waves for Measuring Spontaneous Polarization in Ferroelectric Liquid Crystals, *Jpn. J. Appl. Phys.* 22 (10) (1983) L661-L663.
- [76] C. B. Sawyer and C. H. Tower, Rochelle salt as a Dielectric, *Phys. Rev.* 35 (1930) 269-273.

- [77] H. Mstsuma, The Ferroelectricity in the Mixtures of Chiral with Non-Chiral Smectic C, *Mol. Cryst. Liq. Cryst.* 49 (1978)105-112.
- [78] B. I. Ostrovski, A. Z. Rabinovich, A. S. Sonin, E. L. Sorking, B. A. Strukov and S.A. Taraskin, Ferroelectric behaviour of different classes of smectic liquid crystal, *Ferroelectrics*. 24 (1980) 309-312.
- [79] M. Imasaki, T Fujimoto, T Nishihara, T. Yoshioka and Y. Narushige, Ferroelectricity in Mixtures of Chiral Smectic C and Smectic A Liquid Crystals, *Jpn. J. Appl. Phys.* 21 (1982) 1100-1100.
- [80] T. Uemoto, K. Yoshino and Y. Inuishi, Ferroelectric Properties of Chiral Smectic Liquid Crystal, *Jpn. J. Appl. Phys.* 18(7) (1979) 1261-1265.
- [81] M. Buivydas, P. Adomenas, S. T. Lagerwall and B. Stebler, The Spontaneous Polarisation and Rotational viscosity in Host-dopant Mixtures, *Ferroelectrics*. 166 (1995) 165-174.
- [82] I. Dahl, S. T. Lagerwall and K. Skarp, Simple model for the polarization reversal current in a ferroelectric liquid crystal. *Phys. Rev. A.* 36(9) (1987) 4380-4390.
- [83] K. Skarp, I. Dahl, S.T. Lagerwall and B. Stebler, Polarisation and viscosity measurements in a ferroelectric liquid crystal by the field reversal method, *Mol. Cryst. Liq. Cryst.* 114 (1984) 283-297.
- [84] S. S. Bawa, A. M. Biradar, K. Saxena and S. Chandra, Direct pulse technique for spontaneous polarization dynamics and molecular reorientation processes in ferroelectric liquid crystals, *Rev. Sci. Inst.* 59 (1988) 2023-2030.
- [85] S.A. Arrhenius, On the reaction rate of the inversion of non-refined sugar upon souring, *Z. Phys. Chem.* 4 (1889) 99-116.

# CHAPTER 3

---

## Effect of lateral fluorination on the properties of four antiferroelectric liquid crystals

3.1	INTRODUCTION	66
3.2	EXPERIMENTAL TECHNIQUES	68
3.3	RESULTS AND DISCUSSIONS	68
3.3.1	POLARIZING OPTICAL MICROSCOPY (POM) AND DSC STUDY	68
3.3.2	OPTIMIZATION OF GEOMETRY	70
3.3.3	X-RAY DIFFRACTION STUDY	71
3.3.4	DIELECTRIC STUDY	76
3.3.4.1	SmC <sub>A</sub> * PHASE	77
3.3.4.2	SmC* AND SmA* PHASE	81
3.3.5	SPONTANEOUS POLARIZATION (P <sub>s</sub> ) MEASUREMENTS	82
3.3.6	OPTICAL TILT ( $\theta_{opt}$ )	84
3.3.7	SWITCHING TIME ( $\tau$ ) AND VISCOSITY ( $\gamma$ )	85
3.4	CONCLUSION	87
3.5	REFERENCES	89

---

Part of the work has been published in Journal of Physics and Chemistry of Solids, Vol.88 (2016), pp. 14-23; AIP Conf. Proc. 1731 (2016) 040015(1-3); Materials Today Proc. 3(2016) 3987-3991.

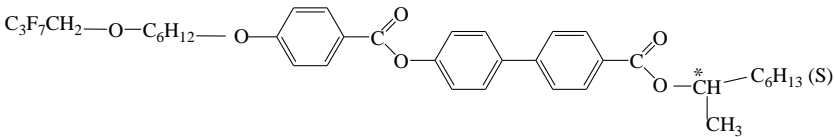
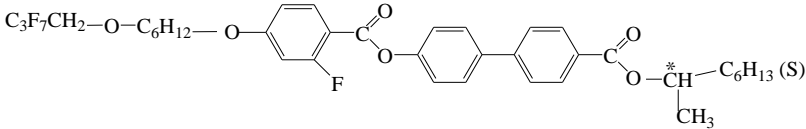
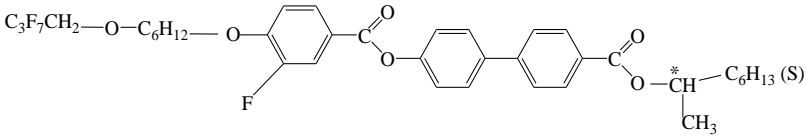
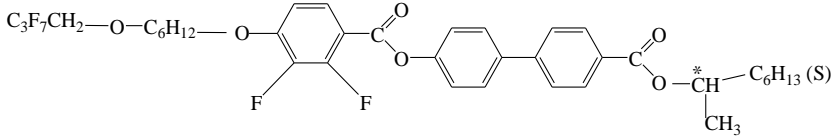


### 3.1 INTRODUCTION

The mesogenic behaviour of a compound is strongly influenced by the structure of the rigid molecular core as well as by the lateral substitutions. Because of the small size of a fluoro-substituent and high strength of the C–F bond, liquid crystals with fluoro-substituent show low birefringence, viscosity and conductivity, high chemical and thermal stability, etc. As a result, many liquid crystal compounds with fluoro-substituents both in the cores and alkoxy chains were designed and synthesized in achiral as well as in chiral systems [2–8]. Liquid crystals with fluorinated chains are also very promising as antiferroelectric materials especially as the thresholdless ones [8–11]. Phase behavior and physical and electro-optical properties of fluorinated derivatives in many aspects are quite different from their protonated analogues which create new possibilities for their applications [10]. A terphenyl based ester compound with CH<sub>3</sub>COO– group at the achiral end exhibits SmC\* and SmA\* phases while the analogous compound with CF<sub>3</sub>COO– group shows SmC<sub>A</sub>\* phase in addition, but stronger polar end group (CNCOO–) shows only SmA\* phase [12]. Induction or enhancement of SmC<sub>A</sub>\* phase due to fluorination has also been reported in reference [13]. Effects of fluorination on the relaxation and switching behaviour of para, ferro and antiferroelectric liquid crystals have been discussed by many authors [10–11, 14–18]. The rigidity of the core structure, nature of chirality and extent of fluorination of the constituent molecules are found to have a pronounced effect on the collective mode relaxation behavior in room temperature FLC mixtures [16]. To study the effect of lateral fluorination in core we have chosen four member of series of a biphenyl benzoate core-based compounds namely (S)-4'-(1-methylheptyloxycarbonyl)biphenyl-4-yl 4-[6-(2,2,3,3,4,4,4-heptafluorobutoxy)hexyl-1-oxy]benzoate, (S)-4'-(1-methylheptyloxy-carbonyl)biphenyl-4-yl4-[6-(2,2,3,3,4,4,4-heptafluorobutoxy) hexyl – 1 - oxy] - 2-fluoro-benzoate, (S)-4'-(1-methylheptyloxycarbonyl)biphenyl-4-yl 4-[6-(2,2,3,3,4,4,4-hepta-fluorobutoxy)hexyl-1-oxy]-3-fluorobenzoate, and (S)-4'-(1-methylheptyloxycarbonyl) biphenyl-4-yl 4- [6-(2,2,3,3,4,4,4-heptafluorobutoxy) hexyl-1-oxy]-2,3-difluorobenzoate (in short **DM0**, **DM1**, **DM2** and **DM3** respectively). These compounds were synthesized by Zurowska *et al.* [18]. Molecular structures of the compounds are shown in **Table 3.1** for ease of discussion. The molecules of the series differ by the number and position of lateral fluorine substitution in the core. All the compounds have a partially

fluorinated achiral chain and an asymmetric C\* atom in methyl heptyl moiety rendering chirality while the carbonyl (–C=O) functional group provides a transverse permanent electric dipole moment. The first compound DM0 is a protonated compound but in DM1 one fluorine atom is introduced at ortho position of the benzoate core, while it is introduced at position meta but in DM3 fluorine atoms are introduced both at ortho and meta positions of the benzoate core structure. All the four compounds exhibit paraelectric, ferroelectric and antiferroelectric phases but in different temperature ranges.

**Table 3.1.** Molecular structures and transition temperatures (°C) of the compounds

Name	Molecular structures and transition temperatures
<b>DM0</b>	 <p>Cr 61.0 SmC<sub>A</sub>* 94.0 SmC* 123.0 SmA* 125.0 Iso (heating) Cr 26 SmC<sub>A</sub>* 83 SmC* 122.2 SmA* 124.4 Iso (cooling)</p>
<b>DM1</b>	 <p>Cr 41.0 SmC<sub>A</sub>* 75.2 SmC* 103.0 SmA* 103.6 Iso (heating) Cr 20 SmC<sub>A</sub>* 65 SmC* 103 SmA* 103.6 Iso (cooling)</p>
<b>DM2</b>	 <p>Cr 57.3 SmC<sub>A</sub>* 80.5 SmC* 108.0 SmA* 112.2 Iso (Heating) Cr 29.3 SmC<sub>A</sub>* 79.2 SmC* 108.2 SmC<sub>A</sub>* 112.2 Iso (cooling)</p>
<b>DM3</b>	 <p>Cr 63.2 SmC<sub>A</sub>* 85.2 SmC* 109.3 SmA* 111.6 Iso (heating) Cr 32.5 SmC<sub>A</sub>* 82.2 SmC* 109.1 SmA* 111.5 Iso (cooling)</p>

## 3.2 EXPERIMENTAL TECHNIQUES

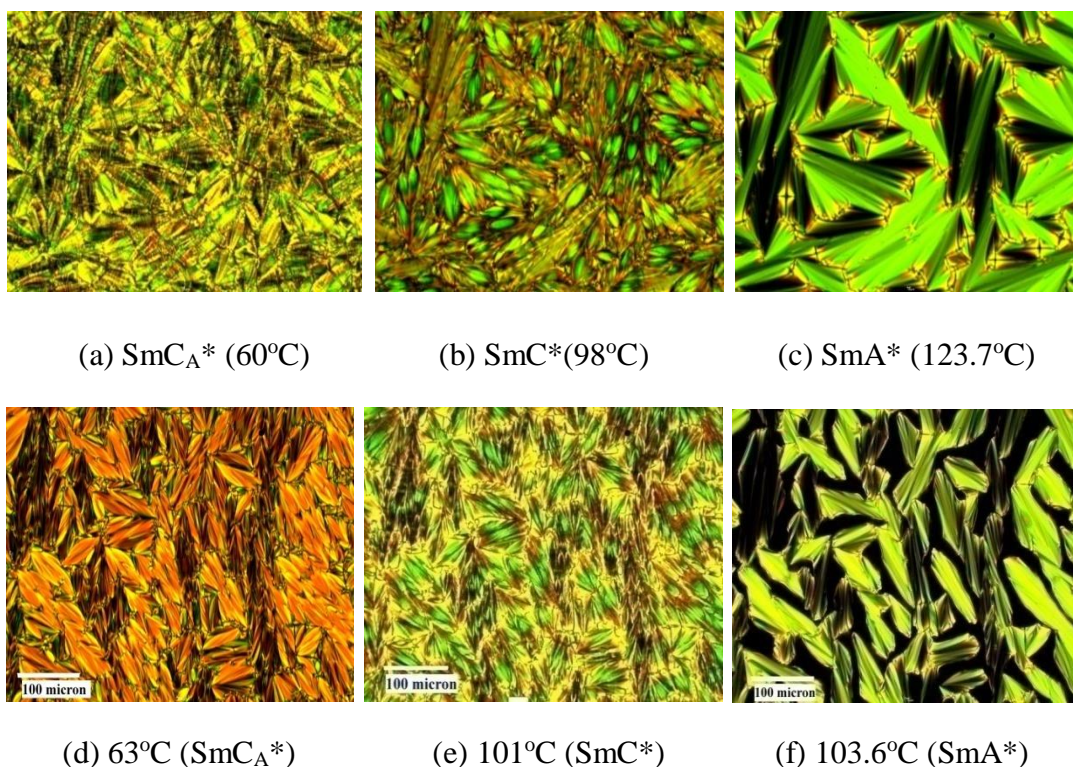
Phase behaviour and transition temperatures of the compounds were investigated by polarizing optical microscopy (POM) and differential calorimetric study (DSC). Mesophase structures were investigated using synchrotron radiation facility at Deutsches Elektronen Synchrotron, Hamburg, Germany. Dielectric and electro-optical studies were performed using Indium–Tin–Oxide (ITO) coated homogeneous (HG) cells of 10  $\mu\text{m}$  thickness. Procedure of preparation of the cells and experimental procedures have been described detail in Chapter 2.

## 3.3 RESULTS AND DISCUSSIONS

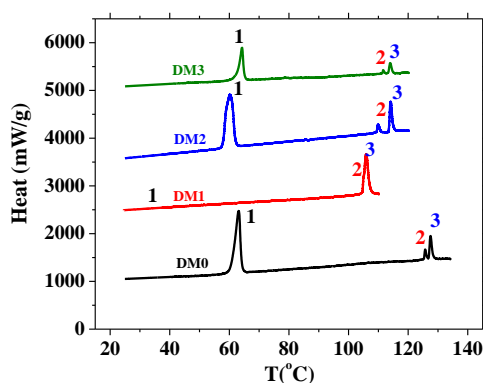
### 3.3.1 POLARIZING OPTICAL MICROSCOPY (POM) AND DSC STUDY

From the texture study under polarizing microscope, transition temperatures were determined and the phases were identified. Transition temperatures were also determined from DSC study, which differs slightly from those obtained from texture study which might be due to the use of two different temperature baths. Phase sequence and the transition temperatures of the compounds, as obtained from texture study, are mentioned in **Table 3.1**. No change in phase sequence is observed due to fluorination at different positions of the benzoate core. However, the melting point is found to decrease by 20°C in DM1 and 3.7°C in DM2 but increases by 2.2°C in DM3; the clearing point decreases by 21.4°C, 12.8°C, and 13.4°C in DM1, DM2 and DM3 respectively; thermal stability of  $\text{SmC}_\text{A}^*$  increases by 1.2°C in DM1, decreases by 9.8°C and 11°C in DM2 and DM3 respectively; the stability of  $\text{SmC}^*$  is decreased in all the fluorinated compounds by 1.2°C, 1.5°C, and 5°C in DM1, DM2 and DM3 respectively. A large super cooling effect is observed in all the compounds in texture study as well as in dielectric and electro-optic measurements.

Textures were observed under planar anchoring conditions for all the compounds. Typical fan shape texture was observed in  $\text{SmA}^*$  phase which was broken in  $\text{SmC}^*$  and  $\text{SmC}_\text{A}^*$  phases, existence of helicoidal structure is visible in the form of parallel equidistant lines more in  $\text{SmC}_\text{A}^*$  phase than in  $\text{SmC}^*$  phase as shown in **Figure 3.1** for DM0 and DM1. Other compounds showed similar textures.



**Figure 3.1.** Exemplary characteristic textures of DM0 in (a) SmCA\*, (b) SmC\* and (c) SmA\* phases and those of DM1 in (e) SmCA\*, (f) SmC\* and (g) SmA\* phases during cooling cycle.



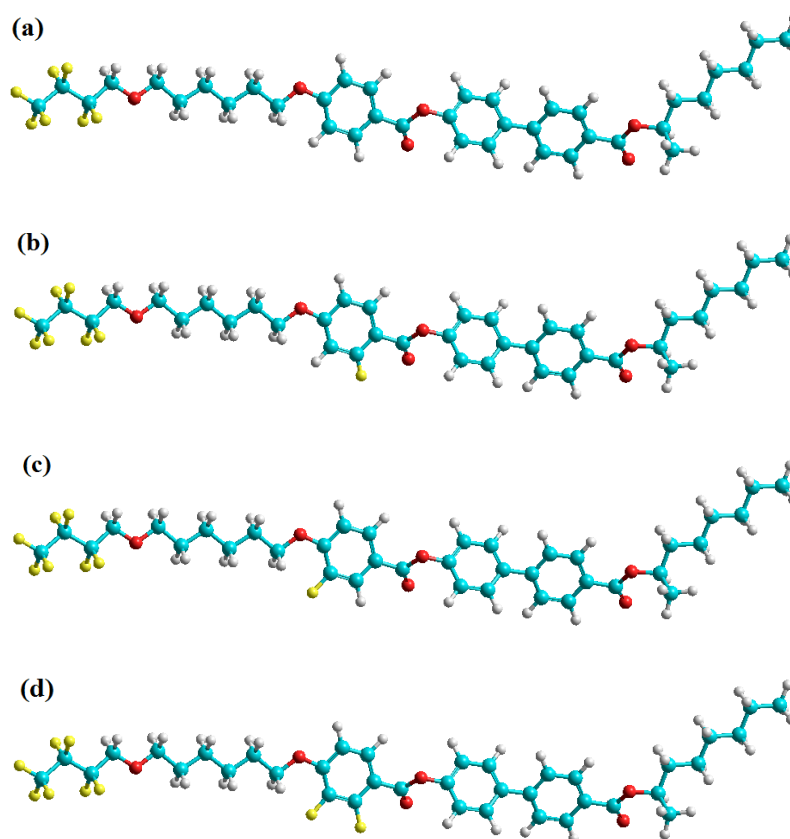
**Figure 3.2.** DSC thermograms of DM0, DM1, DM2 and DM3 during heating cycle.

DSC thermograms of the compounds showing the variation of heat flow with temperature during heating cycle are shown in **Figure 3.2**. Anomaly 1 represents melting, 2 represents SmC\*–SmA\* transition and 3 represents SmA\*–Isotropic transition. SmCA\*–SmC\* transition is not visible in the thermogram of all compounds due to finite hysteresis in temperature and a small change in enthalpy at the phase transitions [19]. This is not very unusual, observed in many other systems [20, 21]. As

for example, the phase change between  $\text{SmC}^*$  and  $\text{SmC}^*\alpha$  could not be detected in MHPO (13F)BC [20]. A similar observation was reported by Marzec *et al.* [21] in the analogous compound MHP(F)O(13F)BC. A very weak anomaly was also observed between  $\text{SmC}^*$  and  $\text{SmC}_A^*$  phase in MOPB(H)PBC [22].

### 3.3.2 OPTIMIZATION OF GEOMETRY

In order to explore the structural conformation of the compounds, their molecular geometries were optimized using PM3 molecular mechanics method in the Hyperchem software package in vacuo [23]. While optimizing the geometry the bond, angle and torsional interactions were considered in the force field along with the van der Waals and electrostatic interactions.



**Figure 3.3.** Optimized structures of the (a) DM0, (b) DM1, (c) DM2 and (d) DM3

Total energy, most extended molecular length, moments of inertia and dipole moment of the compounds as obtained from the geometry optimization, are compared in **Table 3.2**. Optimized lengths of the molecules, as expected, are almost the same and their total energy is also almost the same.

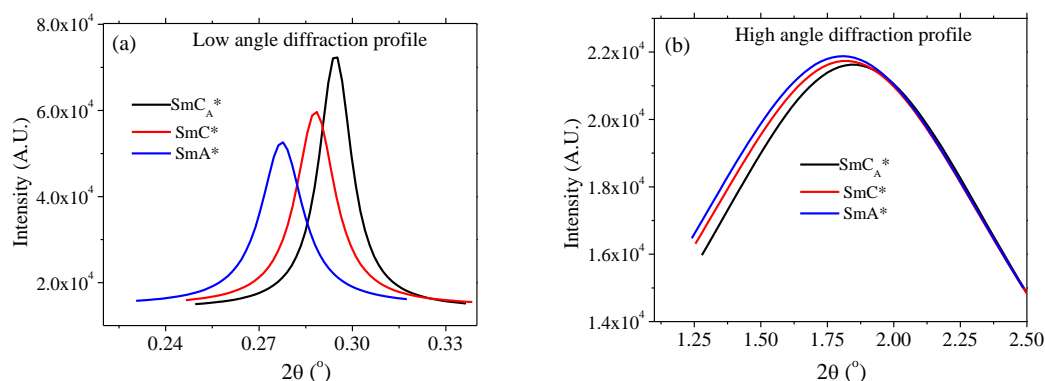
The dipole moment of DM0 is found to be 4.73 Debye. In DM1 and DM2, due to introduction of one lateral fluorine in the core, the dipole moment increased almost by 1.00 Debye and in DM3, when two lateral fluorine is introduced, the dipole moment increased almost by 2.00 Debye. Major increase in dipole moment is found to be transverse to the molecular long axis, as expected. Similarly the moments of inertia along x-axis in DM0 is the least ( $2235 \times 10^{-46} \text{ kgm}^2$ ) and it increases due to lateral substitution of one fluorine atom (heavier than hydrogen) in DM1 and DM2 ( $2314 \times 10^{-46} \text{ kgm}^2$  and  $2321 \times 10^{-46} \text{ kgm}^2$ ) and due to addition of two lateral fluorine in DM3 it increases further to  $2447 \times 10^{-46} \text{ kgm}^2$ . So the dipole moment and moment of inertia increases almost linearly with the increase of the number of lateral fluorine substitutions.

**Table 3.2.** Few important parameters of the molecules in optimized geometry

Sample	Optimized Molecular Length (Å)	Energy (kcal/mole)	Moment of Inertia in $10^{-46} \text{ kgm}^2$			Dipole Moment (Debye)			
			About x-axis	About y-axis	About z-axis	Components			Total
						x	Y	z	
DM0	38.37	-9788	2235	103770	104698	-1.55	-3.68	-2.53	4.73
DM1	37.91	-9799	2314	104918	106049	-1.97	-4.40	-3.14	5.75
DM2	37.93	-9800	2321	104892	106020	-1.95	-4.37	-3.17	5.74
DM3	38.39	-9802	2447	104336	105453	-1.15	-5.98	-3.11	6.84

### 3.3.3 X-RAY DIFFRACTION STUDY

Synchrotron X-ray diffraction photographs were recorded throughout the mesophases from the isotropic phase to room temperature during cooling. Transition temperatures observed from X-ray studies are found to be shifted to the higher side by about 3 degrees than those observed from optical microscopy which might be the result of using two different temperature baths. Intensity profile of the fitted (a) low and (b) high angle diffraction features are shown in **Figure 3.4**. Average intermolecular distance (D) and layer spacing (d) were calculated using the angles of the relevant Bragg peaks obtained from fitted profiles.

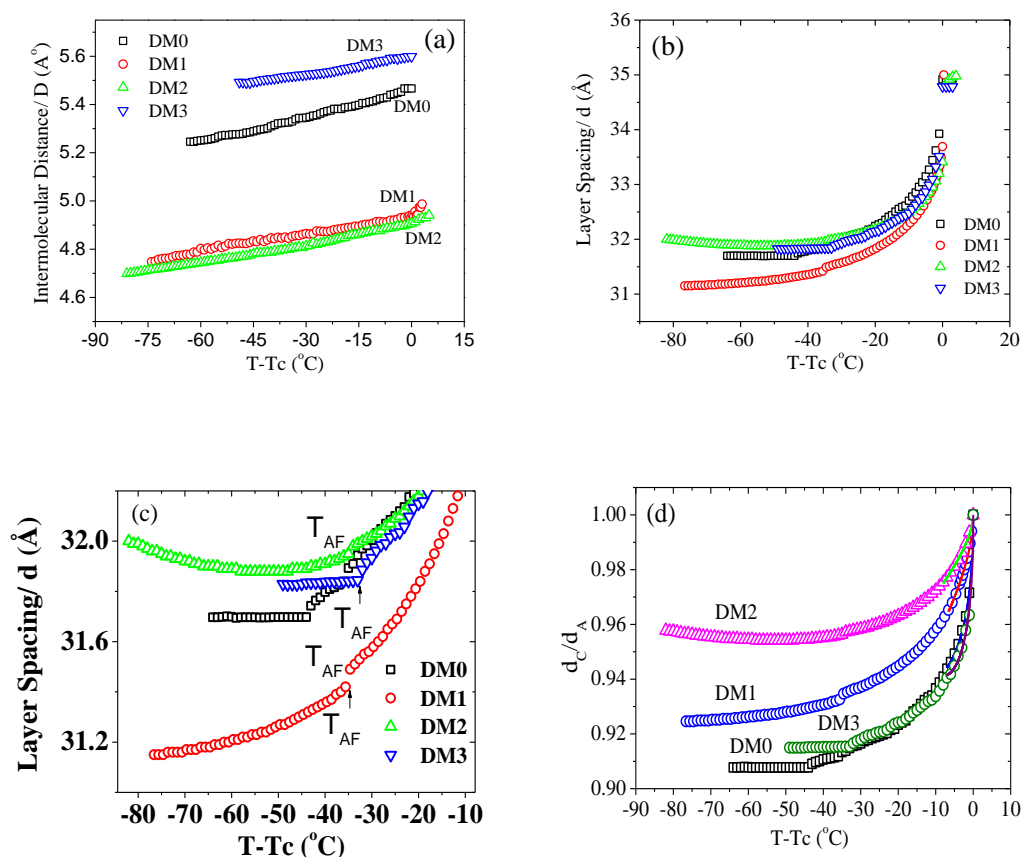


**Figure 3.4.** Intensity profile of the (a) low and (b) high angle diffraction features.

The temperature dependence of average intermolecular distance ( $D$ ) and layer spacing ( $d$ ) are shown in **Figure 3.5**. In the singly fluorinated compounds (DM1 and DM2) the average intermolecular distances are found to be less than the protonated (DM0) but in the doubly fluorinated compound (DM3) it becomes more than that of protonated (DM0). The average intermolecular distance ( $D$ ) is found to decrease slowly with decreasing temperature without showing any significant change at the transitions in all the compounds [**Figure 3.5(a)**]. The  $D$ -values in DM0 decreases from  $5.47\text{\AA}$  to  $5.24\text{\AA}$ , but it decreases from  $4.94\text{\AA}$  to  $4.74\text{\AA}$  in DM1 and from  $4.93\text{\AA}$  to  $4.70\text{\AA}$  in DM2 and from  $5.59$  to  $5.49\text{\AA}$  in DM3. So due to single lateral fluorination the average  $D$ -value decreases almost by  $0.5\text{\AA}$  and due to double lateral fluorination average  $D$ -value increases by  $0.2\text{\AA}$ .

On the other hand, smectic layer spacing ( $d$ ) of all the compounds decreases rapidly on cooling from  $\text{SmA}^*-\text{SmC}^*$  transition point ( $T_c$ ), the rate of fall decreases gradually as the temperature goes deeper into the  $\text{SmC}^*$  phase. Anomalous changes are observed at para to ferroelectric transition ( $T_c$ ) and ferro to antiferroelectric transition ( $T_{AF}$ ) in all the compounds as shown in **Figure 3.5(b)**, anomalies in the later transition is visible in **Figure 3.5(c)**. Such behavior was also reported in a fluorinated terphenyl compound [24]. In  $\text{SmA}^*$  phase maximum value of layer spacing for DM0 is  $34.9\text{\AA}$  and its value is found to increase by  $\sim 0.1\text{\AA}$  in DM1 and DM2 ( $35.0\text{\AA}$ ) whereas it decreases by  $\sim 0.1\text{\AA}$  in DM3 ( $34.8\text{\AA}$ ) although these values are substantially less than the molecular lengths as observed from optimized geometry (**Table 3.2**). It may be as a result of the tilt of the molecules with azimuthal

degeneracy as in de Vries phase [25] or the molecules may have different conformations than in vacuo condition or both.

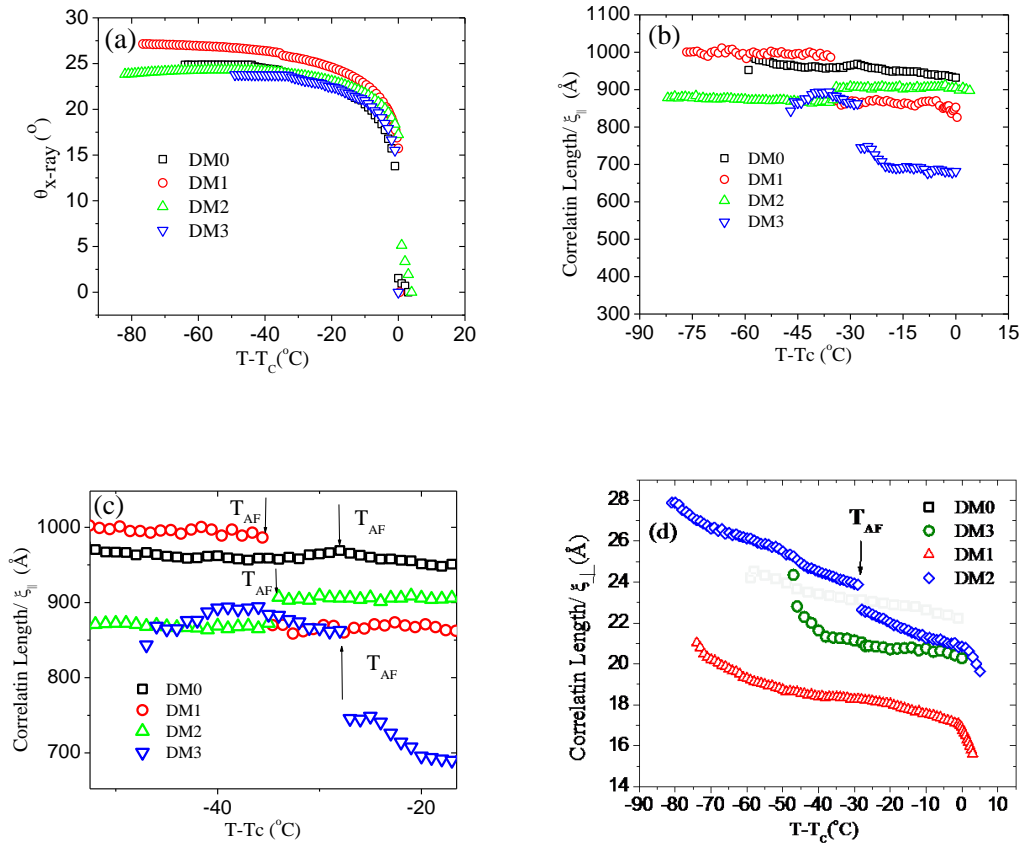


**Figure 3.5.** Temperature dependence of (a) intermolecular distance and (b) smectic layer spacing of the compounds, (c) anomalous change of layer spacing at  $T_{AF}$  is seen, (d) fitted data near  $T_c$  as discussed in the text.

It is further noted that the temperature dependence of layer spacing in SmC\* phase is parabolic. Under rigid rod approximation of the mesogenic molecules and for a second order transition approaching the tricritical point in the generalized mean-field theory, Following Hartley *et al.* [26] but keeping up to fourth order terms in the expansion of  $\cos\theta$  it can be shown that near  $T_c$ ,  $d_c/d_A \approx 1 - a/|T - T_c|^{1/2} + b/|T - T_c|$ , when  $\beta$  is taken as  $1/4$ . Observed data fitted nicely to the above equation (**Figure 3.5(d)**) signifying that the SmC\*–SmA\* transition was a tricritical type in all the systems.

In all the compounds, on cooling, tilt increase rapidly near  $T_c$ , the rate of increment is slow as moved away from  $T_c$  as depicted in **Figure 3.6(a)**. It remains essentially constant in the antiferroelectric phase and small discontinuity is observed

at the ferro to antiferroelectric transition. The maximum value of tilt in DM0 is  $24.8^\circ$  which in DM1 increases to  $27.1^\circ$  but in DM2 and DM3 decrease to  $23.8^\circ$ .



**Figure 3.6.** Temperature variation of (a) tilt angle ( $\theta$ ) of the compounds (b) correlation lengths across the smectic layers [ $\xi_{||}$ ] (c) magnified view of (b) near  $T_{AF}$  showing a discontinuity and (d) correlation lengths within the smectic layers ( $\xi_{\perp}$ ).

To probe the extent of correlation of the molecules across the smectic layers, correlation lengths ( $\xi_{||}$ ) have been calculated from the fitted intensity profile of the low and high angle diffraction features using Lorentzian fit function of origin 8.5. The maximum correlation length in  $\text{SmC}_A^*$  of DM0 is found to be  $986\text{\AA}$  across the smectic layers which is equivalent to about 28 molecular lengths. Corresponding values are  $1006\text{\AA}$  in DM1,  $878\text{\AA}$  in DM2 and  $894\text{\AA}$  in DM3 [Figure 3.6(b)], which are equivalent to almost 29, 25 and 25 molecular lengths respectively. Thus in the antiferroelectric phase correlation length across the plane is significantly less in DM2 and DM3 compared to DM0 but higher in DM1. In  $\text{SmC}^*$  phase the maximum value of  $\xi_{||}$  in DM0 is  $969\text{\AA}$ , its value decreases in DM1, DM2, and DM3 to  $870\text{\AA}$ ,  $907\text{\AA}$ ,

and 748 Å respectively. Thus in the ferroelectric phase the value of  $\xi_{||}$  value decreases systematically with the number of fluoro-substitution. Similar correlation lengths have been reported recently in the ferroelectric SmC\* phase of a terphenyl based compound [27].

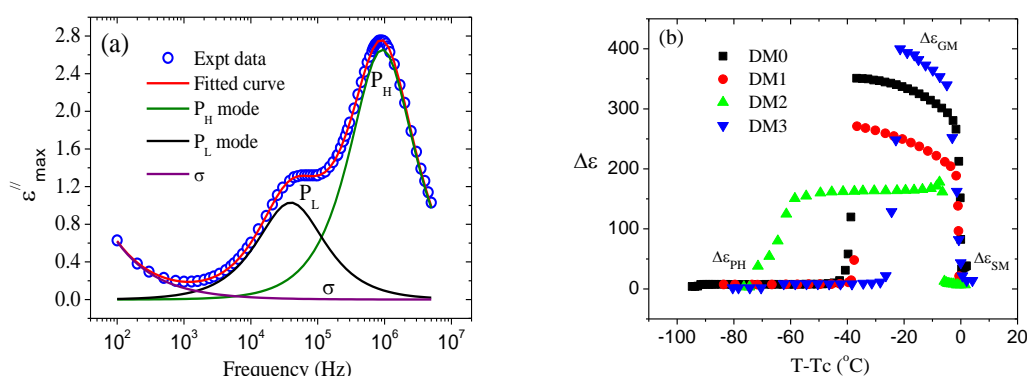
**Table 3.3.** Comparison of a few important parameters obtained from diffraction study

Parameter	DM0	DM1	DM2	DM3
Range of D (Å)	5.24-5.47	4.74-4.94	4.70-4.93	5.49-5.59
Maximum value of d (Å)	34.9	35.0	35.0	34.8
Range of d (Å)	31.7-34.9	31.2-35.0	32.0-35.0	31.8-34.8
Maximum tilt $\theta$ (°)	24.8	27.1	23.8	23.8
Range of $\xi_{  }$ in SmC <sub>A</sub> * (Å)	960-986	986-1006	872-878	862-894
Range of $\xi_{  }$ in SmC* (Å)	930-969	850-870	900-907	681-748
Maximum $\xi_{  }$ (Å) in SmC <sub>A</sub> *	986	1006	878	894
Maximum $\xi_{  }$ (Å) in SmC*	969	870	907	748
Maximum $\xi_{\perp}$ (Å) in SmC <sub>A</sub> *	24.5	21.0	27.9	24.3
Maximum $\xi_{\perp}$ (Å) in SmC*	23.1	18.4	22.6	20.9

As expected with decreasing temperature the correlation length increases in DM0, DM1, and DM3 and a substantial increase is observed at SmC\*–SmC<sub>A</sub>\* transition in these compounds. But in DM2 the value of  $\xi_{||}$  shows anomalous behaviour, it shows a down step at the SmC\*–SmC<sub>A</sub>\* transition and also shows a decreasing trend with temperature in both the phases. On the other hand, correlation lengths within the layers ( $\xi_{\perp}$ ) in SmC<sub>A</sub>\* phase are 24.5 Å, 21.0 Å, 27.9 Å, and 24.3 Å in DM0, DM1, DM2 and DM3 respectively, highest in DM2. In SmC\* these values are 23.1 Å, 18.4 Å, 22.6 Å and 20.9 Å respectively. Thus in the ferroelectric phase the value of  $\xi_{\perp}$  also decreases with the number of fluoro-substitution. Temperature dependence of these correlations are shown in **Figure 3.6(d)** and in all the compounds these increase with decreasing temperature as expected. However, it has to be kept in mind that we have not made any correction for the profile of the incident beam which certainly accounts for a part of the diffracted line width thus underestimates the correlation length.

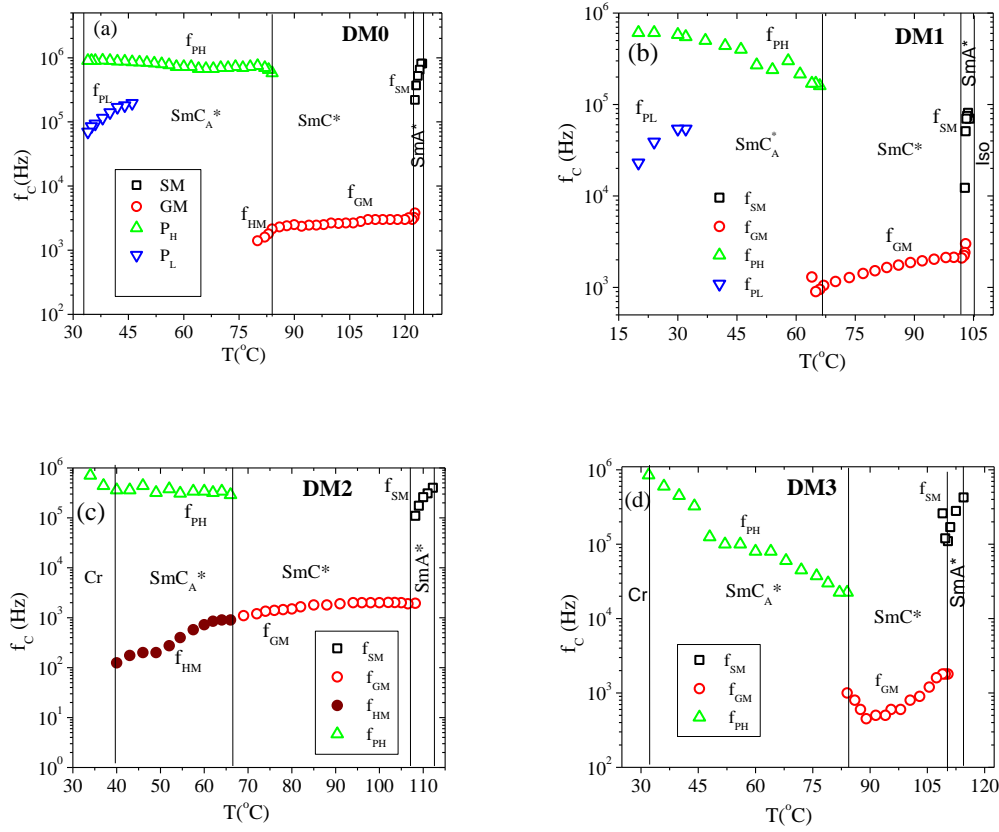
### 3.4 DIELECTRIC STUDY

Dielectric absorption spectra were fitted to the modified Cole-Cole function as mentioned in **Chapter 2** and a fitted spectrum only in SmC<sub>A</sub>\* phase of DM0 is shown in **Figure 3.7(a)** as an example. It may be mentioned here that we have two peaks in this case. Fitted parameters are  $\Delta\epsilon_{PL} = 2.16 \pm 0.02$ ,  $f_{PL} = 39550 \pm 227$ ,  $\alpha_{PL} = 0.030 \pm 0.002$ ;  $\Delta\epsilon_{PH} = 5.38 \pm 0.04$ ,  $f_{PH} = 926610 \pm 2254$ ,  $\alpha_{PH} = 0.003 \pm 0.001$ ,  $\sigma = 8.59 \times 10^{-10} \pm 0.02 \times 10^{-11}$ . All the compounds possess large dielectric increments ( $\Delta\epsilon$ ) in the ferroelectric SmC\* phase as shown in **Figure 3.7(b)**.



**Figure 3.7.** (a) Fitted absorption spectra in SmC<sub>A</sub>\* phase of DM0 at 33°C showing clearly the P<sub>L</sub> and P<sub>H</sub> modes, (b) Temperature dependence of dielectric increment ( $\Delta\epsilon$ ).

Dielectric increment of protonated DM0 is 351, due to fluorination at ortho position (DM1) the  $\Delta\epsilon$  decreases by 80 and due to fluorination at meta position (DM2) the  $\Delta\epsilon$  decreases further by ~90, although both the compounds possess the higher value of dipole moment. However, in case of DM3 due to fluorination at both positions, the  $\Delta\epsilon$  increases to 400, which is more than the protonated DM0. Moreover, the  $\Delta\epsilon$  increases with the decrease of temperature in SmC\* phase in all compounds except DM2 where it decreases. So the value of  $\Delta\epsilon$  is not directly related to the dipole moment of the molecule but depends upon interaction of the atoms within the molecule, intermolecular interactions, etc. Several relaxation modes are observed in different phases which are discussed in the next section.

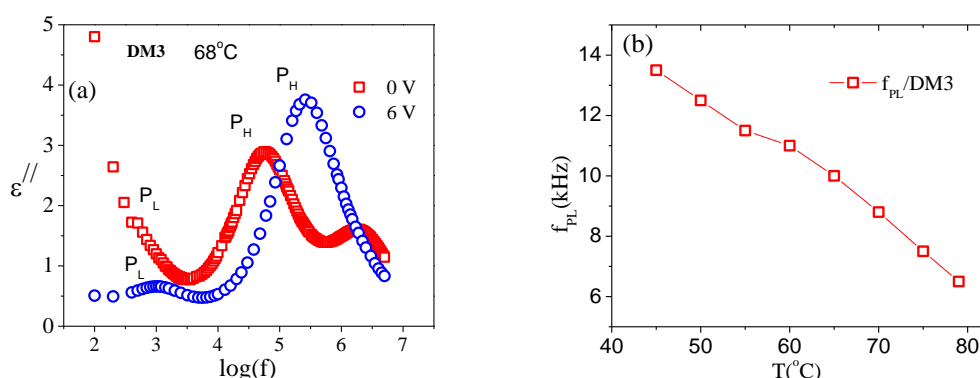


**Figure 3.8.** Temperature dependence of critical frequencies of all the modes observed in (a) DM0, (b) DM1, (c) DM2 and (d) DM3.

### 3.3.4.1 $\text{SmC}_A^*$ PHASE

Temperature dependences of critical frequencies of all the observed modes are shown in **Figure 3.8** for all the compounds. In the antiferroelectric phase, two collective relaxation processes are usually observed in kHz and hundred kHz ranges which respectively are connected with in-phase ( $P_L$ ) and anti-phase ( $P_H$ ) reorientations of the molecules in adjacent smectic layers. In DM0,  $P_L$  is observed at temperatures far below  $T_{AF}$  ( $\text{SmC}^* \text{--} \text{SmC}_A^*$ ) transition.  $T_{AF}$  takes place at  $83^\circ\text{C}$  but  $P_L$  starts at  $45^\circ\text{C}$ . A similar fact is also observed in DM1. But in DM2 a low frequency mode is observed to appear just from the  $\text{SmC}^* \text{--} \text{SmC}_A^*$  transition. This low frequency ( $f_c \sim \text{few hundred Hz}$ ) mode is a sharp one and its  $\Delta\epsilon$  has high value ( $\sim 12$ ) compared to  $P_L$  and it appears in continuation of Goldstone mode of  $\text{SmC}^*$  phase and observed over a large temperature range well inside  $\text{SmC}_A^*$  phase. This observed mode in  $\text{SmC}_A^*$  (not characteristic of  $\text{SmC}_A^*$ ) is identified as hereditary mode [31]. However, no such mode was reported before [29-30]. The reason for the appearance of this mode is the

coexistence of the  $\text{SmC}_A^*$  and  $\text{SmC}^*$  phase when cooled slowly from the isotropic phase. As the hereditary mode is very strong, the weak  $P_L$  mode was annihilated and was not observed in DM2 [31]. But in double laterally fluorinated DM3 although  $P_L$  is observed throughout the  $\text{SmC}_A^*$  phase but at much lower frequency (not in continuation with GM, not shown in **Figure 3.8(d)**) and observed mode is very weak compared to other compounds DM0 and DM1, which might be due to large ionic contribution in permittivity. That indeed the case in DM3 is confirmed by the fact that  $P_L$  peaks become clear, although slightly shifted when a DC bias field ( $0.6\text{V}/\mu\text{m}$ ) is applied which reduced the ionic contribution (**Figure 3.9**).



**Figure 3.9.** (a) Clear evidence of  $P_L$  in DM3 on application of small bias field ( $0.6\text{V}/\mu\text{m}$ ) voltage, (b) Temperature dependence of  $f_{PL}$  of DM3

In DM0, the critical frequencies ( $f_{PL}$ ) decreases with decreasing temperature from 195 kHz to 30 kHz similarly in DM1, it decreases with decreasing temperature from 54 kHz to 23 kHz. However, the temperature dependence of  $f_{PL}$  is also found to be different in DM3, it increases from about 6.5 kHz to 13.5 kHz (**Figure 3.9(b)**) with the decrease of temperature (this observation is in bias field as mentioned above).

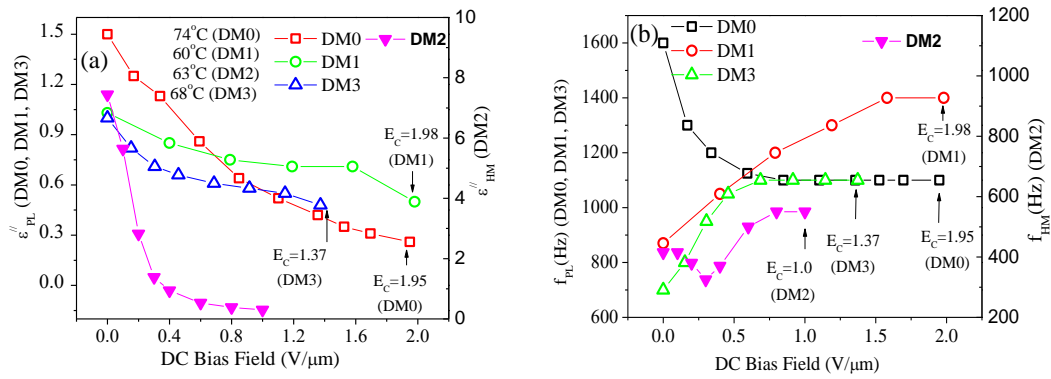
On the other hand, high frequency anti-phase antiferroelectric mode has been observed throughout the  $\text{SmC}_A^*$  phase in all the compounds, critical frequencies ( $f_{PH}$ ) being much higher in DM0 compared to fluorinated compounds as observed in  $P_L$ . However,  $f_{PH}$  increases with decreasing temperature in all the compounds, in DM0 from 580 kHz to 925 kHz, DM1 from 170 kHz to 610 kHz, DM2 from 290 kHz to 710 kHz and in DM3 from 22.5 kHz to 125 kHz (**Figure 3.8**). Thus the behaviour of the in-phase and the anti-phase antiferroelectric modes is significantly influenced by the number and the position of the fluorine substitutions.

From the fitted spectra (**Figure 3.7(a)**)  $\alpha_{PL}$  and  $\alpha_{PH}$  values are found to be 0.003 and 0.030 respectively, signifying that both the processes are Debye type. Diverse reports on range and temperature dependence of critical frequencies of both the modes are found in the literature. For example, Y. P. Panarin *et al.* [32] reported  $P_L$  process at  $\sim 2.5$  kHz and  $P_H$  from 10 kHz to 70 kHz in a laterally fluorinated biphenyl carboxylate compound. The range of the  $P_L$  and  $P_H$  processes obtained by A. Fafara *et al.* [33] are 10 kHz-20 kHz and 900 kHz-2MHz respectively in a different non-fluorinated biphenyl carboxylate compound and both processes were temperature independent. Buividas *et al.* [28] reported  $P_L$  mode at about 400 Hz–20 kHz and  $P_H$  around 200 kHz to 2 MHz in a non-fluorinated biphenyl compound with different chain type and both the modes were found to be sharply temperature-dependent.

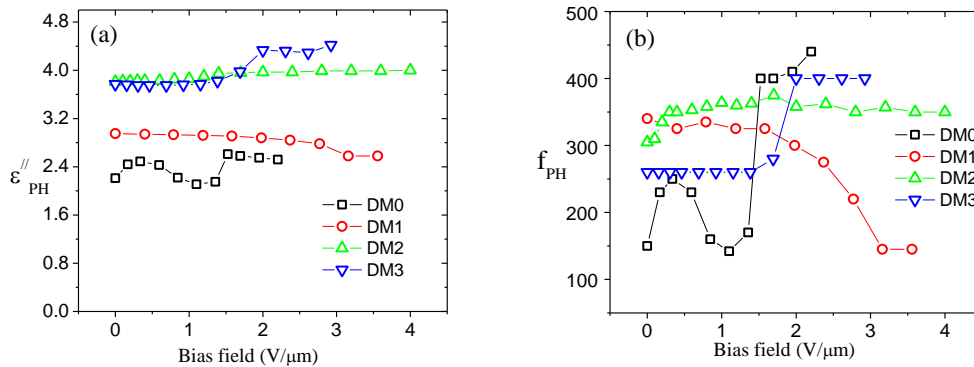
Next, we explored how the behaviour of both the relaxation processes ( $P_L$ ,  $P_H$ ) is influenced by the DC bias field. It is observed that the strength of dielectric absorption ( $\epsilon''_{max}$ ) of  $P_L$  decreases gradually with bias and finally suppresses at the critical field of 1.95 V/ $\mu m$  in DM0, 1.98 V/ $\mu m$  in DM1 and 1.37 V/ $\mu m$  and DM3 respectively (**Figure 3.10(a)**). The dielectric absorption of DM2 at 63°C has a high value (7.44) at zero field and decreases with bias sharply up to 0.3 V/ $\mu m$  then it suppresses at 1.0 V/ $\mu m$ . So the bias variation of the low frequency mode in DM2 is quite different from  $P_L$  and make resemblance with that of GM mode in SmC\* phase [31]. This confirms that the mode is not  $P_L$  rather hereditary mode arising due to the incomplete antiferroelectric conformation. The critical frequency  $f_{PL}$  initially decreases with bias and finally remains constant in DM0 while in DM1 it increases with increasing bias and in DM3 initially increases and then slowly becomes a constant. However, the constant value of  $f_{PL}$  in DM3 is the same as the constant value of DM0 (1100 Hz) [**Figure 3.10(b)**]. The critical frequency of the hereditary mode ( $f_{HM}$ ) observed in DM2, decreases from 415 Hz (at 0 bias field) to 325 Hz (0.3 V/ $\mu m$ ) and then increases to 550 Hz at 1.0 V/ $\mu m$ . So the range and variation of critical frequency of low frequency mode ( $f_{HM}$ ) with bias is different from that of  $P_L$  but makes resemblance with that of GM.

On the other hand, absorption strength and critical frequency of the  $P_H$  mode in all the compounds remains almost constant with bias, except considerable discontinuity at transitions, increase near the critical fields at which  $P_L$  was suppressed (except DM1) [**Figure 3.11(a)**]. Similarly, the critical frequency of  $P_H$  mode ( $f_{PH}$ )

shows a discontinuity near the critical fields in DM0 and DM3, in DM1 it decreases gradually and in DM2 it remains almost constant. In all compounds, the mode did not vanish within dc field 4.0 V/ $\mu\text{m}$  [Figure 3.11(b)]. No appreciable change was reported by Buividas *et al.* [28] in both the  $P_L$  and  $P_H$  critical frequencies but  $P_H$  was found to vanish at a sufficient bias field, whereas Perkowski *et al.* [34] observed increased strength of both the modes with bias. Molecular conformation, as well as strength and orientation of transverse dipole moments, maybe the cause of such conflicting dynamical response.



**Figure 3.10.** Bias field dependence of (a)  $\epsilon''_{PL}$  and  $\epsilon''_{HM}$  and (b)  $f_{PL}$  and  $f_{HM}$ .



**Figure 3.11.** Bias field dependence of (a)  $\epsilon''_{PH}$  and (b)  $f_{PH}$ .

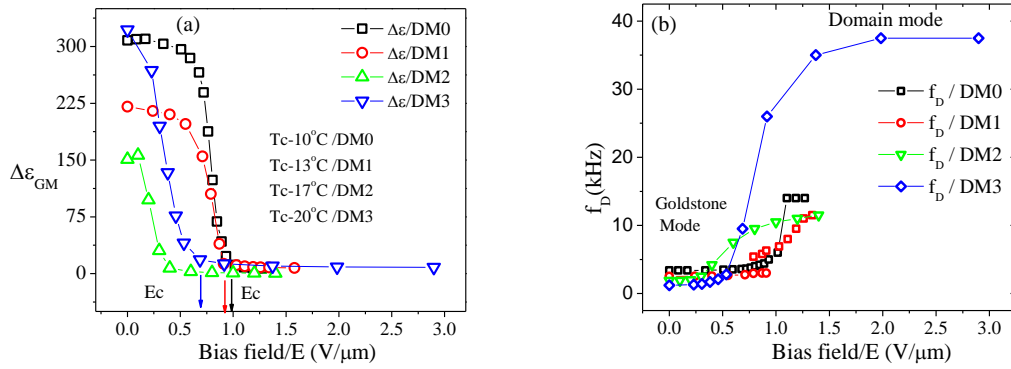
### 3.3.4.2 SmC\* and SmA\* PHASE

Characteristic Goldstone mode (GM) is observed in the ferroelectric smectic phase of all the compounds. GM critical frequency ( $f_{GM}$ ) is found to increase with temperature in all compounds; in DM0 increases from 1400 Hz to 3800 Hz, in DM1 it increases from 900 Hz to 2400 Hz, in DM2 it increases from 1100 Hz to 1950 Hz, and

in DM3 from 450 Hz to 1800 Hz [Figure 3.8]. Anomalous behavior is observed in doubly fluorinated DM3 while approaching  $\text{SmC}_A^*$  transition [Figure 3.8(d)]. It is observed that the  $f_{GM}$  decreases in all fluorinated compounds compared to protonated one and the higher is the number of fluorine substitution more is the decrease in  $f_{GM}$ .

Soft mode (SM) is found in all the compounds, however, in compounds DM0, DM1 and DM2, the mode is observed only in  $\text{SmA}^*$  phase while in DM3 it is also found to penetrate nearly 1.5°C inside the  $\text{SmC}^*$  phase and produces a V shape at  $T_c$  as expected from mean-field theory [35] as shown in Figure 3.8(d). The SM critical frequency ( $f_{SM}$ ) is also found to decrease in fluorinated compounds DM1 (12.5 kHz–81 kHz), DM2 (110 kHz–400 kHz) and DM3 (110 kHz–425 kHz) compared to protonated DM0 (220 kHz–810 kHz). In DM1 the  $f_{SM}$  is the least and in DM2 and DM3 it is almost the same. It is further seen from the Figure 3.8(b) that  $f_{GM}$  increases slowly with decreasing temperature but the  $f_{SM}$  decreases sharply. This is in accordance with the generalized Landau model of Carlson *et al.* [36]. So due to fluorination critical frequencies of both the GM and SM decrease significantly.

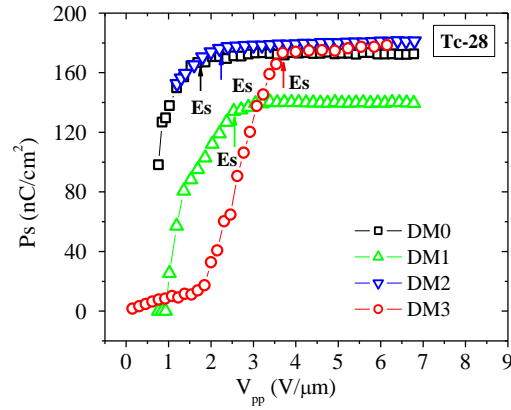
That the Goldstone mode in  $\text{SmC}^*$  phase is a result of phase fluctuation of the molecules is evident from the fact that it diminishes gradually by the application of DC electric field in addition to the measuring ac field and suppresses completely at a certain value of DC field, called critical field ( $E_c$ ), which corresponds to complete unwinding of the helix. DC field required to suppress the GM in DM0 is 0.93 V/ $\mu\text{m}$ , in DM1 is 0.91 V/ $\mu\text{m}$ , in DM2 is 0.4 V/ $\mu\text{m}$  and for DM3 it is 0.68 V/ $\mu\text{m}$  as shown in Figure 3.12(a). So the  $E_c$  decreases due to lateral fluorination. However under strong bias field a residual mode, with dielectric spectrum different from GM, is observed, this mode is known as domain mode (DM) [37–39]. The critical frequency of this mode ( $f_{DM}$ ) increases nonlinearly with increasing bias field and finally remains constant at 14 kHz in DM0, 11.5 kHz in DM1, DM2 and in DM3 at 37.5 kHz as depicted in Figure 3.12(b). Thus  $f_{DM}$  is roughly 4 times in DM0, 4.6 times in DM1, 6 times in DM2 and 20 times in DM3 of respectively compared to  $f_{GM}$ . Czerwiec *et al.* reported 2 and 10 fold increase in two non-fluorinated compounds [37].



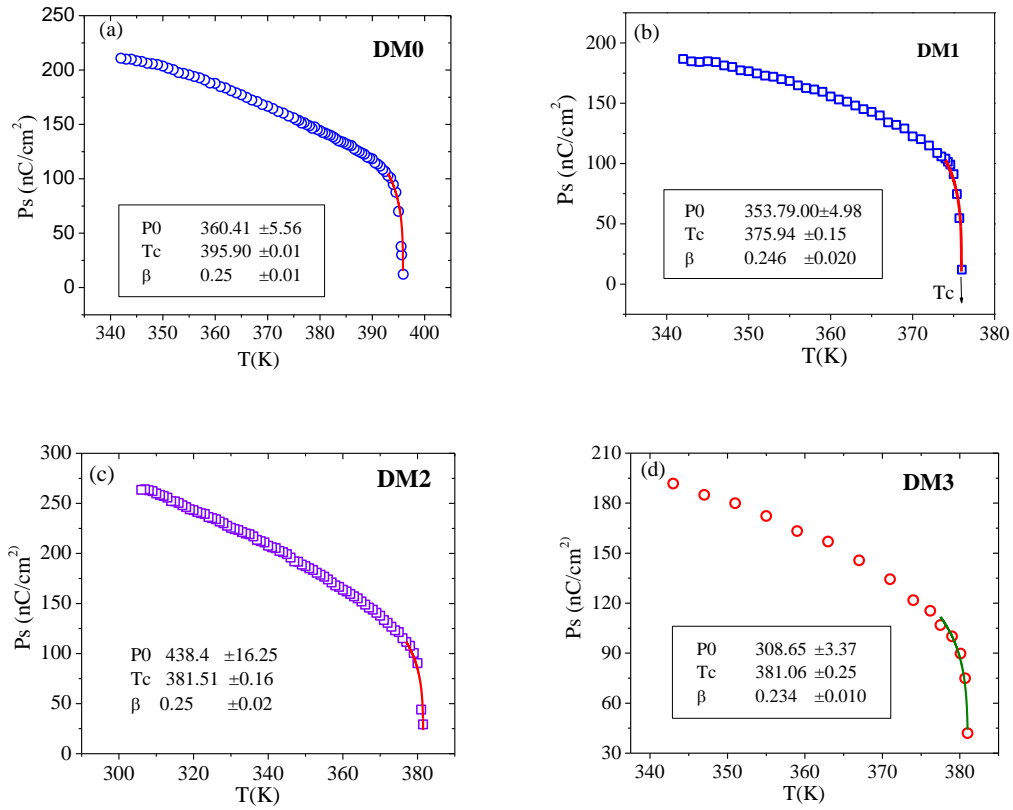
**Figure 3.12.** Bias field dependence of (a) dielectric increment ( $\Delta\epsilon_{GM}$ ) of Goldstone mode and (b) critical frequencies of domain mode ( $f_{DM}$ )

### 3.3.5 SPONTANEOUS POLARIZATION ( $P_s$ ) MEASUREMENTS

The samples were heated to the isotropic phase and then cooled at a slow rate of 0.2°C/min. well within SmC\* phase and at a fixed temperature the spontaneous polarization was measured as a function of ac field ( $E$ ). It is observed that  $P_s$  increases rapidly with increasing field and reaches a maximum at a certain value of the field called the saturation field ( $E_s$ ) [Figure 3.13]. As the electric field increases from zero, the interaction of the polarization vectors with the field causes gradual unwinding of the helix as well as polarization reversal. At the critical field  $E_s$ , helix is completely unwound, bulk domains are formed where all the dipoles are oriented in the direction of the field and the field causes only polarization reversal. In other words, the saturation field is the minimum field required for the operation of FLC based display devices. In protonated DM0 the  $E_s$  is found to be 2.03 V/ $\mu\text{m}$  at 95°C [Tc–28]. In singly fluorinated DM1 and DM2,  $E_s$  is observed to increase to 2.40 V/ $\mu\text{m}$  at 75°C [Tc–28] and 2.54 V/ $\mu\text{m}$  at 80°C [Tc–28] respectively and in DM3, due to double lateral fluorination it increases further to 3.69 V/ $\mu\text{m}$  at 80°C [Tc–28]. Thus, due to fluorine substitution in DM1, DM2 and DM3, the transverse component of dipole moment increases and hence more driving force i.e. stronger electric field is required to unwind the helix.



**Figure 3.13.** Field dependence of spontaneous polarization ( $P_s$ ) at  $T_c = 28^\circ\text{C}$



**Figure 3.14.** Temperature dependence of  $P_s$  at saturation field of (a) DM0, (b) DM1, (c) DM2, and (d) DM3. Fitted curves near  $T_c$  are also shown.

### 3.3.6 OPTICAL TILT ( $\theta_{opt}$ )

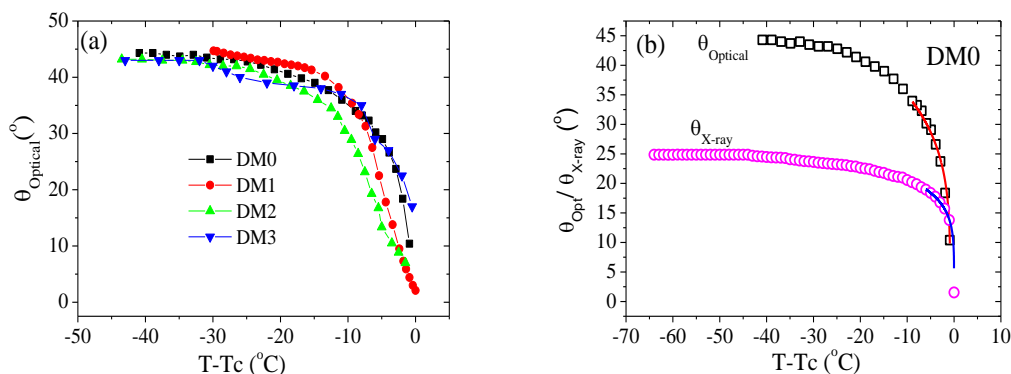
The temperature dependence of  $P_s$  has been shown in **Figure 3.14(a-d)**. With decrease of temperature the  $P_s$  increases rapidly near  $T_c$  and slowly away from  $T_c$ ,

reaching a maximum of 210.8 nC/cm<sup>2</sup> in DM0 at 69°C, 186.4 nC/cm<sup>2</sup> in DM1 at 69°C, 263.5 nC/cm<sup>2</sup> in DM2 at 33°C and 191.7 nC/cm<sup>2</sup> in DM3 at 70°C. In SmC<sub>A</sub>\* it falls very rapidly to zero.  $P_s$  does not show any discontinuity at SmC\*–SmC<sub>A</sub>\* transition since  $P_s$  was measured with high field. Such behavior was reported before [24, 37, 40]. Near  $T_c$  the  $P_s$  data was fitted to the mean-field equation [41]

$$P_s = P_o(1 - T/T_c)^\beta \quad (3.1)$$

and from the fitted data the  $T_c$  values are found to match well with the observed critical temperatures in all the compounds. However, order parameter critical exponent  $\beta$  is found to be 0.25, 0.25, 0.25 and 0.23 in DM0, DM1, DM2, and DM3 respectively, such values have been reported before [42, 43]. For a pure second order transition,  $P_s$ , the secondary order parameter of the phase, should continuously reach to zero with critical exponent  $\beta=0.5$  whereas a  $\beta$  value of 0.25 is expected in the case of second order transition approaching the tricritical point [44,45]. Thus the paraelectric to ferroelectric transition is tricritical in nature revealed from both X-ray and polarization study.

The optical tilts are found to increase rapidly with decrease of temperature from  $T_c$  reaching nearly 45° in SmC<sub>A</sub>\* phase in all the compounds [Figure 3.15(a)] indicating that the compounds are orthoconic antiferroelectric in nature. On the other hand, although the x-ray tilts ( $\theta_{x-ray}$ ) of the compounds show similar temperature variation but their maximum values are found to vary between 23.8°–27.1°, as shown before in Figure 3.6(a). Thus x-ray tilts are much less than the optical tilts. Similar results were reported before by several other authors [46-48], although the existence of higher x-ray tilt than optical tilt was also observed by Meier *et al.*[49]. X-ray tilt is a result of the tilt of the electron-density function of the whole molecule, whereas optical tilt arises due to the tilt of only the rigid polarisable group of the molecule, thus the two tilts may differ. This difference has also been explained considering zig-zag shape of the molecules [46]. The zig-zag molecular shape arises out of the rigid core which tilt independently whereas the melted end chains are on the average closer to the layer normal. Both the tilts are found to fit nicely to the power-law with  $\beta = 0.25$  near  $T_c$  in all compounds signifying again the tricritical nature of SmC\*–SmA\* transition. Fitted curve for DM0 is shown in Figure 3.15(b).



**Figure 3.15.** (a) Variation of optical tilts with reduced temperature of DM0, DM1, DM2, and DM3, (b) Fitted X-ray tilt and Optical Tilt of DM0.

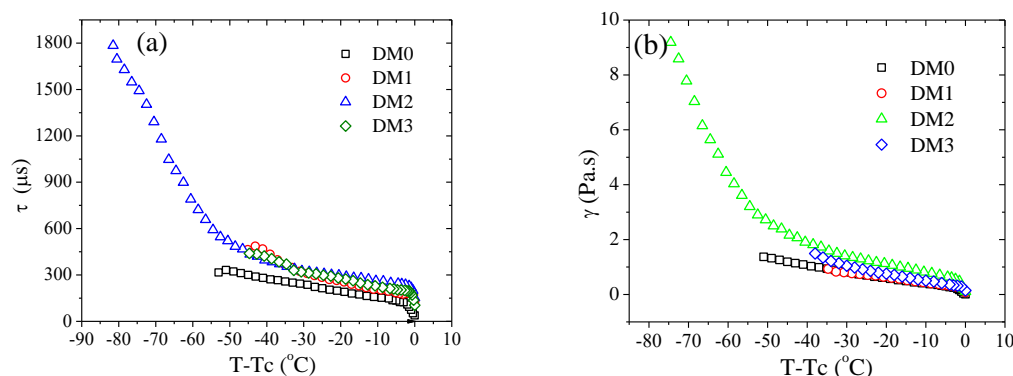
### 3.3.7 SWITCHING TIME ( $\tau$ ) AND VISCOSITY ( $\gamma$ )

The compounds show sub-millisecond switching time ( $\tau$ ) (except in  $\text{SmC}_A^*$  phase of DM2), however, a comparatively slower response is observed in all the laterally fluorinated compounds in  $\text{SmC}^*$  phase; in DM1, DM2 and DM3  $\tau_{\text{max}} \sim 500 \mu\text{s}$  compared to non-fluorinated DM0 in which  $\tau_{\text{max}} \sim 340 \mu\text{s}$ . In a phenyl based nonfluorinated compound switching time was reported at around  $10.5 \mu\text{s}$  [22] which was increased to around  $88 \mu\text{s}$  [42] in the terminally fluorinated compound, supporting the present observation that fluorination causes slower response. Further,  $\tau$  increases sharply with decreasing temperature in DM2 and clear anomalies are observed at the onset of the antiferroelectric phase [Figure 3.16(a)].

The torsional viscosity ( $\gamma$ ) of the materials has been calculated using the following relation [50]

$$\gamma = \tau \cdot Ps \cdot E \quad (3.2)$$

here  $E$  is the applied field. Due to fluorination  $\gamma$  is found to increase as shown in Figure 3.16(b). Assuming the temperature dependence of  $\gamma$  is Arrhenius type, activation energy ( $Ea$ ), which is the energy barrier for the dipole relaxation, was calculated and found to be  $38.19 \text{ kJ/mol}$  in DM0,  $44.52 \text{ kJ/mol}$  in DM1,  $26.66 \text{ kJ/mol}$  in DM2 and  $44.34 \text{ kJ/mol}$  in DM3.



**Figure 3.16.** Comparison of (a) switching times ( $\tau$ ) and (b) viscosities ( $\gamma$ ) of the compounds.

A selected list of parameters of the compounds of the series along with literature values of related compounds has been given in **Table 3.4** for ease of comparison.

**Table 3.4.** A selected list of parameters of DM0, DM1, DM2, and DM3 and related compounds

Parameters	DM0	DM1	DM2	DM3	Other compounds		
$\mu(D)$	4.73	5.75	5.74	6.84			
$\Delta\epsilon_{GM}$	350	271	178	400	92[42]	25.8[24]	400[33]
$f_{GM}(\text{Hz})$	1400-3800	900-3000	1100-1950	450-1800	4700[42]	400-900[24]	
$f_{SM}(\text{kHz})$	220-810	12.5-81	110-400	110-425	2-70[24]		
$f_{PL}(\text{kHz})$	30-195	23-54	---	6.5-13.5	0-2[42]	10-20[33]	
$f_{PH}(\text{kHz})$	580-925	170-610	290-710	22.5-125	10-50[42]	900-2000 [33]	
$D(\text{\AA})$ (max)	5.47	4.94	4.93	5.59	6.00[42]		
$d$ ( $\text{\AA}$ ) (max)	34.9	35.0	35.0	34.8	34.3[42]	29.2[50]	
$\xi_{  }(\text{\AA})$ (max)	986	1006	878	894	1180[27]		
$P_s$ (max)							
(nC/cm <sup>2</sup> )	210.8	186.4	263.5	191.7	120 [24]	195 [50]	300 [33]
$\tau$ ( $\mu\text{s}$ )			484(SmC*),				
(max)	340	486	1784 (SmC <sub>A</sub> *)	500	88[42]	10.5[50]	
$\gamma$ (Pa.s)			2.5 (SmC*),				
(max)	1.37	0.93	9.2 (SmC <sub>A</sub> *)	1.49	0.37[42]	2.0[24]	0.42[50]
$\beta$	0.25	0.246	0.25	0.234	0.45[24]	0.32[50]	
$E_a$ (kJ mol <sup>-1</sup> )	38.19	44.52	26.66	44.34	97.09[42]	48.14[24]	

### 3.4. CONCLUSION

Based on the POM, DSC, X-ray, dielectric and electro–optic studies the effect of lateral fluorination in the core may be summarized as follows:

1. No change in phase sequence is observed due to lateral fluorination, however, due to fluorination at ortho and meta position (DM1, DM2) the melting point is found to decrease, however, for fluorination at both position (DM3), it increases. Clearing point decreases in all the fluorinated compounds; thermal stability of SmC<sub>A</sub>\* phase increases by in DM1 but decreases in DM2 and DM3; the stability of SmC\* phase is found to decrease in all the fluorinated compounds.
2. Dipole moment increases in all the fluorinated compounds, more in doubly fluorinated compound than the protonated one. Increase in dipole moment is mainly transverse in nature.
3. The average intermolecular spacing is found to decrease in singly fluorinated compounds however, it increases in the doubly fluorinated compound.
4. Layer spacings in orthogonal SmA\* phase increases in DM1 and DM2 whereas it is found to decrease in DM3, these spacings are substantially less than the optimized molecular lengths implying that the molecules are in different conformations than in *vacuo* condition or the molecules are tilted with azimuthal degeneracy as in de Vries phase or both. The temperature variation of layer spacing shows a parabolic nature near T<sub>c</sub>, implying that SmA\*–SmC\* transition is nearly tricritical in nature in all the systems.
5. With decreasing temperature correlation length [ $\xi_{||}$ ] across the smectic plane increases. The average value  $\xi_{||}$  phase is observed to decrease due to fluorination in SmC\*. At ferro to antiferroelectric transition, a substantial jump is observed. The  $\xi_{||}$  value in SmC<sub>A</sub>\* phase is less for DM2 and DM3 but higher for DM1 than DM0.
6. All the compounds exhibit very large dielectric increments in SmC\* phase but in DM1 and DM2 its value is less and in DM3 it is more than the core protonated compound. Thus values of  $\Delta\epsilon$  are not proportional to the dipole moments of the molecules.
7. Four relaxation modes (P<sub>L</sub>, P<sub>H</sub>, GM, and SM) are observed and their critical frequencies are found to decrease in all fluorinated compounds. Similarly less amount of critical field is required to suppress both the P<sub>L</sub> and GM in the

fluorinated compounds. Under a strong bias field although domain mode is observed in all the compounds, however, saturated  $f_{DM}$  of DM1 and DM2 is found to decrease and in DM3 it increases to almost two and half times that of DM0.

8. Significantly higher field is required for saturation of the spontaneous polarization in all the laterally fluorinated compounds than in the protonated compound. Tricritical nature of the SmA\*–SmC\* transition is also supported by temperature-dependence of  $P_s$ .
9. Fluorination results in the slower response under a square pulse.

Thus finally we like to conclude that lateral fluorination in the core substantially changes the dynamics of the ferro and antiferroelectric phases as well as several other macroscopic and microscopic properties.

### 3.5 REFERENCES

- [1] M. Hird, Ferroelectricity in liquid crystals—materials, properties and applications, *Liq. Cryst.* 38 (2011) 1467–1493.
- [2] P. J. Collings, Ferroelectric liquid crystals: The 2004 Benjamin Franklin Medal in Physics presented to Robert B. Meyer of Brandeis University, *Journal of the Franklin Institute.* 342 (2005) 599–608.
- [3] J. Wen, M. Tian, Q. Chen, Novel fluorinated liquid crystals. II. The synthesis and phase transitions of a novel type of ferroelectric liquid crystals containing 1,4-tetrafluorophenylene moiety, *Liq. Cryst.* 16 (1994) 445–453.
- [4] Y. Xu, W. Wang, Q. Chen, J. Wen, Synthesis and transition temperatures of novel fluorinated chiral liquid crystals containing 1,4-tetrafluorophenylene units, *Liq. Cryst.* 21 (1996) 65–71.
- [5] R. Dąbrowski, J. Gąsowska, J. Otón, W. Piecek, J. Przedmojski, M. Tykarska, High tilted antiferroelectric liquid crystalline materials, *Displays* 25 (2004) 9–19.
- [6] R. Dąbrowski, P. Kula, Z. Raszewski, W. Piecek, J.M. Otón, A. Spadło, New Orthoconic Antiferroelectrics Useful for Applications, *Ferroelectrics.* 395 (2010) 116-132.
- [7] D. Ziobro, R. Dąbrowski, M. Tykarska, W. Drzewiński, M. Filipowicz, W. Rejmer, K. Kuśmierek, P. Morowiak, W. Piecek, Synthesis and properties of new ferroelectric and antiferroelectric liquid crystals with a biphenyl benzoate rigid core, *Liq. Cryst.* 39 (2012) 1011–1032.
- [8] H. T. Nguyen, J. C. Rouillon, A. Babeau, J. P. Marcerou, G. Sigaud, Synthesis, Properties and crystal structure of chiral semiperfluorinated liquid crystals with ferro and anticlinic smectic phases, *Liq. Cryst.* 26(1999) 1007–1019.
- [9] R. Dabrowski, Liquid crystals with fluorinated terminal chains and antiferroelectric properties, *Ferroelectrics.* 243 (2000) 1–18.

- [10] S. Seomun, T. Gouda, Y. Takanishi, K. Ishikawa, H. Takezoe, Bulk optical properties in binary mixtures of antiferroelectric liquid crystal compounds showing V-shaped switching, *Liq. Cryst.* 26 (1999) 151–161.
- [11] J. Dziaduszek, R. Dabrowski, K. Czuprynski, N. Bennis, Ferroelectric Compounds with Strong Polar Cyano Group in Terminal Position, *Ferroelectrics*. 343(2006)3–9.
- [12] J. Rutkowska, P. Perkowski, W. Piecek, J. Kedzierski, Z. Raszewski and J. Zielinski, Dielectric Spectroscopy of the Fluorinated AFLC's and Their Protonated Analogs, *Ferroelectrics*. 343 (2006) 151–160.
- [13] D. M. Potukuchi, A. K. George, C. Carboni, S. H. Alharthi, J. Naciri, Low Frequency Dielectric Relaxation, Spontaneous Polarization, Optical Tilt Angle and Response Time Investigations in a Flourinated Ferroelectric Liquid Crystal, N125F2(R\*), *Ferroelectrics*. 300(2004) 79–93.
- [14] D. M. Potukuchi, A. K. George, Phase Transitions and Characterization in a Chiral Smectic-A deVries Liquid Crystal by Low-Frequency Dielectric Spectroscopy, *Mol. Cryst. Liq. Cryst.* 487 (2008)92–109.
- [15] P. K. Mandal, S. Halder, A. Lapanik, and W. Haase, Induction and Enhancement of Ferroelectric Smectic C Phase in Multi-Component Room Temperature Mixtures, *Jpn. J. Appl. Phys.* 48 (2009) 011501(1-6)
- [16] K. Hiraoka, A. D. L. Chandani, E. Gorecka, Y. Ouchi, H. Takezoe, and A. Fukuda, Electric-Field-Induced Transitions among Antiferroelectric, Ferrielectric and Ferroelectric Phases in a Chiral Smectic MHPOBC, *Jpn. J. Appl. Phys.* 29 (1990) L1473-L1476.
- [17] Ł. Kolek, M. Massalska-Arodź, M. Paluch, K. Adrjanowicz, T. Rozwadowski, D. Majda, Dynamics in ferro- and antiferroelectric phases of a liquid crystal with fluorinated molecules as studied by dielectric spectroscopy, *Liq. Cryst.* 40 (2013)1082-1088.
- [18] M. Zurowska, R. Dabrowski, J. Dziaduszek, K. Czuprynski, K. Skrzypek, M. Filipowicz, Synthesis and Mesomorphic Properties of Chiral Esters Comprising Partially Fluorinated Alkoxyalkoxy Terminal Chains and a 1-methylheptyl Chiral Moiety, *Mol. Cryst. Liq. Cryst.* 495 (2008) 145-157.

- [19] J. Hamato, Y. Hanakai, Hirokazu Furue, H. Uehara, S. Saito, K. Murashiro, Phase Sequence in Smectic Liquid Crystals Having Fluorophenyl Group in the Core, *Jpn. J. Appl. Phys.* 33 (1994) 5498-5502.
- [20] P. K. Mandal, B. R. Jaishi, W. Haase, R. Dabrowski, M. Tykarska and P. Kula, Optical microscopy, DSC and dielectric relaxation spectroscopy studies on a partially fluorinated ferroelectric liquid crystalline compound MHPO(13F)BC. *Phase Transit.* 79 (2006) 223–235.
- [21] M. Marzec, A. Mikulko, S. Wrobel, R. Dabrowski, M. Darius and W. Haase, Alpha sub-phase in a new ferroelectric fluorinated compound, *Liq. Cryst.* 31 (2004) 153–159.
- [22] A. K. Srivastava, R. Dhar, V. K. Agrawal, S. H. Lee, and R. Dabrowski, Switching and electrical properties of ferro- and antiferroelectric phases of MOPB(H)PBC, *Liq. Cryst.* 35 (2008) 1101–1108.
- [23] Hyperchem 6.03, Hypercube Inc., Gainesville, FL, USA.
- [24] S. Haldar, K. C. Dey, D. Sinha, P. K. Mandal, W. Haase, P. Kula, X-ray diffraction and dielectric spectroscopy studies on a partially fluorinated ferroelectric liquid crystal from the family of terphenyl esters, *Liq. Cryst.* 39(10) (2012) 1196–1203.
- [25] A. de Vries. The description of the smectic A and C phases and the smectic A–C phase transition of TCOOB with a diffuse-cone model. *J. Chem. Phys.* 71 (1979) 25-31.
- [26] C. S. Hartley, N. Kapernaum, J. C. Robert, Frank Giesselmann, and R. P. Lemieux, Electroclinic effect in chiral SmA\* liquid crystals induced by atropisomeric biphenyl dopants: amplification of the electroclinic coefficient using achiral additives, *J. Mat. Chem.* 16 (2006) 2329-2337.
- [27] D. Sinha, A. Debnath, and P. K. Mandal, Hexatic and blue phases in a chiral liquid crystal: optical polarizing microscopy, synchrotron radiation and dielectric study, *Mat. Research Exp.* 1(2014)1-13.
- [28] M. Buivydas, F. Gouda, G. Andersson, S. T. Lagerwall, B. Stebler, Collective and non-collective excitations in antiferroelectric and ferroelectric liquid

- crystals studied by dielectric relaxation spectroscopy and electro-optic measurements, *Liq. Cryst.* 23(5) (1997) 723.
- [29] P. Perkowski, K. Ogrodnik, D. Lada, W. Piecek, J. Ruthkowska, Z. Raszewski, M. Zurowska, R. Dabrowski, X. Sun. Dielectric measurements of new antiferroelectric liquid crystals. 16(3) (2008) 277-280.
- [30] S. Ghosh, P. Nayek, S. Kr. Roy, T. P. Majumder and R. Dabrowski. Dielectric relaxation spectroscopy and electro-optical studies of a new, partially fluorinated orthoconic antiferroelectric liquid crystal material exhibiting V-shaped switching, *Liq. Cryst.* 37(4) (2010) 369–375.
- [31] K. C. Dey, P. K. Mandal, and R. Dabrowski, Influence of Bias on Dielectric Properties of Mesophases of a Laterally Fluorinated Antiferroelectric Liquid Crystal. *Springer Proceedings in Physics*, ‘Recent Trends in Materials Science and Applications’. Volume 89 (2016) 475-483.
- [32] Y. P. Panarin, O. Kalinovskaya, J. K. Vij, The Relaxation Processes in Helical Antiferroelectric Liquid Crystals, *Ferroelectrics*. 213 (1998) 101-108.
- [33] A. Fafara, M. Marzec, W. Haase, S. Wrobel, D. Kilian, M. Godlewska, K. Czuprinski, R. Dabrowski, Antiferroelectric Liquid Crystals Studied by Different Methods, *Ferroelectrics*. 245 (2000) 81-89.
- [34] P. Perkowski, K. Ogrodnik, W. Piecek, M. Zurowska, Z. Raszewski, R. Dabrowski, L. Jaroszewicz, Influence of the bias field on dielectric properties of the  $\text{SmC}_A^*$  in the vicinity of the  $\text{SmC}^* - \text{SmC}_A^*$  phase transition. *Liq. Cryst.* 38(16) (2011) 1159-1167.
- [35] F. Gouda, K. Skarp, S. T. Lagerwall, Dielectric studies of the soft mode and Goldstone mode in ferroelectric liquid crystals, *Ferroelectrics*. 113 (1991) 165-206.
- [36] T. Carlsson, B. Zeks, C. Filipic, A. Levstik, Theoretical model of the frequency and temperature dependence of the complex dielectric constant of ferroelectric liquid crystals near the smectic-C'-smectic- A phase transition, *Phys. Rev. A*. 42(2) (1990) 877-889.

- [37] J. M. Czerwiec, R. Dabrowski, K. Garbat, M. Marzec, M. Tykarska, A. Wawrzyniak, S. Wrobel, Dielectric and electro-optic behaviour of two chiral compounds and their antiferroelectric, *Liq. Cryst.* 39(12) (2012) 1503-1511.
- [38] M. Marzec, W. Haase, E. Jacob, M. Pfeiffer, S. Wrobel, The existence of four dielectric modes in the planar oriented  $S_C^*$  phase of a fluorinated substance, *Liq. Cryst.* 14 (2) (1993) 1967-1976.
- [39] S. Wrobel, G. Cohen, D. Davidov, W. Hasse, M. Marzec, M. Pfeiffer, Dielectric, electro-optic and x-ray studies of a room temperature ferroelectric mixture, *Ferroelectrics*. 166 (1995) 211-222.
- [40] M. Marzec, A. Mikułko, S. Wrobel, R. Dabrowski, M. Darius, W. Haase, Alpha sub-phase in a new ferroelectric fluorinated compound, *Liq. Cryst.* 31(2) (2004) 153–159.
- [41] B. Zeks and M. Cepic, A phenomenological model of antiferroelectric liquid crystals, *Liq. Cryst.* 14(2) (1993) 445–451.
- [42] D. Goswami, D. Sinha, A. Debnath, P. K. Mandal, S. K. Gupta, W. Haase, D. Ziobro, R. Dabrowski, Molecular and dynamical properties of a perfluorinated liquid crystal with direct transition from ferroelectric  $SmC^*$  phase to isotropic phase, *J. Mol. Liq.* 182 (2013) 95-101.
- [43] P. K. Mandal, B. R. Jaishi, W. Hasse, R. Dabrowski, M. Tykarska, P. Kula, Optical microscopy, DSC and dielectric relaxation spectroscopy studies on a partially fluorinated ferroelectric liquid crystalline compound MHPO(13F)BC, *Phase Transit.* 79(3) (2006) 223-235.
- [44] L. D. Landau, *Statistical Physics*, Pergamon Press, Oxford, 1980.
- [45] R. J. Birgeneau, C. W. Garland, A. R. Kortan, J. D. Lister, M. Meichle, B. M. Ocko, C. Rosenblatt, L. J. Yu, and J. Goodby, Smectic-A-smectic-C transition: Mean field or critical, *Phys. Rev. A.* 27(1983)1251.
- [46] R. Bartolino, J. Doucet and G. Durand, Molecular tilt in the smectic C phase: a zig-zag model, *Ann. de Phys.* 3 (1978) 389–395.
- [47] E. N. Keller, E. Nachaliel, and D. Davidov, Evidence for the “zig-zag” model of the smectic-C phase in the liquid crystal 4'-butoxyphenylester 4-

- decyloxybenzoic acid (4OP10O8): A high resolution x-ray study, *Phys. Rev. A.* 34 (5) (1986) 4363-4369.
- [48] M. S. Spector, P. A. Heiney, J. Naciri, B. T. Weslowski, D. B. Holt, and R. Shashidhar, Electroclinic liquid crystals with large induced tilt angle and small layer contraction, *Phys. Rev. E.* 61(2) (2000) 1579-1584.
- [49] J. G. Meier, M. Nobili, T. Carlsson, P. Rudquist, A. S. Petrenko, J. W. Goodby, M. Brunet, and S. T. Lagerwall, Possible model of an antiferroelectric twist grain boundary phase, *Phys. Rev. E.* 76 (2007) 011704(1-9).
- [50] L. A. Beresnev, L. M. Blinov, M. A. Osipov, S. A. Pikin, Ferroelectric Liquid Crystals, *Mol. Cryst. Liq. Cryst.* 158A (1988) 3–150.



# CHAPTER 4

---

## Formulation of a binary eutectic antiferro-electric liquid crystal mixture

4.1	INTRODUCTION	101
4.2	EXPERIMENTAL TECHNIQUES	102
4.3	RESULTS AND DISCUSSION	104
4.3.1	POLARIZING OPTICAL MICROSCOPY AND DSC STUDY	104
4.3.2	DIELECTRIC STUDY	106
4.3.2.1	SmC <sub>A</sub> * PHASE	106
4.3.2.2	SmC* PHASE	110
4.3.2.3	SmA* PHASE	113
4.3.3	ELECTRO-OPTIC STUDY	117
4.4	CONCLUSION	119
4.5	REFERENCES	120

---

Part of the work has been published in (i) Journal of Molecular Liquids, Vol.243 (2017), pp. 484-493, and (ii) Springer Proceedings in Physics, ‘Recent Trends in Materials Science and Applications, Vol. 89 (2016) 475-483.



## 4.1 INTRODUCTION

Antiferroelectric liquid crystals (AFLCs) of low melting point and stable phase in the desired temperature range of operation are of great importance. Although the synthesis of AFLCs with low melting point is not impossible [1], some problems are experienced in the stability of the phase. So preparing a mixture (binary or multi-component) is a useful technique [1]. However, the nature and concentration of the host and dopant influences the phase behaviour and properties of the resulting mixture enormously. It was observed in our laboratory that when one of the partially fluorinated compound (DM1), discussed in Chapter 3, was used as a dopant in an achiral host mixture, resulted in an electroclinic mixture with large field induced tilt and very small layer contraction at lower concentrations [2]. However, the same dopant at higher concentrations in the same host mixture resulted in a wide range ferroelectric mixtures with a few hundred microsecond switching time [3]. A different fluorinated chiral dopant, with oligomethylene spacer  $[C_4F_9-COO-(CH_2)_3O-Ph-Ph-OOC-Ph-O-CH^*(CH_3) C_6H_{13}]$  (4F3R), was found to produce a ferroelectric mixture with much faster response time in the same host mixture [4]. On the other hand, a binary mixture of one protonated oligomethylene spacer based chiral compound  $[C_4H_9-COO (CH_2)_6-O-Ph-Ph-OOC-Ph-O-CH^*(CH_3) C_6H_{13}]$  (4H3R), and one achiral biphenyl pyrimidine compound  $[C_8H_{17}O- Ph-Ph-Ph(N_2)-C_8H_{17}]$ , one of the component of the above host mixture, was found to exhibit room temperature ferroelectric mixture with moderate spontaneous polarization and sub-millisecond switching time [5]. Intermolecular attractive forces, like Van der Waals forces, hydrogen bonds and electron donor-acceptor interactions influence the configurations of molecular arrangements in the mesophases of a mixture. Each of these forces, collectively or separately, may be responsible for increasing or decreasing the stability of the liquid crystalline phases and appearance of new intermediate phases in some cases. Transition temperatures of binary mixtures are generally found to be in between those of the pure components [6]. But in case of eutectic mixture, the melting point is highly depressed.

In order to investigate how the properties of our studied biphenyl benzoate core-based homologous series change when mixed with one another, we select two compounds DM0, which is laterally protonated and DM3, which is laterally doubly fluorinated at benzoate core. As described in Chapter 3, these compounds have almost

the same melting points and with comparatively narrow range of antiferroelectric phase.

Five binary mixtures were formulated by mixing 20, 40, 50, 60 and 80 wt.% of DM3 in DM0, but observing that the 50 wt.% mixture (M3) is an eutectic mixture it was studied in detail by employing polarizing optical microscopy, dielectric spectroscopy and electro-optic techniques. The results of these studies are discussed in this Chapter and have been compared with those of the pure compounds [7].

It is worth mentioning here that a eutectic mixture is defined as a mixture of two or more components which usually do not interact to form a new chemical compound but which, at certain ratio, inhibit the crystallization process of one another resulting in a system having a lower melting point than either of the components [8]. The eutectic point of a binary mixture with respect to concentration and temperature can easily be found out by investigation of the phase diagram of the system [9].

## 4.2 EXPERIMENTAL TECHNIQUES

Mixtures of DM0 and DM3 were prepared by solution method. The desired weights of both the compounds were dissolved in chloroform and were sonicated for 1 hour using an ultrasonic mixture, GT Sonic Professional, Apex, India. The solution was then heated at a constant temperature  $\sim 60^{\circ}\text{C}$  for four hours in order to evaporate the chloroform completely from the solution. The complete evaporation of chloroform was confirmed by regaining the weight of the mixture. Phase behaviour and transition temperatures of the mixtures were investigated by polarizing optical microscopy (POM) ( $@ \pm 0.2^{\circ}\text{C}/\text{min}$ ) and differential calorimetric study (DSC) ( $@ 3^{\circ}\text{C}/\text{min}$ ). Dielectric and electro-optical studies were performed using Indium–Tin–Oxide (ITO) coated homogeneous (HG) cells of  $10 \mu\text{m}$  thickness. The sample was aligned applying an ac field of amplitude  $1.0 \text{ V}/\mu\text{m}$  and frequency  $10 \text{ Hz}$  during the cooling. Detailed procedure of preparation of the cell and experimental techniques are discussed in Chapter 2.

In order to study the molecular behaviour near transition from  $\text{SmA}^*-\text{SmC}^*$ , the temperature of the mixture was cooled very slowly at the rate of  $0.1^{\circ}\text{C}/\text{min}$ , from isotropic phase under the fixed bias fields of 0.5, 1.0, 1.5 and  $2.0 \text{ V}/\mu\text{m}$  and the dependence of  $\text{SmA}^*-\text{SmC}^*$  transition temperature ( $T_c$ ), critical frequency of soft mode ( $f_{SM}$ ), and dielectric increment ( $\Delta\epsilon_s$ ) were measured. The frequency response

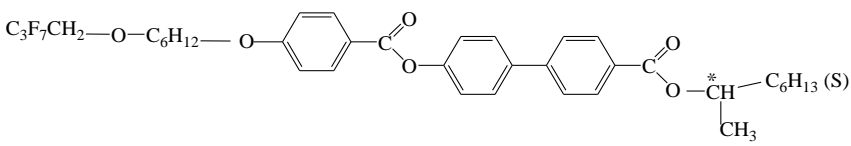
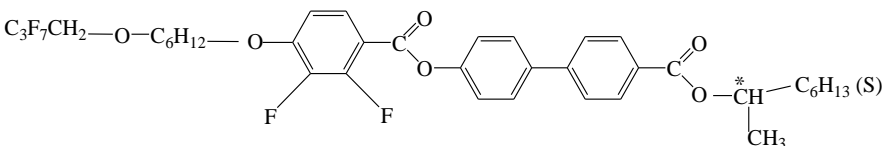
curves were fitted to the modified Cole–Cole equation to extract the dielectric increment ( $\Delta\epsilon$ ), relaxation frequency ( $f_c$ ) and symmetry parameter ( $\alpha$ ) of different modes.

As detailed in Chapter 2 the spontaneous polarization ( $P_s$ ) of the eutectic mixture was determined using polarization reversal current method [10]. The response time ( $\tau$ ), which is the most important parameter from the application point view, was determined using the square pulse method described in Chapter 2 [7, 11, 12]. The rotational viscosity ( $\gamma$ ) of the mixture was calculated using the formula [13]

$$\gamma = \tau \cdot P_s \cdot E \quad (4.1)$$

where  $E$  is the applied field.

**Table 4.1.** Formulae structures of DM0 and DM3, their transition temperatures and transition temperatures of the eutectic mixture M3.

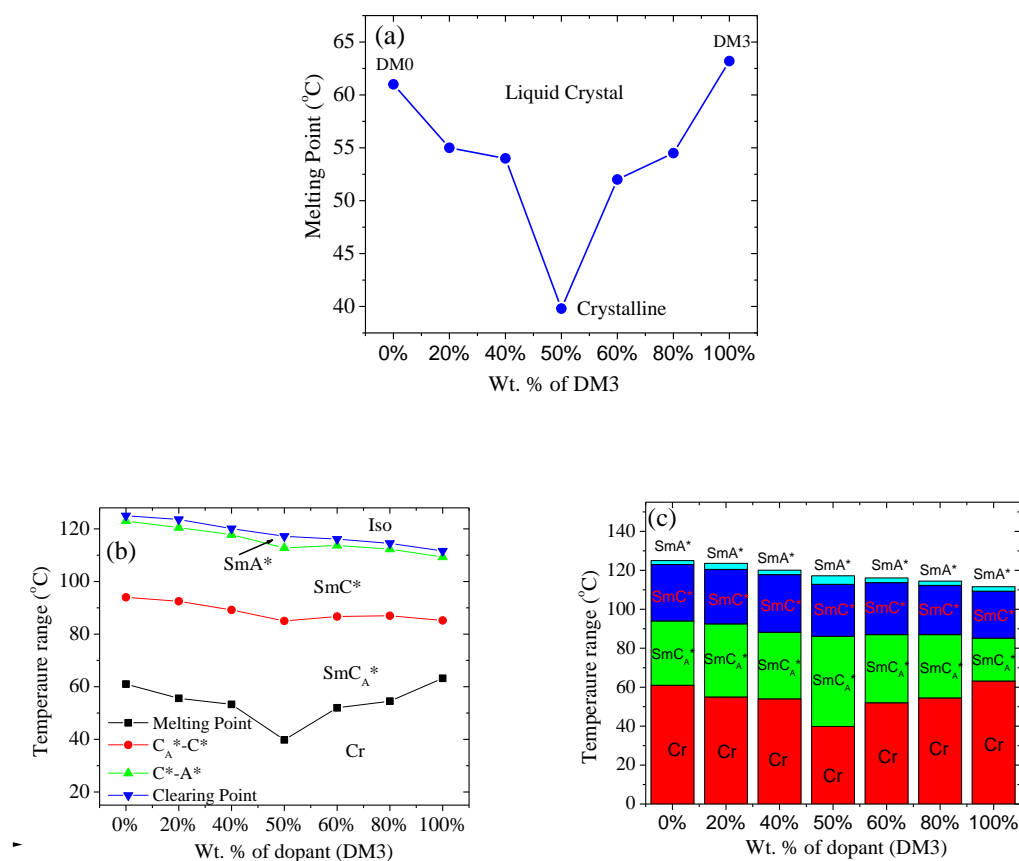
Name	Molecular structures and transition temperatures(in °C)
<b>DM0</b>	 <p>Cr 61.0 SmC<sub>A</sub>* 94.0 SmC* 123.0 SmA* 125.0 Iso (heating) Cr 26 SmC<sub>A</sub>* 83.0 SmC* 122.2 SmA* 124.4 Iso (cooling)</p>
<b>DM3</b>	 <p>Cr 63.2 SmC<sub>A</sub>* 85.2 SmC* 109.3 SmA* 111.6 Iso (heating) Cr 32.5 SmC<sub>A</sub>* 82.2 SmC* 109.1 SmA* 111.5 Iso (cooling)</p>
<b>M3</b> (Eutectic Mixture)	<p><b>DM0 + DM3 (50 wt. % of each)</b></p> <p>Cr 39.8 SmC<sub>A</sub>* 86.1 SmC* 112.8 SmA* 117.2 Iso (heating) Cr (~ -8.0) SmC<sub>A</sub>* (73.6) SmC* (112) SmA* (117.0) Iso (cooling)</p>

### 4.3. RESULTS AND DISCUSSIONS

#### 4.3.1 POLARIZING OPTICAL MICROSCOPY (POM) AND DSC STUDY

All the mixtures are found to exhibit paraelectric, ferroelectric and antiferroelectric phases. Although no new phase is observed, however, the transition temperatures are found to change significantly. Initially, we prepared 20, 40, 60 and 80 wt.% mixtures and the melting point was found to decrease gradually till 60 wt.% and at 80 wt.% it was found to increase although remained less than the pure compounds. Plotting the melting points of the mixtures with concentration an arc-like curve was obtained which meant that with increasing relative wt.% of DM3 the melting point initially decreased and then increased beyond a certain concentration.

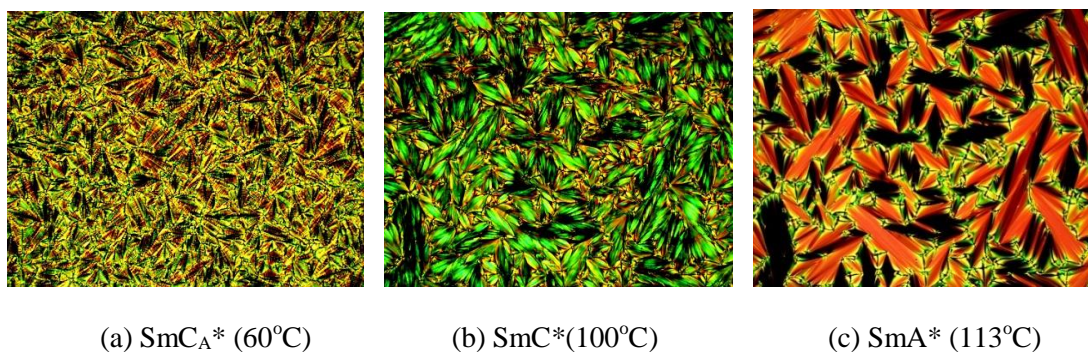
So we decided to prepare a mixture with equal wt. % of DM3 and DM0 and the melting point of this mixture was observed to be the lowest (39.8°C), far below than those of the mixtures of the nearest concentrations (40 wt. % and 60 wt. %). We considered this mixture (M3) to be eutectic. We, of course, did not prepare mixtures near M3 with a concentration difference of less than 10%. The phase sequence and transition temperatures of the mixing compounds and the eutectic mixture (both during heating and cooling) are shown in **Table 4.1**. The transition temperatures of all the mixtures with varying concentrations, obtained during heating are furnished in **Table 4.2**. Although no significant change in thermal stability of the phases (except  $\text{SmC}_A^*$ ) is observed, the mixture M3 remains in  $\text{SmC}_A^*$  phase till about  $-8^\circ\text{C}$  due to super cooling effect and then crystallized. It is to be noted that pure compounds also show super cooling behaviour. Sometimes new phases appear in the mixed systems where the molecules differ in polarity [14–20]. In the present case, the molecules are of the same polarity, probably that is why no new phases are observed. The phase diagram and bar diagram of different phases of the mixtures are represented in **Figure 4.1**.



**Figure 4.1.** (a) Diagram of state showing melting points of the binary mixtures of DM0 and DM3, (b) Phase diagram (c) bar diagram of different phases of the mixtures (heating cycle).

**Table 4.2.** Transition temperatures of mixtures (DM0+DM3) as obtained from texture study during heating

DM3 (wt.%)	Mixture		Transition Temperatures (°C)							
0	DM0	Cr	61.0	SmC <sub>A</sub> *	94.0	SmC*	123.0	SmA*	125.0	Iso
20	M1	Cr	55.0	SmC <sub>A</sub> *	92.5	SmC*	120.5	SmA*	123.6	Iso
40	M2	Cr	54.0	SmC <sub>A</sub> *	88.2	SmC*	117.8	SmA*	120.1	Iso
50	M3	Cr	39.8	SmC <sub>A</sub> *	86.1	SmC*	112.8	SmA*	117.2	Iso
60	M4	Cr	52.0	SmC <sub>A</sub> *	87.0	SmC*	113.7	SmA*	116.1	Iso
80	M5	Cr	54.5	SmC <sub>A</sub> *	87.0	SmC*	112.3	SmA*	114.5	Iso
100	DM3	Cr	63.2	SmC <sub>A</sub> *	85.2	SmC*	109.3	SmA*	111.6	Iso



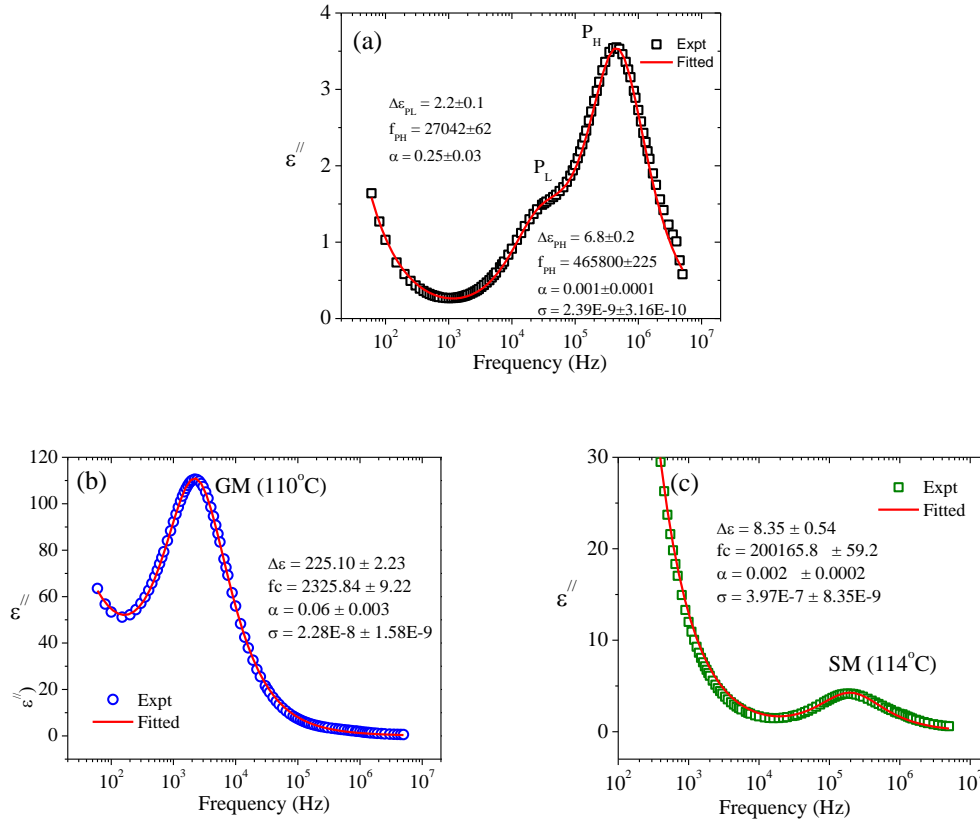
**Figure 4.2.** Observed textures of M3 in (a) SmC<sub>A</sub>\*, (b) SmC\* and (c) SmA\* phases

## 4.3.2 DIELECTRIC STUDY

### 4.3.2.1 SmC<sub>A</sub>\*PHASE

Representative fitted absorption spectra depicting different relaxation modes (P<sub>L</sub>, P<sub>H</sub>, GM and SM) observed in the eutectic mixture M3 are shown in **Figure 4.3**. The temperature dependence of critical frequencies of all the observed modes in all phases and their absorption strengths are presented in **Figure 4.4**. In the absorption spectra, the mixture exhibits two collective modes in SmC<sub>A</sub>\* phase: one in low frequency region and other in high frequency region. Usually, they are termed as P<sub>L</sub> and P<sub>H</sub> mode of relaxations [7, 21–25]. P<sub>L</sub> is observed to appear at temperatures far below the transition temperature T<sub>AF</sub> (SmC\*–SmC<sub>A</sub>\*) during cooling; transition takes place at 72.5°C but P<sub>L</sub> arises from 40°C [**Figure 4.4**]. Similar phenomenon was noticed in the pure compound DM0 in which T<sub>AF</sub> was 84°C and P<sub>L</sub> began at 46°C [7]. In the mixture, the P<sub>L</sub> mode is strong enough and its dielectric absorption strength ( $\epsilon''_{PL}$ ) and critical frequency ( $f_{PL}$ ) are observed to decrease with decreasing temperature ( $\epsilon''_{PL}$ : 1.54–1.39 and  $f_{PL}$ : 37.5–22 kHz) [**Figure 4.4**]. A similar strong P<sub>L</sub> was observed in DM0 in which absorption strength was observed to decrease from 1.9 to 0.25. However, P<sub>L</sub> was not observed in DM3 due to large ionic contribution. But when a weak bias was applied, it was revealed from T<sub>AF</sub> (79 °C) and the absorption intensity  $\epsilon''_{PL}$  went stronger (6.5–13.5 kHz) with decreasing temperature unlike in DM0 and M3. Critical frequencies of P<sub>L</sub> of M3 are found to decrease with decreasing temperature from 37.5 kHz to 22 kHz which is intermediate between those of the pure compounds DM0 (195 kHz to 30 kHz, decreasing with decreasing T) and DM3 (6.5 kHz to 13.5 kHz, increasing with decreasing T), but not proportional to their concentration. The slope of variation of  $f_{PL}$  with temperature is positive and very high

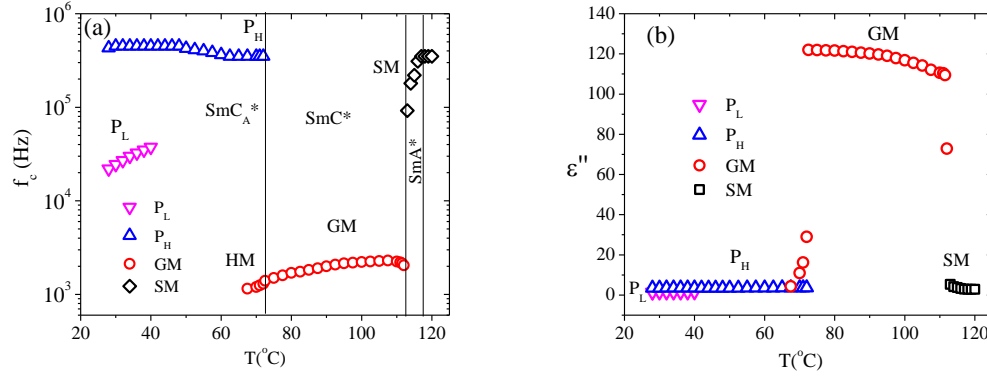
in DM0 (10.70) whereas it is small negative in case of DM3 ( $-0.20$ ). But in the mixture M3, although in it pure compounds were mixed in 50 wt. % of each, the slope is still positive but has a lower value (1.30) in comparison to DM0. So it may be inferred that the slope of  $f_{PL}$  versus temperature curve decreases with increasing wt.% of DM3 and at a certain wt.% it becomes zero and then on a further increase of concentration of DM3, it becomes negative.



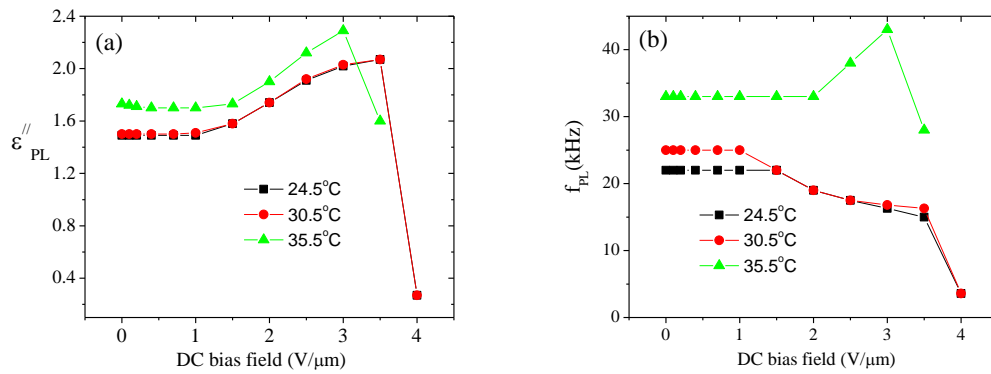
**Figure 4.3.** Fitted absorption spectra of the mixture M3 (a) in  $SmC_A^*$  phase at 30°C showing two modes  $P_L$  and  $P_H$ , (b) in  $SmC^*$  phase at 110°C and showing GM and (c) in  $SmA^*$  phase at 114°C showing soft mode. Fitted parameters are also shown.

On the other hand, the  $P_H$  mode of the mixture appears just from the transition  $T_{AF}$ . The critical frequency of  $P_H$  mode ( $f_{PH}$ ) is observed to increase gradually from 350 kHz to 450 kHz with the decrease of temperature [Figure 4.4]. Similar behaviour was seen in pure DM0 and DM3. The observed values of  $f_{PH}$  of the mixture are less than that of DM0 (580 kHz to 925 kHz) but higher than that of DM3 (22.5 kHz to 125 kHz) and the values are nearly proportional to their concentration. However, the absorption strength of  $P_H$  mode ( $\epsilon''_{PH}$ ) remains almost unchanged with temperature,

decreases from 3.66 (72 °C) to 3.53 (28°C) over the entire temperature range of  $\text{SmC}_A^*$  phase during cooling. Similar nature of variation of  $\varepsilon_{PH}''$  was observed in DM0 ( $\varepsilon_{PH}''$ : 2.8–2.75) and DM3 ( $\varepsilon_{PH}''$ : 3.14–2.72).



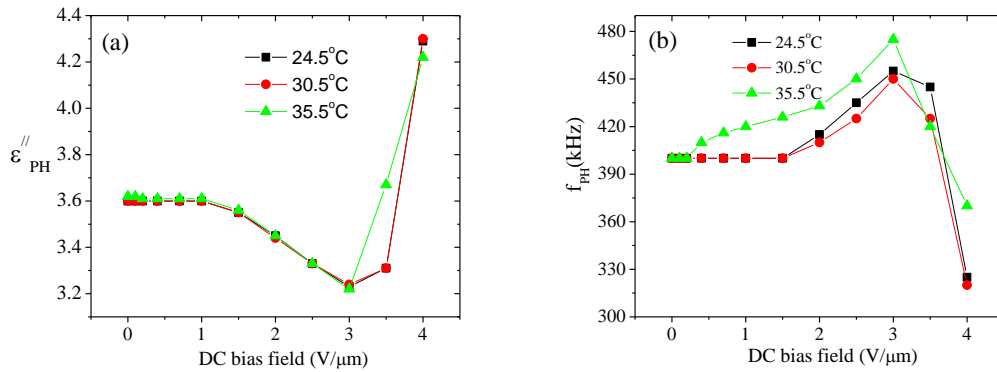
**Figure 4.4.** (a) Critical frequencies of all the observed collective modes of relaxations – soft mode in  $\text{SmA}^*$ , Goldstone mode in  $\text{SmC}^*$ , in-phase ( $P_L$ ) and anti-phase ( $P_H$ ) modes in  $\text{SmC}_A^*$  (b) their absorption strengths.



**Figure 4.5.** Bias field dependence of (a)  $\varepsilon_{PL}''$  and (b)  $f_{PL}$  of M3 at different temperatures in  $\text{SmC}_A^*$  phase.

The dielectric spectroscopy in the presence of bias field is very crucial to probe the molecular dynamics of a liquid crystalline phase. The mixture M3 was, therefore, studied under varying bias fields in  $\text{SmC}_A^*$  phase at three fixed temperatures 24.5°C, 30.5°C and 35.5°C in the low temperature regime of  $\text{SmC}_A^*$  phase. Both the collective modes are found to be influenced by the bias field. The absorption strength of the  $P_L$  mode remains initially constant and then increases gradually with bias at all three temperatures and begins to fall at field 3.5 V/μm at 24.5°C and 30.5°C and at 3.0 V/μm at 35.5°C and is suppressed at field 4.0 V/μm at

all temperatures [Figure 4.5(a)]. But in the pure compounds DM0 and DM3, the  $\varepsilon_{PL}''$  was found to decrease with the gradual increase of bias and finally suppressed at 1.95 V/ $\mu\text{m}$  and 1.37 V/ $\mu\text{m}$  respectively. It is clear that in the mixture the bias dependence of  $\varepsilon_{PL}''$  is opposite to that of its constituent compounds in which  $\varepsilon_{PL}''$  decreased gradually with bias. The critical field for suppression of the  $P_L$  mode is also found to increase significantly in the mixture. A similar increase of absorption strength of  $P_L$  mode with bias was reported earlier by several authors [21, 22, 25].



**Figure 4.6.** Bias field dependence of (a)  $\varepsilon_{PH}''$  and (b)  $f_{PH}$  of M3 at different temperatures in  $\text{SmC}_A^*$  phase.

The critical frequency of  $P_L$  mode ( $f_{PL}$ ) remains initially constant with increasing bias field and then decreases and finally suppressed [Figure 4.5(b)]. At 24.5°C, the  $f_{PL}$  remains constant at 22 kHz up to 1.5 V/ $\mu\text{m}$ , then it decreases gradually and suppressed at 4.0 V/ $\mu\text{m}$ . Similarly at 30.5°C, it remains constant at 25 kHz up to 1.0 V/ $\mu\text{m}$  and then decreases gradually with bias and is suppressed at 4.0 V/ $\mu\text{m}$ . But at 35.5°C the value of  $f_{PL}$  is considerably higher (~33 kHz) and increases with bias after 2.0 V/ $\mu\text{m}$  unlike at 24.5°C and at 30.5°C, however, finally it is also suppressed at 4.0 V/ $\mu\text{m}$ .

On the other hand, the value of  $\varepsilon_{PH}''$  decreases gradually with bias from 3.62 to 3.22 up to 3.0 V/ $\mu\text{m}$  at all three temperatures and then at 24.5°C and 30.5°C, it begins to increase and after field 3.5 V/ $\mu\text{m}$ , it increases sharply to reach 4.3 at 4.0 V/ $\mu\text{m}$ ; but at 35.5°C it increases sharply right from 3.0 V/ $\mu\text{m}$  and reaches the same value (4.3) at 4.0 V/ $\mu\text{m}$  (at which  $P_L$  is suppressed) [Figure 4.6(a)]. The critical frequency  $f_{PH}$  remains initially constant at 400 kHz up to 1.5 V/ $\mu\text{m}$  at 24.5°C and 30.5°C and up to 0.2 V/ $\mu\text{m}$  at 35.5°C, then increases gradually with field up to 3.0 V/ $\mu\text{m}$  and then begins to decrease. After field 3.5 V/ $\mu\text{m}$   $f_{PH}$  decreases sharply (to 325 kHz at 24.5°C,

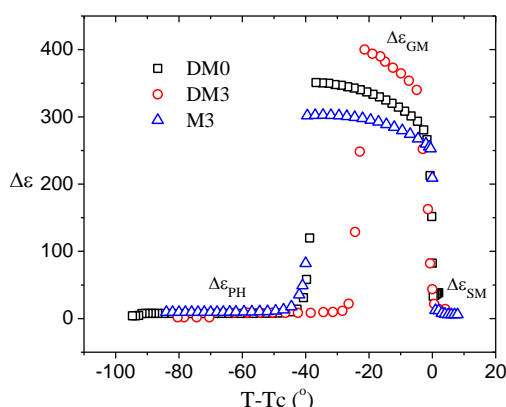
to 320 kHz at 30.5°C kHz) at 4.0 V/ $\mu\text{m}$ , but at 35.5°C this sharp decrease in  $f_{PH}$  starts after 3.0 V/ $\mu\text{m}$  and reaches 370 kHz at 4.0 V/ $\mu\text{m}$  [**Figure 4.6(b)**]. This implies that the absorption strength  $\varepsilon''_{PH}$  gets stronger and the relaxation frequency  $f_{PH}$  decreases sharply after a certain value of bias field (at all temperatures) at which the  $P_L$  mode begins to suppress.

The strong correlation of bias dependence of absorption strengths of  $P_L$  and  $P_H$  modes indicates that their origin should be correlated. J. Hou *et al.* [21] reported that the modes  $P_L$  and  $P_H$  might arise due to in-phase and anti-phase fluctuation of molecules in the adjacent smectic layers and at a sufficiently high field the transition from antiferroelectric to the ferroelectric conformation was induced and both the modes were suppressed at the same bias field. However, assuming antiferroelectric polarization, Yu. Panarin *et al.* [26] explained the low frequency mode as antiferroelectric Goldstone mode and strength of this mode was found to be ~3% of Goldstone mode of  $\text{SmC}^*$  phase. This is in good agreement with our experimental results. Even the complete suppression  $P_L$  mode at a sufficient bias field can also be successfully explained since bias field unwinds the helical structure, but getting stronger  $P_L$  with bias, also observed before [22, 24], cannot be explained.  $P_L$  was designated as antiferroelectric Goldstone mode for some similarity with its  $\text{SmC}^*$  counterpart [22] but it might not carry all the properties of ferroelectric Goldstone mode, moreover, the origin of polarization in  $\text{SmC}_A^*$  and  $\text{SmC}^*$  phases are different. Neither of the above models enlighten about stronger  $P_H$  mode at the suppression of  $P_L$ .

#### 4.3.2.2 $\text{SmC}^*$ PHASE

The dielectric response of a ferroelectric system exhibiting  $\text{SmC}^*$  and  $\text{SmA}^*$  phase consists of four modes of relaxations two of which are Goldstone mode (GM) and soft mode, related to the collective director fluctuations, lie in a few hundred Hz to a few hundred kHz range and have been studied within our frequency domain (50 Hz–5 MHz). The other two modes are molecular, related to the fluctuation of polarization and observed in the frequency range of several hundred kHz to a few GHz. Although the reorientation about the short molecular axes takes place in the range of several hundred kHz to several MHz it is not usually visible by dielectric

spectroscopy when the planar orientation of the molecules exists in the measuring cell.



**Figure 4.7.** Comparison of dielectric increment ( $\Delta\epsilon$ ) of M3 with those of its constituents.

GM arises from the phase fluctuation of the director and its amplitude is high and hence the dielectric increment ( $\Delta\epsilon_{GM}$ ) is high and corresponding relaxation frequency ( $f_{GM}$ ) is low. Both  $\Delta\epsilon_{GM}$  and  $f_{GM}$  are feebly temperature dependent. The weak temperature dependence of dielectric increment can be explained by considering coupling between tilt and polarization in the free energy density of classical Landau model and that of the critical frequency ( $f_c$ ) is due to the temperature dependent elastic constant, rotational viscosity and pitch of the helix on which  $f_c$  depends [27-28]. Observed temperature dependence of dielectric strength ( $\Delta\epsilon$ ) of the Goldstone mode of the mixtures is similar, however, it is lower (302) in the eutectic mixture compared to pure DM0 (350) and DM3 (400) as shown in **Figure 4.7**. This figure also shows the typical temperature dependence of dielectric strength in a compound having antiferroelectric, ferroelectric and paraelectric phases.

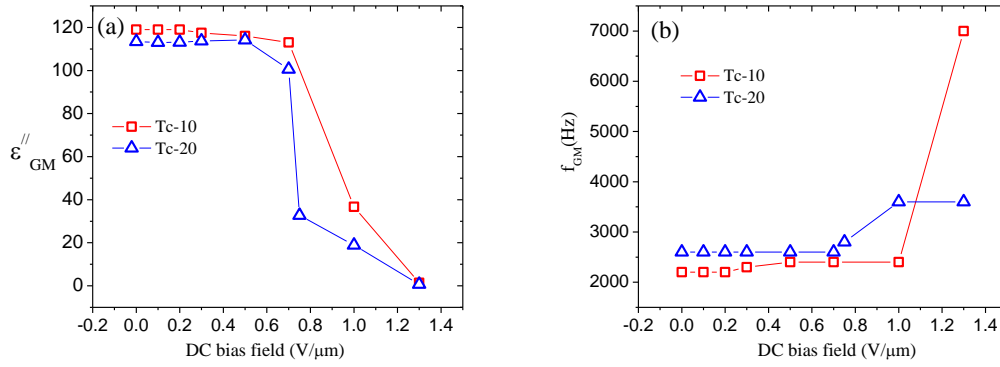
The critical frequency of Goldstone mode of M3 decreases from 2250 Hz to 1150 Hz with the decrease of temperature [**Figure 4.4**]. A similar decrease  $f_{GM}$  was observed by Goswami *et al.* [28] in a ferroelectric compound having a direct transition from  $SmC^*$  to Isotropic phase. The temperature dependence of  $f_{GM}$  in ferroelectric liquid crystals was also reported by several authors [29-31]. The mode was observed to penetrate almost 5.0 °C into the  $SmC_A^*$  phase (transition  $SmC^*$ – $SmC_A^*$  takes place at 72.5°C and GM persists till 67.5°C). This mode in the regime of  $SmC_A^*$  phase is usually termed as hereditary mode (HM) which arises due to the

incomplete conformation of molecular arrangement [7, 22]. The dielectric increment of this mode is larger than  $P_L$  mode and is suppressed at the lower field [21, 32]. The field dependent dielectric study on GM in  $SmC^*$  phase is performed at two temperatures:  $T_c-10$  (i.e. 102°C) and  $T_c-20$  (i.e. 92°C) in the mixture. The depression of the absorption strength of Goldstone mode ( $\epsilon''_{GM}$ ) starts at 0.7 V/ $\mu m$  and suppressed at 1.3 V/ $\mu m$  at both the temperatures [Figure 4.8(a)]. The dc bias electric field at which Goldstone mode is suppressed is termed as the critical field ( $E_c$ ). The value of  $E_c$  is the same (1.3V/ $\mu m$ ) at both the temperatures, although its temperature dependence was observed at lower fields. The critical field for the suppression of Goldstone mode ( $E_c$ ), dielectric increment ( $\Delta\epsilon'_{GM}$ ) and critical frequency ( $f_{GM}$ ) of M3 and those of the pure compounds at  $T_c-10$  have been listed in Table 4.3 for comparison.  $E_c$  in M3 is found to be almost double compared to DM0. However  $\Delta\epsilon_{GM}$  was less than the pure compounds while  $f_{GM}$  was found to have intermediate values.

**Table 4.3.** Comparison of  $E_c$  at  $T_c-10$ ,  $\Delta\epsilon_{GM}$ , and  $f_{GM}$  of the mixture M3 with DM0 and DM3

Parameter	DM0	DM3	M3
$E_c$ (V/ $\mu m$ )	0.68	0.93	1.3
$\Delta\epsilon_{GM}$	310	322	289
$f_{GM}$ (Hz)	1200–2800	450–1800	1150–2250

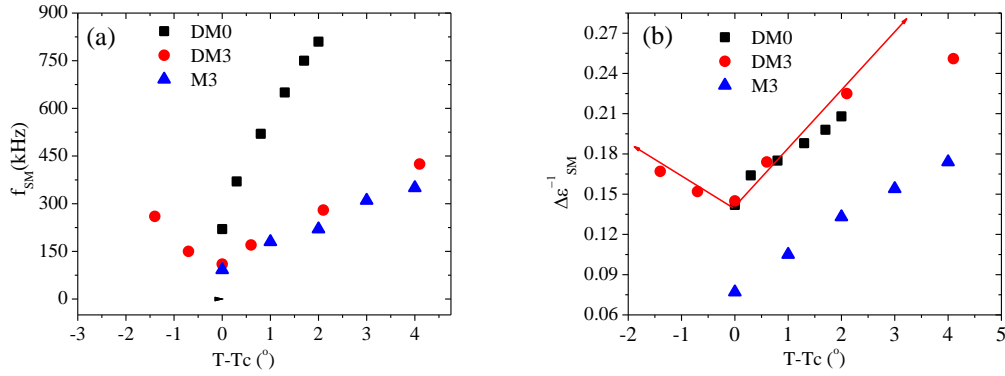
The  $f_{GM}$  at  $T_c-10$  remains almost constant at 2200 Hz up to the bias field 1.0 V/ $\mu m$  before it increases sharply to 7.0 kHz at 1.3 V/ $\mu m$  until suppression. Similarly at  $T_c-20$ ,  $f_{GM}$  remains constant at 2600 Hz up to field 0.7 V/ $\mu m$  and then increases to 3600 Hz and remains constant till the suppression [Figure 4.8(b)]. This large increase in  $f_{GM}$  at  $T_c-10$  and small increase at  $T_c-20$  just before its suppression does not, however, represent the appearance of domain mode (DM) because, usually the DM has critical frequency about 2–10 times higher than that of GM and remains unchanged with increasing dc bias, as was observed in the pure compounds [7]. Suppression of Goldstone mode by the electric field is due to the unwinding of the helical structure [33–34]. During this structural change, the molecules become rigid and hence critical frequency of fluctuation shifts to higher ranges.



**Figure 4.8.** Bias dependence of (a) absorption strength  $\epsilon''_{GM}$  and (b) critical frequency  $f_{GM}$  of the mixture M3 compared at two temperatures  $T_c-10$  and  $T_c-20$ .

#### 4.3.2.3. SmA\* PHASE

Near SmA\*–SmC\* transition the molecules lying in orthogonal bookshelf geometry undergo a collective tilt fluctuation, the amplitude of which is small [dielectric increment~ 5–10] and the corresponding relaxation frequency is high [~ few hundred kHz] and this mode is known as soft mode (SM). On approaching SmA\* to SmC\* transition, binding forces (also corresponding elastic modulus) of the molecules get soft against this fluctuation, which results in increasing amplitude (hence dielectric permittivity) and decreasing relaxation frequency with decreasing temperature. After the SmA\*–SmC\* transition, the molecules get tilted and relaxation mode due to phase fluctuation with large amplitude begins to arise (GM), but the tilt fluctuation persists and its amplitude decreases and corresponding relaxation frequency increases. So the dielectric increment ( $\Delta\epsilon_{SM}$ ) or absorption ( $\epsilon''_{SM}$ ) diverges, and the critical frequency ( $f_{SM}$ ) converges near  $T_c$  producing a ‘V’ shape following Curie–Weiss law [35]. Temperature dependence of  $f_{SM}$  and  $\epsilon''_{SM}$  of M3 in comparison to DM0 and DM3, without bias field, is shown the **Figure 4.9**. Soft mode is detected in both DM0 and M3 only in SmA\* phase, while it is observed in both SmA\* and SmC\* phases in DM3 depicting the ‘V’ shape variation of  $f_{SM}$  and  $\Delta\epsilon_{SM}^{-1}$  with temperature. The range of critical frequencies of soft mode in SmA\* phase in M3 [92–310 kHz] is lower



**Figure 4.9.** Temperature variation of (a)  $f_{SM}$  and (b)  $\Delta\epsilon_{SM}^{-1}$  of DM0, DM3 and M3 without bias.

than that in DM0 [220–810 kHz] and DM3 [110–425 kHz] but the soft mode dielectric increment of M3 is higher [5.75–13.00] than that of DM0 [4.8–7.03] and DM3 [3.98–6.9]. In the presence of high bias field ( $>E_c$ ), SM is also observed in SmC\* phase in DM0 and M3. For example, at  $T_c-10$ , in DM0 the SM is observed at 700 kHz with bias field of 1.0 V/ $\mu\text{m}$ , while in M3 it is observed at 325 kHz with bias field of 1.6 V/ $\mu\text{m}$ . The influence of bias on the dielectric properties of the soft mode near SmC\*–SmA\* was investigated by several authors [36–38]. Gouda *et al.* [36] investigated experimentally the influence of the bias field on the soft mode part of dielectric constant and observed only close to  $T_c$  it was influenced. They gave a theoretical explanation of the observed phenomena. J. Schacht *et al.* [37] using Landau free energy expression established a linear dependence of the minimum value of  $f_{SM}$  and minimum value of  $\Delta\epsilon_{SM}^{-1}$  with reduced temperature in the vicinity of  $T_c$ . C. Bahr *et al.* [38] studied the influence of dc electric field on a first order SmA\* to ferroelectric SmC\* liquid crystal phase transition and observed that the discontinuity of tilt angle, polarization vanishes when the field strength exceeds a critical value.

Soft mode normally appears in SmA\* phase just above the SmA\* to SmC\* transition temperature ( $T_c$ ), but in a dc bias field, the SM begins to appear from temperature higher than  $T_c$ , implying that the  $T_c$  is influenced by the bias field. The  $T_c$  is observed to increase linearly with increasing bias in the mixture M3 [Figure 4.10]. This phenomenon was theoretically explained using the classical Landau model [27, 38]. The Gibbs free energy density for helix free SSFLC cell in presence of bias field ( $E$ ), is expressed as

$$g = g_0 + \frac{1}{2}a\theta^2 + \frac{1}{2}b\theta^4 + \frac{P^2}{2\varepsilon_0\chi_\infty} - CP\theta - PE \quad (4.2)$$

where,  $a$  and  $b$  are the first and second coefficient in the Gibbs free energy expansion, and  $a$  is assumed to be linearly dependent on  $(T - T_c)$  and is expressed as

$$a = \alpha(T - T_c) \quad (4.3)$$

$\chi_\infty$ , is high frequency dielectric susceptibility and  $C$  is the coupling coefficient of tilt ( $\theta$ ) and polarization ( $P$ ). The important feature of the model is the presence of coupling between tilt and polarization in the free energy density of the system.

Introducing  $x = T - T_c$  and  $y = 1/\Delta\varepsilon$ , Schacht *et al.* [37] obtained,

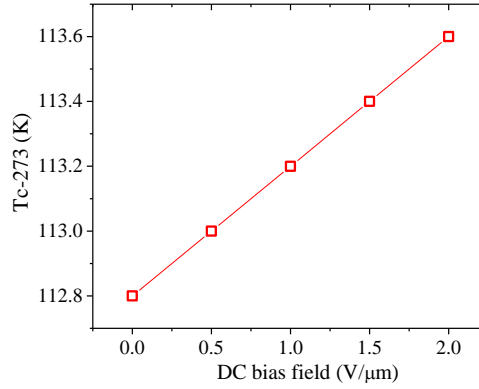
$$y_m = \frac{2\alpha x_m}{\varepsilon_0\chi_\infty^2 C^2} \quad (4.4)$$

where  $x_m$  and  $y_m$  are the values of  $x$  and  $y$  at the minimum condition.

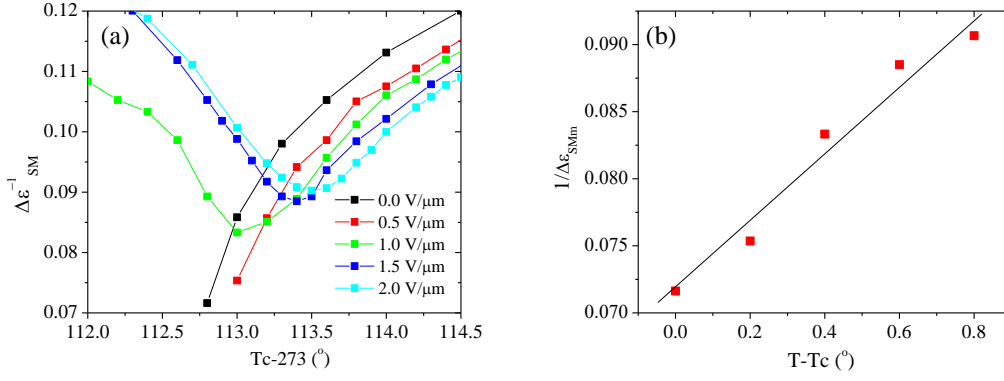
Similarly, the minimum of relaxation frequency  $f_{SMm}$  is obtained as

$$f_{SMm} = \frac{\alpha}{\pi\gamma_\theta} x_m \quad (4.5)$$

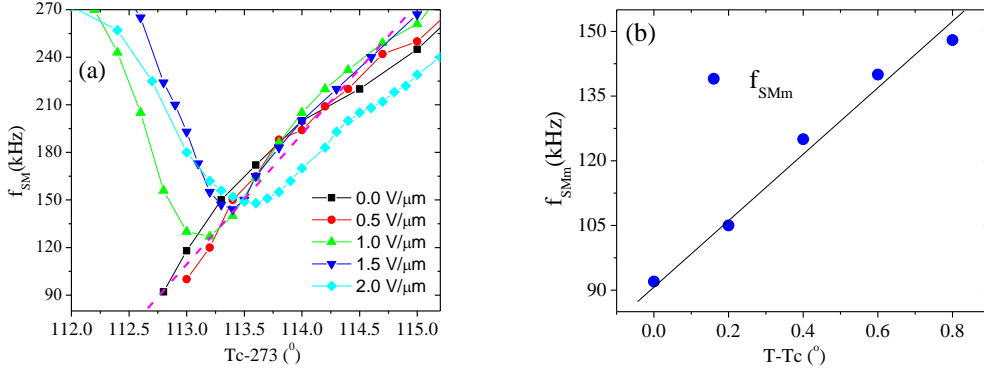
$\gamma_\theta$  is the dissipation coefficient of relaxation of  $\theta$  of the soft mode.



**Figure 4.10.** Critical temperature ( $T_c$ ) as a function of bias electric field.



**Figure 4.11.** (a) Inverse of dielectric increment of soft mode ( $\Delta\epsilon_{SM}^{-1}$ ) as a function of reduced temperature at different bias field, (b) Minimum value of inverse of dielectric increment of soft mode ( $\Delta\epsilon_{SMm}^{-1}$ ) as a function of  $(T - T_c)$ .



**Figure 4.12.** (a) Relaxation frequency of the soft mode ( $f_{SM}$ ) as a function of reduced temperature at different bias field, (b) Minimum value of relaxation frequency of the soft mode ( $f_{SMm}$ ) as a function  $(T - T_c)$ .

Above equations (4) and (5) imply that the minima  $y_m$  and  $f_{SMm}$  will lie on a line. The plot of  $\Delta\epsilon_{SM}^{-1}$  vs  $T$  for different bias field has been shown in the **Figure 4.11(a)**, where the minimum values of ( $\Delta\epsilon_{SM}^{-1}$ ) lie on the dotted line obeying the relation (4). The linear nature of the minimum values of  $\Delta\epsilon_{SMm}^{-1}$  as a function of  $T - T_c$  is shown in **Figure 4.11(b)**. Similarly,  $f_{SM}$  vs  $T$  for different bias field has been shown in the **Figure 4.12(a)**, where the minimum values of  $f_{SM}$  ( $f_{SMm}$ ) lie on a dotted line obeying the relation (5). The dependence of  $f_{SMm}$  on  $T - T_c$  has been shown in **Figure 4.12(b)**. The bias dependence of critical temperature ( $T_c$ ), minimum relaxation frequency of soft mode ( $f_{SMm}$ ), and dielectric strength ( $\Delta\epsilon_{SMm}^{-1}$ ) are compiled in **Table 4.4** for ease of comparison.

**Table 4.4.** Field dependence of  $T_c$ ,  $f_{SMm}$  and  $\Delta\epsilon_{SMm}^{-1}$ 

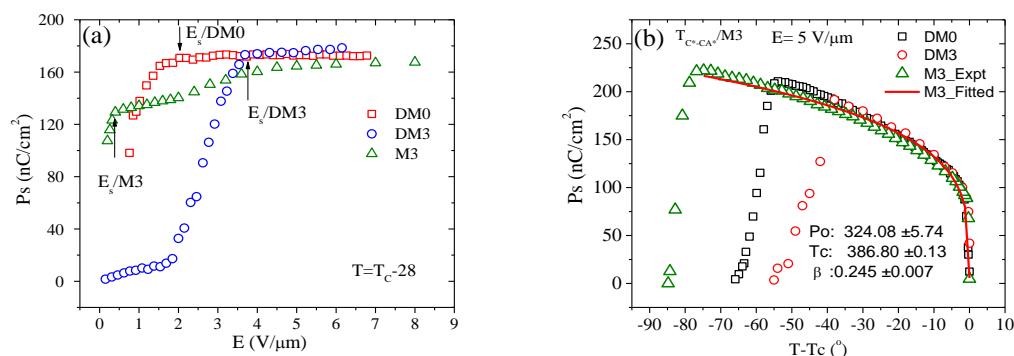
Field (V/ $\mu$ m)	$T_c$ -273.5 (K)	$f_{SMm}$ (kHz)	$\Delta\epsilon_{SMm}$	$\Delta\epsilon_{SMm}^{-1}$
0.0	112.8	92	13.96	0.0716
0.5	113.0	105	13.27	0.0753
1.0	113.2	125	11.75	0.0851
1.5	113.4	140	11.30	0.0885
2.0	113.5	148	11.08	0.0908

### 4.3.3 ELECTRO-OPTIC STUDY

The ac field dependence of spontaneous polarization ( $P_s$ ) of M3 in comparison to those of DM0 and DM3 at ( $T_c$ -28) is shown in **Figure 4.13(a)**.  $P_s$  increases with the field ( $E$ ) initially and then becomes saturated at the saturation field  $E_s$ . The saturation field is found to be 2.03 V/ $\mu$ m for DM0 and 3.69 V/ $\mu$ m for DM3. However, in M3 the dependence of  $P_s$  on  $E$  at the same reduced temperature is slightly different. Increase of  $P_s$  in the field range 0.4 – 2.0 V/ $\mu$ m is slower.  $P_s$  reaches the saturation value of 162.0 nC/cm<sup>2</sup> at 4.0 V/ $\mu$ m, which is at the midway of those of DM0 (170.8 nC/cm<sup>2</sup>) and DM3 (173.3 nC/cm<sup>2</sup>).  $P_s$  as a function of temperature at the saturated field (5V/ $\mu$ m) has been depicted in **Figure 4.13(b)**. The maximum value of  $P_s$  in DM0 is 210.8 nC/cm<sup>2</sup> at 69°C, 191.7 nC/cm<sup>2</sup> at 70°C in DM3 whereas in M3 it is 221.7 nC/cm<sup>2</sup> at 42°C. Experimental  $P_s$  values of M3 were fitted to the mean-field equation [39]

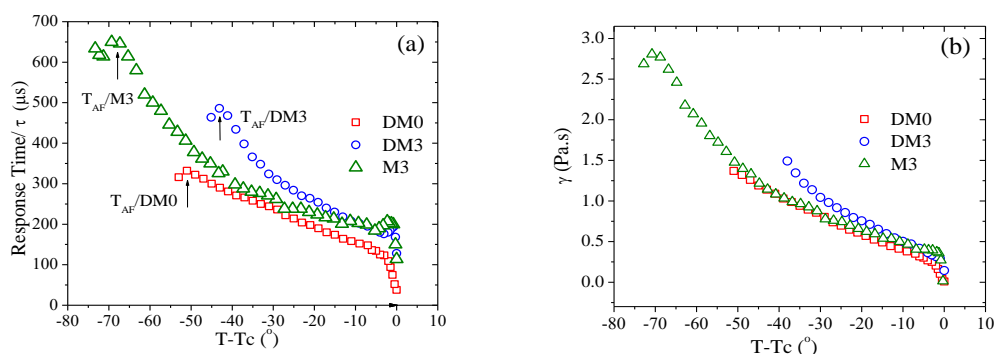
$$P_s = P_o(1 - T/T_c)^\beta \quad (4.6)$$

From the fitted curve, the transition temperature  $T_c$  is determined which matches nicely with the experimental result. The critical exponent  $\beta$  is obtained as 0.25; such  $\beta$  value is expected in the case of second order transition approaching the tricritical point [40-41]. Thus the paraelectric to ferroelectric transition of the mixture is tricritical in nature. The mixing compounds DM0 and DM3 also showed similar nature of transition as discussed in Chapter 3 [7].



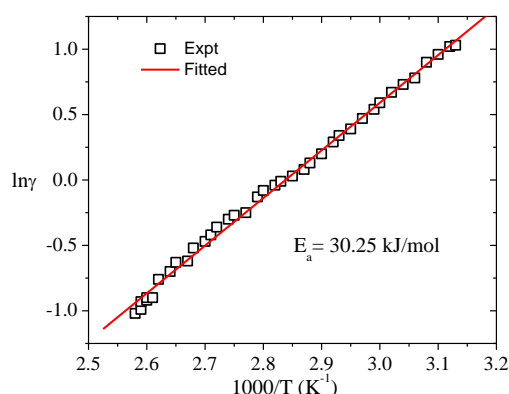
**Figure 4.13.** (a)  $P_s$  as a function of applied field in DM0, DM3 and M3 at  $T_c - 28$ , (b) Comparison of  $P_s$  as a function of temperature of M3, DM0 and DM3

The value of the response time ( $\tau$ ) of the mixture is found to be about 100  $\mu$ s near  $T_c$  and up to 50°C below  $T_c$  its value is intermediate of DM0 and DM3. Beyond that, it increases gradually till SmC\*–SmC<sub>A</sub>\* transition and reaches maximum value of 650  $\mu$ s [Figure 4.14(a)].



**Figure 4.14.** Comparison of (a) response time ( $\tau$ ) and (b) rotational viscosity ( $\gamma$ ) as a function of the temperature of M3, DM0 and DM3

Temperature dependence of rotational viscosity ( $\gamma$ ), calculated from the measured  $P_s$  and  $\tau$  values, is shown in Figure 4.14(b). That  $\gamma$  follows the Arrhenius law is evident by the fact that,  $\ln \gamma$  vs  $1000/T$  plot shows a linear behavior as shown in Figure 4.16. There is a slight change of gradient at 74°C which is the transition from SmC\* to SmC<sub>A</sub>\* phase. The activation energy ( $E_a$ ) determined from the plot is 30.25 kJ/mol which is less than those of the pure compounds DM0 (38.19 kJ/mol) and DM3 (44.34 kJ/mol).



**Figure 4.15.**  $\ln\gamma$  vs  $1000/T$  plot for the mixture M3.

#### 4.4. CONCLUSION

A eutectic antiferroelectric mixture is formed using 50 wt.% of two pure compounds, one of them is DM0 which is protonated in its core and the other is DM3, which is doubly fluorinated in the core. It shows the same phase sequence  $\text{Cr-SmC}_A^*-\text{SmC}^*-\text{SmA}^*-\text{Iso}$  as in the pure compounds but with increased range of  $\text{SmC}_A^*$  phase. The behaviour of the mixture is not always proportional to the concentration of the protonated and the fluorinated components. In the eutectic mixture, the critical frequencies of all the collective relaxation modes ( $P_L$ ,  $P_H$ , GM, and SM) are found to lie in between the pure compounds. However,  $P_L$  and SM critical frequencies are not proportional to the concentration of the pure compounds but for  $P_H$  and GM they are almost proportional. The critical field for the suppression of the  $P_L$  and Goldstone modes is increased significantly. The GM mode dielectric increment decreased significantly. Like the pure compounds, the hereditary mode is observed in the mixture, however, no domain mode is observed, unlike the pure compounds.  $\text{SmC}^*-\text{SmA}^*$  transition temperature ( $T_c$ ) is found to increase linearly with bias field and the phenomenon has been explained using the Landau model. Spontaneous polarization is found to be in between those of the pure compounds. Switching time also exhibits similar behaviour and observed to be about a few hundred microseconds. The rotational viscosity is increased slightly but the activation energy is decreased compared to the pure compounds.

## 4.5 REFERENCES

- [1] T. Geelhaar, Ferroelectric mixtures and their physico-chemical properties, *Ferroelectrics*. 85(1988) 329-349.
- [2] A. Debnath, D. Sinha, and P. K. Mandal, Wide range room temperature electroclinic liquid crystal mixture with large induced tilt and very small layer contraction, *J. App. Phys.* 119 (2016)124103(1-5).
- [3] A. Debnath, D. Sinha, P. K. Mandal, and R. Dabrowski, Formulation of a Room Temperature Ferroelectric Liquid Crystal Mixture with Sub-millisecond Switching Time, *AIP Conf. Proc.* 1665 (2015) 040004(1-3).
- [4] A. Debnath and P. K. Mandal, Wide range room temperature ferroelectric liquid crystal mixture with micro-second order switching, *J. Mol. Liq.* 221(2016) 287-297.
- [5] A. Debnath, P. K. Mandal, D. Weglowska and R. Dabrowski, Induction of a room temperature ferroelectric SmC\* phase in binary mixtures with moderate spontaneous polarization and sub-millisecond switching time, *RSC Adv.* 6 (2016) 84369-84368.
- [6] S. Delica, M. Estonactoc, M.C. Micaller, L. Cada and Z. Domingo, Phase Diagram of Binary Mixture TM74A:E48 Liquid Crystals, *Mol. Cryst. Liq. Cryst.* 366 (2001) 101-106.
- [7] K. C. Dey, P. K. Mandal, R. Dabrowski, Effect of lateral fluorination in antiferroelectric and ferroelectric mesophases: synchrotron X-ray diffraction, dielectric spectroscopy and electro-optic study, *J. Phys. and Chem. Solids*. 88 (2016) 14-23.
- [8] P. W. Stott, A. C. Williams, B. W. Barry, Transdermal delivery from eutectic systems: enhanced permeation of a model drug, ibuprofen, *J. Control Release*. 50 (1998) 297-308.
- [9] D. Demus, C. Fietkau, R. Schubrt and H. Kehlen, Calculation and Experimental Verification of Eutectic Systems with Nematic Phases, *Mol. Cryst. Liq. Cryst.* 25(1974) 215-233.
- [10] K. Miyasato, S. Abe, H. Takezoe, A. Fukuda, E. Kuze, Direct Method with

- Triangular waves for Measuring Spontaneous Polarization in Ferroelectric Liquid Crystal, Jpn. J. Appl. Phys. 22(10) (1983) L661-L664.
- [11] S. S. Bawa, A. M. Biradar, K. Saxena and S. Chandra, Direct pulse technique for spontaneous polarization dynamics and molecular reorientation processes in ferroelectric liquid crystals, Rev. Sci. Inst. 59 (1988) 2023-2030.
- [12] K. A. Jasjit, K. K. Raina. Polarization Switching and Dielectric Relaxations in Ferroelectric Liquid Crystals, Jpn. J. Appl. Phys. 39 (2000) 4076-4081.
- [13] L. A. Beresnev, L. M. Blinov, M. A. Osipov, S. A. Pikin, Ferroelectric Liquid Crystals, Mol. Cryst. Liq. Cryst. 158A (1988) 1-150.
- [14] S. Gauza, R. Dabrowski, K. Czuprynski, W. Drzewinski, K. Kenik, Induced Antiferroelectric Smectic  $C_A^*$  Phase Structural Correlations, Ferroelectrics. 276 (2002) 207-217.
- [15] M. Brodzik and R. Dabrowski, Induction of the smectic  $A_d$  phase in polar systems II. Role of steric effects in the smectic  $A_d$  phase induction, Liq. Cryst. 20 (1996) 99-102.
- [16] R. K. Bamezai, S. Sharma, S. B. Raina, and H. Kresse, Phase diagrams and dielectric studies of binary mixtures exhibiting intermediate nematic and induced smectic phases, Phase Transit. 78(6) (2005) 471-479.
- [17] S. Diele, G. Pelzl, A. Madicke, D. Demus, and W. Weissflog, The Steric Influence on the Formation of Smectic Layers in Binary Systems, Mol. Cryst. Liq. Cryst. 191 (1990) 37-47.
- [18] S. Haddawi, S. Diele, H. Kresse, G. Pelzl and W. Weissflog, Stabilization and Destabilization of the  $S_A$  Phase in Mixtures of 4-Nitrobenzyl-2,5-bis (4-n-alkoxybenzoyloxy)benzoates, Cryst. Res. Technol. 29(5) (1994) 745-757.
- [19] B. Wazzynska, Binary mixtures of smectic  $A_1$ s with abnormal behaviour, Liq. Cryst. 3(1) (1988) 85-99.
- [20] M. Marcos, E. Melendez, M.B. Ross and J.L. Serrano, Influence of Polar End Groups on Induced Smectic Phase Appearance, Mol. Cryst. Liq. Cryst. 167 (1989) 239-252.
- [21] J. Hou, J. Schacht, F. Giebelmann and P. Zugenmaier, Temperature and bias-

- field dependences of dielectric behaviour in the antiferroelectric liquid crystal, (R)-MHPOBC, *Liq. Cryst.* 22(4) (1997) 409-417.
- [22] M. Buivydas, F. Gouda, G. Andersson, S. T. Lagerwall, B. Stebler, Collective and non-collective excitations in antiferroelectric and ferroelectric liquid crystals studied by dielectric relaxation spectroscopy and electro-optic measurements, *Liq. Cryst.* 23(5) (1997) 723-739.
- [23] Yu. Panarin, O. Kalinovskaya, and J. K. Vij, The investigation of the relaxation processes in antiferroelectric liquid crystals by broad band dielectric and electro-optic spectroscopy, *Liq. Cryst.* 25 (2) (1998) 241-252.
- [24] Y. P. Panarin, O. Kalinovskaya, J. K. Vij, The Relaxation Processes in Helical Antiferroelectric Liquid Crystal, *Ferroelectrics*. 213 (1998) 101-108.
- [25] P. Perkowski, K. Ogrodnik, W. Piecek, M. Zurowska, Z. Raszewski, R. Dabrowski, L. Jaroszewicz, Influence of the bias field on dielectric properties of the  $\text{SmC}_A^*$  in the vicinity of the  $\text{SmC}^* - \text{SmC}_A^*$  phase transition, *Liq. Cryst.* 38(16) (2011) 1159-1167.
- [26] Yu. Panarin, O. Kalinovskaya, and J. K. Vij, Observation and investigation of the ferroelectric subphase with high  $q_T$  parameter, *Phy. Rev. E*. 55(4) (1997) 4345-4353.
- [27] T. Carlsson, B. Zeks, C. Filipic, A. Levstik, Theoretical model of the frequency and temperature dependence of the complex dielectric constant of ferroelectric liquid crystals near the smectic-C'-smectic-A phase transition, *Phys. Rev. A*. 42(2) (1990) 877-889.
- [28] D. Goswami, D. Sinha, A. Debnath, P. K. Mandal, S. K. Gupta, W. Haase, D. Ziobro, R. Dabrowski, Molecular and dynamical properties of a perfluorinated liquid crystal with direct transition from ferroelectric  $\text{SmC}^*$  phase to isotropic phase, *J. Mol. Liq.* 182 (2013) 95-101.
- [29] S. Haldar, K. C. Dey, D. Sinha, P. K. Mandal, W. Haase, P. Kula, X-ray diffraction and dielectric spectroscopy studies on a partially fluorinated ferroelectric liquid crystal from the family of terphenyl esters, *Liq. Cryst.* 39(10) (2012) 1196-1203.
- [30] P. Arora, A. Mikulko, F. Podgornov, W. Haase, Dielectric and Electro-Optic

- Properties of New Ferroelectric Liquid Crystalline Mixture Doped with Carbon Nanotubes, *Mol. Cryst. Liq. Cryst.* 502 (2009) 1-8.
- [31] A. Mikulko, P. Arora, A. Glushchenko, A. Lapanik, W. Haase, Complementary studies of BaTiO<sub>3</sub> nanoparticles suspended in a ferroelectric liquid-crystalline mixture, *Euro phys. Lett.* 87(2009) 27009 (1-5).
- [32] K. Hiraoka, Y. Takanishi, K. Skarp, H. Takezoe and A. Fukuda, Electric-Field-Induced Apparent Tilt Angle and Devil's Staircase in SmC<sub>a</sub>\* of an Antiferroelectric Chiral Smectic Liquid Crystal. *Jpn. J. Appl. Phys.* 30 (1991) L1819-L1825.
- [33] M. Marzec, R. Dabrowski, A. Fafara, W. Haase, S. Hiller, S. Wrobel, Goldstone mode and domain mode relaxation in ferroelectric phases of 4'-[(S,S) - 2,3 - epoxyhexyloxy] phenyl 4-(decyloxy)benzoate (EHPDB), *Ferroelectrics*. 180 (1996) 127-135.
- [34] K. C. Dey, P. K. Mandal, R. Dabrowski, Effect of bias on dielectric properties of SmC<sub>A</sub>\* and SmC\* phases of a perfluorinated antiferroelectric liquid crystal, *Materials Today Proc.* 3 (2016) 3987-3991.
- [35] F. Gouda, K. Skarp, S.T. Lagerwall, Dielectric studies of the soft mode and Goldstone mode in Ferroelectric liquid crystal, *Ferroelectrics*. 113 (1991) 165-206.
- [36] F. Gouda, G. Anderson, S. T. Lagerwall, K. Skarp, B. Stebler, T. Carlson, B. Zeks, and A. Levstik, Experimental and theoretical study of the influence of a bias electric field on the dielectric properties of the chiral smectic A\* phase, *Liq. Cryst.* 6(2) (1989) 219-231.
- [37] J. Schacht, F. Giesselmann, P. Zugenmaier and W. Kuczynski, Dielectric studies of the bias field effect on the soft mode of a ferroelectric liquid crystal, *Ferroelectrics*. 209 (1998) 483-503.
- [38] C. Bahr and G. Heppke, Influence of electric field on a first-order smectic-A — ferroelectric-smectic-C liquid-crystal phase transition: A field-induced critical point, *Phys. Rev. A* 41(8) (1990) 4335-4342.
- [39] B. Zeks and M. Cepic, A phenomenological model of antiferroelectric liquid crystals. *Liq. Cryst.* 14(2) (1993) 445–451.

- [40] L. D. Landau, Statistical Physics, Pergamon Press, Oxford, 1980.
- [41] R. J. Birgeneau, C. W. Garland, A. R. Kortan, J. D. Lister, M. Meichle, B. M. Ocko, C. Rosenblatt, L. J. Yu and J. Goodby, Smectic-A—smectic-C transition: Meanfield or critical, Phys. Rev. A 27(1983) 1251-1254.

# CHAPTER 5

---

## Formulation of a room temperature multi-component high tilt antiferroelectric liquid crystal mixture

5.1	INTRODUCTION	127
5.2	EXPERIMENTAL TECHNIQUES	128
5.3	RESULTS AND DISCUSSION	129
5.3.1	POLARIZING OPTICAL MICROSCOPY (POM)	129
5.3.2	DSC STUDY	131
5.3.3	SYNCHROTRON RADIATION STUDY	131
5.3.4	DIELECTRIC STUDY	134
5.3.5	ELECTRO-OPTIC STUDY	140
5.4	CONCLUSION	143
5.5	REFERENCES	145

---

Part of the work has been communicated for publication in the Journal Philosophical Magazine.



## 5.1 INTRODUCTION

Antiferroelectric liquid crystals (AFLCs) are promising materials for fast switching display devices and photonic applications because of their fascinating electro-optic properties: tri-stable switching, micro-second response, intrinsic analog gray-scale capability, hemi-spherical viewing angle (in-plane switching geometry) and no-ghost effect [1]. In spite of having such properties, they did not get much success in display industry due to their disadvantages mainly in light leakage in the dark state, poor contrast and problem in alignment [2, 3]. Further development of faster but complex FLC and AFLC based display technology was decelerated due to the development of active matrix display with improved nematic materials [4]. But the increasing demand on switching speed for 3D vision displays and for field-sequential-colour (FSC) generation displays, have led to a renewed interest in faster LC display technologies in the last few years and therefore the development of ferroelectric and antiferroelectric liquid crystals has got an impetus [5].

Orthoconic antiferroelectric liquid crystals (OAFLCs) [6-7] are materials with almost 45° tilt, having high-speed switching of conventional antiferroelectric materials with an additional unique feature: under surface stabilized structure, they behave like a uniaxial crystal with optic axis along normal to the boundary surfaces and therefore when light falls perpendicularly to the glass substrate, it passes as if through isotropic medium and hence the dark state is perfectly dark irrespective of the irregularities in the smectic layer alignment. This means that high-contrast AFLC devices can be realized with very relaxed alignment requirements.

But in spite of synthesis of numerous new antiferroelectric compounds [8-13], it is found that no single compound satisfies the optimum conditions of parameters required for the applications in display technology. The useful technique to obtain a room temperature liquid crystal with broad temperature range, desired helical parameters and electro-optic parameters of anticlinic phase is the formulation of mixtures [14]. The property of mixture depends on the nature and concentration of the host and the dopant. The van der Waals forces, hydrogen bonds and electron donor–acceptor interaction etc. collectively or separately are responsible for the change of properties.

Molecular, dielectric and electro-optic properties of four pure AFLC compounds DM0, DM1, DM2 and DM3 have been described in Chapter 3 [15]. Binary mixture of

two of these compounds DM0 and DM3 (50 wt.% of each) showed eutectic behaviour [16-17] and antiferroelectric phase ( $\text{SmC}_A^*$ ) was observed at  $39.8^\circ\text{C}$  whereas in the pure compounds it was observed at  $61^\circ\text{C}$  and  $63.2^\circ\text{C}$  respectively. The antiferroelectric phase crystallized below about  $-8^\circ\text{C}$  and some properties exhibited linear additive behavior [18]. In continuation of these works, we have formulated a mixture (M6) by mixing 25 wt.% of each of the four compounds DM0, DM1, DM2 and DM3 in order to obtain a room temperature AFLC. Properties of these pure compounds have been described in chapter 3. In the present Chapter we have studied various properties of the formulated mixture important for display applications and compared them with those of the pure compounds.

**Table 5.1.** Phase sequence and transition temperatures ( $^\circ\text{C}$ ) of the mixture as obtained from POM study during heating. Figures within parentheses are transition temperatures during cooling.

Mixture	Phase sequence and transition temperatures
M6	<b>DM0 + DM1 + DM2 + DM3 (25 wt.% of each)</b> (~ -8) $\text{SmC}_A^*$ (65) $81.5 \text{ SmC}^*$ (109) $110 \text{ SmA}^*$ (112) $112.5 \text{ IsO}$

## 5.2 EXPERIMENTAL TECHNIQUES

The compounds DM0, DM1, DM2 and DM3 were mixed in equal wt.% by solution method. The desired weights of all the compounds were dissolved in chloroform and sonicated for 1 hour using an ultrasonic mixer (GT Sonic Professional, Apex, India). The solution was then heated at constant temperature  $\sim 60^\circ\text{C}$  for four hours in order to evaporate the chloroform completely from the solution. Complete evaporation of chloroform was confirmed by regaining the weight of the mixture. The phase behaviour and transition temperatures of the mixture were investigated by polarizing optical microscopy (POM) (@  $\pm 0.1^\circ\text{C}/\text{min}$ ) and differential calorimetric study (DSC) (@  $3^\circ\text{C}/\text{min}$ ). Mesophase structures were investigated by diffraction experiment using synchrotron radiation facility (PETRA III beam line at P07 Physics Hutch station) at Deutsches Elektronen Synchrotron, Hamburg. Dielectric and electro-optical studies were performed using Indium–Tin–oxide (ITO) coated homogeneous (HG) cells of  $10 \mu\text{m}$  thickness. Detailed procedures

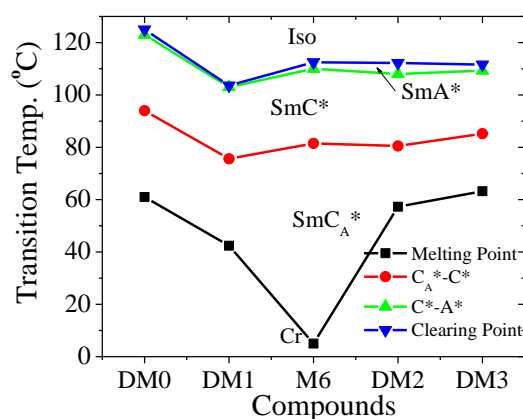
of preparation of the cell and experimental arrangements have been explained in **Chapter 2**.

### 5.3 RESULTS AND DISCUSSIONS

#### 5.3.1 POLARIZING OPTICAL MICROSCOPY (POM)

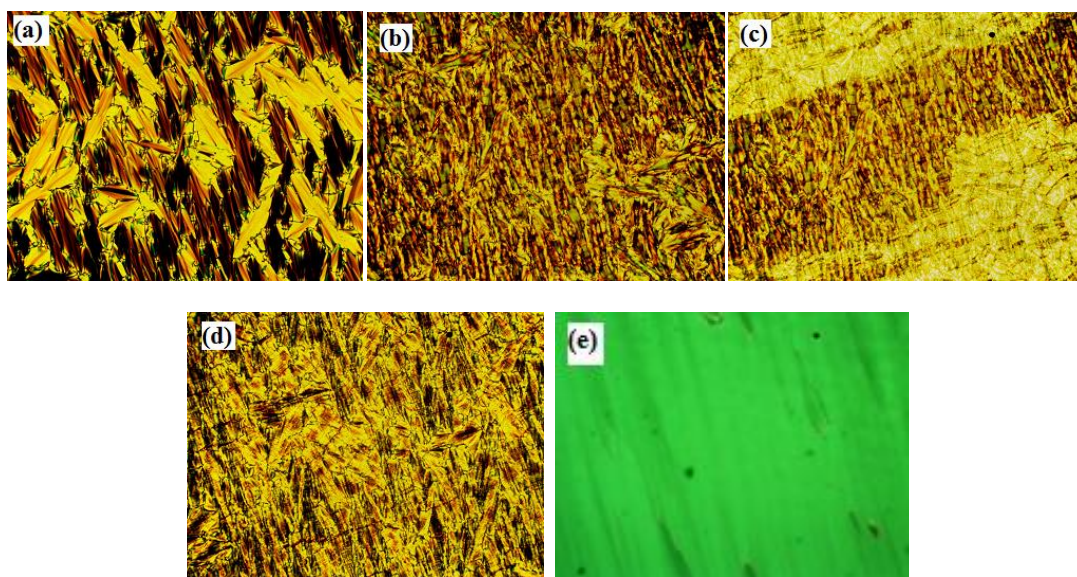
The phase sequence and transition temperatures of the mixture determined using polarizing optical microscopy are shown in **Table 5.1**. The phase diagram of the pure compounds and the mixture during heating is presented in **Figure 5.1**. The phase sequence was found to be the same as that of the pure compounds *viz.*, Cr–SmC<sub>A</sub>\*–SmC\*–SmA\*–Iso. The SmC<sub>A</sub>\*–SmC\*, SmC\*–SmA\* and SmA\*–Iso transition temperatures were found to be almost equal to the mean of the corresponding phase transition temperatures of the pure compounds. However, the melting point of the mixture depressed drastically to about 5°C, compared to 39.8°C in binary mixture. As a result the thermal range of the SmC<sub>A</sub>\* phase was found to increase substantially.

Fan shaped texture was observed in SmA\* phase which was converted into broken fan in SmC\* and SmC<sub>A</sub>\* phases more in the later phase [**Figure 5.2**]. No change in the texture of SmC<sub>A</sub>\* phase was observed after keeping the mixture in a refrigerator for more than 15 days signifying the stability of SmC<sub>A</sub>\* phase till about -8°C. Moreover, monodomain texture was obtained throughout the SmC\* and SmC<sub>A</sub>\* phases when the mixture was cooled under electric field of 5.0 V/ $\mu$ m [**Figure 5.2(e)**] although no such behaviour was noticed in the pure compounds.

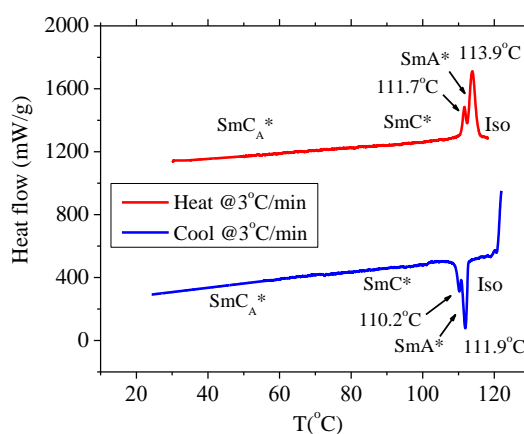


**Figure 5.1.** Phase diagram of the pure compounds and the mixture during heating.

It might be mentioned here, as described in Chapter 4, that in a multi-component host, the dopants DM1 and DM2 showed only ferroelectric phase while the dopant DM0 and DM3 exhibited both ferroelectric and antiferroelectric phases when mixed in large concentration (60 wt.%) [19]. But when the dopant DM1 was mixed in less concentration (10 wt.%) in the same host mixture the resulted mixture was found to exhibit only paraelectric phase having large electroclinic coefficient [20]



**Figure 5.2.** Observed textures of the mixture in different phases (a) SmA\* (110.5°C), (b) SmC\* (105°C), (c) SmC\*-SmC<sub>A</sub>\* transition, (d) SmC<sub>A</sub>\* (20°C), (e) monodomain texture under electric field (5.0 V/μm) in SmC\* phase.



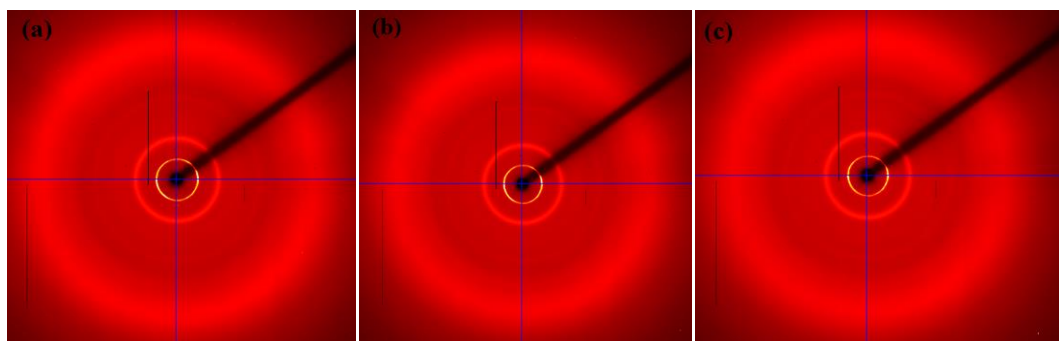
**Figure 5.3.** DSC thermograms of M6 during heating and cooling

### 5.3.2 DSC STUDY

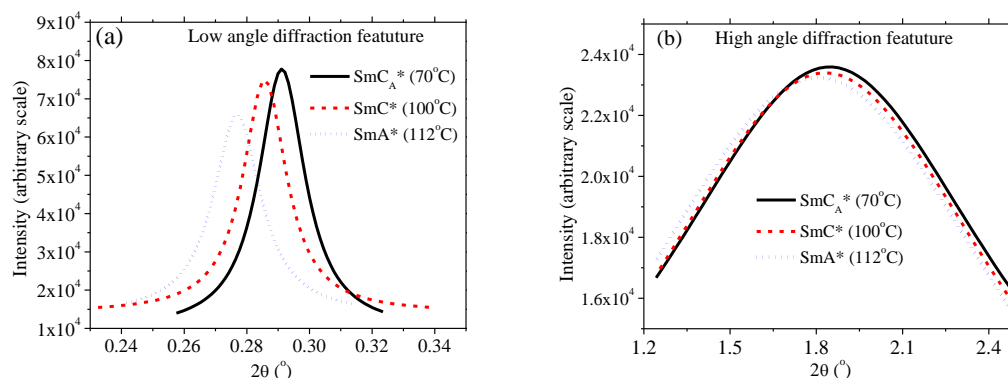
The DSC thermograms of the mixture during heating and cooling are presented in **Figure 5.3**. At Iso–SmA\* and SmA\*–SmC\* transitions a significant change of molecular structures takes place therefore the order parameter changes significantly which was manifested in the DSC curve by anomaly [21]. The intermediate transitions between SmC\* and SmC<sub>A</sub>\* phases or between the sub-phases are not always possible to detect by DSC due to finite hysteresis in temperature and a small change in enthalpy at the phase transitions [22]. But in this mixture anomaly of small peak height in the thermogram at SmC\*– SmC<sub>A</sub>\* transition was detectable in the magnified view. The transition temperatures observed in DSC was found to differ slightly from those of POM studies which might be due to different sample environment and thermal history.

### 5.3.3 SYNCHROTRON RADIATION STUDY

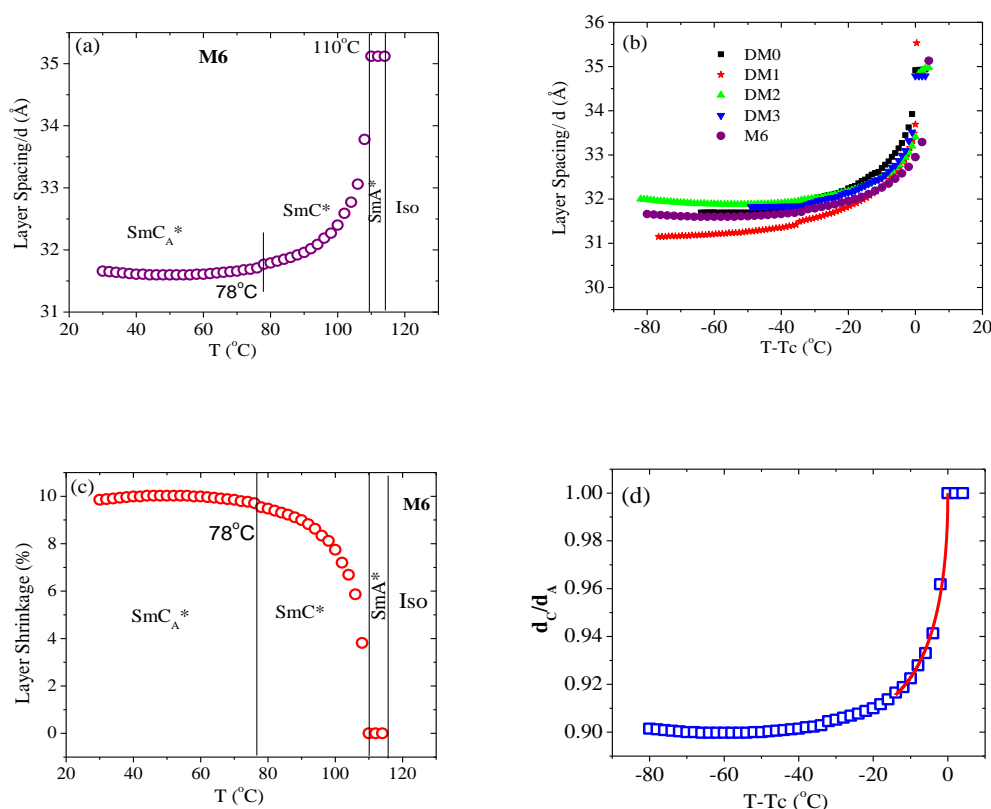
In the diffraction photographs one low angle sharp diffraction ring and one high angle diffuse diffraction ring were observed. The lower angle feature arises due to smectic layer spacing whereas higher angle one corresponds to average intermolecular distance within the layers. Diffraction photographs and their intensity profiles in different phases are shown in **Figure 5.4** and **Figure 5.5** respectively. Peaks of the intensity profiles were found to shift gradually towards low angle side with increasing temperature signifying increase of layer spacing and intermolecular distance with temperature. The intensity of the low angle inner ring was much higher than high angle outer ring as expected.



**Figure 5.4.** Synchrotron x-ray diffraction photographs at (a) 70 °C (SmC<sub>A</sub>\*), (b) 100 °C (SmC\*) and (c) 112 °C (SmA\*).



**Figure 5.5.** X-ray diffraction profiles at 70 °C ( $\text{SmC}_A^*$ ), 100 °C ( $\text{SmC}^*$ ) and 112 °C ( $\text{SmA}^*$ ) of the (a) low angle and (b) high angle diffraction features.



**Figure 5.6.** Temperature dependence of layer spacing of the (a) mixture and (b) pure compounds, (c) layer shrinkage of the mixture and (d) fitted layer spacing near T<sub>c</sub> as discussed in the text.

The temperature evolution of the layer thickness ( $d$ ), intermolecular distance ( $D$ ) and percent layer shrinkage are plotted in **Figure 5.6**. The value of  $d$  was maximum (35.1  $\text{\AA}$ ) in orthogonal  $\text{SmA}^*$  phase which was almost equal to the average of the maximum layer spacings of the pure compounds (35.05 $\text{\AA}$ ). Layer spacings

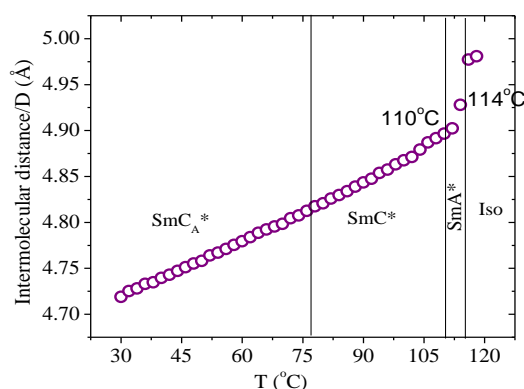
decreased sharply near  $T_c$  and then slowly it became minimum (31.6 Å) in the  $\text{SmC}_A^*$  phase which was also almost equal to the average of the minimum layer spacing of the pure compounds [**Figure 5.6(a)**]. With decreasing temperature percent layer shrinkage sharply increased from  $T_c$  till  $T_{AF}$  and in  $\text{SmC}_A^*$  phase maximum layer shrinkage was about 10%.

It was further noticed that the temperature dependence of  $d$  near  $T_c$  was parabolic in nature. According to generalized mean field theory, the tilt  $\theta \propto (T - T_c)^\beta$ , where for the critical exponent  $\beta$  a value of  $(1/2)$  was expected in a pure second order transition and a value of  $(1/4)$  was expected in case of second order transition approaching tricritical point (TCP) [23-24]. Following Hartley *et al.* [25] but keeping up to fourth order terms in the expansion of  $\cos\theta$  it can be shown that near  $T_c$

$$d/d_A \approx 1 - a|T - T_c|^{1/2} + b|T - T_c| \quad (5.1)$$

when  $\beta$  is taken as  $1/4$ . Observed data fitted nicely to the above equation (**Figure 5.6(d)**) signifying that the  $\text{SmC}^* - \text{SmA}^*$  transition was a tricritical type.

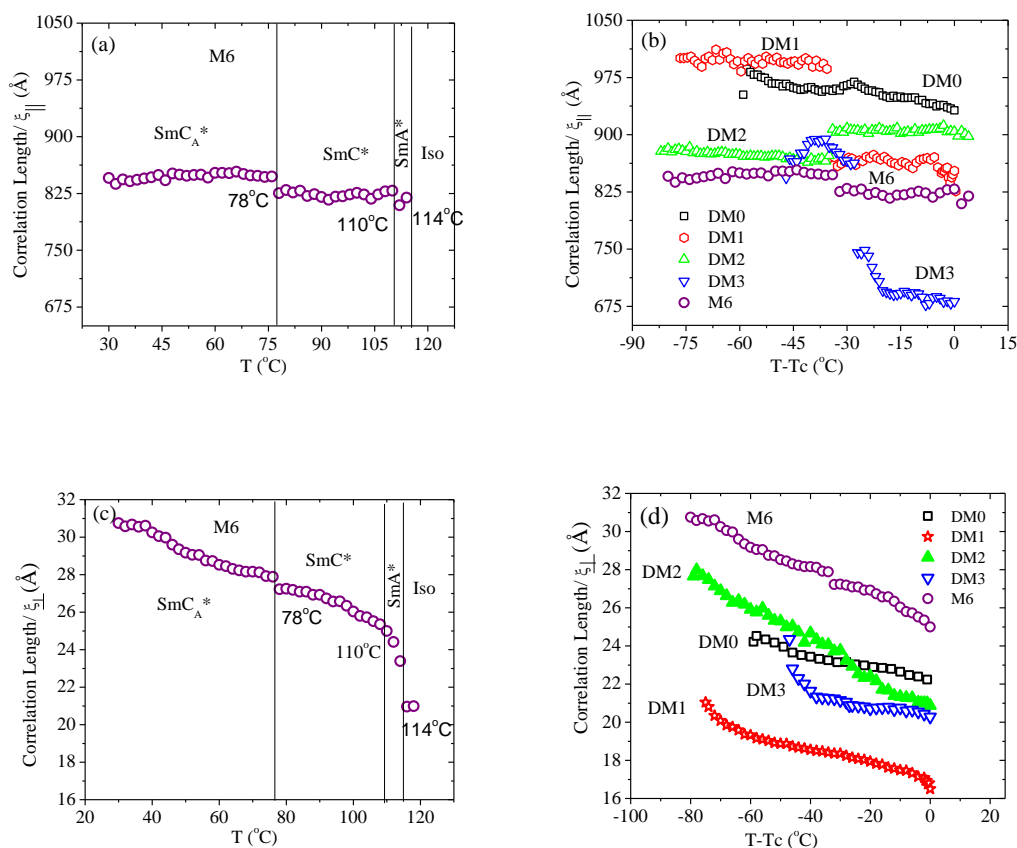
The minimum value of intermolecular distance ( $D$ ) of the mixture was found to be 4.7 Å in  $\text{SmC}_A^*$  phase and increased almost linearly with temperature and became maximum (4.97 Å) in  $\text{SmA}^*$  phase as shown in **Figure 5.7**. However unlike the layer thickness, the intermolecular distance was found to be less than the average value of those of the pure compounds.



**Figure 5.7.** Temperature dependence of intermolecular distance ( $D$ ) of the mixture.

In the mixture the correlation length across the layers ( $\xi_{||}$ ) in  $\text{SmA}^*$  phase was lowest (810–813 Å) and increased slightly in  $\text{SmC}^*$  phase (818–828 Å) which further

increased in  $\text{SmC}_A^*$  phase (846–850 Å) [Figure 5.8]. Similar correlation lengths were obtained earlier by our group in other systems [26–27]. However  $\xi_{||}$  was more in the pure compounds except in DM3 and discontinuous changes were observed at  $\text{SmC}^*-\text{SmC}_A^*$  transition except in DM0 [15]. On the other hand the correlation lengths within the layers ( $\xi_{\perp}$ ) were significantly larger in the mixture in all the phases and found to increase with decreasing temperature as observed in all the pure compounds.

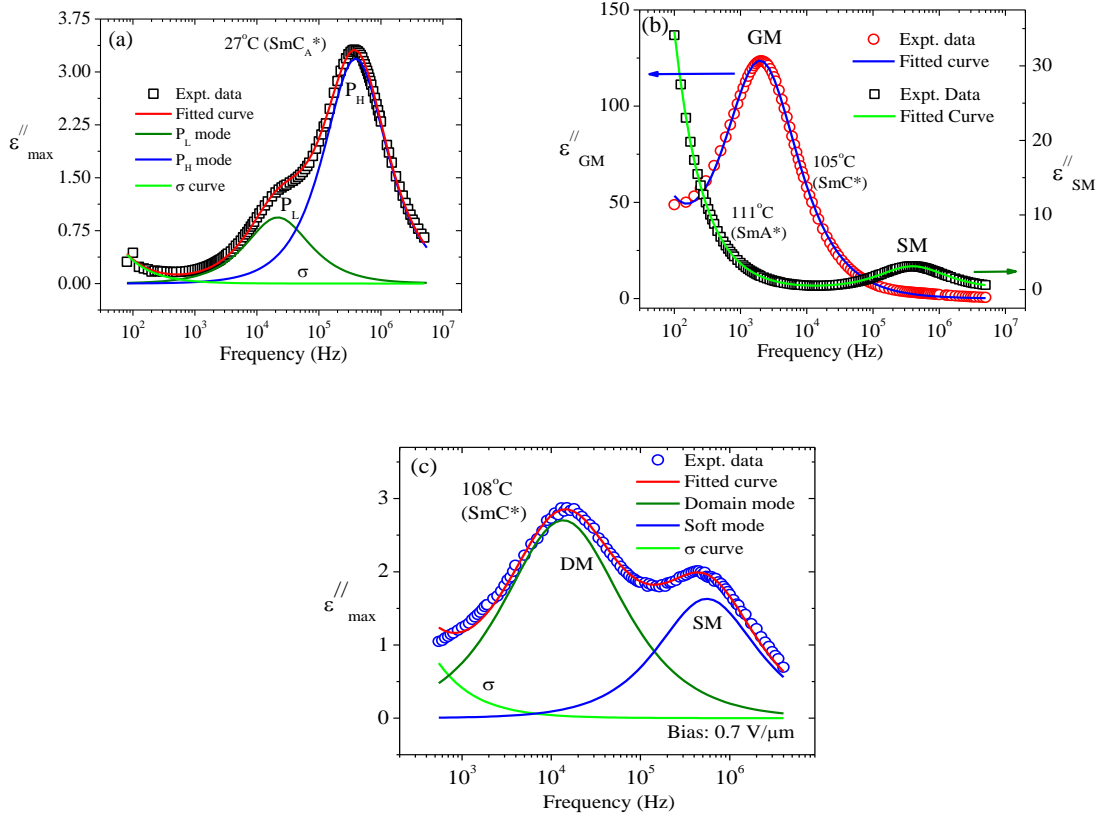


**Figure 5.8.** Temperature dependence of correlation lengths across the layers ( $\xi_{||}$ ) in the (a) mixture and (b) pure compounds and that of within the layers ( $\xi_{\perp}$ ) in the (c) mixture and (d) pure compounds.

### 5.3.4 DIELECTRIC STUDY

In order to elucidate the dynamics of the molecules within the phases the dielectric behaviour of the mixture was investigated in planar geometry in the frequency domain 50Hz – 5MHz. The transverse components of the dielectric permittivity (real  $\epsilon'$  as well as imaginary part  $\epsilon''$ ) were measured in all phases. From the temperature evolution of the critical frequency ( $f_c$ ) and the dielectric increment

( $\Delta\epsilon$ ) the various collective modes of relaxations present in different phases were identified. Exemplary fitted spectra showing clearly the different modes of relaxations are shown in **Figure 5.9**.

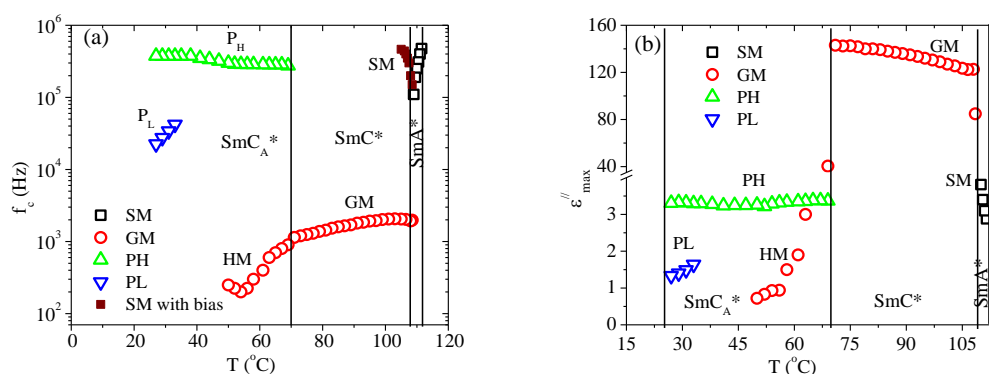


**Figure 5.9.** Fitted absorption spectrum (a) in SmC<sub>A</sub>\* phase at 27°C showing P<sub>L</sub> and P<sub>H</sub> (fitted parameters of P<sub>L</sub>  $\Delta\epsilon = 2.0 \pm 0.3$ ,  $f_c = 21723 \pm 76$  Hz,  $\alpha = 0.04 \pm 0.005$ ,  $\sigma = 1.83E - 9 \pm 1.6E - 10$ , fitted parameters of P<sub>H</sub> are  $\Delta\epsilon = 6.7 \pm 0.4$ ,  $f_c = 390330 \pm 255$  Hz,  $\alpha = 0.03 \pm 0.003$ ) (b) in SmC\* and SmA\* phases at 105°C and at 111°C showing GM and SM (fitted parameters of GM are  $\Delta\epsilon = 282.8 \pm 3.5$ ,  $f_c = 2008.2 \pm 15$  Hz,  $\alpha = 0.09 \pm 0.006$ ,  $\sigma = 3.84E - 10 \pm 3.0E - 11$ , fitted parameters of SM are  $\Delta\epsilon = 6.74 \pm 0.5$ ,  $f_c = 394982 \pm 535$  Hz,  $\alpha = 0.05 \pm 0.007$ ,  $\sigma = 1.92E - 7 \pm 1.6E - 9$ ) and (c) in SmC\* phase under bias 0.7 V/μm at 108°C showing DM and SM (fitted parameters of DM are  $\Delta\epsilon = 7.2 \pm .8$ ,  $f_c = 13600 \pm 112$  Hz,  $\alpha = 0.18 \pm 0.02$ ,  $\sigma = 1.5E - 8 \pm 2.3E - 9$ ).

The mixture was found to exhibit two collective modes in SmC<sub>A</sub>\* phase: one in the low frequency region known as in-phase antiferroelectric mode (P<sub>L</sub>) and other in the high frequency region identified as anti-phase antiferroelectric mode (P<sub>H</sub>) [28–32]. The P<sub>L</sub> was found to appear from 33°C, far below the SmC\*–SmC<sub>A</sub>\* transition

( $T_{AF}$ ) during cooling. The critical frequencies ( $f_{PL}$ ) and dielectric absorption strengths ( $\epsilon''_{PL}$ ) of  $P_L$  mode were observed to decrease with decreasing temperature ( $f_{PL}$ : 42–22.5 kHz and  $\epsilon''_{PL}$ : 1.64–1.33) as shown in **Figure 5.10**.  $P_L$  was also found to appear at temperatures lower than  $T_{AF}$  in DM0 [15] and in the binary mixture of DM0 and DM3 [16]. However, although the observed  $P_L$  frequency range was similar to that of DM1, in DM0 it was much higher whereas in DM2 and DM3 much lower.

In contrary to the decreasing trend of  $f_{PL}$ , the critical frequency of  $P_H$  mode ( $f_{PH}$ ) was observed to increase gradually from 275 kHz to 375 kHz with the decrease of temperature but  $\epsilon''_{PH}$  remains almost unchanged with temperature over the entire  $SmC_A^*$  phase [Figure 5.10]. Lower limit of  $f_{PH}$  of the mixture (275 kHz) was nearer to that in DM2 (290 kHz), the upper frequency limit (375 kHz) was far below than in all the pure compounds (lowest was 610 kHz in DM1). However the nature of temperature dependence of  $f_{PH}$  and  $\epsilon''_{PH}$  were similar to that in the pure compounds [15].

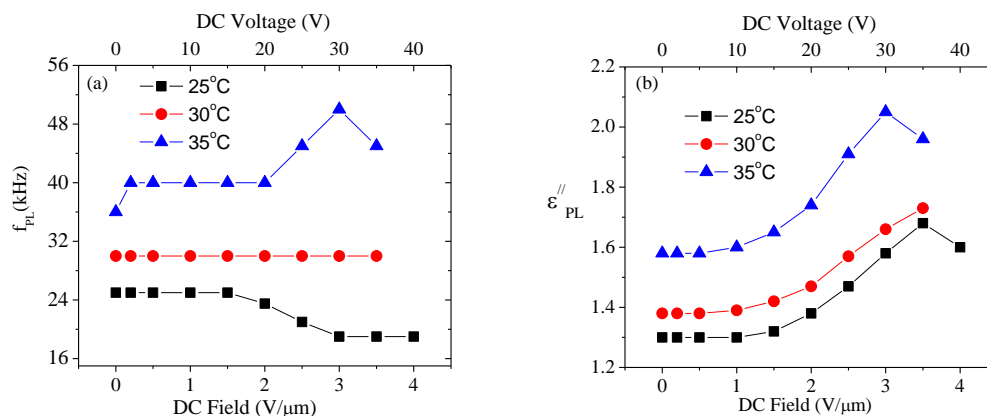


**Figure 5.10.** Temperature dependence of (a) the critical frequencies of soft mode, Goldstone mode,  $P_L$  mode and  $P_H$  mode and (b) the maximum dielectric absorptions ( $\epsilon''_{max}$ ) at critical frequencies of the corresponding modes.

To further probe the dynamics of the molecules, bias dependent dielectric measurements were made at selected temperatures 35°C, 30°C and 25°C varying the bias fields within range of 0 to 4.0 V/ $\mu$ m. These results have been presented in **Figure 5.11**. The critical frequency of  $P_L$  mode ( $f_{PL}$ ) remained constant at 30°C but at 25°C and 35°C it respectively decreased and increased beyond 2.0 V/ $\mu$ m [Figure 5.11(a)]. In the pure compounds the  $f_{PL}$  was found to decrease with bias. However, the absorption strength of the  $P_L$  mode ( $\epsilon''_{PL}$ ) was found to increase with field till 3.5

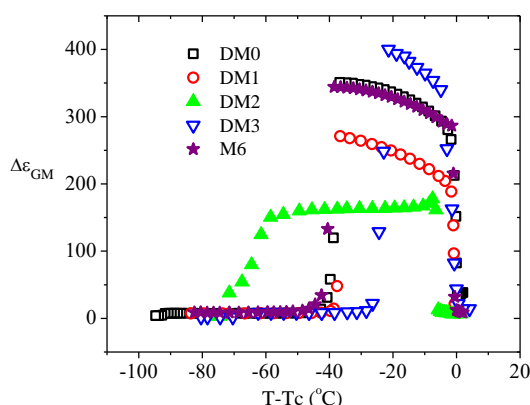
V/ $\mu\text{m}$  beyond which the mode got suppressed except at 25°C where it persisted even upto 4.0V/ $\mu\text{m}$  as shown in **Figure 5.11(b)**. Critical field for suppression of  $P_L$  was less in the pure compounds, about 2.0 V/ $\mu\text{m}$ .

On the other hand the critical frequency  $f_{PH}$  remained constant till a bias field of about 2.0V/ $\mu\text{m}$  beyond which it increased and got suppressed at about 4.0 V/ $\mu\text{m}$  at all three temperatures. But the absorption  $\varepsilon''_{PH}$  is found to decrease gradually with field, except sudden rise before suppression.



**Figure 5.11.** Bias field dependence of (a)  $f_{PL}$  and (b)  $\varepsilon''_{PL}$  of M6.

Dielectric spectra in SmC\* phase exhibited a strong absorption, which arose due to the phase fluctuation of the molecular directors, was identified as Goldstone mode (GM) [**Fig. 5.9(b)**]. The critical frequency ( $f_{GM}$ ) was found to decrease with decreasing temperature from 2050 Hz (103°C) to 1140 Hz (71°C) [**Figure 5.10(a)**] whereas the dielectric increment was found to increase 286.6 (107°C) to 344.2 (71°C) [**Figure 5.10(b)**]. Range of  $f_{GM}$  was like that of DM1 and DM2 but less than DM0 and greater than DM3. But  $\Delta\varepsilon_{GM}$  was almost equal to that of DM0, less than in DM3 and greater than in the other two pure compounds as seen clearly from **Figure 5.12**. Hereditary mode (HM) [29, 33] was also observed in SmC<sub>A</sub>\* phase upto 50°C with decreasing critical frequency and decreasing absorption strength in continuation with GM in SmC\*.

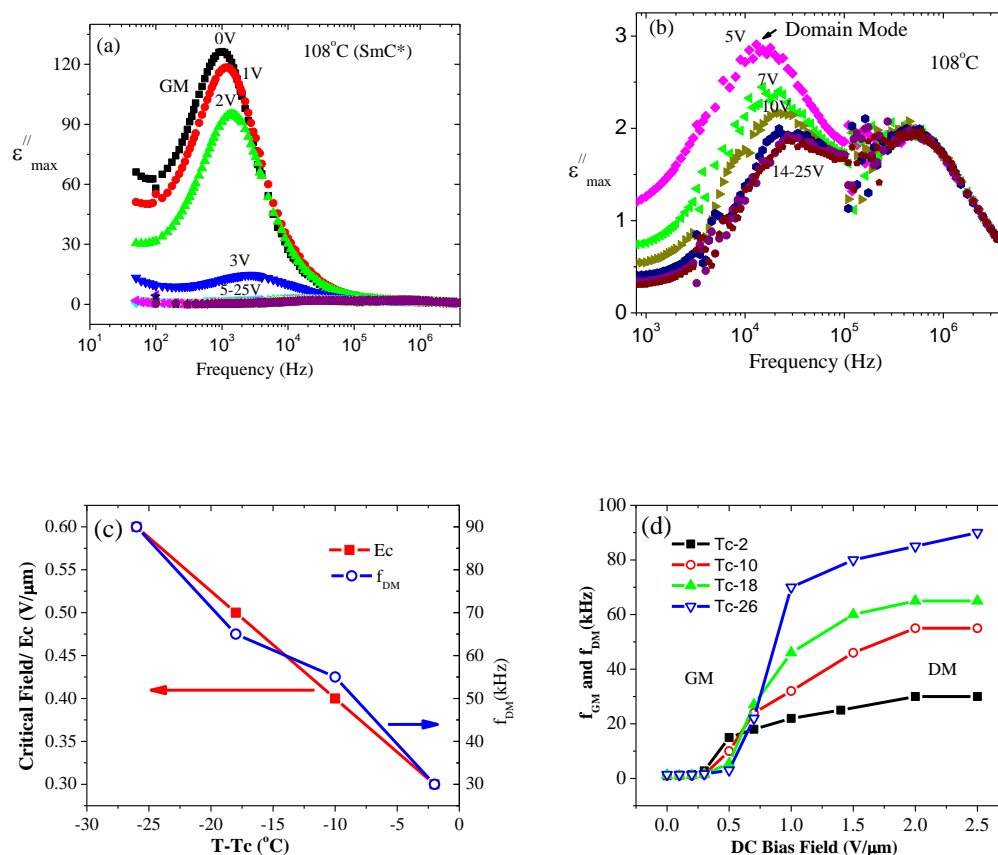


**Figure 5.12.** Dielectric increment ( $\Delta\epsilon_{GM}$ ) of Goldstone mode of the mixture in comparison to pure compounds.

The Goldstone mode contribution to the dielectric absorption strength decreased gradually under dc bias and suppressed at a particular bias field called critical field ( $E_c$ ) [Figure 5.13(a)]. In order to study the temperature dependence of  $E_c$ , dielectric spectra were taken under bias at four selected temperatures:  $T_c - 2$ ,  $T_c - 10$ ,  $T_c - 18$  and  $T_c - 26$ . The critical field ( $E_c$ ) was observed to increase with decreasing temperature from 0.3 V/ $\mu\text{m}$  at ( $T_c - 2$ ) to 0.6 V/ $\mu\text{m}$  at ( $T_c - 26$ ) [Figure 5.13(c)]. A similar temperature dependence of  $E_c$  was reported earlier [34-35].

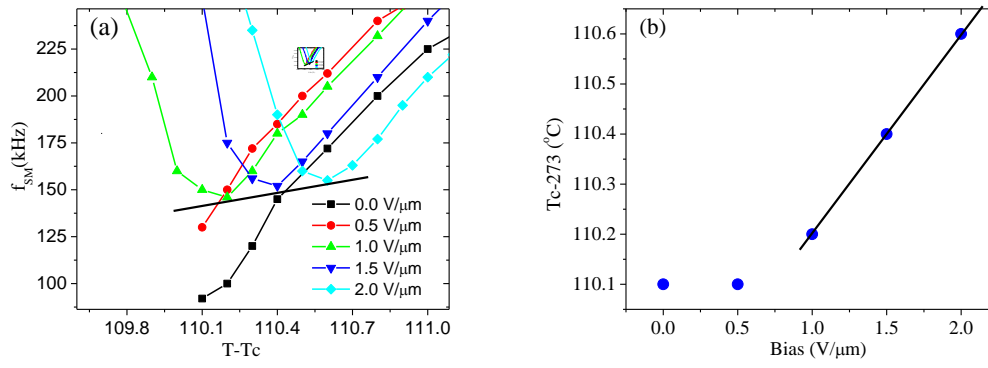
It has been reported that ferroelectric liquid crystals with high spontaneous polarization (as in M6 discussed in section 5.3.5) can form solid ferroelectric like domain after suppression of GM [34-36]. Relaxation mode arising out of such domain is termed as domain mode. Domain mode (DM) was observed in the mixture M6 at much higher frequencies than GM. A fitted absorption curve showing domain mode (DM) was shown in Figure 5.9(c). The strength of the mode was found to decrease gradually with bias [Figure 5.13(b)]. But the critical frequency ( $f_{DM}$ ) increased with bias to attain finally a saturation value at any fixed temperature [Figure 5.13(d)], however, it increased with decrease of temperature. Assuming the temperature dependence of  $f_{DM}$  Arrhenius type [37], the activation energy ( $E_a$ ) was calculated to be 48.7 kJ/mol. M. Marzec *et al.* [34] obtained  $E_a$  value of 32.0 kJ/mol. in the ferroelectric phase, much less than in the present mixture. Debnath *et al.* observed  $E_a$  values 23.01, 27.38, 27.26 and 28.83 kJ/mol. in the mixtures of any one of the DM series compounds in a achiral phenyl pyrimidine host matrix [19] and in four mixtures

of different concentrations of 4H6R in achiral host 8OBBP8 they observed  $E_a$  values as 51.15, 13.04, 14.21 and 17.53 kJ/mol. [27].



**Figure 5.13.** (a) Effect of bias on Goldstone mode, (b) Appearance of domain mode with bias, (c) Linear dependence of  $E_c$ , and  $f_{DM}$  with reduced temperature ( $T-T_c$ ), (d) Bias dependence of  $f_{GM}$  and  $f_{DM}$  at different temperatures.

Soft mode (SM) was observed in SmA\* phase which arises due to the fluctuation in the tilt angles of the molecular directors [38]. The dielectric increment of the mode was found to increase and corresponding relaxation frequency decreased due to the softening of the binding forces of the molecules with decrease of temperature as shown in **Figure 5.10(a), (b)**. The strong GM in SmC\* phase was found to mask the soft mode. But it could be observed when GM was suppressed under the bias field of 2.0 V/ $\mu\text{m}$  and the critical frequency ( $f_{SM}$ ) was found to increase sharply from 150 kHz at 109°C to 465 kHz at 105°C in SmC\* phase [**Figure 5.10(a)**]. Thus  $f_{SM}$  was observed to increase on either side of  $T_c$  according to Curie-Weiss law [38].



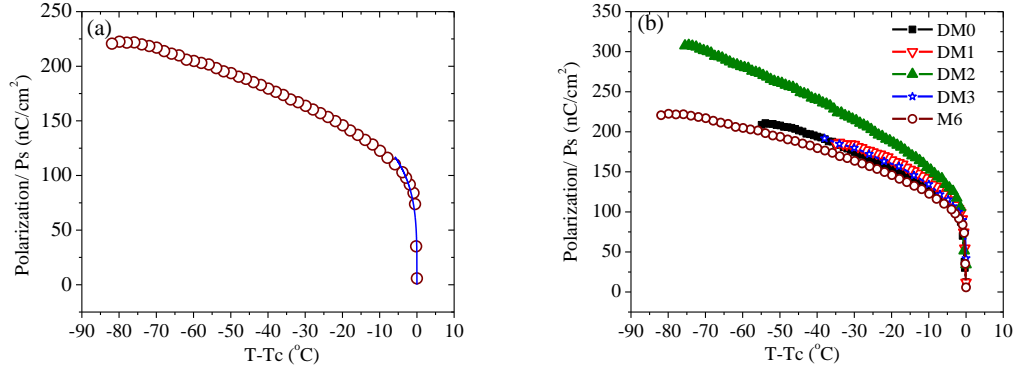
**Figure 5.14.** Temperature dependence of (a)  $f_{SM}$  at selected bias field near  $T_c$  and (b) bias field dependence of  $T_c$ .

To investigate how the ferroelectric to paraelectric transition temperature  $T_c$  changes with bias field, dielectric spectra were taken upto  $\pm 2.5^\circ\text{C}$  on both sides of  $T_c$  at steps of  $0.1^\circ\text{C}$  under fixed bias field of 0.0, 0.5, 1.0, 1.5, and  $2.0\text{ V}/\mu\text{m}$ . Following Landau theory Schacht *et al.* [39, 40] showed that when the critical frequency  $f_{SM}$  and the inverse of dielectric strength ( $\Delta\epsilon_{SM}^{-1}$ ) of SM are plotted as a function of temperature for a fixed bias, the minima of  $f_{SM}$  (or  $\Delta\epsilon_{SM}^{-1}$ ), correspond to the transition temperature  $T_c$  at that fixed bias. For M6 this is shown in **Figure 5.14(a)** for  $f_{SM}$ . The obtained value of  $T_c$  was observed to remain unchanged at  $110.1^\circ\text{C}$  upto a bias field  $0.5\text{ V}/\mu\text{m}$ , but after that it increased almost linearly with bias to  $110.6^\circ\text{C}$  as shown in **Figure 5.14 (b)**.

### 5.3.5 ELECTRO-OPTIC STUDY

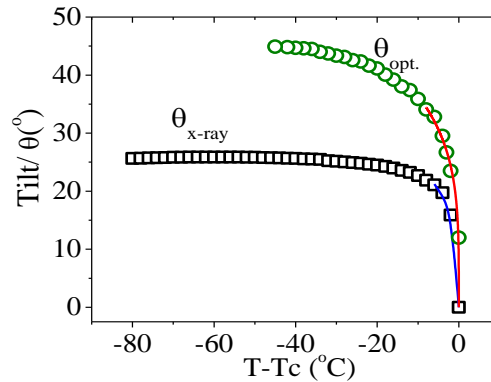
By electro-optic method we measured the spontaneous polarization ( $P_s$ ), optical tilt angle ( $\theta$ ) and switching time ( $\tau$ ) of mixture M6. Temperature dependence of spontaneous polarizations ( $P_s$ ) is depicted in the **Figure 5.15(a)**. The maximum value was found to be  $222.5\text{ nC}/\text{cm}^2$  and decreased rapidly with temperature. However, the  $P_s$  of the mixture was found to be slightly less in comparison to the pure DM0 and DM3, but much less than DM1 and DM2, especially DM2 as shown in **Figure 5.15(b)**. The binary mixture of DM0 and DM3 also showed similar behaviour as described in chapter 4 [16]. Thus in both the binary and the quaternary mixtures  $P_s$  did not show additive behaviour. Observed  $P_s$  data fitted near  $T_c$  nicely to the equation  $P_s = P_0(T - T_c)^\beta$ , considering  $\beta = 1/4$  as discussed before [**Figure 5.15(a)**]. Fitted  $T_c$

was  $109.9 \pm 0.2$  °C which was very close to the actual  $T_c$  (110.0 °C) and critical exponent  $\beta$  was  $0.25 \pm 0.01$ . This also supported our previous inference that the SmC\*–SmA\* transition was TCP type.



**Figure 5.15.** (a) Temperature variation of  $P_s$  of M6, the fitted line is also shown. (b) Comparison of  $P_s$  of the mixture with the pure compounds.

The optical tilt ( $\theta_{opt.}$ ) of the mixture was found to increase sharply with the decrease of temperature near  $T_c$  and reached nearly 45° in SmC<sub>A</sub>\* phase [Figure 5.16]. Thus the mixture also showed orthoconic antiferroelectric nature like the pure compounds. On the other hand, the X-ray tilt showed similar temperature dependence [Figure 5.16] but its maximum value was 25.8°, much less compared to the optical tilt. The maximum value of  $\theta_{X-ray}$  in the pure compounds was also around 25°.

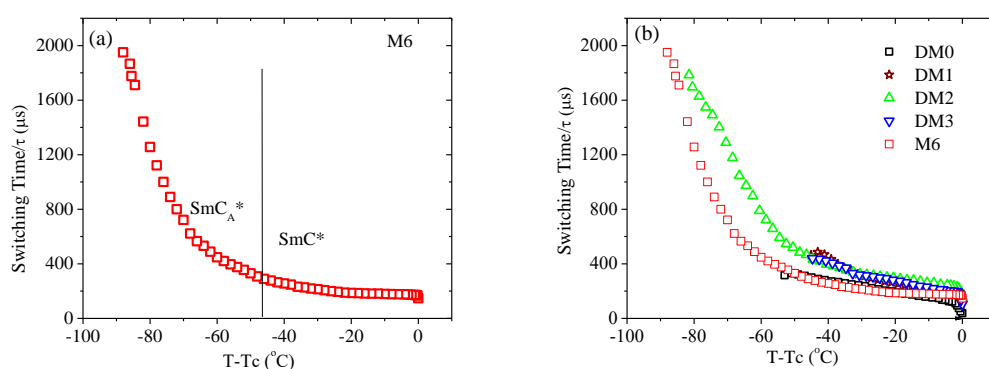


**Figure 5.16.** Temperature dependence of optical tilt ( $\theta_{opt.}$ ) and X-ray tilt ( $\theta_{X-ray}$ ) of M6. Power law fitted lines near  $T_c$  are also shown as discussed in text.

Similar results were reported before by several authors [27, 41-44], although existence of higher x-ray tilt than optical tilt was also observed by Meier *et al.*[41]. Reason of this discrepancy has been explained in chapter 3. However, both types of

tilts could be fitted nicely to the power law with  $\beta = 0.25 \pm 0.02$  near  $T_c$  [Figure 5.16] as observed before signifying again the TCP nature of  $SmC^* - SmA^*$  transition.

The switching time ( $\tau$ ), which represents the response of the material to an applied electric field, is an important parameter from the application point of view. The lower is the switching time, the faster will be the response. Switching time of the mixture showed similar nature of temperature dependence as in the pure compounds.  $\tau$  increased with decrease of temperature and reached a value of  $308\mu s$  at the onset of  $SmC_A^*$  phase, thereafter it increased rapidly reaching a maximum value of  $1950\mu s$  as shown in Figure 5.17(a). However  $\tau$  of the pure compounds DM0, DM1, DM2 and DM3 at the onset of  $SmC_A^*$  were  $332\mu s$ ,  $348\mu s$ ,  $484\mu s$  and  $330\mu s$  respectively [Figure 5.17(b)]. A similar temperature dependence of switching time was observed by Fitas *et al.* in an induced high tilt antiferroelectric liquid crystal mixture W-316-3 [45]. In the mixture in  $SmC^*$  phase the  $\tau$  increased slowly nearly from  $0.01$  ms to  $0.1$  ms and at the transition  $SmC^*-SmC_A^*$  it showed a discontinuity and then increased sharply in  $SmC_A^*$  phase nearly to  $3.5$  ms. Dwivedi *et al.* observed that the switching time vary approximately  $2-5$  ms with the applied field in a high tilt antiferroelectric pure compound [46]. Similarly in a high tilt antiferroelectric compound having similar structure to that of DM0, only differing in number of oligomethelene spacer, Verma *et al.* measured switching time of about  $45$  ms in antiferroelectric phase while observing its variation with applied field [47]. Selected important parameters of the mixture and the pure compounds are furnished in Table 5.2 for ease of comparison.



**Figure 5.17.** (a) Temperature dependence of switching time ( $\tau$ ) of M6 (b) comparison of  $\tau$  of M6 with the pure compounds.

**Table 5.2.** A Selected list of parameters of mixture M6 and pure compounds DM0, DM1, DM2 and DM3.

Parameters	Values in the pure compounds and in the mixture				
	DM0	DM1	DM2	DM3	M6
$\Delta\epsilon_{max}$	350	270	178	400	344
$f_{GM}(\text{Hz})$	1400-3800	900-2000	1100-1950	450-1800	1140-2050
$f_{SM}(\text{kHz})$	220-810	12.25-81	110-400	110-425	110-475
$f_{PL}(\text{kHz})$	30-195	23-54	0.125-0.9	6.5-13.5	22.5-42.0
$f_{PH}(\text{kHz})$	580-925	160-610	290-440	22.5-125	250-900
$D_{max}(\text{\AA})$	5.46	4.94	4.95	5.59	4.97
$d_{max}(\text{\AA})$	34.92	35.53	34.98	34.78	35.1
$\xi_{  }(\text{max})$	963	1000	871	894	850
$\theta_{opt.}(\text{max})$	44.3	44.9	44.7	45.0	44.9
$P_s(\text{nC/cm}^2)(\text{max})$	210.8	186.7	308	191.7	222.5
$\tau(\mu\text{s})$ (at the onset of $\text{SmC}_A^*$ )	332	348	484	330	308
$\gamma_\phi(\text{Pa.s})(\text{max})$	1.37	0.93	2.72	1.49	0.14
$E_a(\text{kJ mol}^{-1})$	38.19	44.52	44.38	44.34	33.41
$E_c$ for GM ( $\text{V}/\mu\text{m}$ )	0.93	0.91	0.4	0.68	0.4

## 5.4 CONCLUSION

A room temperature multi-component high tilt antiferroelectric mixture was prepared mixing four antiferroelectric compounds of a homologous series in equal wt.%. Although the phase sequence was observed to remain same as in the pure compounds ( $\text{Cr-SmC}_A^*-\text{SmC}^*-\text{SmA}^*-\text{Iso}$ ), the range of  $\text{SmC}_A^*$  phase was increased significantly and extended far below room temperature ( $\sim -8^\circ\text{C}$  to  $65^\circ\text{C}$ ). Some properties of the mixture were found to be equal to the average of the pure compounds. Optical tilt was nearly  $45^\circ$  showing orthoconic nature of the mixture like the pure compounds. The layer spacing ( $d$ ) in  $\text{SmC}_A^*$  phase shrunk almost by 10% from its value in  $\text{SmA}^*$  phase. A parabolic nature of variation of  $d$  with temperature near  $T_c$  with critical exponent value of 0.5 signified that the  $\text{SmC}^*-\text{SmA}^*$  transition was tricritical in nature. Temperature variation of spontaneous polarization ( $P_s$ ) and tilt ( $\theta$ ) near  $T_c$  also supported this inference. Correlation lengths across and within the layers were found to increase from paraelectric to ferroelectric to antiferroelectric phases. Four collective modes viz.  $P_L$ ,  $P_H$ , GM and SM were observed. Domain mode

was also exhibited under sufficient dc bias.  $f_{SM}$  and  $\Delta\epsilon_{SM}$  were found to follow Curie–Weiss law.  $T_c$  was found to increase with bias which was explained using Landau model. The mixture exhibited sub-millisecond switching, near the onset of  $\text{SmC}_A^*$  phase, observed switching time was around  $308\mu\text{s}$ .

## 5.5 REFERENCES

- [1] R. Dabrowski, J. Gasowska, J. Oton, W. Piecek, J. Przedmojski, and M. Tykarska, High tilted antiferroelectric liquid crystalline materials, *Displays*. 25 (2004) 9–19.
- [2] S.T. Lagerwall, *Ferroelectric and antiferroelectric liquid crystals*, New York (NY): Wiley-VCH; (1998).
- [3] P. Rudquist, Orthoconic antiferroelectric liquid crystals, *Liq. Cryst.* 40(12) (2013)1678–1697.
- [4] J.W. Goodby, The nanoscale engineering of nematic liquid crystals for displays, *Liq. Cryst.* 38(2011)1363–1387.
- [5] P. Rudquist, Smectic LCD Modes, in *Handbook of visual display technology*, J. Chen, W. Cranton, and M. Fihn, eds., Springer, Berlin, 2012, pp. 1445–1467.
- [6] S.T. Lagerwall, K. Dhawe, P. Rudquist, H. Pauwels, W. Drzewinski, and R. Dabrowski, Solution of the dark state problem in antiferroelectric liquid crystal displays, *Appl. Phys. Lett.* 76 (2000) 3528–3530.
- [7] K. Dhawe, A. Dahlgren, P. Rudquist, J.P.F.Lagerwall, G. Andersson, M. Matuszczyk, S.T. Lagerwall, R. Dabrowski, and W. Drzewinski, Antiferroelectric liquid crystals with 45° tilt – a new class of promising electro-optic materials, *Ferroelectrics*. 244 (2000)115–128.
- [8] P. Kula, R. Dabrowski, K. Kening, and D. Chyczewska, New antiferroelectric compounds from chiral terphenyls, *Ferroelectrics*. 343 (2006)19-26.
- [9] P. Kula, J. Herman, P. Perkowski, M. Mrukiewicz, and L.R. Jaroszewicz. On the influence of the chiral side linking bridge type upon the syclinic vs. anticlinic balance in the case of 2', 3' -difluoroterphenyl derivatives, *Liq. Cryst.* 40 (2013)256-266.
- [10] R. Dabrowski, P. Kula, Z.Raszewski, W. Piecek, J.M. Oton, and A. Spadlo. New Orthoconic Antiferroelectrics useful for Applications, *Ferroelectrics*. 395 (2010)116-132.
- [11] M. Zurowska, R. Dabrowski, J. Dziaduszek, K. Skrzypek, M. Filipowics, W. Rejmer, K. Czuprynski, N. Bennis, J.M. Otton, Influence of alkoxy chain length

- and fluorosubstitution on mesogenic and spectral properties of high tilted antiferroelectric esters, *J. Mater Chem.* 21 (2011)2144-2153.
- [12] M. Żurowska, R. Dąbrowski, J. Dziaduszek, K. Czupryński, K. Skrzypek, and M. Filipowicz, Synthesis and Mesomorphic Properties of Chiral Esters Comprising Partially Fluorinated Alkoxyalkoxy Terminal Chains and a 1-methylheptyl Chiral Moiety, *Mol. Cryst. Liq. Cryst.* 495 (2008)145 [497]–157 [509].
- [13] P. Kula, R. Dąbrowski, and M. Tykarska, Orthoconic antiferroelectric liquid crystals containing a terphenyl rigid core, *Phase Trans.* 80 (6) (2007)771–780.
- [14] T. Geelhaar, Ferroelectric mixtures and their physico-chemical properties, *Ferroelectrics.* 85(1988)[329]/717-[349]/737.
- [15] K. C. Dey, P. K. Mandal, and R. Dabrowski, Effect of lateral fluorination in antiferroelectric and ferroelectric mesophases: synchrotron X-ray diffraction, dielectric spectroscopy and electro-optic study, *J. Phys. Chem. Solids.* 88 (2016)14-23.
- [16] E.C.H. Hsu and J. F. Johnson, Prediction of Eutectic Temperatures, Compositions and Phase Diagrams for Binary Mesophase Systems, *Mol. Cryst. Liq. Cryst.* 27 (1974) 95-104.
- [17] A. V. Ivashenko, V. V. Titov, E. I. Kovshev, Liquid Crystalline Compounds: III On Applicability of Schröder-Van Laar Equations to Liquid Crystals Mixtures, *Mol. Cryst. Liq. Cryst.* 33 (1976) 195-200.
- [18] K. C. Dey, and P. K. Mandal, Formulation of a binary eutectic antiferroelectric liquid crystal mixture: Comparison of dielectric and electro-optic properties with the pure compounds, *J. Mol. Liq.* 243 (2017)484 –493.
- [19] A. Debnath, and P. K. Mandal, Effect of fluorination on the phase sequence, dielectric and electro-optical properties of ferroelectric and antiferroelectric mixtures, *Liq. Cryst.* 44 (2017)2192–2202
- [20] A. Debnath, D. Sinha, and P. K. Mandal, Wide range room temperature electroclinic liquid crystal mixture with large induced tilt and very small layer contraction, *JAP.* 119 (2016)124103(1-4)

- [21] A. Wiegeleben and D. Demus. Calorimetric Investigations in Liquid Crystalline Terephthalylidene-bis- [ 4-n-alkylanilines], *Crystal Res. & Technol.* 17(1982), 161-165.
- [22] Yu. Panarin, O. Kalinovskaya, and J. K. Vij, Observation and investigation of the ferroelectric sub-phases with high  $q_T$  parameter, *Phy. Rev. E.* 55(4)(1997)4345-4353.
- [23] B. Zeks, Landau Free Energy Expansion for Chiral Ferroelectric Smectic Liquid Crystal, *Mol. Cryst. Liq. Cryst.* 114 (1984)259-270.
- [24] R. Shashidhar, B. R. Ratna, G. G. Nair, S. Krishna Prasad, Ch. Bahr, and G. Heppke, Mean-Field to Tricritical Crossover Behaviour near the Smectic-A-Smectic-C\* Tricritical Point, *Phys. Rev. Lett.* 61(5) (1988)547-549.
- [25] C. S. Hartley, N. Kapernaum, J. C. Roberts, F. Giesselmann, and R. P. Lemieux, Electroclinic effect in chiral SmA\* liquid crystals induced by atropisomeric biphenyl dopants: amplification of the electroclinic coefficient using achiral additives, *J. Mater. Chem.* 16 (2006)2329–2337.
- [26] D. Sinha, A. Debnath, and P.K. Mandal, Hexatic and blue phases in a chiral liquid crystal: optical polarizing microscopy, synchrotron radiation and dielectric study, *Mater. Res. Express.* 1 (2014)1-13.
- [27] A. Debnath, P. K. Mandal, D. Weglowska, and R. Dabrowski, Induction of a room temperature ferroelectric SmC\* phase in binary mixtures with moderate spontaneous polarization and sub-millisecond switching time. *RSC Advances*, 6 (2016)84369-84378.
- [28] J. Hou, J. Schacht, F. Giebelmann, and P. Zugenmaier, Temperature and bias-field dependences of dielectric behaviour in the antiferroelectric liquid crystal, (R)-MHPOBC, *Liq. Cryst.* 22(4) (1997)409-417.
- [29] M. Buivydas, F. Gouda, G. Andersson, S.T. Lagerwall, and B. Stebler, Collective and non-collective excitations in antiferroelectric and ferroelectric liquid crystals studied by dielectric relaxation spectroscopy and electro-optic measurements, *Liq. Cryst.* 23(5) (1997)723-739.

- [30] Yu. Panarin, O. Kalinovskaya, and J. K. Vij, The investigation of the relaxation processes in antiferroelectric liquid crystals by broad band dielectric and electro-optic spectroscopy, *Liq. Cryst.* 25 (2) (1998)241-252.
- [31] Y. P. Panarin, O. Kalinovskaya, and J. K. Vij, The relaxation processes in helical antiferroelectric liquid crystals, *Ferroelectrics.* 213 (1998)101-108.
- [32] P. Perkowski, K. Ogrodnik, W. Piecek, M. Zurowska, Z. Raszewski, R. Dabrowski, and L. Jaroszewicz, Influence of the bias field on dielectric properties of the  $\text{SmC}_A^*$  in the vicinity of the  $\text{SmC}^*-\text{SmC}_A^*$  phase transition, *Liq. Cryst.* 38(16) (2011)1159-1167.
- [33] S. Ghosh, P. Nayek, S.K. Roy, T. P. Majumder, and R. Dabrowski, Dielectric relaxation spectroscopy and electro-optical studies of a new, partially fluorinated orthoconic antiferroelectric liquid crystal material exhibiting V-shaped switching, *Liq. Cryst.* 37(4) (2010)369-375.
- [34] M. Marzec, R. Dabrowski, A. Fafara, W. Haase, S. Hiller, and S. Wrobel, Goldstone mode and domain mode relaxation in ferroelectric phases of 4'-[(S,S) - 2,3 - epoxyhexyloxy] phenyl 4-(decyloxy)benzoate (EHPDB), *Ferroelectrics.* 180 (1996)127-135.
- [35] K. C. Dey, P. K. Mandal, and R. Dabrowski, Influence of Bias on Dielectric Properties of Mesophases of a Laterally Fluorinated Antiferroelectric Liquid Crystal, in *Recent Trends in Materials Science and Applications*, Springer Proceedings in Physics. 89 (2016) 475-483.
- [36] W. Haase, S. Hiller, M. Pfeiffer, and L.A. Beresnev, The domain mode in ferroelectric liquid crystals; electro-optical and dielectric investigations, *Ferroelectrics.* 140 (1993)37-44.
- [37] S.A. Arrhenius, On the reaction rate of the inversion of non-refined sugar upon souring, *Z. Phys. Chem.* 4 (1889)99-116.
- [38] F. Gouda, K. Skarp, and S.T. Lagerwall, Dielectric studies of the soft mode and Goldstone mode in ferroelectric liquid crystals, *Ferroelectrics.* 113 (1991)165-206.

- [39] J. Schacht, F. Giesselmann, P. Zugenmaier, and W. Kuczynski, Dielectric studies of the bias field effect on the soft mode of a ferroelectric liquid crystal, *Ferroelectrics*. 209 (1998)483-503.
- [40] T. Carlsson, B. Zeks, C. Filipic, and A. Levstik, Theoretical model of the frequency and temperature dependence of the complex dielectric constant of ferroelectric liquid crystals near the smectic-C\* –smectic-A phase transition, *Phys. Rev. A*. 42(2) (1990)877-889.
- [41] J. G. Meier, M. Nobili, T. Carlsson, P. Rudquist, A. S. Petrenko, J. W. Goodby, M. Brunet, and S. T. Lagerwall, Possible model of an antiferroelectric twist grain boundary phase, *Phys. Rev. E*. 76 (2007)011704(1-9).
- [42] R. Bartolino, J. Doucet and G. Durand, Molecular tilt in the smectic C phase: a zig-zag model, *Ann. de Phys.* 3 (1978)389–395.
- [43] E. N. Keller, E. Nachaliel, and D. Davidov, Evidence for the “zig-zag” model of the smectic-C phase in the liquid crystal 4'-butoxyphenylester 4-decyloxybenzoic acid (4OP10O8): A high resolution x-ray study, *Phys. Rev. A*. 34 (5) (1986)4363-4369.
- [44] M. S. Spector, P. A. Heiney, J. Naciri, B. T. Weslowski, D. B. Holt, and R. Shashidhar, Electroclinic liquid crystals with large induced tilt angle and small layer contraction, *Phys. Rev. E*. 61(2) (2000)1579-1584.
- [45] J. Fitas, M. Marzec, K. Kurp, M. Żurowska, M. Tykarska & A. Bubnov. Electro-optic and dielectric properties of new binary ferroelectric and antiferroelectric liquid crystalline mixtures. *Liq. Cryst.* 44(9) (2017) 1468-1476.
- [46] A. Dwivedi, R. Dhar, R. Dabrowski, and M. Tykarska, Characteristic switching and dielectric parameters of ferro- and antiferroelectric phases of (S)-(+)-(1-methylheptyloxycarbonyl) phenyl 4-(6-perfluoropentanoyloxyhex-1-oxy) biphenyl-4-carboxylate, *J. Phys. D: Appl. Phys.* 42 (2009)095402(1-10).
- [47] R. Verma, R. Dabrowski, and R. Dhar, Thermodynamic, electrical and electro-optical features of the racemic mixture of an antiferroelectric liquid crystal suitable for displays, *Liq. Cryst.* 42(12) (2015)1785-1797.



# CHAPTER 6

---

## Effect of multi-walled carbon nanotubes on dielectric and electro-optic properties of a high tilt antiferroelectric liquid crystal

6.1	INTRODUCTION	153
6.2	EXPERIMENTAL TECHNIQUES	154
6.3	RESULTS AND DISCUSSION	155
6.3.1	OPTICAL POLARIZING MICROSCOPY	155
6.3.2	DIELECTRIC STUDY	158
6.3.3	ELECTRO-OPTIC STUDY	164
6.4	CONCLUSION	168
6.5	REFERENCES	169

---

Part of the work has been published in Phase Transitions Vol. 92(3) (2019), pp. 302–315.



## 6.1 INTRODUCTION

Carbon nanotubes are the most important allotrope of carbon, after its discovery by Sumio Iijima [1] they find applications in diversified fields like – electromechanical devices, hydrogen storage, field emission devices, nanometer-sized electronic devices, sensors and probes etc., due to their fascinating properties of high conductivity with essentially no heating. They possess exceptional stiffness and strength with high modulus of elasticity [2, 3], and enhanced surface area due to its high porosity. Mainly there are two types of carbon nanotubes: (a) single-walled carbon nanotubes (SWCNT) and (b) multi-walled carbon nanotubes (MWCNT). SWCNTs consist of a single graphite sheet wrapped into a cylindrical tubular shape whereas MWNTs consist of a number of such SWCNTs placed coaxially one within another with weak coupling and that is why MWCNTs are almost similar to SWCNTs in respect of electronic properties. Due to one dimensional electronic structure, they have high conductivity along their lengths and almost non-conducting along their diameter [4]. Liquid crystals, on the other hand, are fascinating self-assembled soft materials in which the molecules are orientationally ordered and maybe partially positionally ordered also. They easily response to small perturbations like the electric field, magnetic field, surface effect, etc. for which they find applications in diversified areas, mainly in display technology. Optimization of the electro-optic properties of liquid crystalline material is essential for the display applications. One approach to achieve optimized LC materials is engineering their molecular structures [5–7]. The alternative process, as discussed in Chapter 4, maybe preparing mixtures (binary, ternary, or multi-component) or by dispersing LCs in a non-mesogenic host mixture [8]. But dispersing carbon nanotubes in liquid crystalline host could be another non-synthesis means. Initially, most of the studies were confined to nanocomposites of nematic liquid crystals [4, 9–14]. The composite system of liquid crystals and carbon nanotubes attracted great interest as they show lower operating voltage, higher contrast ratio and faster switching speeds [9] because a minute addition of CNTs makes a huge change in the properties of nematic LCs. CNTs were first aligned along the director ( $\mathbf{n}$ ) of molecules by dispersing them in nematic media by Lynch *et al.* [10]. From the measurement of angular distribution Dierking *et al.* [4] showed that nanotubes are mainly oriented along the director. Enhanced conductivity and lowered threshold voltage for Freedericksz transition from planar to homeotropic configuration

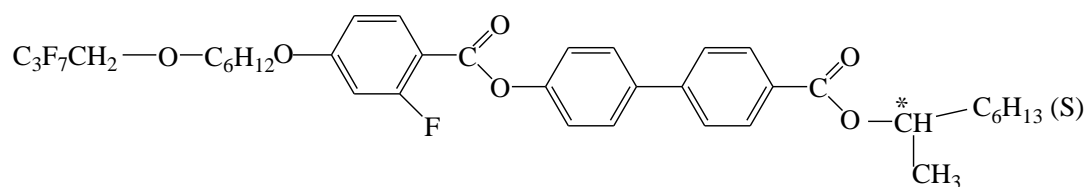
of the SWCNT doped nematic liquid crystals were observed by Dierking *et al.* [4]. Two important issues for high performance of liquid crystalline displays (LCD) are to reduce the charge impurity for reducing the transient current and to increase the resistivity in order to increase the voltage holding ratio (VHR) [11]. Chen *et al.* [12] observed much lower transient current in the insulating nano particle doped LCD cells which indicated the decrease of moving ion density. A high voltage holding ratio was also observed in the doped cells. Lee *et al.* [13] investigated MWCNT doped twisted nematic liquid crystal system by optical transition under application of a dc voltage and observed a reduced dc driving voltage and an improved switching behaviour. An increase of effective elastic constant of doped LC–CNT dispersion due to a small amount of CNT dopant in twisted nematic liquid crystal cell was also observed by Huang *et al.* [14]. In the recent past, few groups studied the CNT composite of ferroelectric liquid crystals (FLCs) [15–17]. Decreases in dielectric increment, a faster switching and enhanced stability of helical structure were observed by P. Arora *et al.* [15] and F.V. Podgornov *et al.* [16] in FLC/MWCNT dispersions. A similar decrease in dielectric strength was also observed in CNT doped deformed helix FLCs by N. Sood *et al.* [17]. But studies on nanocomposites of antiferroelectric liquid crystals are rare. In one communication reductions of viscosity and switching time in CNT composite were reported [18]. Large change in electrical conductivity with small change in CNT concentration was also reported [19]. Therefore, in order to observe the change of properties biphenyl benzoate core-based compound (DM1) in presence of tiny external particles (nano scale), a small amount of a multi-walled –COOH functionalized carbon nanotubes has been mixed and the properties of the nanocomposite are discussed in comparison to the pure compound in this chapter.

## 6.2 EXPERIMENTAL TECHNIQUES

The molecular structure of the pure compound named as DM1, whose properties have been discussed in Chapter 3, is again shown in **Figure 6.1** for ease of discussion. This compound was used as the host.

Multiwall carbon nanotubes functionalized with –COOH, purchased commercially from Time Nano (China), was used as the dopant. The length of MWCNTs is spread over 0.5–2.0  $\mu\text{m}$  and diameter spread over 8–15 nm. To prepare the nanocomposite, the MWCNTs were dispersed in chloroform and sonicated for about 40 minutes using an ultrasonic mixture (GT Sonic Professional, Apex, India).

The desired amount of the prepared dispersion was added to the pure AFLC to make the concentration of MWCNT 0.12 wt.%. The whole mixture was again dissolved in chloroform and sonicated for an hour to get a homogeneous mixture. Then the mixture was heated at 60°C to evaporate the chloroform. The resulting AFLC/MWCNT mixture was introduced into a planar EHC cell of thickness 5  $\mu\text{m}$  by capillary action in the isotropic phase. The texture of the mixture was studied using Olympus BX41 polarizing microscope. Dielectric spectroscopy and frequency dependent conductance measurement was performed using computer-controlled HIOKI 3532–50 impedance analyzer from 50 Hz – 5 MHz, confining the cell within Mettler FP82HT hot stage and the temperature was controlled with Mettler FP90 central processor with accuracy  $\pm 0.1^\circ\text{C}$ . The dielectric spectra of AFLC/CNT composite were fitted using the modified Cole-Cole equation [20] as detailed in Chapter 2.



**Figure 6.1.** Molecular structure of the antiferroelectric liquid crystal (DM1)

## 6.3 RESULTS AND DISCUSSIONS

### 6.3.1 OPTICAL POLARIZING MICROSCOPY

The phase sequence and transition temperatures ( $^\circ\text{C}$ ) of the pure and the AFLC/MWCNT composite, obtained from optical polarising microscopy in the heating cycle are shown below. Transition temperatures during cooling ( $@0.1^\circ\text{C}/\text{min.}$ ) are mentioned within the bracket. The considerable supercooling effect is noticed in the pure as well as in the nanocomposite.

Pure Compound: Cr (20) 41  $\text{SmC}_\text{A}^*$  (65) 75.2  $\text{SmC}^*$  (103) 103  $\text{SmA}^*$  (103.6) 103.6 Iso

Nanocomposite: Cr ( $<19^\circ\text{C}$ ) 39  $\text{SmC}_\text{A}^*$  (48) 70  $\text{SmC}^*$  (101) 102.5  $\text{SmA}^*$  (102.2) 103.3 Iso

Although the phase sequence of the MWCNT system is observed to remain unchanged, the transition temperatures are found to change considerably. The melting point is decreased by 2  $^\circ\text{C}$ , the clearing point is decreased slightly by 0.3  $^\circ\text{C}$ , the

transition temperature from  $\text{SmC}_A^*$  to  $\text{SmC}^*$  is decreased by 5.2 °C, and that of  $\text{SmC}^*$  to  $\text{SmA}^*$  is decreased by 0.5 °C during heating. But during cooling, the clearing point is decreased by 1.4 °C, transition temperature from  $\text{SmA}^*$  to  $\text{SmC}^*$  decreased by 2.0 °C while  $\text{SmC}^*$ - $\text{SmC}_A^*$  transition temperature is decreased by 17°C. Due to the change of transition temperatures, the stability of phases was also changed [Table 6.1]. The stability of  $\text{SmA}^*$  phase, especially of  $\text{SmC}^*$  phase is increased but that of  $\text{SmC}_A^*$  is decreased considerably. In the literature both changed and unchanged transition temperatures are reported in LC-nanocomposites.

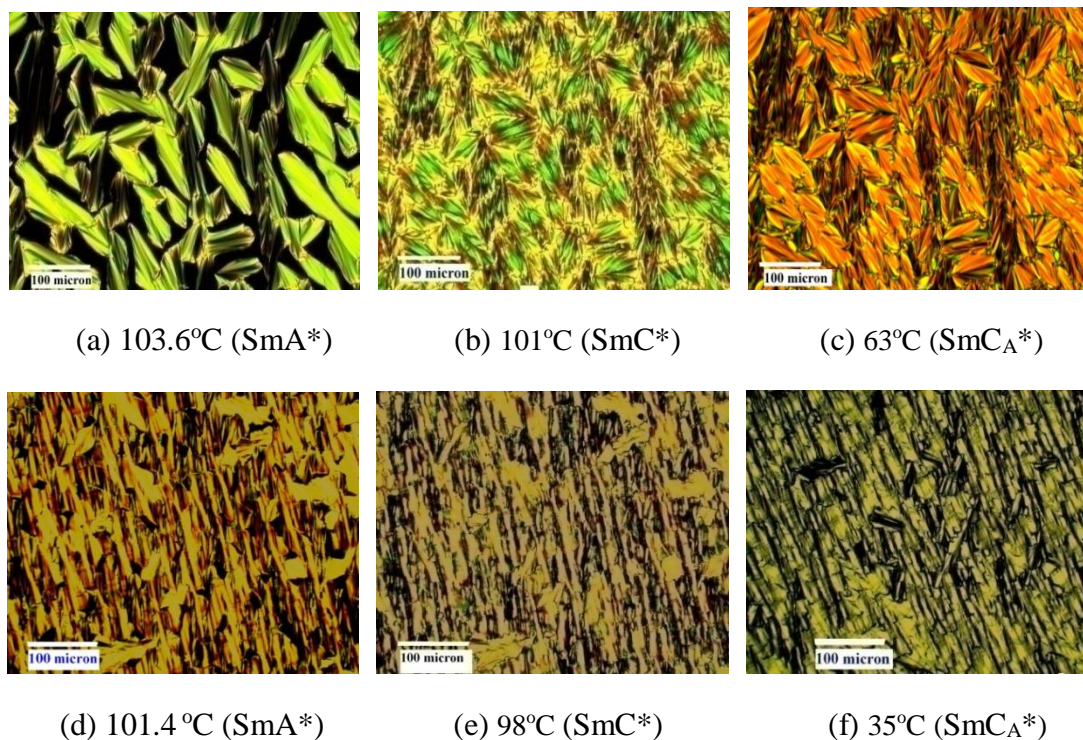
**Table 6.1.** Comparison of phase stability of pure and CNT doped systems

Compound	Phase stability in the heating cycle (°C)		
	(cooling data within parenthesis)		
	$\text{SmC}_A^*$	$\text{SmC}^*$	$\text{SmA}^*$
Pure AFLC	34.2 (45.0)	27.8 (38.0)	0.6 (0.6)
Pure+CNT	31.0 (29.0)	32.5 (53.0)	0.8 (1.2)

A decrease of isotropic to cholesteric and cholesteric to  $\text{SmC}^*$  transition temperatures by 3°C were observed in a 0.1% CNT doped ferroelectric liquid crystal by Neeraj *et al.* [21]. They also noticed a textural change in the nanocomposite. An increase of nematic to isotropic transition temperature by 3.3°C and a change of texture were observed by Pandey *et al.* [22] in 5CB dispersed with 0.1 wt% of GNPs. However, no significant influence of the carbon nanotubes on the transition temperatures and textures was observed by F.V. Podgornov *et al.* [16] in an FLC and by S. Ghosh *et al.* [18] in an AFLC system. An increase in melting point (1-2°) was observed when an FLC mixture was doped with  $\text{TiO}_2$  [23] but thresholdless V-shape switching was reported when  $\text{TiO}_2$  was doped in a pure FLC [24].

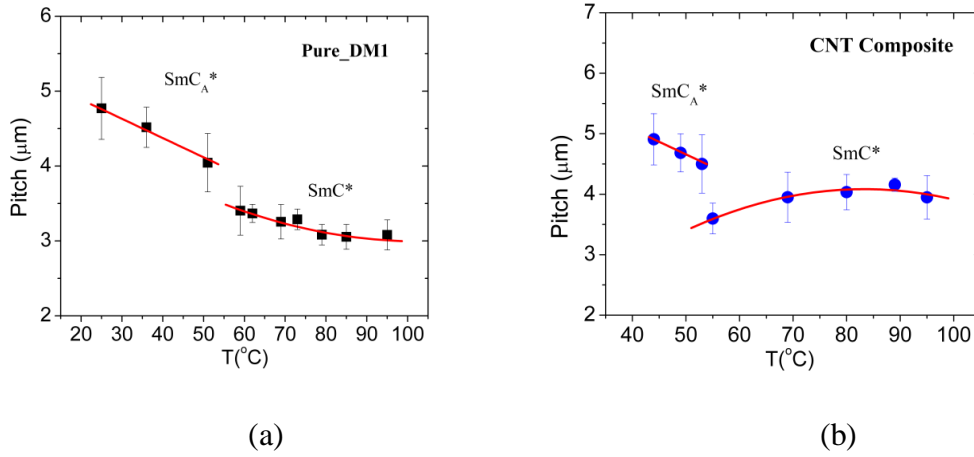
Textures were observed under planar anchoring condition for both the systems [Figure 6.2]. Representative textures of the pure AFLC in  $\text{SmA}^*$ ,  $\text{SmC}^*$  and  $\text{SmC}_A^*$  phases are shown in Figures 6.2(a)-(c), whereas those of the nanocomposite are shown in Figures 6.2(d)-(f). Typical fan shape texture was observed in the  $\text{SmA}^*$  phase which was broken in the  $\text{SmC}^*$  and  $\text{SmC}_A^*$  phases. Existence of helicoidal structure was visible in the form of parallel equidistant lines more in  $\text{SmC}_A^*$  phase than in  $\text{SmC}^*$  phase. A clear change in colour was also noticed at the phase transition

points. In the CNT doped system the textures became more homogeneous because of the better alignment of the molecular directors, other features of the textures remain unaltered. Helicoidal lines were more prominent in CNT doped  $\text{SmC}_A^*$  phase as was the case in pure system. No evidence of CNT aggregates was seen in any of the textures.



**Figure 6.2.** Textures of  $\text{SmA}^*$ ,  $\text{SmC}^*$  and  $\text{SmC}_A^*$  phases of the pure compound in (a)-(c) and those of the composite in (d)-(f).

From the measurement of the spatial period of the stripes at different locations of the textures, values of the helical pitch were estimated [25]. Temperature dependence of the pitch in both the ferroelectric and antiferroelectric phases along with estimated errors is shown in **Figure 6.3**. In the pure compound, the pitch is observed to increase slightly within the  $\text{SmC}^*$  phase with decreasing temperature, shows a discontinuous change at  $\text{SmC}^*$ - $\text{SmC}_A^*$  transition and then in the  $\text{SmC}_A^*$  phase it increases further. But in the nanocomposite the only behavioural change is that the pitch decreases slightly with decreasing temperature in  $\text{SmC}^*$  phase. Similar temperature dependence of helical pitch were observed by J. Li *et al.* [26] in several pure systems, a decrease of the pitch with decreasing temperature was also reported by Martinot-lagarde *et al.* [25].



**Figure 6.3.** Temperature variation of pitch in  $\text{SmC}^*$  and  $\text{SmC}_A^*$  phases of (a) pure and (b) MWCNT composite.

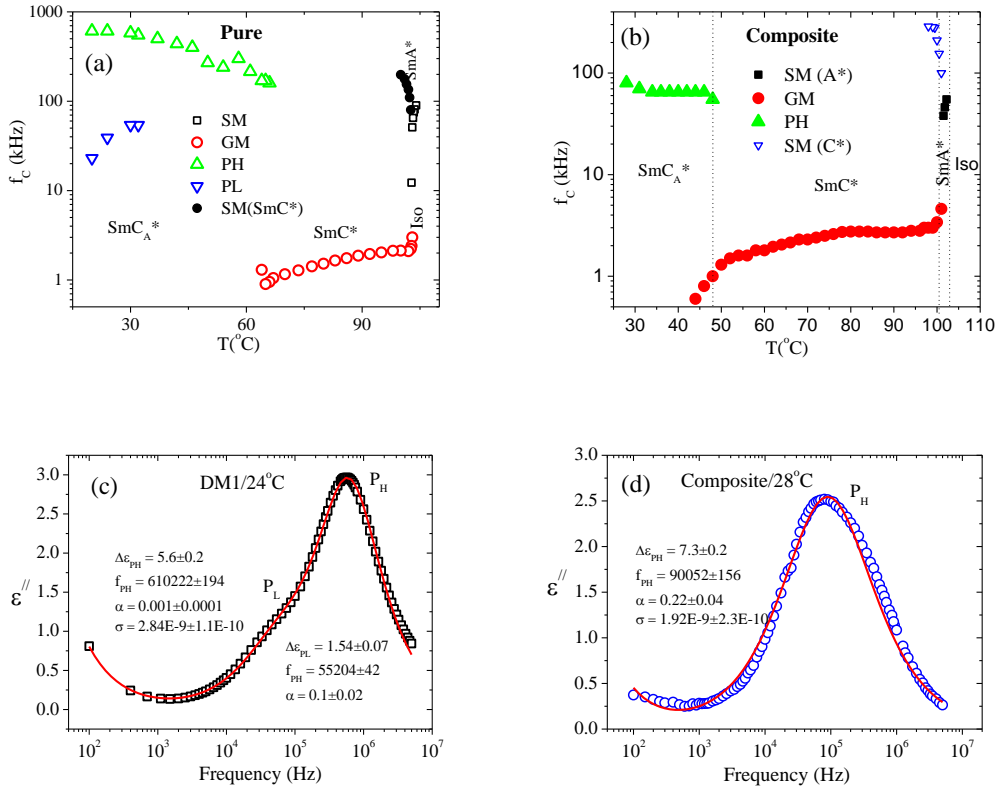
### 6.3.2 DIELECTRIC STUDY

To explore the molecular dynamics of the pure as well as of its nanocomposite, we have studied their relaxation behaviour in homogeneous geometry. The transverse component (real  $\epsilon'$  as well as imaginary part  $\epsilon''$ ) of the dielectric permittivity was measured in the 50 Hz to 5 MHz frequency domain during cooling starting from the isotropic phase down to the room temperature. From the temperature evolution of critical frequency ( $f_c$ ) and the strength of dielectric absorption ( $\epsilon''$ ) the modes of relaxations present in different phases of the composite were identified. Soft mode in  $\text{SmA}^*$  phase, Goldstone mode in  $\text{SmC}^*$  phase, in-phase and anti-phase antiferroelectric modes ( $P_L$ ,  $P_H$ ) in  $\text{SmC}_A^*$  phase were observed in the pure compound [19] as discussed in Chapter 3 whereas in its MWCNT composite all those modes were observed except the  $P_L$  mode in  $\text{SmC}_A^*$  phase as depicted in **Figure 6.4**.

The critical frequency of high frequency anti-phase mode ( $f_{PH}$ ) in the pure system is observed to increase from 160 kHz to 610 kHz whereas in the doped system it increases from 55 kHz to 80 kHz. Thus the value of  $f_{PH}$  is observed to reduce and the range becomes narrower due to doping. The reduction of  $f_{PH}$  is clearly seen in the exemplary fitted curve in the  $\text{SmC}_A^*$  phase of the pure and the doped system [**Figure 6.4(c)**]. It is also observed that the absorption strength of the high frequency antiferroelectric mode ( $\epsilon''_{PH}$ ) decreases in the doped system. In the pure system  $\epsilon''$  varies from 2.16 to 3.01 whereas in CNT doped system it varies from 2.41 to 2.52.

In the pure compound, the  $P_L$  mode is observed to appear far below the  $SmC^*$ - $SmC_A^*$  transition during cooling (transition takes place at  $66^\circ\text{C}$  whereas  $P_L$  appears at  $32^\circ\text{C}$ ). Its critical frequency ( $f_{PL}$ ) decreases with the decrease of temperature from 54 kHz at  $32^\circ\text{C}$  to 23 kHz at  $20^\circ\text{C}$ ; absorption strength ( $\epsilon''_{PL}$ ) is also found to decrease from 1.26 to 1.09.

As discussed in previous Chapters the soft mode arises from the tilt fluctuation of the molecules in  $SmA^*$  phase. When the temperature approaches  $SmA^*$ - $SmC^*$  transition ( $T_c$ ) from above, the binding forces of the molecules soften resulting in the increase of amplitude of fluctuations and the decrease of relaxation frequency. When the temperature is lowered below  $T_c$  the situation is reversed. Therefore,  $f_{SM}$  depicts V-shape temperature dependence near the transition [27].



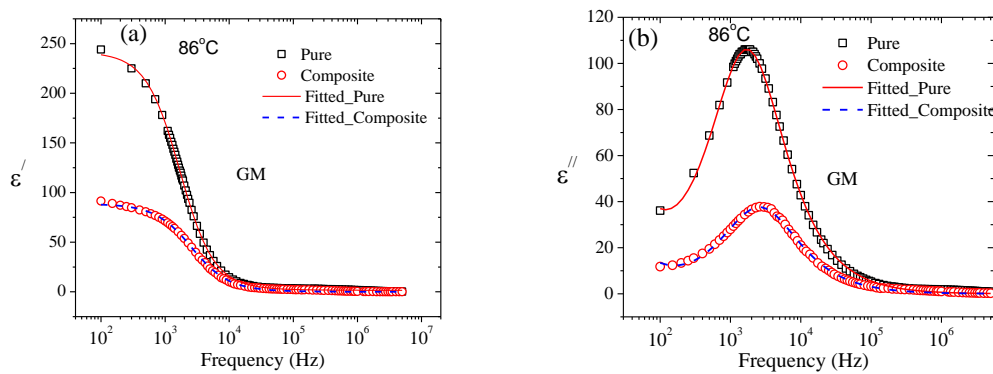
**Figure 6.4.** Temperature dependence of critical frequencies ( $f_c$ ) of all modes of (a) pure AFLC, (b) nanocomposite, (c) fitted absorption ( $\epsilon''$ ) curve in  $SmC_A^*$  phase of pure AFLC and (d) its CNT composite. Soft mode in the  $SmC^*$  phase seen under bias field.

Since the range of the  $SmA^*$  phase is very small in both the systems, only a few data points could be collected. Studying these data it is observed that the critical

frequency of the soft mode ( $f_{SM}$ ) in SmA\* phase of the pure compound increases with temperature from 12.5 kHz to 81 kHz whereas that of the composite increases from 38 kHz to 55 kHz. Doping of the rigid and stiff rod-like MWCNTs in a soft liquid crystalline system enhances the modulus of elasticity of the medium [28] which in turn makes it less flexible. Consequently, the critical frequency of the tilt fluctuations ( $f_{SM}$ ) in the CNT doped system increases.

The soft mode in the SmC\* phase but in the vicinity of  $T_c$  could also be studied by suppressing the Goldstone mode after applying a strong bias field. The  $f_{SM}$  is found to increase sharply from 80 kHz to 198 kHz in the pure compound and in the nanocomposite it is increased from 100 kHz to 288 kHz as shown in **Figure 6.4** indicating an increase of  $f_{SM}$  in the doped system. However, in both the systems, the critical frequencies of the soft mode are observed to increase on both sides of  $T_c$  by following Curie-Weiss law [27].

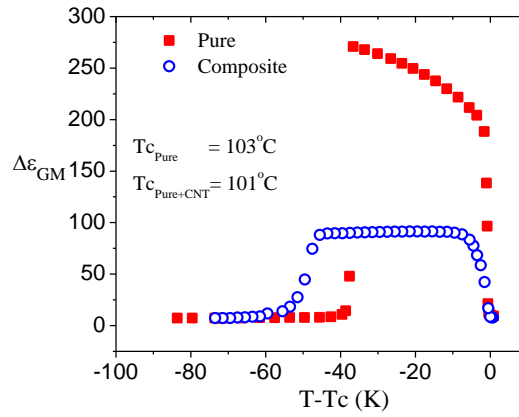
Prominent collective relaxation mode in SmC\* phase is the Goldstone mode which arises due to fluctuations in the azimuthal angle of the directors, hence also called a phason mode. The Goldstone mode (GM) was observed in both the systems, however, GM continued with decreasing critical frequency in the CNT composite about  $4^\circ$  below the SmC\*–SmC<sub>A</sub>\* transition [**Figure 6.4(b)**]. This mode in SmC<sub>A</sub>\* phase within a few degrees just after the transition is due to the incomplete molecular arrangement of SmC<sub>A</sub>\* phase and is termed as hereditary mode [29]. Exemplary fitted dispersion and absorption curves of the pure and the MWCNT composite in SmC\* phase at  $86^\circ\text{C}$  are shown in **Figure 6.5**.



**Figure 6.5.** Comparison of the fitted (a) dispersion ( $\epsilon'$ ) and (b) absorption ( $\epsilon''$ ) curves in the SmC\* phase at  $86^\circ\text{C}$ . Fitted parameters for pure compound are  $\Delta\epsilon_{GM} = 236.78 \pm .86$ ,  $f_{GM} = 1732.70 \pm 8.42 \text{ Hz}$ ,  $\alpha = 0.07 \pm 0.002$ ,  $\sigma = 1.14E - 7 \pm$

$4.5E - 9$  and that for nanocomposite are  $\Delta\epsilon_{GM} = 86.04 \pm .47$ ,  $f_{GM} = 2608.94 \pm 20.00 \text{ Hz}$ ,  $\alpha = 0.09 \pm 0.002$ ,  $\sigma = 5.08E - 8 \pm 2.57E - 9$ .

It is seen that the real part of the dielectric permittivity ( $\epsilon'$ ) at 100 Hz decreases from 239 to 88 due to CNT doping. The range of critical frequency of Goldstone mode ( $f_{GM}$ ) of the pure AFLC is 900 Hz to 2400 Hz but in the composite, it increases from 1300 Hz to 4600 Hz. Doping of MWCNT reduces the dielectric increment ( $\Delta\epsilon_{GM}$ ) significantly over the entire range of Goldstone mode as depicted in **Figure 6.6**.



**Figure 6.6.** Temperature dependence of dielectric increment ( $\Delta\epsilon_{GM}$ ) of the pure AFLC and its CNT composite.

Reduction of the real part of permittivity due to doping of CNTs in ferroelectric, deformed helix ferroelectric and antiferroelectric liquid crystals was reported by various groups [16–18]. Decrease of dielectric increment ( $\Delta\epsilon_{GM}$ ) and increase of critical frequency ( $f_{GM}$ ) can be explained using generalized Landau theory of T. Carlsson *et al.* [30]. Considering the bi-quadratic coupling between the tilt and the polarization they derived the following relations for  $\Delta\epsilon_{GM}$  and  $f_{GM}$ .

$$\Delta\epsilon_{GM} = \frac{1}{2\epsilon_0 K_\phi q^2} \left[ \frac{Ps}{\theta} \right]^2 \quad (6.1)$$

$$\text{and } f_{GM} = \frac{K_\phi q^2}{2\pi\gamma_{GM}} \quad (6.2)$$

Since twist elastic constant  $K_\phi$  increases due to dispersion of rigid carbon nano particle in soft liquid crystal medium, spontaneous polarization ( $Ps$ ) decreases and tilt angle  $\theta$  remains unaltered (discussed in section 3.4), the relation (2) infers that  $\Delta\epsilon_{GM}$

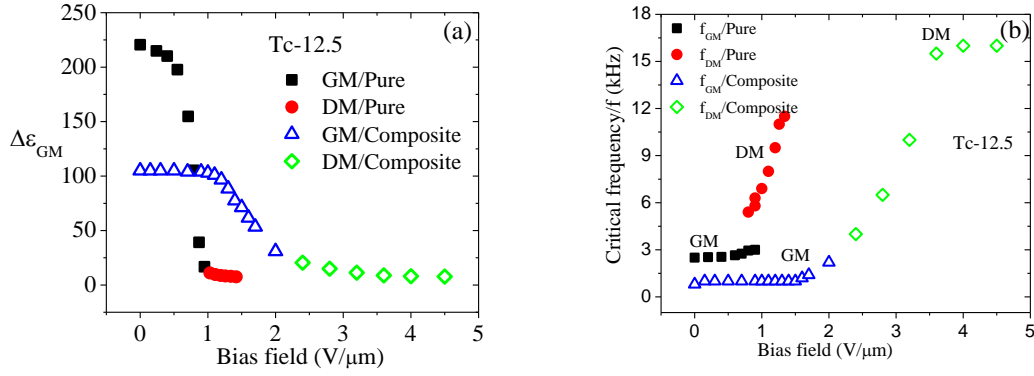
should decrease. Similarly increase of  $K_\phi$  and reduction of  $\gamma_{GM}$  (discussed in section 3.4) explains increased  $f_{GM}$  from relation (3). The ranges of critical frequencies of different modes of pure AFLC and its CNT composite are furnished in **Table 6.2** for ease of comparison.

Goldstone mode begins to reduce with increasing bias field in both the pure and the doped material [**Figure 6.7**]. In the case of the pure AFLC as GM decreases with bias field a new mode begins to arise at a bias field of 0.80 V/ $\mu\text{m}$  in the higher frequency region; however, GM is completely suppressed at 0.90 V/ $\mu\text{m}$ . In the CNT composite, GM is completely suppressed at 2.40 V/ $\mu\text{m}$  but in both the systems at higher fields a new relaxation mode arises with higher critical frequencies. At high field solid ferroelectric like domains are formed in both the systems which give rise to this mode and the mode is termed as domain mode (DM) [31]. The absorption strength of this mode is smaller ( $\sim 10$ ) and the critical frequency ( $f_{DM}$ ) is 2 to 4 fold higher than that of  $f_{GM}$ . In some cases, 10 fold increase of  $f_{DM}$  is also reported [32].

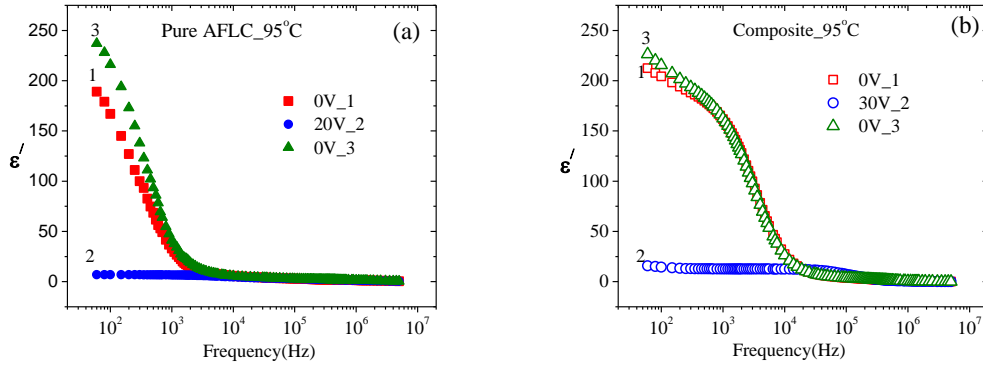
**Table 6.2.** Comparison of different critical frequencies of the pure and the CNT composite

Parameter	Pure DM1	DM1+CNT
$f_{PL}$	54-23 kHz	Not found
$f_{PH}$	160 -610 kHz	55-80 kHz
$f_{SM}$	12.5-81 kHz	38-55 kHz
$f_{GM}$	900-2400 Hz	1300-4600 Hz
$f_{DM}$	5.4-11.5 kHz	2.2-15.5 kHz

The critical frequencies of domain mode ( $f_{DM}$ ) in both the pure and CNT doped composite increase sharply with the increasing bias field. In pure AFLC  $f_{DM}$  increases from 5.4 kHz at 0.8 V/ $\mu\text{m}$  to 11.5 kHz at 1.36 V/ $\mu\text{m}$  and is suppressed at 1.42 V/ $\mu\text{m}$  [33] whereas in its CNT doped composite  $f_{DM}$  increases from 2.2 kHz at 2.40V/ $\mu\text{m}$  to 15.5 kHz at 3.60V/ $\mu\text{m}$  and then remains constant at 16 kHz up to 4.50V/ $\mu\text{m}$ , finally suppressed at 4.50 V/ $\mu\text{m}$ . It was noted before that about two and half times more bias field was required to suppress the Goldstone mode in the AFLC/CNT composite compared to the pure. These suggest that the helical structure is more stable in the AFLC/CNT composite which implies the increased ordering of the molecules.



**Figure 6.7.** (a) Dielectric increments and (b) critical frequencies as a function of dc bias field of the pure AFLC and its composite at  $T_c = 12.5$ .



**Figure 6.8.** Frequency dependent dielectric dispersion ( $\epsilon'$ ) curves in  $\text{SmC}^*$  phase under the bias field of 0V (curve 1), 30V (curve 2) and again 0V (curve 3) of the (a) pure AFLC and (b) its nanocomposite.

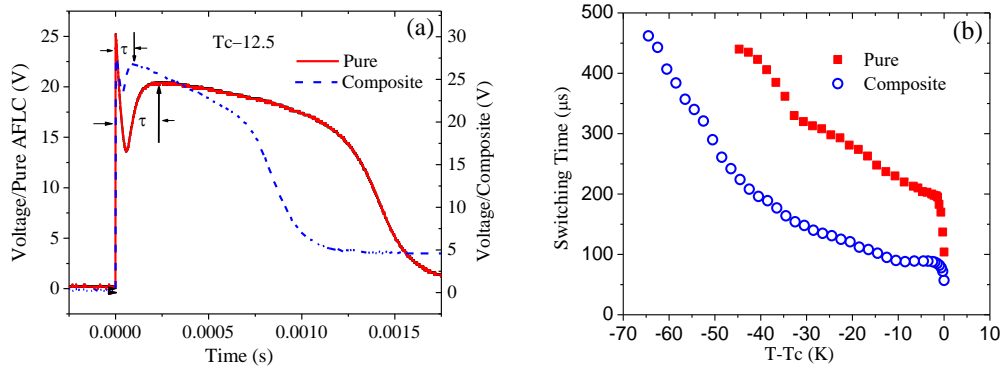
The memory effect of the pure and CNT doped composite was also investigated. The real part of the permittivity ( $\epsilon'$ ) was measured as a function of frequency at  $95^\circ\text{C}$  ( $\text{SmC}^*$  phase) at bias fields of 0V, then 30V and again at 0V after a time delay of 8 minutes [Figure 6.8]. At 0V, the value of  $\epsilon'$  is high due to Goldstone mode relaxation and at 30V, it is very small due to suppression of the GM at such high bias field. After a time delay of 8 minutes,  $\epsilon'$  was observed to regain the value obtained before applying 30V. Therefore, both the pure and the nanocomposite do not remain in the unwinding state after withdrawal of the high bias field, which essentially implies that they do not have any memory effect.

### 6.3.3 ELECTRO-OPTIC STUDY

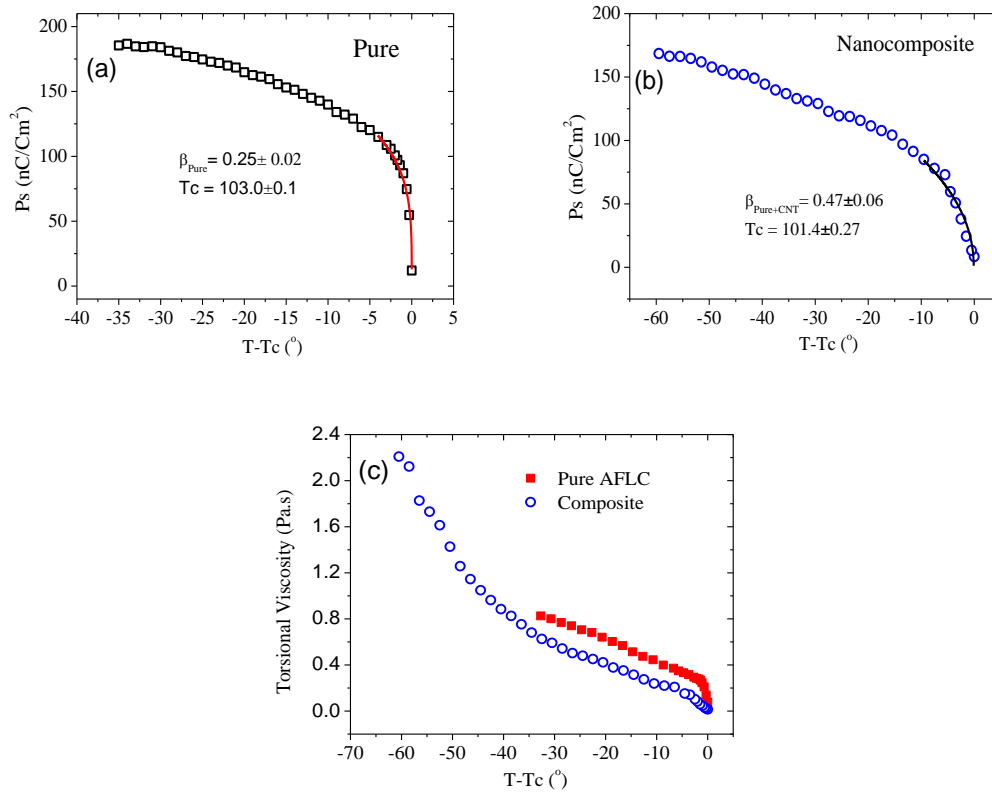
Switching time ( $\tau$ ) is the most important physical parameter for addressing the fast LC display devices. In the undoped liquid crystal devices the response time is higher due to the presence of ion impurities, so to achieve faster display devices the ion density should be reduced. Doping of LCs with CNTs is one of the suitable means to achieve it [12, 34]. An improved response time (almost 50% less) was observed in a CNT doped deformed helix ferroelectric liquid crystal (DHFLC) by J. Prakash *et al.* [35]. A rapid decrease in the rise time with increasing concentration of CNT was observed in a negative dielectric anisotropy nematic host by C.Y. Huang *et al.* [36]. Faster response time in the nano tube doped cells than in pure FLC mixture cell was observed by F.V. Podgornov *et al.* [16]. Improvement of response time of FLC material in both thin and thick cells upon doping copper oxide decorated MWCNTs was observed by A. Malik *et al.* [34]. In a CNT doped AFLC cell, almost 40% faster response time compared to the pure system was observed by S. Ghosh *et al.* [18]. This decrease in response time in CNT doped nematic, FLC and AFLC system is attributed to the decrease in the viscosity, since switching time is directly related to the viscosity ( $\gamma$ ) as follows [37–39]

$$\gamma = \tau \cdot P_s \cdot E \quad (6.3)$$

where  $E$  is the electric field applied and  $P_s$  is the spontaneous polarization. As discussed in Chapter 2 the delay in occurring of polarization bump in time axis due to polarization reversal of square wave pulse is considered as the measure of the response time of ferroelectric materials. As an example, time delays in the pure AFLC and its CNT composite are compared at  $T_c-12.5$  in **Figure 6.9(a)**. The delay of the polarization bump in the nanocomposite is almost 56% less than that of the pure compound. Temperature variation of switching time is compared in **Figure 6.9(b)** which shows that the switching is much faster in the nanocomposite in the entire ferroelectric and antiferroelectric phases as was reported in the literature. At 60°C in  $\text{SmC}_A^*$  phase, the switching time is found to decrease from 435  $\mu\text{s}$  to 224  $\mu\text{s}$  and at 94 °C in  $\text{SmC}^*$  phase it reduces to 89  $\mu\text{s}$  from 220  $\mu\text{s}$ .



**Figure 6.9.** (a) The delay of polarization bump of pure AFLC and its CNT composite occurring in time axis at  $T_c-12.5$  (b) Variation of switching time with temperature.



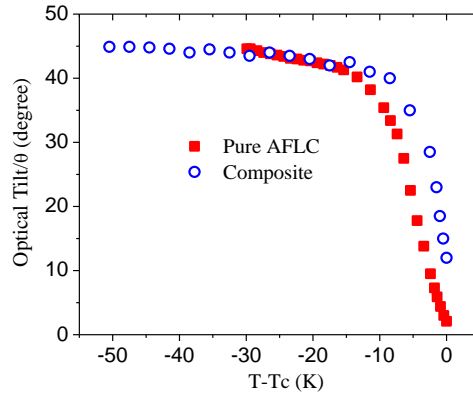
**Figure 6.10.** Temperature dependence of spontaneous polarization of (a) Pure AFLC and (b) Nanocomposite, fitted curves near  $T_c$  is also shown, (c) Temperature dependence of rotational viscosity of the pure and the CNT composite.

The spontaneous polarization ( $P_s$ ) of the AFLC/MWCNT is also found to reduce significantly in the doped system as shown in **Figure 6.10**. CNTs having an unmatched aspect ratio, unmatched electrical properties and distinct dielectric anisotropies, when doped in the anisotropic liquid crystalline host, change the

spontaneous polarization. A decreased value of  $P_s$  was reported by J. Prakash *et al.* [35] in a CNT doped deformed helix FLC system. The  $P_s$  data were fitted to the mean field equation near  $T_c$  and in the pure compound a  $\beta$  value of 0.25 was obtained which suggests the ferroelectric to paraelectric transition is tricritical in nature (also discussed in chapter 3) whereas in the nanocomposite the  $\beta$  value obtained 0.47 which is near to 0.5 and suggests the ferroelectric to paraelectric transition is second order.

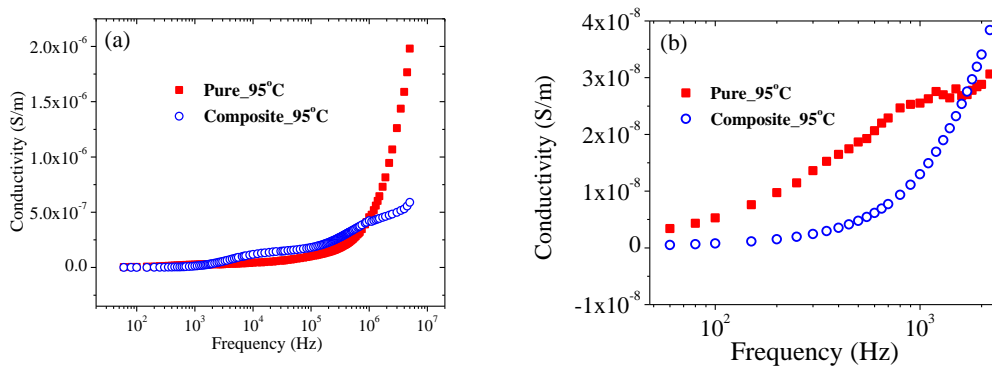
The rotational viscosities, as estimated by the formula (4), are depicted as a function of temperature in **Figure 6.10(c)**. In the pure compound, it varies from 0.08 to 0.82 Pa.s and in the composite it reduces and varies from 0.3 to 0.62 Pa.s up to 34.7 K below  $T_c$ , thus viscosity also reduces substantially in the composite.

The increase of the orientational order parameter in the CNT doped nematic liquid crystals is reported by several authors [22, 40]. Increased nematic–isotropic transition temperature, signifying increased orientational order, in gold nano particle (GNP) doped NLC composite has been observed [22]. A substantial increase of the nematic order parameters are reported in BaTiO<sub>3</sub> and Sn<sub>2</sub>P<sub>2</sub>S<sub>6</sub> particle doped NLC systems [40]. In the case of FLCs and AFLCs, the molecular tilt ( $\theta$ ) is considered as the primary order parameter which was also observed to increase by several authors on CNT doping [41–43]. The tilt angle of an FLC was observed to increase approximately from 25° to 28° when doped with –COOH functionalized MWCNTs [41]. A similar increase in the tilt angle was reported by Kumar *et al.* [42] in Pd nano particle doped FLC system. Fivefold increase of optical tilt was also reported in GNP doped ferroelectric liquid crystal (FLC) mixtures [43]. However, in the present study, no change in tilt angle is observed in the doped system in the low temperature regime, at high temperatures the tilt is found to increase as shown in **Figure 6.11**. Since the pure AFLC under investigation is orthoconic in nature, the tilt is around 45°, therefore, we cannot expect any further increase in its value at low temperature except an improvement in their dispersion. An almost similar result was reported in a CNT doped orthoconic AFLC having similar molecular structure only difference was in the position of the lateral Fluorine atom [18].

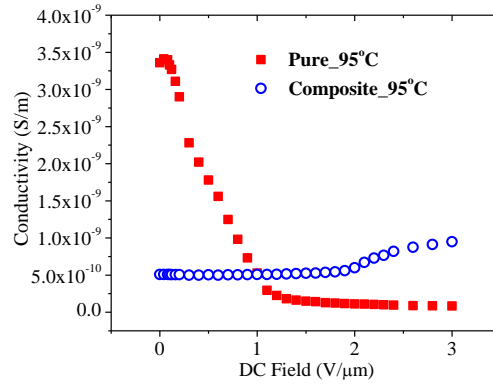


**Figure 6.11.** Variation of optical tilt as a function of reduced temperature ( $T-T_c$ ).

The frequency dependent conductivities ( $\sigma$ ) of the pure and the AFLC/MWCNT composite at 95°C in SmC\* phase were measured using the same dielectric cell and the obtained results are depicted in **Figure 6.12(a)**. In the low frequency region  $\sigma$  is found to be substantially less in the nanocomposite due to trapping of the impurity charges by the CNTs. This is clearly shown in **Fig. 6.12(b)**. This is also revealed by the fact that in the pure system  $\sigma$  decreases sharply with the field at low frequency (60 Hz) whereas in the nanocomposite it remains almost constant [**Figure 6.13**]. However, with frequency  $\sigma$  becomes higher in the doped system. High value of conductivity in the undoped sample at lower fields is due to the presence of the impurity ions which arise due to aligning layers and during the synthesis of the LC materials [44, 45] and disappear at higher fields. CNTs having higher electron affinity trap the ions, thereby decrease the ion density in the composite at lower fields. The increase of conductivity at higher fields in the composite may be due to the mobility of trapped ions.



**Figure 6.12.** (a) Variation of conductivity as a function of frequency, (b) Magnified view is shown in the low frequency region.



**Figure 6.13.** Variation of conductivity as a function of dc bias field.

#### 6.4. CONCLUSION

Properties of an AFLC and its MWCNT doped composite have been studied and compared. Due to the addition of a small fraction (0.12 wt.%) of MWCNT in the AFLC the phase boundaries are lowered and the stability of the SmA\* and the SmC\* phases are found to increase but that of SmC<sub>A</sub>\* phase is decreased. Distinct textural changes are observed in different phases. Pitch of the helicoidal structure was found to increase with decreasing temperature in the pure compound in both the tilted phases, the opposite trend is observed in the composite in the SmC\* phase. In the antiferroelectric phase, the in-phase antiferroelectric mode is absent in the doped system whereas the absolute values and the ranges of the anti-phase antiferroelectric mode critical frequency ( $f_{PH}$ ) and the absorption strength ( $\epsilon''_{PH}$ ) are found to decrease in the doped system. However, the reduction of the dielectric increment ( $\Delta\epsilon_{GM}$ ) and increase of critical frequency ( $f_{GM}$ ) of the Goldstone mode in the composite have been observed and explained using generalized Landau theory. Two fold increase of the critical field for suppression of the Goldstone mode in the composite is found, which signifies the helical structure in the nanocomposite is more stable than in the pure compound. Doping of rigid MWCNTs increases the modulus of elasticity of the composite and hence increases SM critical frequency. Moreover, significant reduction of spontaneous polarization and switching time is observed in the composite. The observed decrease in response time in the doped system is attributed to the decrease in the rotational viscosity ( $\gamma$ ). A lower value of conductivity in the composite signifies trapping of impurity ions by the CNTs.

## 6.5 REFERENCES

- [1] S. Iijima, Helical microtubules of graphitic carbon, *Nature (London)*. 354(1991)56-58.
- [2] R. H. Baughman, A. A. Zakhidov, W.A. de Heer, Carbon Nanotubes- the Route Toward Applications, *Science*. 297(2002) 787–792.
- [3] X. Yu, R. Rajamani, K.A. Stelson, T. Cui, Carbon nanotube-based transparent thin film acoustic actuators and sensors, *Sensors and Actuators A*. 132 (2006) 626–631.
- [4] I. Dierking, C. Scalia, P. Morales, D. LeClere, Aligning and reorienting carbon nanotubes with nematic liquid crystals, *Advanced Materials*. 16(11) (2004) 865–869.
- [5] M. Zurowska, R. Dabrowski, J. Dziaduszek, K. Czuprynski, K. Skrzypek, M. Filipowicz, Synthesis and Mesomorphic Properties of Chiral Esters Comprising Partially Fluorinated Alkoxyalkoxy Terminal Chains and a 1-methylheptyl Chiral Moiety, *Mol. Cryst. Liq. Cryst.* 495(2008)145–157.
- [6] D. Ziobro, R. Dabrowski, M. Tykarska, W. Drzewinski, M. Filipowicz, W. Rejmer, W. Kusmierk, P. Morowiak, W. Piecek, Synthesis and properties of new ferroelectric and antiferroelectric liquid crystals with a biphenyl benzoate rigid core, *Liq. Cryst.* 39 (2012)1011–1032.
- [7] Y. Aoki, H. Nohira, New antiferroelectric liquid crystals with a trifluoromethyl group at the chiral centre, *Liq. Cryst.* 19(1) (1995)15–19.
- [8] T. Geelhaar, Ferroelectric mixtures and their physico-chemical properties, *Ferroelectrics*. 85 (1988) 329–349.
- [9] H. Qi, T. Hegmann, Impact of nanoscale particles and carbon nanotubes on current and future generations of liquid crystal displays, *J. Mate. Chem.* 18(28) (2008) 3288–3294.
- [10] M.D. Lynch, and D.L. Patrick, Organizing Carbon Nanotubes with Liquid Crystals, *Nano Lett.* 2(11) (2002) 1197–1201.
- [11] T. Takanishi, T. Takahashi, H. Mada, and S. Saito, Transient Behavior of Voltage Holding Ratio in Nematic Liquid Crystal Cells, *Jpn. J. Appl. Phys.* 41 (2002) 3752–3757.

- [12] P. S. Chen, C.C. Huang, Y.W. Liu, C.Y. Chao, Effect of insulation nanoparticles addition on ion current and voltage-holding ratio in nematic liquid crystal cells. *Appl. Phys. Lett.* 90 (2007) 211111(1–3).
- [13] W. Lee, C. Wang, Y. Shih, Effect of carbon nanosolids on the electro-optical properties of a twisted nematic liquid crystal host, *Appl. Phys. Lett.* 85(4) (2004) 513–516.
- [14] C.Y. Huang, H. C. Pan, C.T. Hsieh, Electro-optical properties of carbon-nanotube doped twisted nematic liquid crystal cell, *Jpn. J. Appl. Phys.* 45 (8A) (2006) 6392–6394.
- [15] P. Arora, A. Mikulko, F. Podgornov, W. Haase, Dielectric and electro-optic properties of new ferroelectric liquid crystalline mixture doped with carbon nanotubes, *Mol. Cryst. Liq. Cryst.* 502 (2009) 1–8.
- [16] F.V. Podgornov, A.M. Suvonova, A.V. Lapanik, W. Haase, Electrooptical and dielectric properties of ferroelectric liquid crystal/single walled carbon nanotubes dispersions confined in thin cells, *Chem. Phys. Lett.* 479 (2009) 206–210.
- [17] N. Sood, S. Khosla, D. Singh and S.S. Bawa. Dielectric investigations of pure and carbon nanotube-doped deformed helix ferroelectric liquid crystals. *Liq. Cryst.* 39(10) (2012) 1169–1174.
- [18] S. Ghosh, Antiferroelectric liquid crystal/carbon nano tube duo for achieving modified electro-optical properties; aiming at display application, *Adv. Mater Lett.* 7(1) (2016) 60–64.
- [19] L. N. Lisetski, N. I. Lebovka, O. Ts. Sidletskiy, V. D. Panikarskaya, N. A. Kasian, S. S. Kositsyn, M. O. Lisunova, and O. V. Melezhyk, Spectrophotometry and electrical conductivity studies of multiwall nanotubes dispersed in nematic liquid crystals, *Functional Materials.* 14 (2007) 233–237.
- [20] W. Haase, S. Wrobel (Ed.), *Relaxation phenomena – Liquid crystals, magnetic systems, polymers, high- $T_c$  superconductors, metallic glasses*, Springer–Verlag, Berlin–Heidelberg, 2003, pp. 20.
- [21] Neeraj, K. K. Raina, Dynamic Responses of Dispersed Ferroelectric Liquid Crystal Composite Materials. *Integrated Ferroelectrics.* 125 (2011) 104–110.
- [22] A.S. Pandey, R. Dhar, S. Kumar, R. Dabrowski. Enhancement of the display parameters of 4'-pentyl-4- cyanobiphenyl due to the dispersion of functionalised gold nano particles. *Liq. Cryst.* 38(1) (2011) 115–120.

- [23] P. Kumar, A. Kishore, A. Sinha, Effect of different concentrations of dopant Titanium Dioxide Nanoparticles on electro-optics and dielectric properties of ferroelectric liquid crystal mixture, *Adv. Mat. Lett.* 7(2) (2016) 104-110.
- [24] P. Kumar, A. Kishore, A. Sinha, Analog switching in the nanocolloids of ferroelectric liquid crystal, *Appl. Phys. Lett.* 108 (2016) 262903.
- [25] P. Martinot-lagarde, R. Duke, G. Durand, Temperature Dependence of Tilt, Pitch and Polarization in Ferroelectric Liquid crystals, *Mol. Cryst. Liq. Cryst.* 75 (1981) 249-286.
- [26] J. Li, H. Takezoe, A. Fukuda, Novel Temperature Dependences of Helical Pitch in Ferroelectric and Antiferroelectric Chiral Smectic Liquid Crystals, *Jpn. J. Appl. Phys.* 30 (1991) 532.
- [27] F. Gouda, K. Skarp, and S.T. Lagerwall, Dielectric studies of the soft mode and Goldstone mode in ferroelectric liquid crystal, *Ferroelectrics*. 113 (1991) 165–206.
- [28] S. Y. Jeon, S. H. Shin, S. J. Jeong, S. H. Lee, Effects of carbon nanotubes on electro-optical characteristics of liquid crystal cell driven by in-plane field, *Appl. Phys. Lett.* 90 (2007) 121901(1–3).
- [29] M. Buivydas, F. Gouda, G. Andersson, S.T. Lagerwall, B. Stebler, Collective and non-collective excitations in antiferroelectric and ferroelectric liquid crystals studied by dielectric relaxation spectroscopy and electro-optic measurements, *Liq. Cryst.* 23(5) (1997) 723–739.
- [30] T. Carlsson, B. Zeks, C. Filipic, A. Levstik, Theoretical model of the frequency and temperature dependence of the complex dielectric constant of ferroelectric liquid crystals near the smectic-C\* –smectic-A phase transition. *Phys. Rev. A.* 42(2) (1990) 877–889.
- [31] W. Haase, S. Hiller, M. Pfeiffer, L.A. Beresnev, The domain mode in ferroelectric liquid crystals-electrooptical and dielectric investigations. *Ferroelectrics*. 140 (1993) 37–44.
- [32] K. C. Dey, P. K. Mandal, R. Dabrowski, Effect of lateral fluorination in antiferroelectric and ferroelectric mesophases: synchrotron X-ray diffraction, dielectric spectroscopy and electro-optic study, *J. of Phys. and Chem. of Solids*. 88 (2016) 14–23.

- [33] K. C. Dey, P. K. Mandal, R. Dabrowski, Effect of bias on dielectric properties of  $\text{SmC}_A^*$  and  $\text{SmC}^*$  phases of a perfluorinated antiferroelectric liquid crystal, *Materials Today: Proc.* 3 (2016) 3987–3991.
- [34] A. Malik, J. Prakash, A. Kumar, A. Dhar and A.M. Biradar, Copper oxide decorated multi-walled carbon nanotubes/ferroelectric liquid crystal composites for faster display devices, *J. of Appl. Phys.* 112 (2012) 054309(1–4).
- [35] J. Prakash, A. Choudhary, D. S. Mehta, A. M. Biradar, Effect of carbon nanotubes on response time of ferroelectric liquid crystals, *Phys. Rev. E.* 80 (2009) 012701(1–4).
- [36] C. Y. Huang, C. Y. Hu, H. C. Pan, K. Y. Lo, Electrooptic Responses of Carbon Nanotube-Doped Liquid Crystal Devices, *Jpn. J. Appl. Phys.* 44(11) (2005) 8077–8081.
- [37] L. A. Beresnev, L. M. Blinov, M. A. Osipov, S. A. Pikin, Ferroelectric liquid crystals, *Mol. Cryst. Liq. Cryst.* 158A (1988) 1–150.
- [38] K. Skarp, Rotational viscosities in ferroelectric smectic liquid crystals, *Ferroelectrics.* 84 (1988) 119–142.
- [39] J. Z. Xue, M. A. Handschy, N.A. Clark, Electrooptic response during switching of a ferroelectric liquid crystal cell with uniform director orientation, *Ferroelectrics.* 73 (1987) 305–314.
- [40] M. Čopič, A. Mertelj, O. Buchnev, Y. Reznikov, Coupled director and polarization fluctuations in suspensions of ferroelectric nanoparticles in nematic liquid crystals, *Phy. Rev. E.* 76 (2007) 011702(1–5).
- [41] P. Ganguly, A. Kumar, S. Tripathi, D. Haranath and A. M. Biradar, Effect of functionalisation of carbon nanotubes on the dielectric and electro-optical properties of ferroelectric liquid crystal, *Liq. Cryst.* 41(6) (2014) 793–799.
- [42] A. Kumar, G. Singh, T. Joshi, G. K. Rao, A. K. Singh and A. M. Biradar, Tailoring of electro-optical properties of ferroelectric liquid crystals by doping Pd nanoparticles, *Appl. Phys. Lett.* 100 (2012) 054102(1–4).
- [43] S. Kaur, S. P. Singh, and A. M. Biradar, Enhanced electro-optical properties in gold nanoparticles doped ferroelectric liquid crystals, *Appl. Phys. Lett.* 91 (2007) 023120.

- [44] S. H. Perlmutter, D. Doroski, G. Model, Degradation of liquid crystal device performance due to selective adsorption of ions, *Appl. Phys. Lett.* 69(9) (1996) 1182–1185.
- [45] G. Barbero, G. Durand, Selective ions adsorption and non local anchoring energy in nematic liquid crystals, *J. Appl. Phys.* 67(5) (1990) 26781.



# CHAPTER 7

---

## Effect of fluorinated achiral chain length on structural, dielectric and electro-optic properties of a laterally fluorinated terphenyl based high tilt antiferroelectric liquid crystals

7.1	INTRODUCTION	177
7.2	EXPERIMENTS	179
7.3	RESULTS AND DISCUSSIONS	180
7.3.1	POLARIZING OPTICAL MICROSCOPY	180
7.3.2	DIFFERENTIAL SCANNING CALORIMETRY	180
7.3.3	OPTIMIZED GEOMETRY	181
7.3.4	SYNCHROTRON RADIATION DIFFRACTION STUDY	183
7.3.5	DIELECTRIC STUDY	186
7.3.6	ELECTRO-OPTIC STUDY	188
7.3.6.1	SPONTANEOUS POLARIZATION	188
7.3.6.2	OPTICAL AND X-RAY TILT	190
7.3.6.3	SWITCHING TIME	191
7.3.6.4	EFFECT OF FIELD ON FERROELECTRIC- ANTIFERROELECTRIC TRANSITION TEMPERATURE	192
7.4	CONCLUSION	193
7.5	REFERENCES	195

---

Part of the work has been accepted for publication in the Journal of Molecular Liquids, Vol. 298 (2020) pp.112056 (1-11)



## 7.1 INTRODUCTION

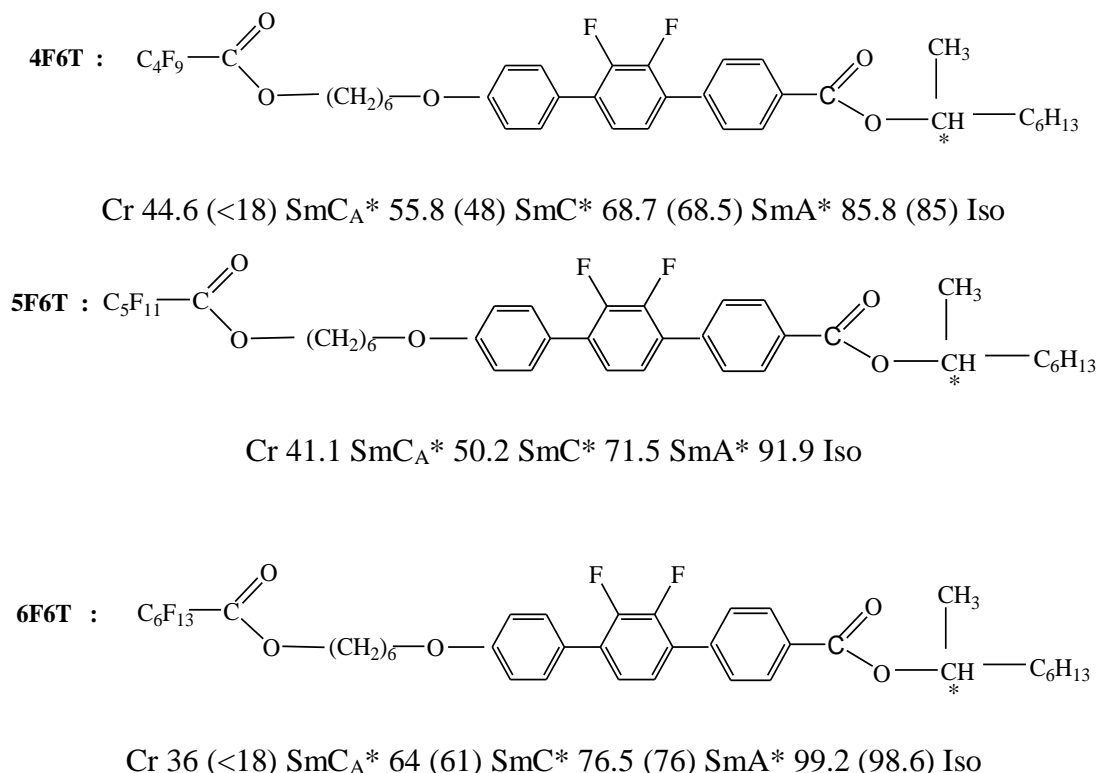
In Chapter 3 we studied the effect of lateral fluorination in the core on the properties of four biphenyl benzoate core AFLCs by various techniques. To probe structure-property relationship further, in this chapter we have investigated the effect of fluorination in achiral chain. For this we have selected two partially fluorinated terphenyl based pure antiferroelectric liquid crystals: (S)-4''-(6-perfluorotetranoyoxyhexyl-1-oxy)-2', - 3'-difluoro - 4 - (1-methylheptyloxy-carbonyl)-[1,1':4',1''] terphenyl [**4F6T**] and (S)-4''-(6-perfluorohexanoyoxyhexyl-1-oxy)-2', - 3'-difluoro - 4 - (1-methylheptyloxy-carbonyl)-[1,1':4',1''] terphenyl [**6F6T**]. These compounds were synthesized by Kula *et al* [1]. The molecular structures of these compounds are shown in **Figure 7.1**. These molecules have laterally fluorinated terphenyl core, methyl heptyl carbonyl ester at the chiral chain at one side of the core and fluorinated achiral chain having ether linkage another side of the core, the achiral chain differ only by the number of the fluorinated carbon atom. 4F6T has 4 fluorinated carbon atom and 6 oligomethelene spacer and 6F6T has 6 fluorinated carbon atom and the same 6 oligomethelene spacer in the achiral chain. Although another compound, (S)-4''-(6-perfluoropentanoyoxyhexyl-1-oxy)-2', - 3'-difluoro - 4 - (1-methylheptyloxy-carbonyl)-[1,1':4',1''] terphenyl [**5F6T**], having 5 fluorinated carbon atom and 6 oligomethelene spacer in the achiral chain, belonging to the above homologous series, has already been studied and published by our group separately before [2], its results are compared with the present compounds for the sake of better understanding of structure-property relations but our emphasis is on 4F6T and 6F6T. The code name of molecules are nFmT, n and m respectively represents the number of C atom in the perfluorinated chain and oligomethylene spacer (n=4, 5, 6 and m=6) [1].

The molecules of this series structurally differ from the DM series, discussed in Chapter 3, by the number of fluorinated carbon atom at achiral chain, instead of alkoxy group in the chain carbonyl group is attached here, the core is doubly fluorinated terphenyl based instead of biphenyl benzoate. Here we discuss the change of properties of these three compounds due to the major change with respect to the biphenyl benzoate core-based series as well as the change of properties of compounds within the series due to the change of the number of fluorinated carbon atom at achiral chain.

Like the previous DM series compounds, these compounds are also having high tilt (nearly  $45^\circ$ ) in the antiferroelectric phase i.e., successive layers are orthogonal to each other, so they are orthoconic antiferroelectric LCs (OAFLCs). For ordinary surface stabilized AFLCs, the contrast ratio is unsatisfactory and light leakage is observed. Surface-stabilized OAFLCs are uniaxial negative with the optic axis perpendicular to the glass plates and therefore provide a perfect dark state between crossed polarizers even if the direction of the smectic layer normal is not homogeneous in the plane of the cell [3–4]. Ferroelectric and antiferroelectric liquid crystals with different core, achiral and chiral chain and their effect on the mesogenic properties have been studied by several groups [5–21]. The nature and extent of influence of chain on mesomorphic properties depends upon (i) length of the chain – whether the chain is fluorinated or non-fluorinated, (ii) nature of the core –biphenyl benzoate or terphenyl or phenyl benzoate etc., (iii) linkage group between achiral chain and core, (iv) linkage group (keto or ether or ester) between chiral chain and core etc. A small influence of the prolongation of the achiral chain on mesomorphic properties was observed in both lactic acid and keto group derivatives while in keto group derivatives substantial changes were observed with increasing chiral chain [10, 21]. Goswami *et al.* [12] reported depression in melting point with increasing achiral chain length and large increase in the thermal range of  $\text{SmC}^*$  phase. On the other hand, Dabrowski *et al.* [22] reported that the fluorination in the achiral chain is responsible for appearing  $\text{SmC}_A^*$  phase and lengthening of the spacer in this part of the molecule increases the range of this phase. There are reports on the increasing trend of  $\text{SmC}^*\text{--SmC}_A^*$  transition and clearing point with increasing number of fluorinated carbon atom in the achiral chain and this increment is higher in case of even number of carbon than odd number [18, 23, 25]. Thus the number of fluorinated carbon in the achiral part is found to influence the mesogenic properties of various liquid crystalline systems.

Our main object is to investigate how the thermal ranges of different phases, smectic layer spacings, dielectric and electro-optic properties of the two compounds (4F6T and 6F6T) are influenced by the achiral chain length. Results of the intermediate homologue 5F6T, studied earlier by our group [2], will also be compared with present observations wherever possible to throw more light on the structure

property relationship. We also want to investigate the suitability of the compounds for formulation of mixtures appropriate for display and other applications.



**Figure 7.1.** Molecular structures and transition temperatures (°C) of the molecules obtained from texture studies during heating; cooling data are shown within parentheses.

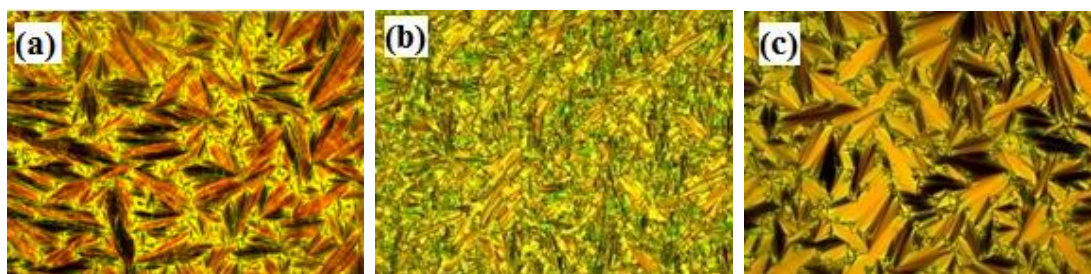
## 7.2 EXPERIMENTS

The compounds were taken in EHC homogeneous cells of 10  $\mu\text{m}$  thickness by capillary action and then cooled slowly (@  $\pm 0.2^\circ\text{C}/\text{min}$ ) in order to get aligned samples. For better alignment, a low frequency ( $\sim 10$  Hz) ac field of amplitude  $0.1\text{V}/\mu\text{m}$  was applied in SmC\* phase. Phase behaviour and transition temperatures of the compounds were investigated by polarizing optical microscopy (POM) (@  $\pm 0.2^\circ\text{C}/\text{min}$ ) and differential calorimetric study (DSC) (@  $3^\circ\text{C}/\text{min}$ ). Dielectric and electro-optical studies were performed using Indium–Tin–Oxide (ITO) (sheet resistances about  $20\Omega/\text{sheet}$ ) coated homogeneous (HG) EHC cells. Detail procedures of preparation of cell and experimental techniques have been discussed in Chapter 2. The frequency response curves were fitted to the modified Cole-Cole equation [26] to extract the dielectric increment ( $\Delta\epsilon$ ) and relaxation frequency ( $f_c$ ) of different modes.

## 7.3 RESULTS AND DISCUSSIONS

### 7.3.1 POLARIZING OPTICAL MICROSCOPY (POM)

Transition temperatures obtained from POM study are shown in **Figure 7.1**. Observed textures in different phases of 6F6T are shown in **Figure 7.2**, 4F6T showed similar textures, so are not presented for brevity. Fan-shaped texture was observed in SmA\* phase which was transformed to broken fans in SmC\* and SmC<sub>A</sub>\* phases. Within the broken fans, parallel strips were observed which arose due to the formation of helix in tilted smectic phases.



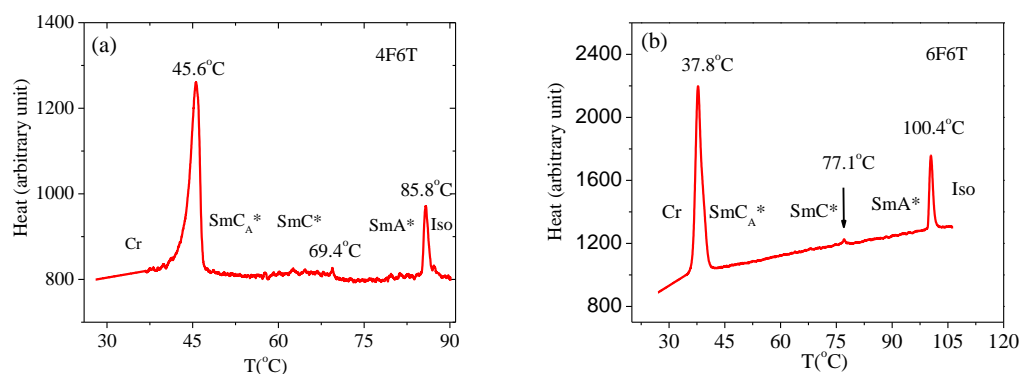
**Figure 7.2.** Textures of 6F6T in different phases (a) SmC<sub>A</sub>\* (40°C), (b) SmC\* (71°C), (c) SmA\* (95°C), magnification 200x.

### 7.3.2 DIFFERENTIAL SCANNING CALORIMETRY (DSC)

The DSC thermograms of the compounds during heating are presented in **Figure 7.3**. As reported in 5F6T [2], SmC<sub>A</sub>\*- SmC\* transition could not be detected in 4F6T and 6F6T which might be due to a very small change in enthalpy. Lack of such thermal signature at transitions involving higher order smectic phases [27] or at transitions involving minimum structural change [28] is not uncommon in liquid crystal systems. The transition temperatures obtained from DSC are slightly higher in some cases than those obtained from POM studies which may be due to finite heating rate (@3.0 °C/min).

A systematic decrease in melting point and increase in clearing point were observed with the increasing length of the fluorinated achiral chain. Such systematic change was also observed in the broadening of SmA\* phase. No such behaviour was noticed in the thermal range of SmC\* and SmC<sub>A</sub>\* phases, rather they exhibit some sort of odd-even effect [23-25, 29]. 6F6T exhibited the highest range of SmC<sub>A</sub>\*

phase. As discussed in the introduction section, increasing range of SmC\* phase was reported in a biphenyl benzoate core-based FLC system [12]. A small influence of the prolongation of the achiral chain on the mesomorphic properties of lactic acid and keto group derivatives was also observed [10, 21].



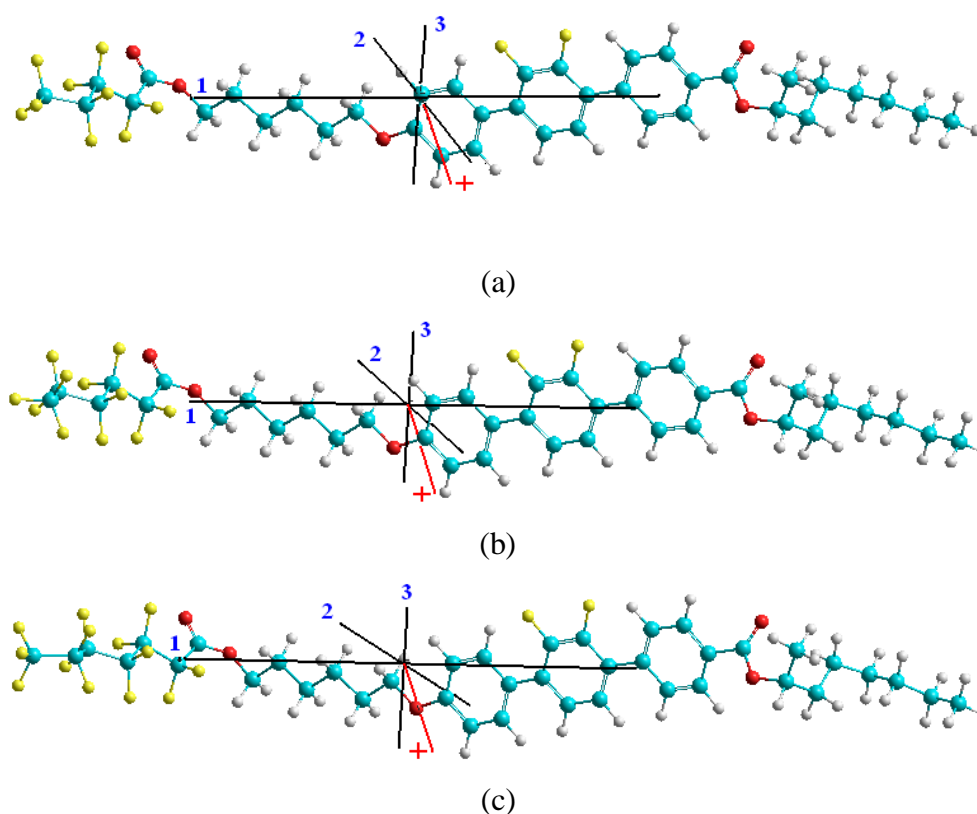
**Figure 7.3.** Typical DSC thermogram obtained for the compounds (a) 4F6T and (b) 6F6T on heating.

**Table 7.1.** Comparison of various thermal parameters obtained from POM study during heating

Sample	Melting Point (°C)	Clearing Point (°C)	Range of phase during heating (°C)		
			SmC <sub>A</sub> *	SmC*	SmA*
4F6T	44.6	85.8	11.2	12.9	17.1
5F6T	41.1	91.9	9.1	21.3	20.4
6F6T	36.0	99.2	28.0	12.5	22.7

### 7.3.3 OPTIMIZED GEOMETRY

The molecular structures of the compounds were optimized by PM3 molecular mechanics calculations in vacuo using Polak–Ribiere algorithm in a commercial package [30] to probe the structure-property relationships. The optimized structures along with moments of inertia axes and directions of dipole moments are presented in **Figure 7.4**. Optimized lengths of 4F6T, 5F6T and 6F6T were found to be 35.15, 35.95 and 36.96 Å respectively. The principal moments of inertia were found to increase systematically in all three directions with increasing fluorinated chain length as shown in **Table 7.2**. However, it should be noted that the optimized molecular structure may not be in the most extended conformation.



**Figure 7.4.** Optimized structures along with the directions of dipole moments (red line) and principal moments of inertia (black line) of (a) 4F6T, (b) 5F6T and (c) 6F6T.

The major components of dipole moments were found to be transverse to the long molecular axes for all the molecules. The molecules showed a quite high value of dipole moments – 5.13 D, 5.01 D and 5.10 D for 4F6T, 5F6T, and 6F6T, respectively. A similar variation in dipole moments was also observed in a series of partially fluorinated biphenyl benzoate rigid core-based ferroelectric liquid crystals [12], observed dipole moments were 5.12 D for 4F4R, 4.95D for 4F5R, 5.05D for 4F3R and 5.23D for 7F3R system. The molecular conformation and chain length both affect the dipole moments in the chiral molecules. Different types of variations of dipole moments with chain lengths were reported in literature [31–34] for achiral systems. Megnassan and Proutiere [31] and Gueu *et al.* [32] observed no significant change in free molecular dipole moment in nCB series for  $n=0$  to 12. Sarkar *et al.* [33] also observed no change in the dipole moments with chain length in the nCHBT series but odd-even effect was dominant. The dipole moments of molecules having even-numbered chain (4F6T and 6F6T) were higher and almost same (5.13D and 5.10 D

respectively) whereas that of odd-numbered chain (5F6T) its value was smaller ( $\sim 5.01D$ ). Thus the odd-even effect was also present in dipole moments of the present compounds as observed in the thermal range of the antiferroelectric phase.

**Table 7.2.** Molecular lengths, energy, principal moments of inertia and dipole moments of the molecules

Sample	Optimized molecular length (Å)	Energy (kCal/mole)	Moments of inertia in $10^{-44} \text{ kgm}^2$			Dipole moment (Debye)			
			About x-axis	about y-axis	about z-axis	Total	Components		
							x	y	z
4F6T	35.15	9729	27.8	913.7	925.4	5.13	+0.25	-5.12	+0.13
5F6T	35.95	10034	36.9	999.2	1017.6	5.01	+0.05	-5.01	+0.02
6F6T	37.96	10340	44.8	1106.6	1131.5	5.10	-0.28	-5.10	+0.10

### 7.3.4 SYNCHROTRON RADIATION DIFFRACTION STUDY

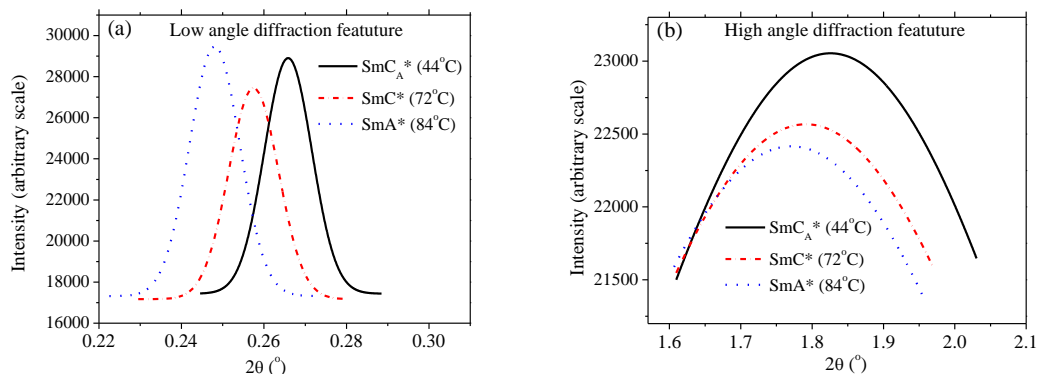
Low and high angle diffraction profiles are shown in **Figure 7.5** for 6F6T, similar features were observed in 4F6T. Temperature dependence of smectic layer thickness ( $d$ ), measured from synchrotron diffraction study, is shown in **Figure 7.6**. Maximum values of layer spacings in  $\text{SmA}^*$  phase ( $34.64\text{\AA}$  in 4F6T and  $37.16\text{\AA}$  in 6F6T) were found to be, in both cases, almost equal to the optimized lengths of the molecules, signifying that the molecular conformation within this phase almost similar to that in vacuo. It decreased rapidly with decrease of temperature near the  $\text{SmA}^*-\text{SmC}^*$  transition ( $T_c$ ) indicating tilting of the molecules. The decrement rate reduced gradually as the temperature went deeper into the  $\text{SmC}^*$  and  $\text{SmC}_A^*$  phase. Average layer spacings were observed to be higher in 6F6T compared to 4F6T almost by  $2.5\text{\AA}$  as expected. A small discontinuity in the layer spacings was observed at  $48^\circ\text{C}$  in 4F6T and  $66^\circ\text{C}$  in 6F6T indicating the transition from  $\text{SmC}^*$  to  $\text{SmC}_A^*$  phase. The lowest values of layer spacing in  $\text{SmC}_A^*$  phase were  $32.11\text{\AA}$  in 4F6T and  $34.50\text{\AA}$  in 6F6T, which means layer shrinkage was roughly 7% in both systems.

Temperature dependence of  $d$  in  $\text{SmC}^*$  phase near  $T_c$ , in both 4F6T and 6F6T, was observed to be parabolic in nature. As discussed in chapter 2, tilt angle  $\theta$  depends on the reduced temperature as  $\theta \propto (T - T_c)^\beta$  according to generalized mean field theory. A value of 0.5 is predicted in a pure second order transition for the critical exponent  $\beta$  and in the case of second order transition approaching tricritical point

(TCP) it is 0.25 [35-36]. Following the argument of Hartley *et al.* [37] and expanding  $\cos\theta$  up to  $\theta^4$  term,  $d_C/d_A$  near  $T_C$  can be written as

$$d_C/d_A \approx 1 - a/T - T_c^{1/2} + b/T - T_c \quad (7.1)$$

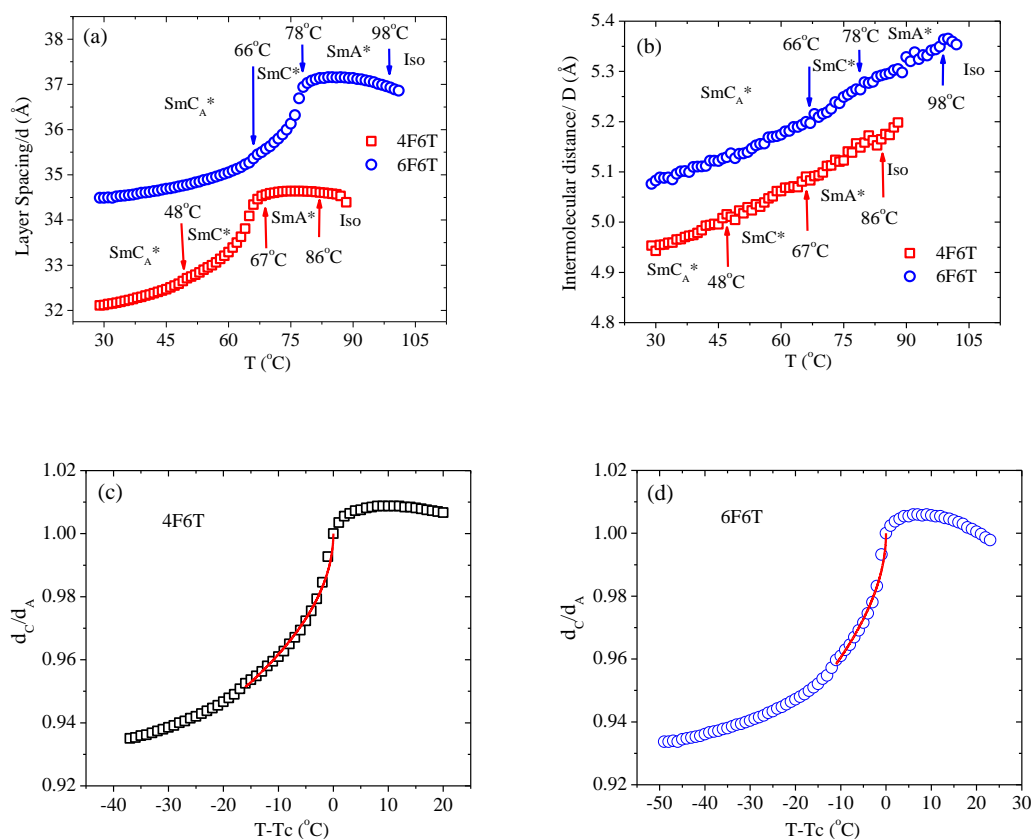
when  $\beta$  is taken as 0.25. Observed data were fitted nicely to the above equation in both the compounds [Figure 7.6(c-d)] signifying that the SmC\*–SmA\* transition was a tricritical type.



**Figure 7. 5.** X-ray diffraction profiles at 44 °C (SmC<sub>A</sub>\*), 72 °C (SmC\*) and 84 °C (SmA\*) of the (a) low angle and (b) high angle diffraction features of 6F6T.

Estimated correlation lengths across the layers ( $\xi_{||}$ ) in 4F6T in SmA\* phase remained almost constant around at 850 Å. At SmA\*-SmC\* and SmC\*-SmC<sub>A</sub>\* transitions small discontinuous changes were observed and  $\xi_{||}$  values were around 860 Å in SmC\* and 870 Å in SmC<sub>A</sub>\* phase [Figure 7.7(a)]. In other words, correlation across the layer was about 24 molecular lengths in SmA\* phase and did not increase much in SmC\* and SmC<sub>A</sub>\* phases.

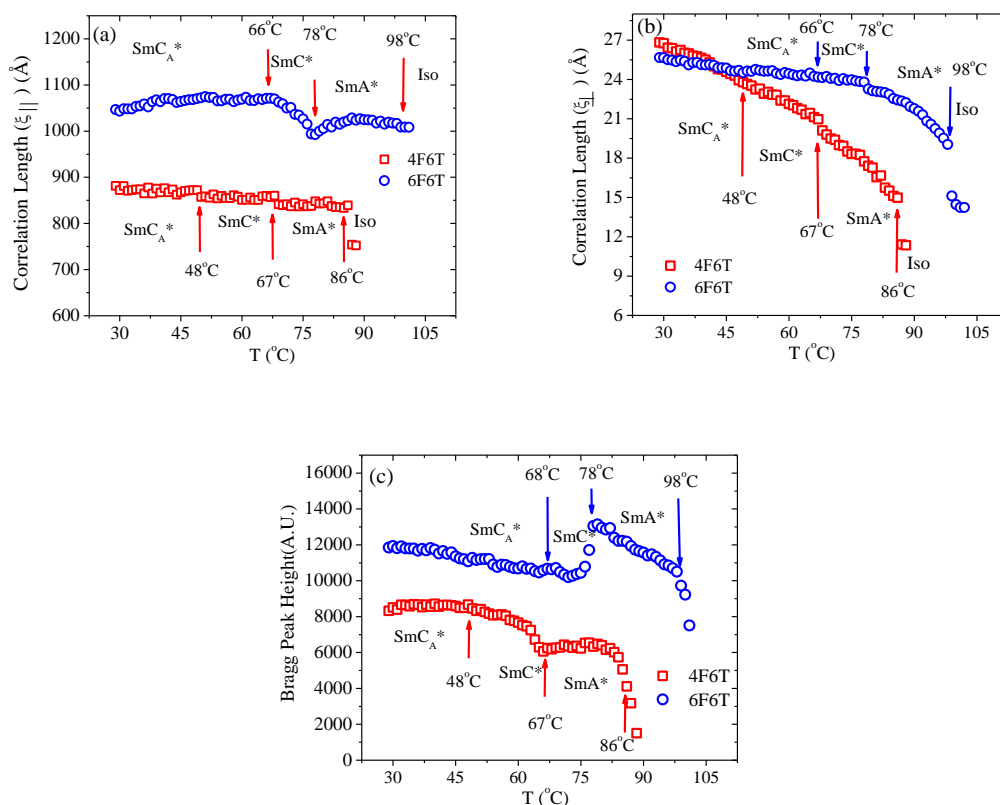
However, in SmA\* phase of 6F6T the  $\xi_{||}$  value initially increased from 1008 Å to 1028 Å with the decrease of temperature and then gradually decreased to 993 Å at SmA\*-SmC\* transition temperature. After the transition, it was observed to increase gradually in the entire SmC\* phase and reached a maximum value of 1071 Å at  $T_{AF}$ , the SmC\*-SmC<sub>A</sub>\* transition temperature. Although  $\xi_{||}$  decreased slightly from 1068 Å to 1046 Å in SmC<sub>A</sub>\* phase, it can be considered to remain almost unchanged at 28 molecular lengths. Almost similar values of correlation lengths ( $\xi_{||}$ ) were observed in biphenyl benzoate core-based laterally fluorinated ferroelectric compounds [986-748 Å] [38], and comparatively higher values were observed in phenyl 4-phenyl benzoate based compound [1450–1160 Å] [39]



**Figure 7.6.** Temperature evolution of (a) layer spacing, (b) intermolecular distance of 4F6T and 6F6T; fitted layer spacings in  $SmC^*$  phase of (c) 4F6T and (d) 6F6T (see text)

In-plane correlation lengths ( $\xi_{\perp}$ ), on the other hand, were observed to increase gradually with the decrease of temperature showing a small discontinuity at the transitions in both the compounds [Figure 7.7(b)]. It varies from 15–26.8 Å in 4F6T and from 19–25.7 Å in 6F6T, showing that the rate of increase is higher in 4F6T than in 6F6T. Comparatively higher in-plane correlation length ( $\xi_{\perp}$ ) was observed in biphenyl benzoate core based laterally fluorinated ferroelectric compounds [21–24.5 Å] [38], and in phenyl benzoate based compound [220–650 Å] [39].

When the low angle Bragg peak intensity of 6F6T was plotted as a function of temperature an anomalous behaviour was seen in the temperature range of 72°C to 77°C which might be considered as a signature of the presence of a *sub-phase*, no such anomaly was observed in 4F6T as depicted in Figure 7.7(c). This phase may be  $SmC^*_{\alpha}$  phase as discussed in the next section.



**Figure 7.7.** Temperature evolution of correlation lengths (a) across the smectic layers ( $\xi_{||}$ ), (b) within the smectic layers ( $\xi_{\perp}$ ) and (c) intensity of the low angle Bragg peak (arbitrary unit) of 4F6T and 6F6T.

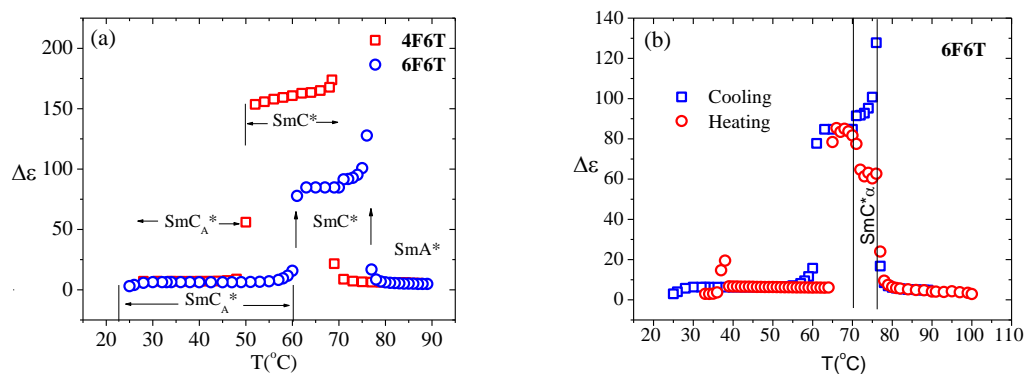
### 7.3.5 DIELECTRIC STUDY

The dielectric increment ( $\Delta\epsilon$ ) of the compounds during the cooling cycle is shown in **Figure 7.8(a)**. Both the compounds were found to possess moderately high value in SmC\* phase. Maximum values of  $\Delta\epsilon$  were found to decrease with increasing fluorinated achiral chain length (4F6T (173.9), 5F6T (92.2 [2]) and 6F6T (84.8)). A gradual decrease of  $\Delta\epsilon$  with decreasing temperature in both the compounds can be explained assuming stronger biquadratic coupling between tilt and polarization compared to bilinear one in the expression for free energy density in the generalized Landau model [40]. A decrease of  $\Delta\epsilon$  with the decrease of temperature was reported in different FLC compounds by several authors [2, 41–43]. An anomaly in the value of  $\Delta\epsilon$  between SmA\* and SmC\* phase in 6F6T during heating as well as cooling was noticed [**Figure 7.8(b)**] indicating the existence of a *sub-phase* in the temperature interval 72°C to 76°C which might be SmC <sub>$\alpha$</sub> \* phase. It behaves in an antiferroelectric

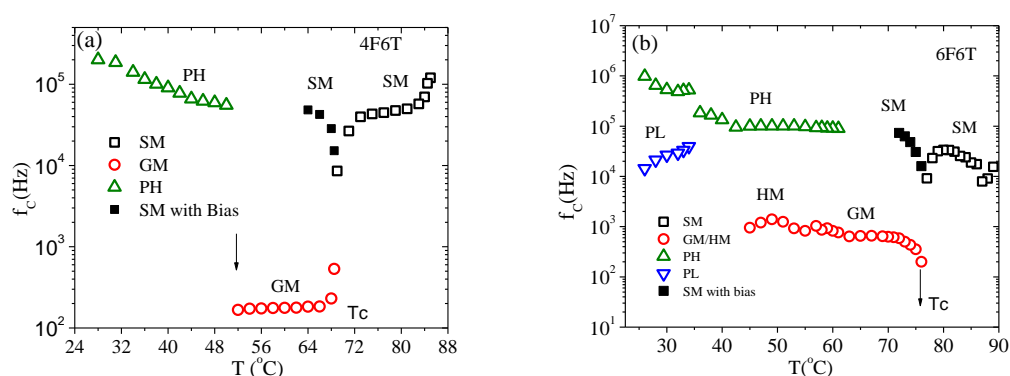
way at its high-temperature region and in a ferroelectric way at its low-temperature region and ferroelectric in between [44–45]. To explain the behaviour of  $\text{SmC}^*_\alpha$  phase Takanishi *et al.* [46] proposed that a sequence of different structural states change structure quasi-continuously in the narrow temperature interval. Missing of this phase in POM and DSC study is not uncommon. Bahr *et al.* [44] argued that no effect can be observed by DSC and polarizing microscopy in the bulk sample, only one transition  $\text{SmC}^*-\text{SmA}^*$  is observed.

The critical frequencies of all modes of relaxations observed in 4F6T and 6F6T are shown in **Figure 7.9**. Soft mode (SM) in  $\text{SmA}^*$  phase and Goldstone mode (GM) in  $\text{SmC}^*$  phase were observed in both the compounds. In  $\text{SmC}_A^*$  phase anti-phase antiferroelectric mode ( $P_H$ ) and in-phase antiferroelectric mode ( $P_L$ ) were observed in 6F6T but in 4F6T only  $P_H$  was observed. The SM critical frequency in 4F6T decreased with decrease of temperature (120 kHz–8.5 kHz). In  $\text{SmC}^*$  phase SM could be observed only under a bias field of 1.2 V/ $\mu\text{m}$ . The critical frequency near  $T_c$  was found to increase sharply, depicting a ‘V’ shape behaviour as expected from mean field theory [47]. On the other hand, in 6F6T the critical frequency of SM increased with decrease of temperature [7.9 kHz–33.6 kHz] in the high temperature region but near  $T_c$  it decreased sharply from 33.6 kHz (80°C) to 9.1 kHz (77°C). In this system also ‘V’ shape behaviour of SM critical frequency was observed near  $T_c$  under a similar bias field. The critical frequency of GM ( $f_{GM}$ ) was found to decrease with decrease of temperature from 540 Hz (68.5°C) to 167 (52°C) in 4F6T whereas in 6F6T the  $f_{GM}$  increased with decrease of temperature from 200 Hz (76 °C) to 765 Hz (61 °C) and then the mode continued upto a few degrees in  $\text{SmC}_A^*$  phase. This mode in  $\text{SmC}_A^*$  phase is known as hereditary mode (HM) [43].

However, no anomaly was observed in critical frequency in the temperature interval of the proposed  $\text{SmC}^*_\alpha$  phase. The critical frequency of high frequency anti-phase mode ( $f_{PH}$ ) in the 4F6T system was observed to increase with decreasing temperature from 55.3 kHz to 200 kHz whereas in the 6F6T system it increased from 90 kHz to 980 kHz, also showing a step increase at 34°C at which  $P_L$  appeared. Like other compounds [38, 48] the critical frequency of  $P_L$  mode in 6F6T decreased with decrease of temperature.



**Figure 7.8.** Dielectric increment  $\Delta\epsilon$  (a) of 4F6T and 6F6T during cooling, (b) of 6F6T during heating and cooling showing anomaly.



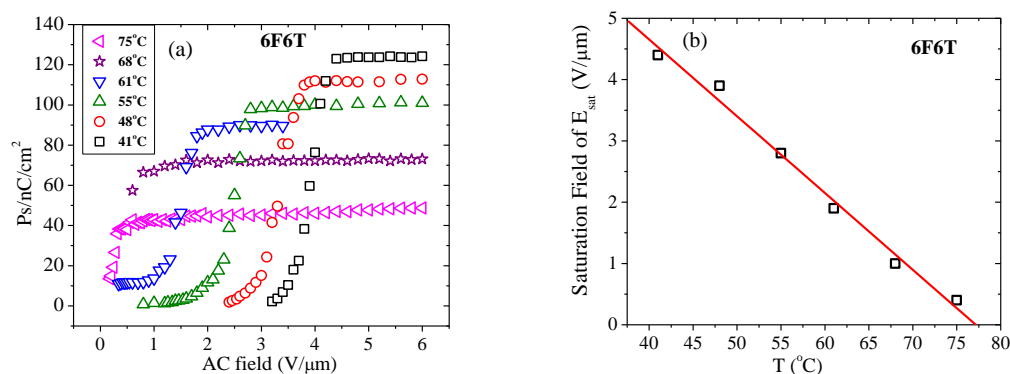
**Figure 7.9.** Temperature dependence of relaxaiton frequencies ( $f_c$ ) of various relaxation modes in (a) 4F6T and (b) 6F6T.

### 7.3.6 ELECTRO-OPTIC STUDY

#### 7.3.6.1 SPONTANEOUS POLARIZATION ( $P_s$ )

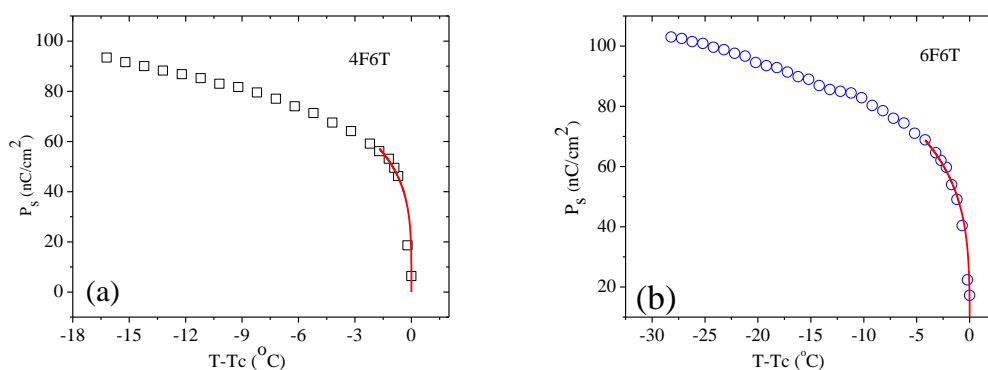
In order to study the field required to obtain saturation polarization,  $P_s$  was measured with an increasing ac field at a particular temperature. With the increasing field, the number of molecules participating in switching increased and after a certain field all the molecules oriented in the direction of the field and the polarization became saturated [Figure 7.10(a)]. The field required for saturation polarization ( $E_{sat}$ ) was found to increase linearly with the decrease of temperature [Figure 7.10(b)], signifying that more driving force was required to align the molecules at lower temperature. 4F6T also showed similar behaviour. In 4F6T the value of  $E_{sat}$

was 1.00 V/ $\mu\text{m}$  at 9.2°C below  $T_c$  whereas in 6F6T its value was more than double (2.26 V/ $\mu\text{m}$ ) at the same temperature below  $T_c$ .



**Figure 7.10.** (a) Polarization versus field in 6F6T at different temperatures and (b) linear increase of saturation field ( $E_{sat}$ ) with decreasing temperature.

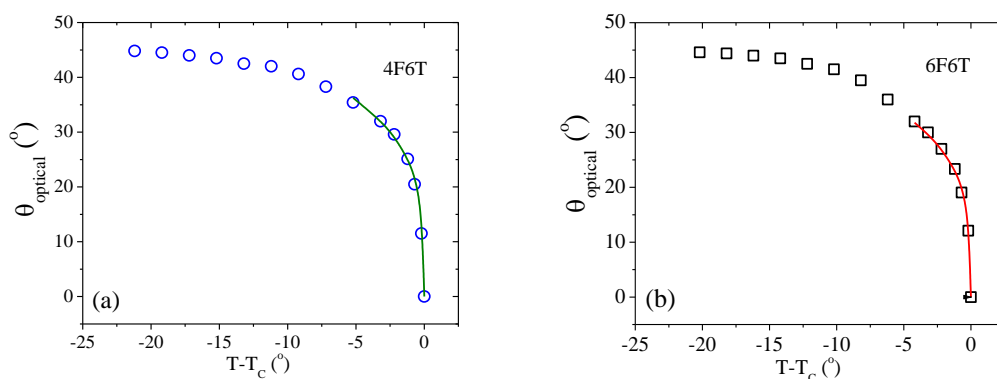
Moderate values of spontaneous polarizations ( $P_s$ ) were observed which are suitable for display applications [49–51].  $P_s$  was found to decrease slowly in the lower temperature region and rapidly in the high temperature region of SmC\* phase as shown in **Figure 7.11**. Maximum value of  $P_s$  was 93.6 nC/cm<sup>2</sup> in 4F6T and 103.0 nC/cm<sup>2</sup> in 6F6T while in 5F6T it was 118.7 nC/cm<sup>2</sup> [2]. A similar increasing trend with the fluorinated achiral chain was observed before [41, 52]. A compound with biphenyl benzoate core and 4 perfluorinated carboxylate C atoms and 3 oligomethylene spacers in achiral chain (4F3R) exhibited  $P_s$  value 41.66 nC/cm<sup>2</sup> [41]. Keeping number of perfluorinated C atom same when oligomethylene spacer was increased to 6 (4F6R), the  $P_s$  value increased to 50 nC/cm<sup>2</sup> and when 8 perfluorinated C atoms and 2 oligomethylene spacers were introduced (8F2R) it became 93 nC/cm<sup>2</sup> [52]. It was inferred that the  $P_s$  increased with an increase of perfluorinated C atoms as well as oligomethylene spacers in the achiral chain but an increase of perfluorinated C atom was more effective. In the present study, the  $P_s$  was observed to increase with the increase of achiral chain length, although in 5F6T the increment was more than in 6F6T which may be due to the odd-even effect [29]. In both the compounds the measured  $P_s$  data were found to fit nicely to the mean-field equation  $P_s = P_o(T - T_c)^\beta$  with  $\beta = 0.25$  near  $T_c$  signifying that the SmC\*–SmA\* transition is a tricritical type [37] as observed in layer spacing.



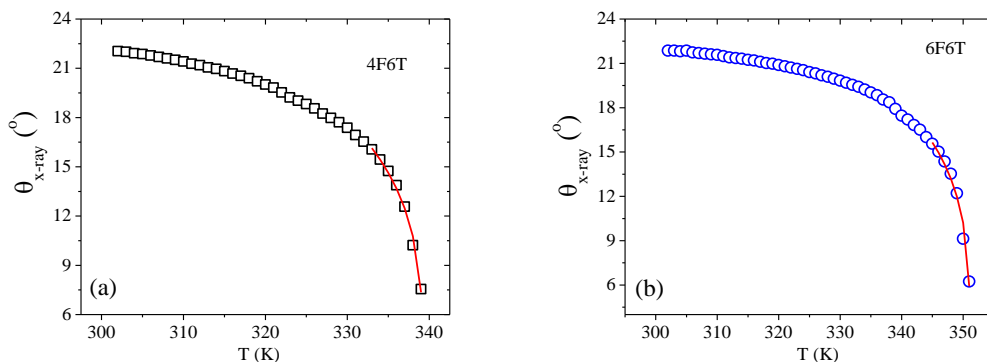
**Figure 7.11.** Temperature variation of spontaneous polarization of (a) 4F6T and (b) 6F6T, fitted curves near  $T_c$  is also shown

### 7.3.6.2 OPTICAL AND X-RAY TILT

The optical tilts ( $\theta_{opt}$ ) were found to increase sharply with the decrease of temperature near  $T_c$  and reached nearly  $45^\circ$  in  $\text{SmC}_A^*$  phase in both the compounds [Figure 7.12], which indicated that both the compounds were orthoconic antiferroelectric in nature. On the other hand, although the x-ray tilts ( $\theta_{x-ray}$ ) of the compounds showed similar temperature variation but their maximum values were  $21.8^\circ$  and  $22.0^\circ$  respectively [Figure 7.13], much less than the optical tilts. As discussed in Chapter 3, in four members of a biphenyl benzoate core-based homologous series (DM series) exhibiting orthoconic antiferroelectric nature, the  $\theta_{x-ray}$  were found to vary within  $23.8^\circ - 27.1^\circ$  [38].



**Figure 7.12.** Temperature variation of optical tilt of (a) 4F6T and (b) 6F6T, fitted curves near  $T_c$  is also shown.



**Figure 7.13.** Temperature variation of x-ray tilt of (a) 4F6T, (b) 6F6T, fitted curves near  $T_c$  is also shown.

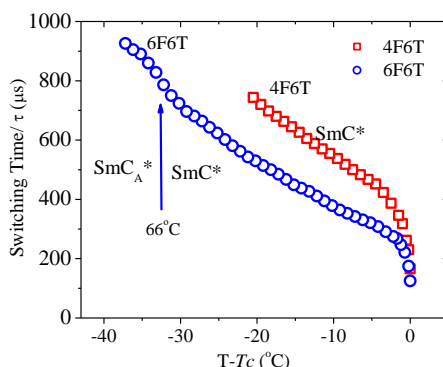
Similar lower values of x-ray tilt than optical tilt were reported before by several other authors [53-55], although the existence of higher x-ray tilt than optical tilt was also observed by Meier *et al.*[56]. This discrepancy has been explained in chapter 3. Tilts in both 4F6T and 6F6T were fitted nicely to the power-law with  $\beta = 0.25$  near  $T_c$  in both the compounds signifying again the tricritical nature of SmC\* – SmA\* transition.

### 7.3.6.3 SWITCHING TIME

The switching time of ferroelectric and antiferroelectric liquid crystals is a very important parameter from the application point of view because to afford a video rate time sequential colour micro-display switching time should be low [14, 57–58]. Both the compounds showed sub-millisecond switching time and it increased with decrease of temperature from  $T_c$  [Figure 7.14]. Similar nature of temperature variation of  $\tau$  was observed in other compounds [38, 59]. The maximum value of  $\tau$  was found to be 744 $\mu$ s in 4F6T and 828 $\mu$ s in 6F6T at  $T_{AF}$ . Within SmC<sub>A</sub>\* phase  $\tau$  increased sharply to 926 $\mu$ s in 6F6T, it could not be measured in 4F6T [Figure 7.14].

In a homologous series of ferroelectric liquid crystals with partially fluorinated biphenyl benzoate core and different number of fluorinated carbon and oligomethylene spacer in achiral chain (nFmR), Goswami *et al.* [59] reported the switching time as 80 $\mu$ s in 4F3R, 122.6 $\mu$ s in 5F3R and 158 $\mu$ s in 6F3R and observed that the  $\tau$  increased with increasing number of fluorinated carbon in achiral chain,

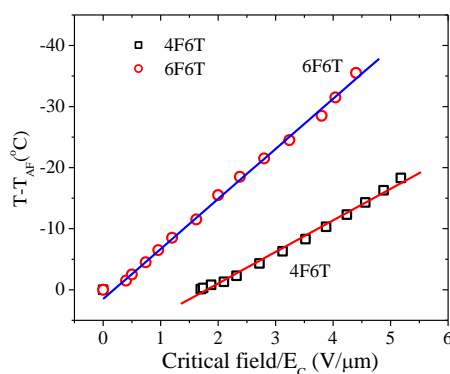
thus with increasing achiral chain length. Same is found to be true in the present compounds.



**Figure 7.14.** Comparison of temperature dependence of switching time.

#### 7.3.6.4 EFFECT OF FIELD ON FERROELECTRIC-ANTIFERROELECTRIC TRANSITION TEMPERATURE ( $T_{AF}$ )

In order to study the effect of ac field on  $\text{SmC}^*-\text{SmC}_A^*$  transition temperature ( $T_{AF}$ ), the optical texture of the compounds were monitored with decreasing temperature under fixed low frequency ( $\sim 10$  Hz) ac fields and the temperatures at which the phase change took place were noted.  $T_{AF}$  was observed to decrease linearly with an increasing field ( $E_c$ ) in both the compounds as shown in **Figure 7.15**. In 4F6T,  $T_{AF}$  was found to depress by  $18.3^\circ\text{C}$  at  $5.18 \text{ V}/\mu\text{m}$  and in 6F6T it depressed by  $35.5^\circ\text{C}$  at  $4.4 \text{ V}/\mu\text{m}$ . The gradient of depression of  $T_{AF}$  was higher in 6F6T ( $\sim 8.19^\circ\text{C}/(\text{V}/\mu\text{m})$ ) than in 4F6T ( $\sim 5.16^\circ\text{C}/(\text{V}/\mu\text{m})$ ).



**Figure 7.15.** AC field dependence of  $\text{SmC}^*-\text{SmC}_A^*$  transition temperature ( $T_{AF}$ ) of 4F6T and 6F6T.

A selected list of parameters of 4F6T, 5F6T, 6F6T are gathered in **Table 7.3** for ease of comparison.

**Table 7.3.** Selected list of parameters of 4F6T, 5F6T, 6F6T

Parameter	4F6T	5F6T	6F6T
$\mu$ (D)	5.13	5.01	5.10
$D$ (Å) (max)	5.17		5.36
$d$ (Å) (max)	34.64		37.16
$\xi_{\parallel}$ (Å) (max)	870		1071
$\xi_{\perp}$ (Å) (max)	26.8		25.7
$\Delta\epsilon_{GM}$ (max)	173.9	92.2	84.4
$f_{GM}$ (Hz)	167-540	590-1190	200-765
$f_{SM}$ (kHz)	8.5-120	2.5-65.8	7.9-33.6
$f_{PL}$ (kHz)			14.3-39.5
$f_{PH}$ (kHz)	55.3-200		90-980
$P_s$ (nC/cm <sup>2</sup> ) (max)	93.6	118.7	103
$\tau$ (μs) (max)	744		926

## 7.4 CONCLUSION

In order to investigate the correlation between structure and property, two terphenyl core based antiferroelectric liquid crystals – 4F6T and 6F6T – differing only in the number of fluorinated carbon at achiral chain have been studied using different experimental techniques and their properties have also been compared with the intermediate homologue 5F6T [2] wherever possible. Although all of them exhibited antiferroelectric-ferroelectric-paraelectric ( $SmC_A^*$ -  $SmC^*$ - $SmA^*$ ) phase sequence, melting point was observed to decrease with increasing achiral chain length but clearing point showed opposite trend, range of  $SmC_A^*$  and  $SmC^*$  phases showed odd-even effect like the molecular dipole moments and spontaneous polarization. Layer spacings, average intermolecular distances and correlation lengths across the smectic planes were also observed to increase with achiral chain length. Temperature dependence of layer spacings suggests tricritical nature of  $SmC^*$ - $SmA^*$  transition which is also supported by temperature dependent x-ray tilt, optical tilt and spontaneous polarization. Dielectric increments decreased with increased achiral chain. Both soft mode and Goldstone mode critical frequencies were found to decrease with decreasing temperature in the lower derivative but opposite behaviour

was observed in the higher derivative. Both the compounds, however, showed Curie–Weiss behaviour in soft mode near  $T_c$ . Goldstone mode critical frequency was much higher in 6F6T. Both  $P_L$  and  $P_H$  modes were observed in  $SmC_A^*$  phase but in 4F6T only  $P_H$  was observed and in 5F6T both modes were absent. Optical tilts exhibited orthoconic nature of the  $SmC_A^*$  phase in both the compounds. However, X-ray tilt was much less and the discrepancy was explained. Both the compounds showed sub-millisecond order switching time which was also found to increase with achiral chain length. Antiferroelectric-ferroelectric transition temperature ( $T_{AF}$ ) was observed to decrease with increasing ac field, effect was more in the higher derivative compared to the lower one.  $SmC_\alpha^*$  phase may be present within a small temperature range between  $SmA^*$  and  $SmC^*$  phases in 6F6T.

It is thus concluded that the thermal range of different phases, smectic layer spacings, various dielectric and electro-optic properties of the two terphenyl based compounds are significantly influenced by the achiral chain length, some of the properties show an increasing trend with chain length whereas some others exhibit opposite trend, even there is an indication of presence of a new phase ( $SmC_\alpha^*$ ) in the higher derivative. Another important conclusion is that the ferroelectric to paraelectric phase transition is tricritical in nature and the ferroelectric-antiferroelectric transition temperature decreases with electric field in both the compounds. Moreover, because of the orthoconic nature of the  $SmC_A^*$  phase with sub-millisecond switching time and moderate spontaneous polarization these two compounds are expected to be suitable for preparation of mixtures suitable for display and non-display applications [14-15, 49-50, 60-67].

## 7.5 REFERENCES

- [1] P. Kula, R. Dąbrowski and M. Tykarska, Orthoconicantiferroelectric liquid crystals containing a terphenyl rigid core, *Phase Transition*. 80(6–7) (2007) 771–780.
- [2] S. Haldar, K. C. Dey, D. Sinha, P.K. Mandal, W. Haase, P. Kula, X-ray diffraction and dielectric spectroscopy studies on a partially fluorinated ferroelectric liquid crystal from the family of terphenyl esters, *Liq. Cryst.* 39(10) (2012) 1196–1203.
- [3] K. Dhare, P. Rudquist, M. Matuszczyk, S. T. Lagerwall, H. Pauwels, R. S. Dabrowski, Antiferroelectric liquid crystals with 45° tilt: new electro-optic effects in liquid crystals. In ‘Liquid Crystal Materials, Devices, and Flat Panel Displays’, Ranganathan Shashidhar, Bruce Gnade, Editors, *Proceedings of SPIE Vol. 3955* (2000) 33–44.
- [4] G. Scalia, P. Rudquist, D. S. Hermann, K. D’have, and S. T. Lagerwall, Fully leaky guided mode study of an orthoconic antiferroelectric liquid crystal cell deviating from perfect horizontal surface stabilization, *J. Appl. Phys.* 91(12) (2002) 9667–9675.
- [5] A. Bubnov, V. Novotna, V. Hamplova, M. Kaspar, M. Glogarova, Effect of multilactate chiral part of liquid crystalline molecule on mesomorphic behaviour, *J. Mol. Struct.* 892(1-3) (2008) 151-157.
- [6] A. Poryvai, A. Bubnov, D. Pocięcha, J. Svoboda, M. Kohout, The effect of the length of terminal n-alkyl carboxylate chain on self assembling and photosensitive properties of chiral lactic acid derivatives, *J. Mol. Liq.* 275 (2019) 829-838.
- [7] B. Barman, B. Das, M. K. Das. V. Hamplova, A. Bubnov, Effect of molecular structure on dielectric and electro-optic properties of chiral liquid crystals based on lactic acid derivatives, *J. Mol. Liq.* 283 (2019) 472-481.
- [8] M. Żurowska, J. Dziaduszek, M. Szala, P. Morawiak, A. Bubnov. Effect of lateral fluorine substitution far from the chiral center on mesomorphic behaviour of highly titled antiferroelectric (S) and (R) enantiomers, *J. Mol. Liq.* 267 (2018) 504-510.

- [9] M. Kohout, A. Bubnov, J. Šturala, V. Novotna and J. Svoboda, Effect of alkyl chain length in the terminal ester group on mesomorphic properties of new chiral lactic acid derivatives, *Liq. Cryst.* 43 (2016) 1472-1485.
- [10] V. Hamplova, A. Bubnov, M. Kaspar, V. Novotna and M. Glogarova, New Series of chiral ferroelectric liquid crystals with the keto group attached to the molecule core, *Liq. Cryst.* 30(04) (2003) 493–497.
- [11] W. L. Tsai, T.C. Lu, H.W. Liu, M.Y. Tsai, C.M. Fu, A comparison of ferroelectric liquid crystals containing diastereomeric propionic acids derived from natural ethyl lactate, *Liq. Cryst.* 27 (2000) 1389.
- [12] D. Goswami, A. Debnath, P. K. Mandal, D. Węłowska, R. Dabrowski and K. Czuprynski, Effect of chain length and fluorination on the dielectric and electro–optic properties of three partially fluorinated biphenyl benzoate rigid core based ferroelectric liquid crystals, *Liq. Cryst.* 43(11) (2016) 1–12.
- [13] K. Kunhnpast, J. Sorubgerm G. Scherowsky, F. Giebelmann and P. Zugenmaier, Ferroelectric liquid–crystalline side group polymers Spacer length variation and comparison with the monomers, *Liq. Cryst.* 14(03) (1993) 861–869.
- [14] A. Debnath and P. K. Mandal, Effect of fluorination on the phase sequence, dielectric and electro–optical properties of ferroelectric and antiferroelectric mixtures, *Liq. Cryst.* 44 (2017) 2192–2202.
- [15] A. Debnath and P. K. Mandal, Dielectric properties of four room temperature ferroelectric and antiferroelectric multi-component liquid crystalline mixtures, *Liq. Cryst.* 46 (2019) 234-248.
- [16] M. Zurowska, R. Dąbrowski, J. Dziaduszek, K. Garbat, M. Filipowicz, M. Tykarska, W. Rejmer, K. Czuprynski, A. Spadlo, N. Bennis, J.M. Oton, Influence of alkoxy spacer length and fluorosubstitution of benzene ring on mesogenic and spectral properties of high tilted antiferroelectric 4'-(S)-1-(methylheptyloxy carbonyl) biphenyl-4-yl-4-(2,2,3,3,4,4,4-heptafluorobutoxy) alkoxybenzoates, *J. Mater. Chem.* 21 (2011) 2144-2153.
- [17] R. Dąbrowski, Liquid crystals with fluorinated terminal chains and antiferroelectric properties, *Ferroelectrics.* 243 (2000) 1-11.

- [18] R. Dąbrowski, J. Gąsowska, J. M. Oton, W. Piecek, J. Przedmojski, M. Tykarska, High tilted antiferroelectric liquid crystalline materials, *Displays*. 25 (2004) 9-19.
- [19] E. Sokol, W. Drzewinski, J. Dziaduszek, R. Dąbrowski, N. Bennis, J.M. Oton, The synthesis and properties of novel partially fluorinated ethers with high tilted anticlinic phase, *Ferroelectrics*. 343 (2006) 41-48.
- [20] R. Dąbrowski, W. Drzewinski, J. Dziaduszek, J. Gąsowska, P. Henderson, P. Kula, J.M. Oton, N. Bennis, Orthoconic antiferroelectric liquid crystals containing biphenyl, terphenyl, or naphthyl mesogenic unit, *Opto-Electron. Rev.* 15 (2007) 32-36.
- [21] M. Kaspar, V. Hamplova, V. Novotna and O. Pachrova, The effect of the alkyl chain length on the mesomorphic properties of new lactic acid derivatives, *Liq. Crys.* 41(08) (2014) 1179–1187.
- [22] R. Dąbrowski, P. Kula, Z. Raszewski, W. Piecek, J. M. Otón and A. Spadło, New Orthoconic Antiferroelectrics Useful for Applications, *Ferroelectrics*. 395 (2010)116–132.
- [23] P. A. Henderson, W. Drzewinski, and R. Dabrowski, Antiferroelectric liquid crystals containing a naphthoate mesogenic unit, *Ferroelectrics*. 343 (2006) 11–18.
- [24] R. Dabrowski, J. Gasowska, J. Oton, W. Piecek, J. Przedmojski, and M. Tykarska, High tilted antiferroelectric liquid crystalline material, *Displays*.25 (2004) 9–19.
- [25] P. Kula, R. Dabrowski, K. Kenig, and D. Chyczewska, New ferroelectric compounds from chiral terphenyls, *Ferroelectrics*. 343 (2006) 19–26.
- [26] W. Haase, S. Wrobel (Ed.), *Relaxation phenomena – Liquid crystals, magnetic systems, polymers, high- $T_c$  superconductors, metallic glasses*, Springer–Verlag, Berlin–Heidelberg, 2003, pp. 20.
- [27] J. Budai, R. Pindak, S.C. Davey, and J.W. Goodby, Structural investigation of the liquid crystal phases of 4-(2'-methylbutyl)phenyl 4'-n-octylbiphenyl-4-carboxylate, *J. Phys. Lett.* 45(1984) L1053-L1062.

- [28] M. Marzec, J. Popczyk, A. Fafara, S. Wróbel & R. Dąbrowski, Antiferroelectric Liquid Crystals Studied by Differential Scanning Calorimetry and Electrooptic Methods, *Ferroelectrics*. 281 (2002) 123–134.
- [29] P. Sarkar, S. Paul and P. Mandal, The Temperature Dependence of Static Dielectric Permittivities and Dipole Moments of Two Mesogens and their Mixture, *Mol. Cryst. Liq. Cryst.* 330 (1999) 87-94.
- [30] Hyperchem 6.03, Hypercube Inc., Gainesville, FL, USA.
- [31] E. Megnassan and A. Proutiere, Dipole Moments and Kerr Constants of 4-*n* Alkyl-4'-Cyanobiphenyl Molecules (from 1CB to 12CB) Measured in Cyclohexane Solutions, *Mol. Cryst. Liq. Cryst.* 108 (1984) 245–254.
- [32] K. P. Gueu, E. Megnassan and A. Proutiere, Dipole Moments of 4-*n* Alkyl-4'-Cyanobiphenyl Molecules (from 0CB to 12CB) Measurements in four solvents and Theoretical Calculations, *Mol. Cryst. Liq. Cryst.* 132 (1986) 303–323.
- [33] P. Sarkar, P. K. Mandal, S. Paul, X-ray diffraction, optical birefringence, dielectric and phase transition properties of the long homologous series of nematogens 4-(trans -4'- *n*-alkylcyclohexyl) isothiocyanatobenzenes, *Liq. Cryst.* 30 (2003) 507–527.
- [34] S. Marcelja, Chain ordering in liquid crystals, I. Even-odd effect, *The J. Chem. Phys.* 60(9) (1974) 3599–3604.
- [35] B. Zeks, Landau Free Energy Expansion for Chiral Ferroelectric Smectic Liquid Crystal, *Mol. Cryst. Liq. Cryst.* 114 (1984) 259-270.
- [36] R. Shashidhar, B. R. Ratna, G. G. Nair, S. Krishna Prasad, Ch. Bahr, and G. Heppke, Mean-Field to Tricritical Crossover Behaviour near the Smectic-A-Smectic-C\* Tricritical Point, *Phys. Rev. Lett.* 61(5) (1988) 547-549.
- [37] C. S. Hartley, N. Kapernaum, J. C. Roberts, F. Giesselmann and R. P. Lemieux, Electroclinic effect in chiral SmA\* liquid crystals induced by atropisomeric biphenyl dopants: amplification of the electroclinic coefficient using achiral additives, *J. Mater. Chem.* 16 (2006) 2329–2337.
- [38] K. C. Dey, P. K. Mandal, R. Dabrowski, Effect of lateral fluorination in antiferroelectric and ferroelectric mesophases: synchrotron X-ray diffraction,

- dielectric spectroscopy and electro–optic study, *Journal of Phys. and Chem. of Solids*. 88 (2016) 14–23.
- [39] D. Sinha, A. Debnath, and P. K. Mandal, Hexatic and blue phases in a chiral liquid crystal: optical polarizing microscopy, synchrotron radiation and dielectric study, *Mat. Research Exp.* 1 (2014)1–13.
- [40] T. Carlsson, B. Zeks, C. Filipic and A. Levstik, Theoretical model of the frequency and temperature dependence of the complex dielectric constant of ferroelectric liquid crystals near the smectic–C\* —smectic– A phase transition, *Phys. Rev. A*. 42(2) (1990) 877–889.
- [41] D. Goswami, D. Sinha, A. Debnath, P.K. Mandal, S. K. Gupta, W. Haase, D. Ziobro, R. Dabrowski, Molecular and dynamical properties of a perfluorinated liquid crystal with direct transition from ferroelectric SmC\* phase to isotropic phase, *J. Mol. Liq.* 182 (2013) 95-103.
- [42] U. Manna, J. K. Song, G. Power, J. K. Vij, Effect of cell surfaces on the stability of chiral smectic–C phases, *Phy. Rev. E*.78 (2008) 021711–0217 (1–8).
- [43] M. Buivydas, F. Gouda, G. Andersson, S.T. Lagerwall, B. Stebler, Collective and non–collective excitations in antiferroelectric and ferrielectric liquid crystals studied by dielectric relaxation spectroscopy and electro–optic measurements, *Liq. Cryst.* 23(5) (1997) 723-739.
- [44] C. Bahr, D. Fliegner, C. J. Booth and J. W. Goodby, Experimental indication of a devil's staircase structure in a smectic liquid crystal, *Phys. Rev. E*. 51(5) (1995) R3823–R3826.
- [45] T. Isozaki, K. Hiraoka, Y. Takanishi, H. Takezoe, A. Fukuda, Y. Suzuki and I. Kawamura, Conoscopic study of the  $Sc\alpha^*$  phase and the Devil's staircase in an antiferroelectric liquid crystal, *Liq. Cryst.* 12 (1992) 59-70.
- [46] Y. Takanishi, K. Hiraoka, V.K. Agarwal, H. Takezoe, A. Fukuda and M. Matsushita, Stability of Antiferroelectricity and Causes for its Appearance in  $SmC^*_\alpha$  and  $SmC_A^*$  phases of a Chiral Smectic Liquid Crystal, MHPOBC, *Jpn. J. Appl. Phys.* 30 (1991) 2023.

- [47] F. Gouda, K. Skarp, S.T. Lagerwall, Dielectric studies of the soft mode and Goldstone mode in ferroelectric liquid crystals, *Ferroelectrics*. 113 (1991) 165.
- [48] K. C. Dey and P. K. Mandal, Effect of multi-walled carbon nanotubes on dielectric and electro-optic properties of a high tilt antiferroelectric liquid crystal. *Phase Transit.* 92(3) (2019) 302–315.
- [49] A. Debnath, P. K. Mandal, D. Weglowska and R. Dbrowski, Induction of a room temperature ferroelectric SmC\* phase in binary mixtures with moderate spontaneous polarization and sub-millisecond switching time, *RSC Adv.* 6 (2016) 84369–84378.
- [50] P. K. Mandal, S. Haldar, A. Lapanik, W. Haase, Induction and Enhancement of Ferroelectric Smectic C\* Phase in Multi-Component Room Temperature Mixtures, *Jpn. J. Appl. Phys.* 48 (2009) 011501–011506.
- [51] W. N. Thurmes, M. D. Wand, R. T. Vohra, K. M. More, FLC materials for micro display applications, *SPIE Conf. Proc.* 3015 (1997) 1–7.
- [52] D. Ziobro, R. Dąbrowski, M. Tykarska, W. Drzewiński, M. Filipowicz, W. Rejmer, K. Kuśmierek, P. Morowiak, W. Piecek, Synthesis and properties of new ferroelectric and antiferroelectric liquid crystals with a biphenyl benzoate rigid core, *Liq. Cryst.* 39 (2012) 1011–1032.
- [53] R. Bartolino, J. Doucet and G. Durand, Molecular tilt in the smectic C phase: a zig-zag model, *Ann. de Phys.* 3 (1978) 389–395.
- [54] E. N. Keller, E. Nachaliel, and D. Davidov, Evidence for the “zig-zag” model of the smectic-C phase in the liquid crystal 4'-butoxyphenylester 4-decyloxybenzoic acid (4OP10O8): A high resolution x-ray study, *Phys. Rev. A.* 34 (5) (1986) 4363–4369.
- [55] M. S. Spector, P. A. Heiney, J. Naciri, B. T. Weslowski, D. B. Holt, and R. Shashidhar, Electroclinic liquid crystals with large induced tilt angle and small layer contraction, *Phys. Rev. E.* 61(2) (2000) 1579–1584.
- [56] J. G. Meier, M. Nobili, T. Carlsson, P. Rudquist, A. S. Petrenko, J. W. Goodby, M. Brunet, and S. T. Lagerwall, Possible model of an

- antiferroelectric twist grain boundary phase, *Phys. Rev. E.* 76 (2007) 011704(1-9).
- [57] M. Wand, W. Thurmes, M. Meadows, FLC displays for high-resolution magnified view and projection applications, *Proc SPIE.* 3635 (1999) 2–7.
- [58] A. Debnath, D. Sinha, P. K. Mandal, Formulation of a room temperature ferroelectric liquid crystal mixture with sub-millisecond switching time, *AIP Conf. Proc. (59th DAE Solid State Symp.)* 1665 (2015) 040004(1–3).
- [59] D. Goswami, D. Sinha, and P. K. Mandal, Dielectric and electro-optic characterization of a partially fluorinated ferroelectric liquid crystal, *AIP Conf. Proc.* 1953 (2018) 050012(1-4).
- [60] A. Debnath and P. K. Mandal, Wide range room temperature ferroelectric liquid crystal mixture with microsecond order switching, *J. Mol. Liq.* 221 (2016) 287-291.
- [61] J. P. F. Lagerwall, F. Giesselmann, Current topics in smectic liquid crystal research, *Chem Phys Chem.* 7 (2006) 20-45.
- [62] S. T. Lagerwall, *Ferroelectric and Antiferroelectric Liquid Crystals*, WILEY-VCH Verlag GmbH. Weinheim, 2007, 1-427.
- [63] J. P. F. Lagerwall, G. Scalia, A new era for liquid crystal research: Applications of liquid crystals in soft matter nano-, bio- and microtechnology, *Curr. Appl. Phys.* 12 (2012) 1387-1412.
- [64] A. Dłubacz, M. Marzec, D. Dardas, M. Żurowska, New antiferroelectric liquid crystal for use in LCD, *Phase Trans.* 89 (2016) 349-358.
- [65] A. Debnath, D. Sinha and P. K. Mandal. Wide range room temperature electroclinic liquid crystal mixture with large induced tilt and very small layer contraction, *J. Appl. Phys.* 119 (2016) 124103(1-4).
- [66] K. C. Dey and P. K. Mandal. Formulation of a binary eutectic antiferroelectric liquid crystal mixture: Comparison of dielectric and electro-optic properties with the pure compounds, *J. Mol. Liq.* 243 (2017) 484 –493.
- [67] A. Debnath, P. K. Mandal, Effect of non-mesogenic chiral terphenylate on the formulation of room temperature ferroelectric liquid crystal mixtures suitable for display applications, *J. Mol. Liq.* 292 (2019) 111317 (1-8).



# CHAPTER 8

---

## Summary and Conclusions



## Summary and Conclusions:

Liquid crystals are very important soft material in the field of material research. With their fascinating physical and electro-optical properties they find application mainly in the display technology as well as in other areas. Antiferroelectric liquid crystals are important class of liquid crystals for their tristate switching, microsecond response, hemispherical viewing angle and no-ghost effect. Moreover, a perfect dark state can be achieved using the orthoconic antiferroelectric liquid crystals as these are uniaxially negative crystal and the optic axis is perpendicular to the glass plates of the cell. Therefore for proper application of these kinds of materials it is very much essential to study their structure-property relationship. These structure-property studies will also help in the understanding of the engineering of the better materials. As no single compounds satisfy the conditions required for display applications, preparing mixture is an alternative means to meet the requirements of the displays. With these aims and objectives we have made detailed investigation on six pure antiferroelectric liquid crystals - **DM0**, **DM1**, **DM2**, **DM3**, **4F6T**, and **6F6T**. The first four compounds are biphenyl benzoate core based (**DM** series) while the remaining two compounds are doubly fluorinated terphenyl core based (**6T** series). We have also investigated in detail three formulated mixtures - a binary eutectic mixture (**M3**) of **DM0** and **DM3** in equal weight percent, a multi-component mixture (**M6**) of equal weight percent of all the **DM** series compounds and a mixture of **MWCNT** and **DM1**. All the nine systems have been studied using POM, DSC, X-ray diffraction, frequency dependent dielectric spectroscopy and electro-optic techniques.

Although the conclusions of these studies have been mentioned while presenting the detailed results in previous chapters in this chapter we summarize below the overall conclusions of the present dissertation. Most of the results have already been published in various scientific journals of international repute, a list of which is given in **Appendix B**.

- All the six pure compounds are found to exhibit antiferroelectric, ferroelectric and paraelectric phases. No change in phase sequence is observed either due to large change in core structure (**DM** series and **6T** series) or due to change in

lateral fluorination in core (**DM** series) or due to increased fluorinated achiral chain length (**6T** series).

- Melting point is found to decrease due to core fluorination at ortho and meta positions (**DM1** and **DM2**) and increasing achiral fluorinated chain length (**4F6T** and **6F6T**), however, for double fluorination in core (**DM3**) it increases. Clearing point also decreases in all the core fluorinated compounds in DM series compared to the protonated core one, while in 6T series it increases with increasing fluorinated chain length.
- Thermal range of the antiferroelectric phase increases in DM1 but decreases in DM2 and DM3 but the range of ferroelectric phase is found to decrease in all the fluorinated compounds. On the other hand, in 6T series compounds thermal ranges of both the phases are found to exhibit odd-even effect.
- All the compounds exhibit quite strong dipole moments. Dipole moment increases with increasing core fluorination but with increasing fluorinated chain length it shows odd-even effect. Fluorinated DM series compounds have higher dipole moments than 6T series compounds.
- The average intermolecular spacing is found to decrease with single fluorination in core, however, it increases with double fluorination in core or with fluorinated chain length.
- Layer spacings in orthogonal SmA\* phase increases with single lateral fluorination in core (DM1 and DM2) whereas it is found to decrease with double fluorination in core (DM3) but it is found to increase with fluorinated chain length (6T series). These spacings are less than the optimized molecular lengths in all systems but substantial in DM series implying that the molecules are in different conformations than in *vacuo* condition or the molecules are tilted with azimuthal degeneracy as in de Vries phase or both.
- Temperature variation of layer spacing in SmC\* phase shows a parabolic nature near the critical temperature  $T_c$ , implying that the paraelectric-ferroelectric (SmA\*–SmC\*) transition is nearly tricritical in nature in all the systems. Temperature dependence of spontaneous polarization also supports this conclusion.
- All the compounds, fluorinated either in core or in chain or in both, are found, considering their tilts, to be of orthoconic antiferroelectric nature. X-ray tilts are, however, much less as observed in many other systems.

- All the compounds exhibit very large dielectric increment ( $\Delta\epsilon$ ) in SmC\* phase but in DM series values are much higher than in 6T series. Maximum value of  $\Delta\epsilon$  is found to decrease with single fluorination and increase with double fluorination in DM series compared to the protonated core compound while it decreases with increasing fluorinated chain length in 6T series.
- Goldstone mode and soft mode critical frequencies are much higher in DM series compounds than in 6T series compounds. Critical frequencies of all the relaxation modes ( $P_L$ ,  $P_H$ , GM and SM) are found to decrease with lateral fluorination in DM series compounds whereas in 6T series GM critical frequency shows an odd-even effect and SM critical frequency decreases with increasing fluorinated chain.
- Although SM is observed within SmA\* phase in all the DM series compounds, but only when the core is doubly fluorinated (DM3) SM is also observed within SmC\* phase near  $T_c$  and it shows Curie–Weiss behaviour. On the other hand, both the 6T series compounds exhibit such behaviour.
- Significantly higher field is required for saturation of the spontaneous polarization with increasing lateral fluorination in core and also with increasing fluorinated chain length. However the maximum values of the spontaneous polarization are much higher in DM series compounds compared to 6T series compounds.
- In all systems sub-millisecond response time is observed. However, increasing fluorination in core and increasing fluorinated chain length, result in the slower response of the molecules under a square pulse.
- Antiferroelectric-ferroelectric transition temperature  $T_{AF}$  is found to decrease with increasing ac field, decrement rate is faster in longer fluorinated chain molecule.
- A eutectic antiferroelectric mixture (M3) is formed when equal weight percent of the protonated core and doubly fluorinated core compounds DM0 and DM3 are mixed. The mixture shows the same phase sequence (Cr–SmC<sub>A</sub>\*–SmC\*–SmA\*–Iso) as in the pure compounds but with increased range of SmC<sub>A</sub>\* phase. But when equal weight percent of all four DM series compounds are mixed (M6) the thermal range of SmC<sub>A</sub>\* phase increases further and the phase persists

much below room temperature. Both the mixtures (M3 and M6) retain the orthoconic nature of the antiferroelectric phase of the pure components.

- Properties of both the mixture are not always found to be proportional to the concentration of the pronated core and the fluorinated core components.
- Four collective relaxation modes ( $P_L$ ,  $P_H$ , GM, and SM) are observed in both the mixtures like the pure compounds, however, their critical frequencies are not always proportional to the concentration of the pure compounds. The critical field for the suppression of the  $P_L$  and Goldstone modes increases significantly in the mixtures. Also, the GM mode dielectric increment decreases significantly. Like the pure compounds, the hereditary mode is observed in both the mixtures, however, domain mode is observed only in the four-component mixture M6.
- ‘V’ shape variation of soft mode critical frequency and inverse of dielectric increment is exhibited by the four –component mixture M6 like the pure compound DM3, but not by the mixture M3 which although it is a mixture of DM0 and DM3.
- Ferroelectric–paraelectric transition temperature ( $T_c$ ) of both the mixtures M3 and M6 is found to increase linearly with bias field which could be explained using the Landau model.
- Spontaneous polarizations of both the mixtures are found to be in between those of the pure compounds. Switching time also exhibits similar behaviour and observed to be less than a millisecond.
- When a small fraction (0.12 wt.%) of functionalized multi-walled carbon nano tube is mixed in one of the core fluorinated DM series compound (DM1) the phase sequence does not alter but the phase boundaries are lowered and the stability of the paraelectric and the ferroelectric phases are found to increase but that of the antiferroelectric phase is decreased. Pitch of the helicoidal structure does not change appreciably in the composite, but it is found to increase with decreasing temperature in both the tilted phases in DM1 but an decreasing trend is observed in the  $SmC^*$  phase of the composite.
- In the antiferroelectric phase of the composite the in-phase antiferroelectric mode is completely suppressed whereas the absolute values and the ranges of the anti-phase antiferroelectric mode critical frequency ( $f_{PH}$ ) and the absorption strength ( $\epsilon''_{PH}$ ) are found to decrease. Moreover, decrease of dielectric increment ( $\Delta\epsilon_{GM}$ ) and increase of critical frequency ( $f_{GM}$ ) of the Goldstone mode are

observed in the composite. Two fold increase of the critical field for suppression of the Goldstone mode in the composite is found, which signifies the helical structure in the nanocomposite is more stable than in the pure compound. Doping of rigid MWCNTs increases the modulus of elasticity of the composite and hence increases SM critical frequency.

- The composite also retains the orthoconic nature of the antiferroelectric phase.
- Spontaneous polarization of the composite is less compared to the pure compound. Most significantly, switching time in the composite is almost half of that of the pure.
- A lower value of conductivity in the composite signifies trapping of impurity ions by the CNTs.

In fine, it is concluded that the nature of core structure, fluorination in the core and chain as well as chain length have pronounced effect in the thermal range of phases and various molecular parameters like dipole moments, layer spacings and tilt angles. These factors also influence significantly the response of the material to an electric field and also their electro-optic behaviour. This study has thrown a significant insight into the structure-property relationship of the materials. That all the materials are having orthoconic antiferroelectric phase and a mixture of four pure compounds have a wide range of antiferroelectric phase far below room temperature with sub-microsecond switching time signify that materials are expected to be useful for formulation of orthoconic antiferroelectric liquid crystal mixture for display applications.



# APPENDIX A

## LIST OF SELECTED BOOKS AND MONOGRAPHS ON LIQUID CRYSTALS

- [1] Ferroelectrics- Physical Effects. Editor: Mickael Lallart. Intech, Croatia; 2011.
- [2] *Relaxation phenomena* – Liquid crystals, magnetic systems, polymers, high-TC superconductors, metallic glasses. W. Haase and S. Wrobel. Springer-Verlag, Berlin-Heidelberg; 2003.
- [3] *The Physics of Ferroelectric and Antiferroelectric Liquid Crystals*. I. Musevic, R. Blinc and B. Zeks. World Scientific, Singapore; 2000.
- [4] *Ferroelectric and antiferroelectric Liquid Crystals*. S.T. Lagerwall. Weinheim, Wiley-VCH; 1999.
- [5] *Handbook of Liquid Crystals*. Vol. 1 “Fundamentals”, 2A “Low Molecular Weight Liquid Crystals I”, 2B “Low Molecular Weight Liquid Crystals II”, 3 “High Molecular Weight Liquid Crystals”, Editors: D. Demus, J. Goodby, G. W. Gray, H. W. Spiess and V. Vill, WILEY-VCH, Verlag GmbH, Weinheim, FRG; 1998.
- [6] *Introduction to Liquid Crystals Chemistry and Physics*. P. J. Collings and M. Hird. Taylor & Francis; 1997.
- [7] *The Surface Physics of Liquid Crystals*. A. A. Sonin. Gordon and Breach Science Publishers; 1995.
- [8] *Liquid Crystals in the Nineties and Beyond*. Editor: S. Kumar. World Scientific; 1995.
- [9] *The Physics of Liquid Crystals*. 2nd Edition. P. G. de Gennes and J. Prost. OUP (Clarendon), London; 1993.
- [10] *Liquid Crystals*. S. Chandrasekhar. Cambridge University Press; 1977.
- [11] *Ferroelectric Liquid Crystals: Principles, Properties and applications*. J. W. Goodby, R. Blinc, N. A. Clark, S. T. Lagerwall, M. A. Osipov, S. A. Pikin, T. Sakurai, K. Yoshino and B. Zeks. Gordon & Breach, Philadelphia; 1991.
- [12] *Thermophysical Properties of Liquid Crystals*. A. L. Tsykalo. Gordon and Breach Science Publishers; 1991.
- [13] *Liquid Crystals Application and Uses*. Vol. 1-3. Editor: B. Bahadur. World Scientific; 1990- 1992.

- [14] *Liquid Crystals: Nature's Delicate Phase of Matter*. P. J. Collings, Princeton Press, Princeton; 1990.
- [15] *Structure of Liquid Crystal Phases*. Lecture Notes in Physics - Vol. 23, P. S. Pershan. World Scientific; 1988.
- [16] *Thermotropic Liquid Crystals, Fundamentals*. G. Vertogen and W. H. de Jeu. Springer-Verlag; 1988.
- [17] *Thermotropic liquid crystals*. G. W. Gray. Wiley, Chichester; 1987.
- [18] *Smectic Liquid Crystals*. G. W. Gray and J. W. Goodby. Glasgow, Leonard Hill; 1984.
- [19] *Advances in Liquid Crystals*. Vol. 1-6. Glenn H. Brown. AP; 1978-1983.
- [20] *Polymeric Liquid Crystals*. Editors: A. Ciferri, W. R. Krigbaum and Robert B. Meyer. AP; 1982.
- [21] *Physical Properties of Liquid Crystalline Materials*. W. H. de Jeu. Gordon and Breach Science Publishers; 1980.
- [22] *Handbook of Liquid Crystals*. H. Kelker and R. Hatz. Verlag Chemie; 1980.
- [23] *Liquid Crystals and Biological Structure*. G. H. Brown and J. J. Wolken. AP; 1979.
- [24] *The Molecular Physics of Liquid Crystals*. Editors: G. R. Lukhurst and G. W. Gray. AP, NY; 1979.
- [25] *Textures of Liquid Crystals*. D. Demus and L. Richter. Verlag Chemie; 1978.
- [26] *Liquid Crystals*. Solid State Physics Suppl. 14. Editor: L. Liebert. AP; 1978.
- [27] *Applications of Liquid Crystals*. G. Meier, E. Sackmann and J. G. Grabmaier. Springer, Verlag; 1975.
- [28] *Introduction to Liquid Crystals*. E. B. Priestley, P. J. Wojtowicz and P. Sheng. Plenum Press; 1975.
- [29] *Liquid Crystals & Plastic Crystals*. Vols 1 and 2. G. W. Gray and P. A. Winsor. Ellis Horwood Ltd.; 1974.
- [30] *The Physics of Liquid Crystals*. P. G. de Gennes. OUP London; 1974.
- [31] *Molecular Structure and Physical Properties of Liquid Crystals*. G. W. Gray. Academic Press (AP); 1962.
- [32] *Textures of liquid crystals*. I. Dierking. WILEY-VCH, GmbH & Co. KGaA; 2003.

# APPENDIX B

## (I) LIST OF PAPERS PUBLISHED IN JOURNALS

- [1] **K. C. Dey**, P. K. Mandal, and R. Dabrowski, Effect of lateral fluorination in antiferroelectric and ferroelectric mesophases: synchrotron X-ray diffraction, dielectric spectroscopy and electro-optic study, **Journal of Physics and Chemistry of Solids**. 88(2016)14-23, doi: 10.1016/j.jpcs.2015.08.016.
- [2] **K. C. Dey**, P. K. Mandal, and R. Dabrowski, Investigation on a laterally fluorinated orthoconic antiferroelectric liquid crystal by different experimental techniques, **AIP Conference Proceedings**. 1731(2016) 040015(1-3), doi: 10.1063/1.4947651.
- [3] **K. C. Dey**, P. K. Mandal, and R. Dabrowski, Effect of bias on dielectric properties of SmC<sub>A</sub>\* and SmC\* phases of a perfluorinated antiferroelectric liquid crystal, **Materials Today Proceedings**. 3(2016) 3987-3991, doi: 10.1016/j.matpr.2016.11.061.
- [4] **K. C. Dey**, P. K. Mandal, and R. Dabrowski, Influence of Bias on Dielectric Properties of Mesophases of a Laterally Fluorinated Antiferroelectric Liquid Crystal. **Springer Proceedings in Physics**, ‘Recent Trends in Materials Science and Applications’. 89 (2016) 475-483, doi: 10.1007/978-3-319-44890-9\_43.
- [5] **K. C. Dey**, and P. K. Mandal, Formulation of a binary eutectic antiferroelectric liquid crystal mixture: Comparison of dielectric and electro-optic properties with the pure compounds, **Journal of Molecular Liquids**. 243 (2017)484 –493, doi: 10.1016/j.molliq.2017.07.117.
- [6] **K. C. Dey** and P. K. Mandal, Effect of multi-walled carbon nanotubes on dielectric and electro-optic properties of a high tilt antiferroelectric

liquid crystal, **Phase Transitions**. 92(3) (2019) 302–315, doi: 10.1080/01411594.2019.1574012.

- [7] **K. C. Dey**, P. K. Mandal, and P. Kula, Effect of fluorinated achiral chain length on structural, dielectric and electro-optic properties of two terphenyl based antiferroelectric liquid crystals, **Journal of Molecular Liquids**. 298 (2020) 112056 (1-11), doi: 10.1016/j.molliq.2019.112056.
- [8] **K. C. Dey**, P. K. Mandal, M. Urbanska, O. Gutowski, and A. Sarma, Formulation and characterization of a room temperature multi-component high tilt antiferroelectric liquid crystal mixture, **Philosophical Magazine**, Communicated for publication.

## **(II) LIST OF PAPERS PRESENTED IN SEMINARS AND CONFERENCES**

- [1] **National Seminar Modern Trends in Material Science (MTMS)-2015**, 5-6<sup>th</sup> India.

**Title:** Investigation on an orthoconic antiferroelectric liquid crystal by temperature dependent dielectric spectroscopy, electro-optic technique and Synchrotron X-ray diffraction. Authors: **K. C. Dey** and P.K. Mandal.

- [2] **National Seminar on Condensed Matter, Laser and Communicaiton-2015**, 27<sup>th</sup> February, 2015, Department of Physics, Burdwan University, West Bengal, India.

**Title:** On the studies of structural aspects and relaxation behaviuor of an orthoconic antiferroelectric liquid crystal (OAFLC) by Synchrotron X-ray diffraction, simulation technique and dielectric spectroscopy. **Author:** **K. C. Dey** and P.K. Mandal.

- [3] **22nd West Bengal State Science and Technology Congress-2015**. 28<sup>th</sup> February - 1<sup>st</sup> March, 2015: University of North Bengal, West Bengal, India.

**Title:** Studies on a laterally fluorinated antiferroelectric liquid crystal by synchrotron X-ray diffraction, dielectric spectroscopy and electro-optic techniques. Author: **K. C. Dey** and P. K. Mandal.

- [4] **Physics and Applied Mathematics Researchers' Meet-2015**, 18-20<sup>th</sup> March 2015, 2015, Indian Statistical Institute, Kolkata, West Bengal, India.

**Title:** Effect of lateral fluoro-substitution on properties of orthoconic antiferroelectric liquid crystal. Author: **K. C. Dey** and P. K. Mandal.

- [5] **60<sup>th</sup> DAE Solid State Symposium-2015**, 21<sup>st</sup> -25<sup>th</sup> Dec, 2015, Amity University, Noida, Delhi, India.

**Title:** Investigation on a Laterally Fluorinated Orthoconic Antiferroelectric Liquid Crystal by Different Experimental Techniques. Author: **K. C. Dey** and P. K. Mandal.

- [6] **International Conference on Recent Trends in Materials Science and Applications-2016**, 29<sup>th</sup> February, 2016, Jamal Mohamed College, Tiruchirappalli, Tamil Nadu- 620020, India.

**Title:** Influence of bias on dielectric properties of mesophases of a laterally fluorinated antiferroelectric liquid crystal. Author: **K. C. Dey** and P. K. Mandal.

- [7] **International Conference on Material Research and Application (ICMRA-2016)**, 11<sup>th</sup> -13<sup>th</sup> March, 2016, CMR Technical Campus, Telengana- 501401, Hyderabad, India.

**Title:** Effect of bias on dielectric properties of SmC<sub>A</sub>\* and SmC\* phases of a perfluorinated antiferroelectric liquid crystal. Author: **K. C. Dey** and P. K. Mandal.

- [8] **National Seminar on Frontiers in Science and Technology towards Development of Nation**, 10<sup>th</sup> -11<sup>th</sup> April, 2016, Acharya B. N. Seal College, Cooch Behar- 736101, West Bengal, India.

**Title:** Ferroelectric and Antiferroelectric Liquid Crystals – Structures and Applications. Author: **K. C. Dey** and P. K. Mandal.

- [9] **International Interdisciplinary Seminar on Contemporary Developments in Social & Basic Sciences in times of Global Crisis (UGC sponsored), 28-29<sup>th</sup> March, 2017, Surya Sen Mahavidyalaya, Siliguri, West Bengal, India.**

**Title:** Dielectric investigations of pure and carbon nanotube–doped antiferroelectric liquid crystals. Author: **K. C. Dey** and P. K. Mandal.

- [10] **Recent Advances in Mathematical Sciences and their Applications (RAMSA-2018), 30<sup>th</sup> -31<sup>st</sup> August, 2018, Surya Sen Mahavidyalaya, Siliguri, West Bengal, India.**

**Title:** Theoretical Conception of Discovery of Ferroelectric Liquid Crystal and Theory of Measurement of Few Electro-optic Parameters. Author: **K. C. Dey**

# INDEX

## A

achiral 7, 17, 19, 21, 22, 62, 69, 70, 94, 101, 138, 139, 147, 175, 177, 178, 180-182, 186, 189, 191-194, 198, 206  
 activation energy 58, 88, 118, 119, 138  
 AFLC 12-14, 16, 19, 21, 127, 128, 155, 156, 159, 161-168  
 anisotropic 43, 165  
 antiferroelectric 1, 6, 12-21, 26-29, 31, 33, 40, 47, 50, 54, 55, 58, 63-65, 67, 69, 70, 75-77, 80-82, 87, 88, 90-97, 101, 102, 104, 110, 111, 119, 120, 122, 123, 125, 127, 128, 130, 135, 141-143, 145-149, 151, 154, 155, 157, 158, 161, 164, 168-172, 175, 177, 178, 183, 186, 190, 191, 193, 195-201, 205-209  
 antiferroelectric phase 12, 21, 50, 76, 77, 80, 88, 102, 128, 142, 168, 178, 183, 206, 208, 209  
 apparent molecular length 40  
 arrhenius law 118  
 arrhenius type 58, 88, 138

## B

bias field 49, 50, 65, 81-85, 91, 95, 108-110, 112-116, 119, 122, 123, 137-140, 148, 149, 159, 160, 162, 163, 168, 187, 208  
 bias fields 102, 108, 136, 163  
 binary mixture 19, 21, 30, 101, 102, 105, 120, 121, 127, 129, 136, 140, 147, 200  
 biphenyl benzoate 21, 22, 69, 101, 154, 177, 178, 184, 185, 190, 205

bistability 11  
 bookshelf geometry 10, 12, 113  
 broken fan 129, 180

## C

chiral 4, 6-9, 16-19, 26, 27, 29-31, 40, 47, 49, 54, 55, 62, 64, 66, 69, 92-94, 96, 101, 123, 145-147, 169, 171, 177, 178, 182, 195-199, 201  
 chiral center 6, 16-18, 169, 195  
 chiral dopant 19, 101  
 chirality 1, 6, 8, 12, 16, 69, 70  
 cholesteric 1, 4, 5, 156  
 CNT 24, 154-166  
 Cole-Cole 33, 45-47, 79, 103, 155, 179  
 cole-cole equation 46, 155, 179  
 cole-cole function 79  
 cole-cole model 33, 46  
 cole-cole plot 45-47  
 collective relaxation 48, 50, 80, 119, 160, 208  
 correlation 6, 42, 51, 77, 78, 90, 110, 133, 134, 143, 184-186, 193  
 correlation length 42, 77, 78, 90, 133, 134, 143, 185, 184-186, 193  
 critical exponent 87, 117, 133, 141, 143, 183  
 critical field 82, 83, 84, 85, 90, 109, 112, 119, 137-139, 168, 192, 208, 209  
 critical frequencies 51, 52, 80-85, 90, 106, 108, 113, 119, 136, 159, 160, 162, 163, 187, 193, 207, 208  
 critical frequency 45-47, 49, 82-84, 102, 106, 107, 109, 111-113, 134, 136-140, 158-163, 168, 187, 194, 207-209

critical temperature 87, 115, 116, 206

## D

Debye 33, 44-47, 62, 74, 82, 183

debye equation 44-46

debye model 33, 44

debye relaxation 45, 47

dielectric 12, 15, 16, 22, 27, 33, 35, 41, 43-50, 52, 53, 55, 56, 59, 62-65, 67, 71, 79, 82, 84, 85, 90, 93-96, 99, 102, 103, 106, 108, 110-116, 119-123, 125, 127, 128, 134, 136-140, 146-149, 151, 154, 155, 158, 161, 163-165, 167, 168, 170-172, 175, 178, 179, 186, 188, 193-196, 198-201, 205, 207, 208

dielectric anisotropy 16, 43, 63, 164

dielectric increment 44, 45, 49, 52, 79, 85, 102, 103, 111-114, 116, 119, 134, 137-139, 154, 161, 163, 168, 179, 186, 188, 193, 207, 208

dielectric permittivities 198

dielectric permittivity 43-45, 48, 52, 53, 113, 134, 158, 161

dielectric relaxation 33, 43, 44, 47, 52, 59, 62-64, 93-96, 121, 122, 147, 148, 171, 199

dielectric response 48, 110

Dielectrics 62

dielectric spectra 45, 46, 49, 137, 138, 140, 155

dielectric spectroscopy 33, 35, 43, 53, 63, 93, 94, 108, 120, 122, 146, 155, 171, 195, 199, 205

diffraction 5, 22, 33, 35, 39-42, 60, 61, 67, 74, 75, 77, 78, 94, 120, 122, 128, 131, 132, 146, 171, 175, 183, 184, 195, 198, 205

diffraction features 42, 74, 75, 77, 132, 184

diffraction pattern 39, 40

diffraction photographs 74, 131

diffraction study 67, 74, 78, 175, 183

dipole 7, 8, 13, 16-18, 62, 70, 73, 74, 79, 83, 85, 88, 90, 181-183, 193, 198, 206, 209

dipole moment 7, 8, 16-18, 62, 70, 73, 74, 79, 85, 90, 182, 183, 193, 198, 206, 209

DOBAMBC 7, 8, 56

domain mode 50, 64, 84, 85, 91, 112, 119, 123, 135, 138, 139, 143, 148, 162, 171, 208

DSC 35, 37-39, 67, 71, 72, 90, 94, 96, 99, 102, 104, 125, 128, 130, 131, 179-181, 187, 205

## E

elastic constant 16, 111, 154, 161

elasticity 153, 160, 168, 209

elastic modulus 113

electric dipole 70

electric field 9, 10, 39, 41, 43, 47, 53-56, 58, 84, 85, 112, 114, 115, 123, 129, 130, 142, 164, 194

Electric-Field-Induced 93, 123

electric polarization 12, 62

electroclinic 19, 30, 94, 97, 101, 120, 130, 146, 147, 149, 198, 200, 201

electron acceptor 17

electron affinity 167

electron-density 87

electron donor 19, 101

electrooptic 26, 53, 54, 63, 172, 198

electro-optic 3, 10-12, 20, 22, 27, 28, 33, 35, 53, 55, 64, 71, 95, 96, 99, 117, 120, 122, 125, 127, 140, 145-149, 151, 153, 164, 170, 171, 175, 178, 188, 194, 195, 201, 205, 209

electro-optical 15, 17, 28, 35, 54, 57, 95, 102, 146, 148, 149, 170-172, 179, 205

eutectic 21, 99, 101-104, 106, 111,

119, 120, 128, 146, 201, 205, 207

## F

fan shape 71, 129, 156

ferroelectric liquid crystal 1, 7, 9, 10, 26, 27, 30, 31, 56, 58, 63, 66, 94, 120, 122, 123, 156, 164, 166, 170, 171, 172, 195, 201

ferroelectric liquid crystals 12, 20, 25-27, 29, 30, 50, 62-66, 92, 94, 95, 111, 121, 138, 148, 149, 154, 170-172, 182, 191, 196, 199, 200

Ferroelectric–paraelectric 208

first order 38, 114

FLC 7, 16, 19, 20, 31, 57, 69, 85, 127, 154, 156, 164, 166, 181, 186, 200, 201

fluorinated 15, 17, 19-22, 29-31, 64, 69-71, 75, 81, 82, 84, 85, 88, 90-96, 101, 119, 122, 146, 148, 169, 175, 177, 178, 180-182, 184-186, 189, 191, 193, 195-197, 201, 205-208

free energy density 111, 114, 115, 186

## G

goldstone mode 48-50, 62, 80, 83, 84, 95, 108, 110-112, 123, 136, 138, 139, 148, 158, 160-162, 168, 171, 187, 193, 194, 200, 207-209

## H

havriliak and negami 47

helical structure 6, 31, 110, 112, 154, 162, 168, 209

helical structure 209

helical superstructure 8

hereditary mode 80-82, 111, 119, 137, 160, 187, 208

homogeneous 9, 12, 47, 48, 71, 102,

128, 155, 157, 158, 178, 179

host mixture 19, 101, 130, 153

## I

induced polarization 43, 44

intermolecular distance 39, 40, 61, 74-76, 131-133, 185, 193

intermolecular interactions 79

intermolecular spacing 90, 206

## L

landau free energy 114, 147, 198

landau model 49, 84, 111, 114, 119, 144, 186, 208

landau theory 140, 161, 168

layer contraction 19, 30, 97, 101, 120, 146, 149, 200, 201

layer shrinkage 132, 133, 183

layer spacing 40, 42, 74-76, 90, 131, 132, 133, 143, 183, 185, 189, 206

layer spacings 90, 132, 178, 183, 185, 193, 206, 209

layer structure 27

layer thickness 132, 133, 183

liquid crystal 1, 3-7, 9-14, 18, 19, 21, 25-31, 38, 40, 56, 58, 61, 63-66, 69, 93-96, 99, 105, 114, 120-123, 127, 142, 145-149, 151, 154-156, 161, 164, 166, 169-173, 195, 197-201, 209

liquid crystal 15, 28, 93, 95, 125, 148, 149, 180, 200

liquid crystal 27, 59, 123, 147, 170, 201

liquid crystal devices 29, 164, 172, 173

liquid crystal display 3, 28, 31, 169

## M

mesogenic 19, 62, 69, 76, 146, 178, 196, 197  
 Mesogens 198  
 mesomorphic 3, 29, 31, 93, 146, 169, 178, 181, 195-197  
 mesophase 7, 8, 16-18, 36, 39, 71, 128, 146  
 MHPOBC 12, 13, 27, 63, 64, 93, 122, 147, 199  
 microsecond 19, 20, 30, 101, 120, 127, 201, 205  
 millisecond 208  
 milliseconds 10  
 molecular structures 18, 23, 69, 70, 103, 131, 153, 154, 155, 166, 179, 181, 195  
 molecular tilt 12, 14, 54, 65, 96, 149, 166, 200  
 multicomponent 19, 101, 125, 130, 205  
 multi-component 19, 29, 93, 143, 153, 196  
 Multi-Component 200  
 multicomponent host 130  
 multicomponent mixture 205  
 multi-walled 21, 151, 153, 154, 172, 200, 208  
 MWCNT 24, 153-155, 158, 160, 161, 165, 167, 168, 205

## N

nanocomposite 19, 21, 52, 153, 154-161, 163-168, 209  
 nematic 1, 4, 5, 8, 15, 19, 25, 39, 40, 43, 61, 120, 121, 127, 145, 153, 154, 156, 164, 166, 169, 170, 172, 173  
 nematics 4-6, 10, 40, 60, 61  
 Nematogens 63, 198  
 non-collective 48, 64, 94, 122, 147,

171  
 non-fluorinated 82, 84, 88, 178  
 non-linear 52  
 non-mesogenic 153, 201

## O

OAFLC 14, 15, 127, 178  
 odd-even 180, 182, 183, 189, 193, 206, 207  
 optical microscopy 22, 33, 35-37, 67, 71, 74, 94, 96, 99, 102, 104, 125, 128, 129, 175, 179, 180  
 optical tilt 67, 86-88, 93, 140, 141, 143, 166, 167, 190, 191, 193  
 optimization 18, 29, 67, 73, 153  
 optimized 18, 73-75, 90, 153, 175, 181-183, 206  
 orientational order 4, 5, 166  
 orientational orders 4  
 Orthoconic antiferroelectric 195

## P

paraelectric 70, 87, 104, 111, 117, 130, 140, 143, 166, 194, 205, 208  
 paraelectric-ferroelectric 206  
 Ph 30, 62, 79-83, 89, 107, 109-111, 136, 137, 143, 159, 162, 188  
 phase 3-12, 14, 16, 17, 19, 21-25, 27, 29, 30, 35-40, 42, 44, 48-53, 59-61, 63-65, 67, 69, 71-85, 87, 88, 90, 92-97, 99, 101, 102, 104-114, 118-123, 127-139, 141-144, 146-149, 151, 155-160, 163, 164, 167, 168, 171, 178-181, 183-187, 189-201, 205-209  
 phase diagram 102, 104, 105, 120, 121, 129, 146  
 phase transition 35, 37, 38, 49, 50, 59, 64, 65, 94, 95, 114, 122, 123, 148, 149, 156, 171, 194, 195, 198  
 phason 49, 50, 160

photonic 14, 15, 127  
 pitch 5, 8, 19, 111, 157, 158, 168, 171, 208  
 $P_L$  mode 80-83, 89, 106-109, 136, 137, 143, 159, 162, 188  
 polarization 3, 7-10, 12, 16-19, 27-30, 33, 35, 43, 44, 48-50, 53-57, 62, 63, 65-67, 85-87, 91, 93, 101, 103, 110, 111, 114, 115, 117, 119-121, 138, 140, 141, 143, 147, 161, 164-166, 168, 171, 172, 175, 186, 188-190, 193, 194, 200, 206, 207, 209  
 polarization reversal 56, 57, 66, 85, 103, 164  
 polarizing microscope 36, 37, 55, 71, 155  
 polarizing microscopy 94, 147, 151, 155, 187, 199  
 polarizing optical 22, 33, 35-37, 67, 71, 99, 102, 104, 125, 128, 129, 175, 179, 180  
 polarizing optical microscopy 22, 33, 35-37, 67, 71, 99, 102, 104, 125, 128, 129, 175, 179, 180

## R

relaxation frequency 49, 52, 103, 110, 111, 113, 115, 116, 139, 159, 179  
 relaxation mode 50, 52, 113, 138, 160, 162  
 relaxation modes 63, 79, 90, 106, 119, 188, 207, 208  
 relaxation processes 50, 52, 63-65, 80, 82, 95, 122, 148  
 response time 11, 19, 44-46, 57, 93, 101, 103, 118, 164, 168, 172, 207  
 rotational viscosities 166, 172  
 rotational viscosity 33, 35, 53, 54, 58, 65, 66, 103, 111, 118, 119, 165, 168

## S

saturation field 85, 86, 117, 189  
 saturation polarization 188  
 second order transition 76, 87, 117, 133, 183  
 second order transition 87, 133  
 single-walled 153  
 $smc^*$  phase 7, 9-11, 16, 17, 36, 49, 50, 53, 71, 75, 77-82, 84, 85, 88, 90, 96, 99, 107, 110, 112, 114, 120, 122, 130, 133, 135, 137, 139, 142, 147, 156-160, 163, 164, 167, 168, 178, 179, 181, 183-187, 189, 199, 200, 206-208  
 $smc^*$  phases 8, 40, 110, 113, 123, 172, 193, 194  
 soft mode 48-50, 62, 84, 95, 107, 108, 110, 113-116, 123, 135, 136, 139, 148, 149, 158-160, 171, 187, 193, 194, 200, 207, 208  
 spontaneous polarization 7, 8, 10, 16-19, 27-30, 33, 35, 50, 53-55, 65-67, 85, 86, 91, 93, 101, 103, 117, 119-121, 140, 143, 147, 161, 164-166, 168, 175, 188, 190, 193, 194, 200, 206, 209  
 SSAFLC 20  
 SSFLC 10, 11, 114  
 SSOAFLCs 20  
 switching speed 10, 18, 19, 127, 153  
 switching time 19, 20, 30, 33, 35, 53, 57, 67, 88, 101, 119, 120, 140, 142, 144, 147, 154, 164, 165, 168, 175, 191, 192, 194, 200, 201, 208, 209  
 synchrotron radiation 40, 41, 71, 94, 125, 128, 131, 147, 175, 183, 199  
 synchrotron x-ray 35, 41, 74, 120, 131, 146, 171, 198

## T

thermogram 38, 39, 72, 130, 131, 180,

181  
 thermotropic 3, 4, 25, 29, 59-61  
 tilt 7, 9-15, 19, 28, 30, 33, 35, 42, 49,  
   53-55, 65, 67, 75-78, 86-88, 93, 96,  
   97, 101, 111, 113-115, 120, 123,  
   125, 127, 133, 139-143, 145, 146,  
   149, 151, 159-161, 166, 167, 171,  
   175, 178, 183, 186, 190, 191,  
   193-195, 200, 201, 209  
 tilt angle 7, 9-11, 14, 33, 35, 53-55,  
   65, 77, 93, 97, 114, 123, 140, 149,  
   166, 183, 200  
 tilts 87, 88, 142, 190, 191, 194, 206

## V

viscosities 89, 166, 172  
 viscosity 6, 16, 18, 19, 33, 35, 53, 54,  
   58, 65-67, 69, 88, 103, 111, 118,  
   119, 154, 164-166, 168

## X

x-ray tilt 87, 88, 141, 175, 190, 191,  
   193, 194, 206

## Z

zig-zag 87, 96, 149, 200



# Effect of fluorinated achiral chain length on structural, dielectric and electro-optic properties of two terphenyl based antiferroelectric liquid crystals

Kartick Ch. Dey<sup>a</sup>, Pradip Kumar Mandal<sup>b,\*</sup>, Przemysław Kula<sup>c</sup>

<sup>a</sup> Department of Physics, Acharya Prafulla Chandra Roy Government College, Matigara, Siliguri 734010, West Bengal, India

<sup>b</sup> Department of Physics, University of North Bengal, Siliguri 734013, West Bengal, India

<sup>c</sup> Institute of Chemistry, Military University of Technology, Warsaw 00908, Poland

## ARTICLE INFO

### Article history:

Received 18 August 2019

Received in revised form 30 October 2019

Accepted 1 November 2019

Available online 9 November 2019

### Keywords:

Orthoconic antiferroelectric liquid crystal

Dielectric increment

Critical frequency

Spontaneous polarization

Switching time

## ABSTRACT

Two antiferroelectric liquid crystals of different fluorinated chain length have been studied. Although both exhibit antiferroelectric ( $\text{SmC}_A^*$ ), ferroelectric ( $\text{SmC}^*$ ) and paraelectric ( $\text{SmA}^*$ ) phases, melting point decreases with increasing achiral chain length but clearing point shows opposite trend. Thermal ranges of  $\text{SmC}_A^*$  and  $\text{SmC}^*$  phases exhibit odd-even effect like the dipole moments and spontaneous polarization. Layer spacings, average intermolecular distances and correlation lengths across the smectic planes also increase with chain length. Temperature dependence of layer spacings, x-ray tilt, optical tilt and spontaneous polarization suggest tricritical nature of  $\text{SmC}^*-\text{SmA}^*$  transition. Dielectric increments decrease with increased achiral chain. Both soft mode and Goldstone mode critical frequencies decrease with decreasing temperature in the lower derivative but opposite behaviour is observed in the higher derivative. Both the compounds show Curie-Weiss behaviour in soft mode near  $\text{SmC}^*-\text{SmA}^*$  transition temperature ( $T_c$ ). Goldstone mode critical frequency is much higher in the higher derivative. Both in-phase and anti-phase antiferroelectric modes are observed in  $\text{SmC}_A^*$  phase in the higher derivative but in the lower derivative only anti-phase antiferroelectric mode is observed. Optical tilts suggest orthoconic nature of the  $\text{SmC}_A^*$  phase of both the compounds. Ferroelectric-antiferroelectric transition temperature decreases with increasing ac field in both compounds.

© 2019 Elsevier B.V. All rights reserved.

## 1. Introduction

Antiferroelectric liquid crystals (AFLCs) are very attractive for display applications for their tristate switching, microsecond response, hemispherical viewing angle and no-ghost effect [1]. In this type of liquid crystals the molecules of successive layers are tilted in opposite direction and hence the dipolar cancellation does not take place via a helix but directly from neighbour to neighbour unlike in ferroelectric liquid crystals. The mesophase consisting of chiral molecules in successive layers with such pattern is termed as antiferroelectric phase ( $\text{SmC}_A^*$ ). Antiferroelectric liquid crystals with molecular tilt nearly  $45^\circ$  are termed as orthoconic antiferroelectric LCs (OAFLCs) since angle between molecules in two neighbouring layers is  $90^\circ$ . For ordinary surface stabilized AFLCs, the contrast ratio is unsatisfactory and light leakage is observed. Surface-stabilized OAFLCs are uniaxially negative with the optic axis perpendicular to the glass plates and therefore provide a perfect dark state between crossed polarizers even if the direction of the smectic layer normal is not homogeneous in the plane of the cell

[1–2]. Ferroelectric and antiferroelectric liquid crystals with different core, achiral and chiral chains have been studied; their effect on the mesogenic properties have been discussed by several groups [3–18]. The nature and extent of influence of the molecular structure on mesomorphic properties depends upon (i) the length of the chain – whether the chain is fluorinated or non-fluorinated, (ii) nature of the core – biphenyl benzoate or terphenyl or phenyl benzoate etc., (iii) linkage group between achiral chain and core, (iv) linkage group between chiral chain and core etc. (keto or ether or ester). A small influence of the prolongation of the achiral chain on mesomorphic properties was observed in both lactic acid and keto group derivatives while in keto group derivatives substantial changes were observed with increasing chiral chain [8,19]. Goswami et al. [10] reported depression in melting point with increasing achiral chain length and large increase in the thermal range of  $\text{SmC}^*$  phase. On the other hand Dabrowski et al. [20] reported that the fluorination in the achiral chain was responsible for appearing  $\text{SmC}_A^*$  phase and lengthening of spacer in this part of molecule increased the range of this phase. There are reports on the increasing trend of  $\text{SmC}^*-\text{SmC}_A^*$  transition and clearing point with increasing number of fluorinated carbon atom in the achiral chain and this increment is higher in case of even number of carbon than odd number [16,21–22].

\* Corresponding author.

E-mail address: [mandalpk.phys@nbu.ac.in](mailto:mandalpk.phys@nbu.ac.in) (P.K. Mandal).

Thus the number of fluorinated carbon in the achiral part is found to influence the mesogenic properties of various liquid crystalline systems.

We are reporting here results of detailed investigation on two antiferroelectric liquid crystals viz. (S)-4''-(6-perfluorotetrahydroxyhexyl-1-oxy)-2', -3'-difluoro - 4 - (1-methyl-heptyloxy-carbonyl)-[1,1':4,1''] terphenyl [4F6T] and (S)-4''-(6-perfluorohexanoyoxyhexyl-1-oxy)-2', -3'-difluoro - 4 - (1-methylheptyloxy-carbonyl)-[1,1':4,1''] terphenyl [6F6T]. The molecules of the series have laterally fluorinated terphenyl core, methyl heptyl carbonyl ester as the chiral chain at one side of the core and fluorinated achiral chain having ether linkage on the other side of the core. Molecular structures of the two compounds are shown in Fig. 1, which differ only by the number of fluorinated carbon atoms in the achiral chain. The code name of molecules is nFmT, n and m respectively represents the number of C atom in the perfluorinated chain and oligomethylene spacer ( $n = 4, 5, 6$  and  $m = 6$ ) attached to the terphenyl core [23]. All the compounds are found to exhibit antiferroelectric, ferroelectric and paraelectric phases.

Our main object is to investigate how the thermal ranges of different phases, smectic layer spacings, dielectric and electro-optic properties of the two compounds (4F6T and 6F6T) are influenced by the achiral chain length. Results of the intermediate homologue 5F6T, studied earlier by our group [24], will also be compared with present observations wherever possible to throw more light on the structure property relationship. We also want to investigate the suitability of the compounds for formulation of mixtures appropriate for display and other applications.

## 2. Experimental

The compounds were investigated by different experimental techniques – polarizing optical microscopy (POM), differential scanning calorimetry (DSC), structural optimization by molecular mechanics, synchrotron radiation scattering, dielectric spectroscopy and electro-optic measurements. The textures of the samples were investigated and phases were identified using Olympus BX41 polarizing microscope fitted with moticam 2500 camera (5.0 megapixel) and was recorded in a PC using motic 2.0 software. The temperature was controlled using Mettler FP90 central processor and FP82HT hot stage. The thermal behaviour of the compounds was investigated using Mettler FP84HT differential scanning calorimeter. The structural aspects of the samples were studied using synchrotron radiation facility (P07 beamline at Physics Hutch station of PETRA III) at DESY, Hamburg, Germany. The details of diffraction experiment were described in our earlier communication [25]. Smectic layer spacing ( $d$ ) and average intermolecular distances ( $D$ ) were determined from the low and high angle diffraction features. The layer spacings ( $d$ ) were determined using Bragg equation,  $2d\sin\theta_d = \lambda$ , and the average intermolecular distances ( $D$ ) were determined using modified Bragg formula,  $2D\sin\theta_D = 1.117\lambda$  [26]. Positional correlation lengths, across ( $\xi_{||}$ ) and within the plane ( $\xi_{\perp}$ ), were estimated using the formula,  $\xi = 2\pi/\text{FWHM}$ , where FWHM was the full

width at half maxima of the low and high angle intensity profile respectively [27–28]. The Bragg peak angles and the FWHMs were determined fitting the relevant intensity profile data to a Lorentzian function using commercial software. Under rigid rod approximation, tilt of the molecules with respect to the layer normal, often referred to as primary order parameter of chiral liquid crystals, was calculated using the formula  $\cos^{-1}(d/d_A)$ , where  $d_A$  is the layer spacing in SmA\* phase.

The dielectric spectroscopic measurements were performed using HIOKI 3532-50 impedance analyzer in frequency range of 50 Hz–5 MHz. Polyimide coated planar EHC cells of thickness 10  $\mu\text{m}$ , made of ITO coated glass electrodes of very low sheet resistance were used for both dielectric and electro-optic measurements. The cell was filled by capillary action keeping the sample in isotropic state and cooled very slowly ( $@0.2^\circ\text{C}/\text{min}$ ) in presence of an ac field of amplitude 10 V and frequency 10 Hz to achieve the proper alignment. Mettler hot stage and controller (accuracy  $\pm 0.1^\circ\text{C}$ ) were used for temperature regulation. An automatic data acquisition arrangement was made with the help of RS232 interface with a PC. The real and imaginary parts of permittivity were fitted non-linearly to the modified Cole–Cole equation (Eq. (1)) [29–30] in order to extract the different dielectric parameters of various modes.

$$\varepsilon^* = \varepsilon' - i\varepsilon'' = \varepsilon(\infty) + \sum_k \frac{\Delta\varepsilon_k}{1 + (i\omega\tau_k)^{1-\alpha_k}} - i \frac{\sigma}{2\pi\epsilon_0} \left( \frac{1}{f^n} \right) \quad (1)$$

Here  $\Delta\varepsilon_k = \varepsilon(0) - \varepsilon(\infty)$  is dielectric increment or strength of  $k$ -th mode of relaxation, ( $\varepsilon(0)$  and  $\varepsilon(\infty)$  being the real part of the low and high frequency limit permittivities),  $\tau_k$  is relaxation time (inverse of critical angular frequency) and  $\alpha_k$  is a symmetry parameter signifying deviation from the Debye type behaviour of  $k$ th mode relaxation process,  $\epsilon_0$  is dielectric permittivity of the free space and  $\sigma$  is the conductivity of the cell that arises due to charge impurities which contributes mainly in the low frequency region,  $n$  is a fitting parameter which is close to 1 in case of ohmic conductivity.

Spontaneous polarization of the compounds was measured by triangular wave technique introduced by Miyasato et al. [31] and was calculated using the formula

$$P_s = \frac{1}{2AR_s} \int V(t)dt \quad (2)$$

Here  $A$  is the effective area of the cell,  $R_s$  is the resistance in series with the LC cell, voltage drop  $V(t)$  across which is measured as a function of time with a digital storage oscilloscope (Tektronix 2012B) and the factor 2 appears because polarization peak occurs twice in a voltage cycle.

The response of the ferroelectric polarizations are not instantaneous to the applied field, the polarization peak appears on the exponential decay curve away on the time scale from the square-pulse edge. The response time is the measure of this delay [32].

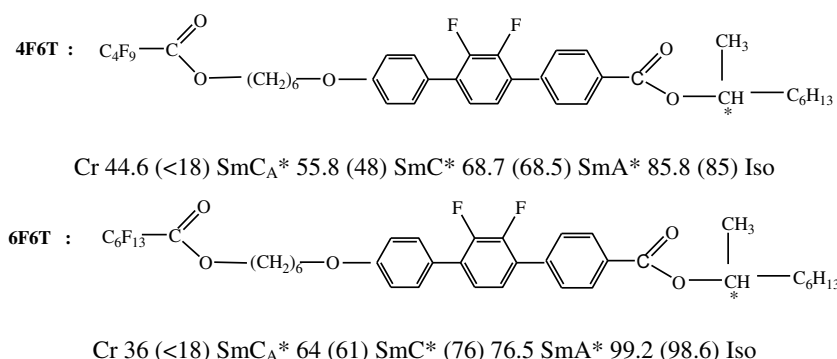


Fig. 1. Molecular structures and transition temperatures ( $^\circ\text{C}$ ) of the molecules obtained from texture studies during heating; cooling data are shown within parentheses.

### 3. Results and discussion

#### 3.1. Polarizing optical microscopy (POM) and differential scanning calorimetric (DSC) study

Transition temperatures obtained from POM study are shown in Fig. 1. Observed textures in different phases of 6F6T are shown in Fig. 2. Fan shaped texture was observed in  $\text{SmA}^*$  phase which was transformed to broken fans in  $\text{SmC}^*$  and  $\text{SmC}_A^*$  phases. Within the broken fans parallel strips were observed which arose due to the formation of helix in tilted smectic phases.

The DSC thermograms of the compounds during heating are presented in Fig. 3. As reported in 5F6T [24],  $\text{SmC}_A^*-\text{SmC}^*$  transition could not be detected in 4F6T and 6F6T which might be due to very small change in enthalpy. Lack of such thermal signature at transitions involving higher order smectic phases [27] or at transitions involving minimum structural change [33] is not uncommon in liquid crystal systems. The transition temperatures obtained from DSC are slightly higher, in some cases, than those obtained from POM studies which may be due to finite heating rate ( $@3.0^\circ\text{C}/\text{min}$ ).

A systematic decrease in melting point and increase in clearing point were observed with increasing length of the fluorinated achiral chain. Such systematic change was also observed in the broadening of  $\text{SmA}^*$  phase. No such behaviour was noticed in the thermal range of  $\text{SmC}^*$  and  $\text{SmC}_A^*$  phases, rather they exhibit some sort of odd even effect [16,21–22,34]. 6F6T exhibited highest range of  $\text{SmC}_A^*$  phase (see Table 1). As discussed in the introduction section, increasing range of  $\text{SmC}^*$  phase was reported in a biphenyl benzoate core based FLC system [10]. A small influence of the prolongation of the achiral chain on the mesomorphic properties of lactic acid and keto group derivatives was also observed [8,19].

#### 3.2. Optimized geometry

The molecular structures of the compounds were optimized by PM3 molecular mechanics calculations in vacuo using Polak–Ribiere algorithm in a commercial package [35] to probe structure-property relationship. The optimized structures along with moments of inertia axes and directions of dipole moments are presented in Fig. 4. Optimized lengths of 4F6T, 5F6T and 6F6T were found to be 35.15, 35.95 and 36.96 Å respectively. The principal moments were found to increase systematically in all three directions with increasing fluorinated chain length as shown in Table 2. However, it should be noted that the optimized molecular structure may not be in the most extended conformation.

The major components of dipole moments were found to be transverse to the long molecular axes for all molecules. The molecules showed quite high value of dipole moments – 5.13 D, 5.01 D and 5.10 D for 4F6T, 5F6T and 6F6T, respectively. A similar variation in dipole moments were also observed in a series of partially fluorinated biphenyl

benzoate rigid core based ferroelectric liquid crystals [10], observed dipole moments were 5.12 D for 4F4R, 4.95 D for 4F5R, 5.05 D for 4F3R and 5.23 D for 7F3R system. The molecular conformation and chain length both affect the dipole moments in the chiral molecules. Different types of variations of dipole moments with chain lengths were reported in literature [36–39] for achiral systems. Megnassan and Proutiere [36] and Gueu et al. [37] observed no significant change in free molecular dipole moment in nCB series for  $n = 0$  to 12. Sarkar et al. [38] also observed no change in the dipole moments with chain length in the nCHBT series but odd–even effect was dominant. The dipole moments of molecules having even numbered chain (4F6T and 6F6T) were higher and almost same (5.13D and 5.10D respectively) whereas that of odd numbered chain (5F6T) its value was smaller ( $\sim 5.01\text{D}$ ). Thus the odd–even effect was also present in dipole moments of the present compounds as observed in the thermal range of the antiferroelectric phase.

#### 3.3. Synchrotron diffraction study

Peaks of low and high angle diffraction profiles of 6F6T are shown in Fig. 5, similar features were observed in 4F6T. Temperature dependence of smectic layer thickness ( $d$ ), measured from synchrotron diffraction study, is shown in Fig. 6. Maximum values of layer spacings in  $\text{SmA}^*$  phase (34.64 Å in 4F6T and 37.16 Å in 6F6T) were found to be, in both cases, almost equal to the optimized lengths of the molecules signifying that the molecular conformation within this phase almost similar to that in vacuo. The layer spacing decreased rapidly with decrease of temperature near the  $\text{SmA}^*-\text{SmC}^*$  transition ( $T_c$ ) indicating tilting of the molecules. Decrement rate reduced gradually as the temperature went deeper into the  $\text{SmC}^*$  and  $\text{SmC}_A^*$  phase. Average layer spacings were observed to be higher in 6F6T compared to 4F6T almost by 2.5 Å as expected. A small discontinuity in the layer spacings was observed at  $48^\circ\text{C}$  in 4F6T and at  $66^\circ\text{C}$  in 6F6T indicating the transition from  $\text{SmC}^*$  to  $\text{SmC}_A^*$  phase. The lowest values of layer spacing in  $\text{SmC}_A^*$  phase were 32.11 Å in 4F6T and 34.50 Å in 6F6T, which means layer shrinkage was roughly 7% in both systems.

Temperature dependence of  $d$  in  $\text{SmC}^*$  phase near  $T_c$  in both 4F6T and 6F6T, was observed to be parabolic in nature. Tilt angle  $\theta$  depends on the reduced temperature as  $\theta \propto (T - T_c)^\beta$  according to generalized mean field theory. A value of 0.5 is predicted in a pure second order transition for the critical exponent  $\beta$  and in case of second order transition approaching tricritical point (TCP) it is 0.25 [40–41]. Following the argument of Hartley et al. [42] and expanding  $\cos\theta$  up to  $\theta^4$  term,  $d_c/d_A$  near  $T_c$  can be written as

$$d_c/d_A \approx 1 - a|T - T_c|^{1/2} + b|T - T_c| \quad (3)$$

when  $\beta$  is taken as 0.25. Observed data fitted nicely to the above equation in both the compounds (Fig. 6(c–d)) signifying that the  $\text{SmC}^*-\text{SmA}^*$  transition was a tricritical type.

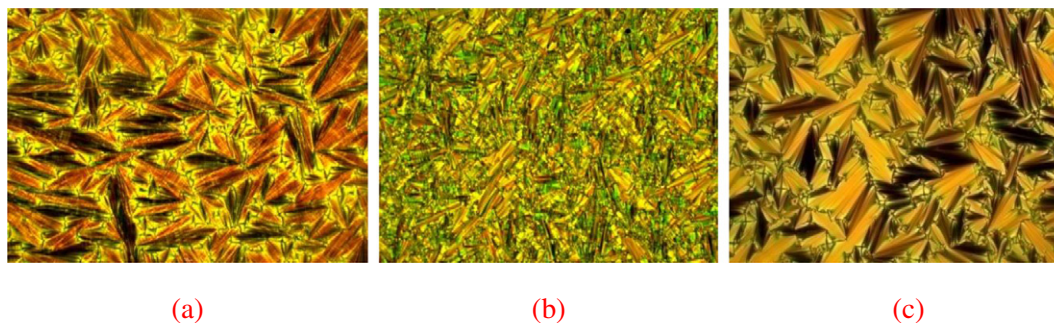


Fig. 2. Textures of 6F6T in different phases (a)  $\text{SmC}_A^*$  ( $40^\circ\text{C}$ ), (b)  $\text{SmC}^*$  ( $71^\circ\text{C}$ ), (c)  $\text{SmA}^*$  ( $95^\circ\text{C}$ ), magnification  $200\times$ .

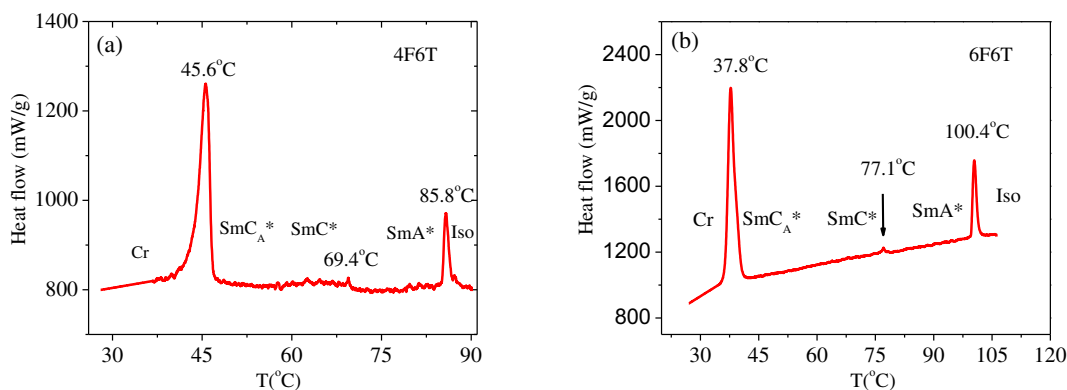


Fig. 3. Typical DSC thermogram obtained for the compounds (a) 4F6T and (b) 6F6T on heating.

On the other hand, average intermolecular distance ( $D$ ) was found to decrease almost linearly with decreasing temperature without showing any significant change at transitions in both the compounds. It decreased from 5.17 Å ( $\text{SmA}^*$ ) to 4.94 Å ( $\text{SmC}_A^*$ ) in 4F6T while in 6F6T from 5.36 Å ( $\text{SmA}^*$ ) to 5.07 Å ( $\text{SmC}_A^*$ ). Thus increase in  $D$  was small due to the increase of achiral chain length by two fluorinated carbon atom.

Estimated correlation lengths across the layers ( $\xi_{||}$ ) in 4F6T in  $\text{SmA}^*$  phase remained almost constant around at 850 Å. At  $\text{SmA}^*$ - $\text{SmC}^*$  and  $\text{SmC}^*$ - $\text{SmC}_A^*$  transitions small discontinuous changes were observed and  $\xi_{||}$  values were around 860 Å in  $\text{SmC}^*$  and 870 Å in  $\text{SmC}_A^*$  phase (Fig. 7(a)). In other words, correlation across the layer was about 24 molecular lengths in  $\text{SmA}^*$  phase and did not increase much in  $\text{SmC}^*$  and  $\text{SmC}_A^*$  phases.

However, in  $\text{SmA}^*$  phase of 6F6T the  $\xi_{||}$  value initially increased from 1008 Å to 1028 Å with decrease of temperature and then gradually decreased to 993 Å at  $\text{SmA}^*$ - $\text{SmC}^*$  transition temperature. After the transition it was observed to increase gradually in the entire  $\text{SmC}^*$  phase and reached a maximum value of 1071 Å at  $T_{AF}$ , the  $\text{SmC}^*$ - $\text{SmC}_A^*$  transition temperature. Although  $\xi_{||}$  decreased slightly from 1068 Å to 1046 Å in  $\text{SmC}_A^*$  phase, it can be considered to remain almost unchanged at 28 molecular lengths. Almost similar values of correlation lengths ( $\xi_{||}$ ) were observed in biphenyl benzoate core based laterally fluorinated ferroelectric compounds [986–748 Å] [25], and comparatively higher values were observed in phenyl 4-phenyl benzoate based compound [1450–1160 Å] [43].

In-plane correlation lengths ( $\xi_{\perp}$ ), on the other hand, were observed to increase gradually with decrease of temperature showing a small discontinuity at the transitions in both the compounds (Fig. 7(b)). It varies from 15 to 26.8 Å in 4F6T and from 19 to 25.7 Å in 6F6T, showing that the rate of increase is higher in 4F6T than in 6F6T. Comparatively higher in-plane correlation length ( $\xi_{\perp}$ ) was observed in biphenyl benzoate core based laterally fluorinated ferroelectric compounds [21–24.5 Å] [25], and in phenyl benzoate based compound [220–650 Å] [43].

When the low angle Bragg peak intensity of 6F6T was plotted as a function of temperature an anomalous behaviour was seen in the temperature range of 72 °C to 77 °C which might be considered as a signature of the presence of a *sub-phase*, no such anomaly was observed in

4F6T as depicted in Fig. 7(c). This phase may be  $\text{SmC}^*_\alpha$  phase as discussed in the next section.

### 3.4. Dielectric spectroscopy

The dielectric increment ( $\Delta\epsilon$ ) of the compounds during cooling cycle is shown in Fig. 8(a). Both the compounds were found to possess moderately high value in  $\text{SmC}^*$  phase. Maximum values of  $\Delta\epsilon$  were found to decrease with increasing fluorinated achiral chain length (4F6T (191.9), 5F6T (92.2[12]) and 6F6T (84.8)). Gradual decrease of  $\Delta\epsilon$  with decreasing temperature in both the compounds can be explained assuming stronger biquadratic coupling between tilt and polarization compared to bilinear one in the expression for free energy density in the generalized Landau model [44]. Decrease of  $\Delta\epsilon$  with decrease of temperature was reported in different FLC compounds by several authors [24,30,45–46]. An anomaly in the value of  $\Delta\epsilon$  between  $\text{SmA}^*$  and  $\text{SmC}^*$  phase in 6F6T during heating as well as cooling was noticed (Fig. 8 (b)) indicating the existence of a *sub-phase* in the temperature interval 72 °C to 76 °C which might be  $\text{SmC}^*_\alpha$  phase. It behaves in an antiferroelectric way at its high-temperature region and in a ferroelectric way at its low-temperature region and ferroelectric in between [47–48]. To explain the behaviour of  $\text{SmC}^*_\alpha$  phase Takanishi et al. [49] proposed that sequence of different structural states change structure quasi-continuously in the narrow temperature interval and Bahr et al. [47] argued that no effect can be observed by DSC and polarizing microscopy in the bulk sample, only one transition  $\text{SmC}^*$ - $\text{SmA}^*$  is observed.

The critical frequencies of all modes of relaxations observed in 4F6T and 6F6T are shown in Fig. 9. Soft mode in  $\text{SmA}^*$  phase, Goldstone mode in  $\text{SmC}^*$  phase were observed in both the compounds. In  $\text{SmC}_A^*$  phase anti-phase antiferroelectric mode ( $P_H$ ) and in-phase antiferroelectric mode ( $P_L$ ) were observed in 6F6T but in 4F6T only  $P_H$  was observed. The SM critical frequency in 4F6T decreased with decrease of temperature (120 kHz–8.5 kHz). In  $\text{SmC}^*$  phase SM could be observed only under a bias field of 1.2 V/ $\mu\text{m}$ . The critical frequency near  $T_c$  was found to increase sharply, depicting a 'V' shape behaviour as expected from mean field theory [50]. On the other hand, in 6F6T the critical frequency of SM increased with decrease of temperature [7.9 kHz–33.6 kHz] in the high temperature region but near  $T_c$  it decreased sharply from 33.6 kHz (80 °C) to 9.1 kHz (77 °C). In this system also 'V' shape behaviour of SM critical frequency was observed near  $T_c$  under a similar bias field. The critical frequency of GM ( $f_{GM}$ ) was found to decrease with decrease of temperature from 540 Hz (68.5 °C) to 167 (52 °C) in 4F6T whereas in 6F6T the  $f_{GM}$  increased with decrease of temperature from 200 Hz (76 °C) to 765 Hz (61 °C) and then the mode continued upto a few degrees in  $\text{SmC}_A^*$  phase. This mode in  $\text{SmC}_A^*$  phase is known as hereditary mode (HM) [30]. However, no anomaly was observed in critical frequency in the temperature interval of the proposed  $\text{SmC}^*_\alpha$  phase. The critical

Table 1  
Comparison of various thermal parameters obtained from POM study during heating.

Sample	Melting point (°C)	Clearing point (°C)	Range of phase during heating (°C)		
			$\text{SmC}_A^*$	$\text{SmC}^*$	$\text{SmA}^*$
4F6T	44.6	85.8	11.2	12.9	17.1
5F6T	41.1	91.9	9.1	21.3	20.4
6F6T	36.0	99.2	28.0	12.5	22.7

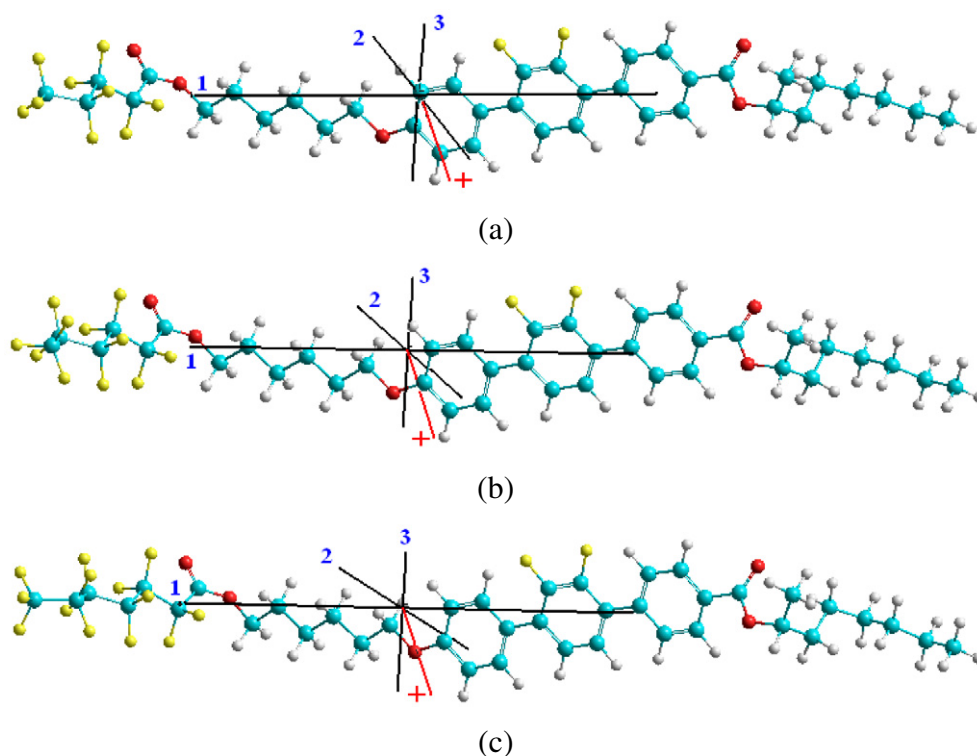


Fig. 4. Optimized structures along with the directions of dipole moments (red line) and principal moments of inertia (black line) of (a) 4F6T, (b) 5F6T and (c) 6F6T.

frequency of high frequency anti-phase mode ( $f_{PH}$ ) in the 4F6T system was observed to increase with decreasing temperature from 55.3 kHz to 200 kHz whereas in the 6F6T system it increased from 90 kHz to 980 kHz, also showing a step increase at 34 °C at which  $P_L$  appeared. Like other compounds [25,51] the critical frequency of  $P_L$  mode in 6F6T decreased with decrease of temperature.

### 3.5. Electro-optic study

#### 3.5.1. Spontaneous polarization ( $P_s$ )

In order to study the field required to obtain saturation polarization,  $P_s$  was measured with increasing ac field at a particular temperature. With the increasing field, the number of molecules participating in switching increased and after a certain field all the molecules oriented in the direction of the field and the polarization became saturated (Fig. 10(a)). The field required for saturation polarization ( $E_{sat}$ ) was found to increase linearly with the decrease of temperature (Fig. 10(b)), signifying that more driving force was required to align the molecules at lower temperature. 4F6T also showed similar behaviour.

Moderate values of spontaneous polarizations ( $P_s$ ) were observed which are suitable for display applications [52–54].  $P_s$  was found to decrease slowly in the lower temperature region and rapidly in the high temperature region of  $SmC^*$  phase as shown in Fig. 11. Maximum value of  $P_s$  was 93.6 nC/cm<sup>2</sup> in 4F6T and 103.0 nC/cm<sup>2</sup> in 6F6T while in 5F6T it was 118.7 nC/cm<sup>2</sup> [24]. Similar increasing trend with

fluorinated achiral chain was observed before [45,55]. A compound with biphenyl benzoate core and 4 perfluorinated carboxylate C atoms and 3 oligomethylene spacers in achiral chain (4F3R) exhibited  $P_s$  41.66 nC/cm<sup>2</sup> [45]. Keeping number of perfluorinated C atom same when oligomethylene spacer was increased to 6 (4F6R), the  $P_s$  increased to 50 nC/cm<sup>2</sup> and when 8 perfluorinated C atoms and 2 oligomethylene spacers were introduced (8F2R) it became 93 nC/cm<sup>2</sup> [55]. It was inferred that the  $P_s$  increased with increase of perfluorinated C atoms as well as oligomethylene spacers in the achiral chain but increase of perfluorinated C atom was more effective. In the present study the  $P_s$  was observed to increase with increase of achiral chain length, although in 5F6T the increment was more than in 6F6T which may be due to the odd even effect [34]. In both the compounds the measured  $P_s$  data were found to fit nicely to the mean-field equation  $P_s = P_o(T - T_c)^\beta$  with  $\beta = 0.25$  near  $T_c$  signifying that the  $SmC^*$ – $SmA^*$  transition is a tricritical type [42] as observed in layer spacing.

#### 3.5.2. Optical and X-ray tilt

The optical tilts ( $\theta_{opt}$ ) were found to increase sharply with the decrease of temperature near  $T_c$  and reached nearly 45° in  $SmC_A^*$  phase in both the compounds (Fig. 12), which indicated that both the compounds were orthoconic antiferroelectric in nature. On the other hand, although the X-ray tilts ( $\theta_{X-ray}$ ) of the compounds showed similar temperature variation but their maximum values were 21.8° and 22.0° respectively (Fig. 13), much less than the optical tilts. In four members

Table 2

Molecular lengths, energy, principal moments of inertia and dipole moments of the molecules.

Sample	Optimized molecular length (Å)	Energy (kCal/mol)	Moments of inertia in 10 <sup>−44</sup> kgm <sup>2</sup>			Dipole moment (Debye)			
			About x-axis	about y-axis	about z-axis	Total	Components		
							x	y	z
4F6T	35.15	9729	27.8	913.7	925.4	5.13	+0.25	−5.12	+0.13
5F6T	35.95	10,034	36.9	999.2	1017.6	5.01	+0.05	−5.01	+0.02
6F6T	37.96	10,340	44.8	1106.6	1131.5	5.10	−0.28	−5.10	+0.10

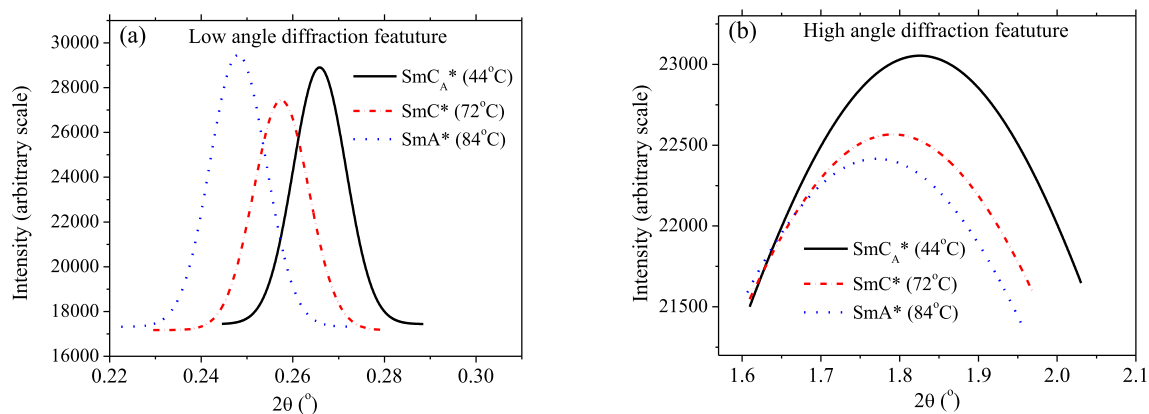


Fig. 5. X-ray diffraction profiles at 44 °C ( $\text{SmC}_A^*$ ), 72 °C ( $\text{SmC}^*$ ) and 84 °C ( $\text{SmA}^*$ ) of the (a) low angle and (b) high angle diffraction features of 6F6T.

of a biphenyl benzoate core based homologous series exhibiting orthoconic antiferroelectric nature, the  $\theta_{X\text{-ray}}$  was found to vary within  $24.2^\circ - 25.8^\circ$  [25]. A similar lower values of X-ray tilt than optical tilt were reported before by several other authors [56–58], although the existence of higher x-ray tilt than optical tilt was also observed by Meier et al. [59]. X-ray tilt is a result of tilt of electron-density function of the whole molecule, whereas optical tilt arises due to tilt of only the rigid polarisable group of the molecule, thus the two tilts may differ. This difference has also been explained considering zig-zag shape of the molecules [56]. The zig-zag molecular shape arose out of the rigid core which

tilted independently whereas the melted end chains are on the average closer to the layer normal. Both tilts were fitted nicely to the power law with  $\beta = 0.25$  near  $T_c$  in both the compounds signifying again the tricritical nature of  $\text{SmC}^* - \text{SmA}^*$  transition.

### 3.5.3. Switching time ( $\tau$ )

The switching time of ferroelectric and antiferroelectric liquid crystals is an important parameter from application point view because to afford a video rate time sequential colour micro-display switching time should be low [12,60–61]. Both the compounds showed sub-

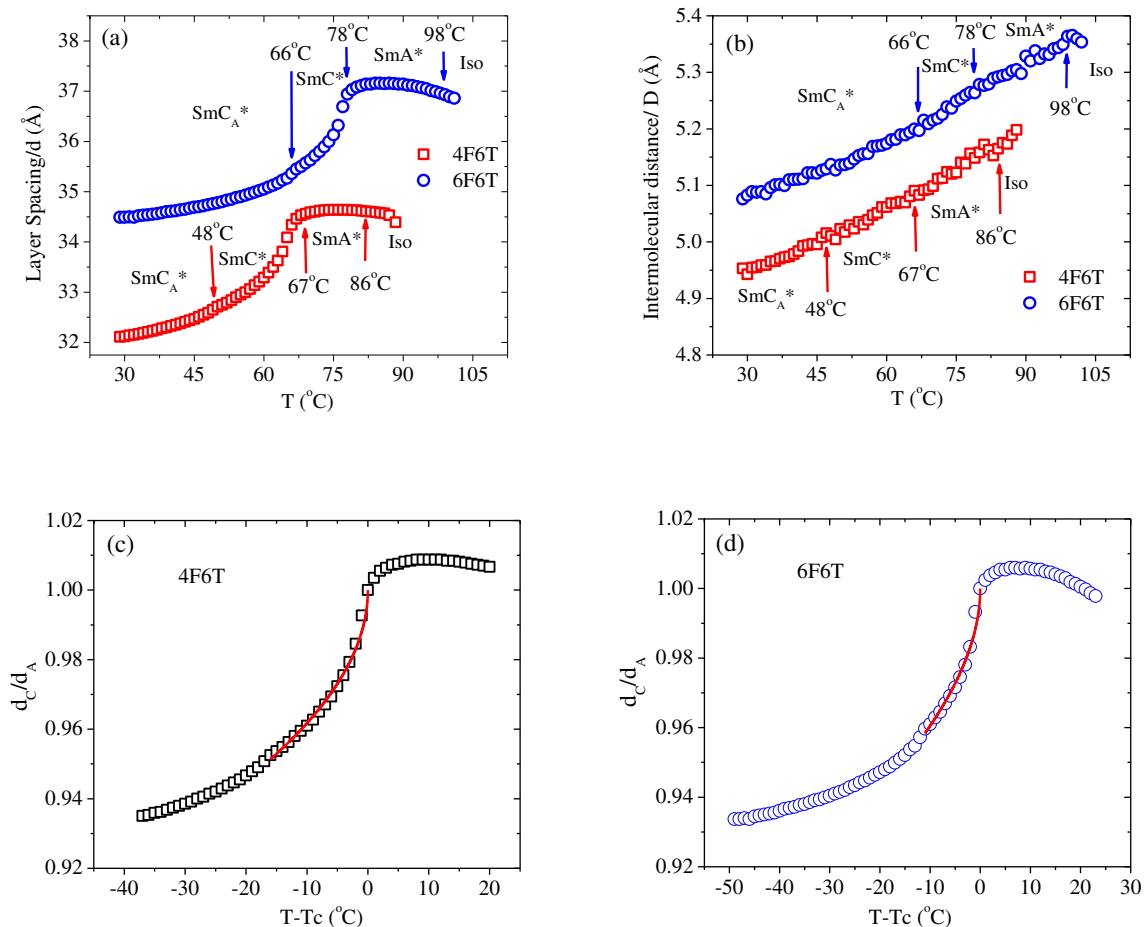
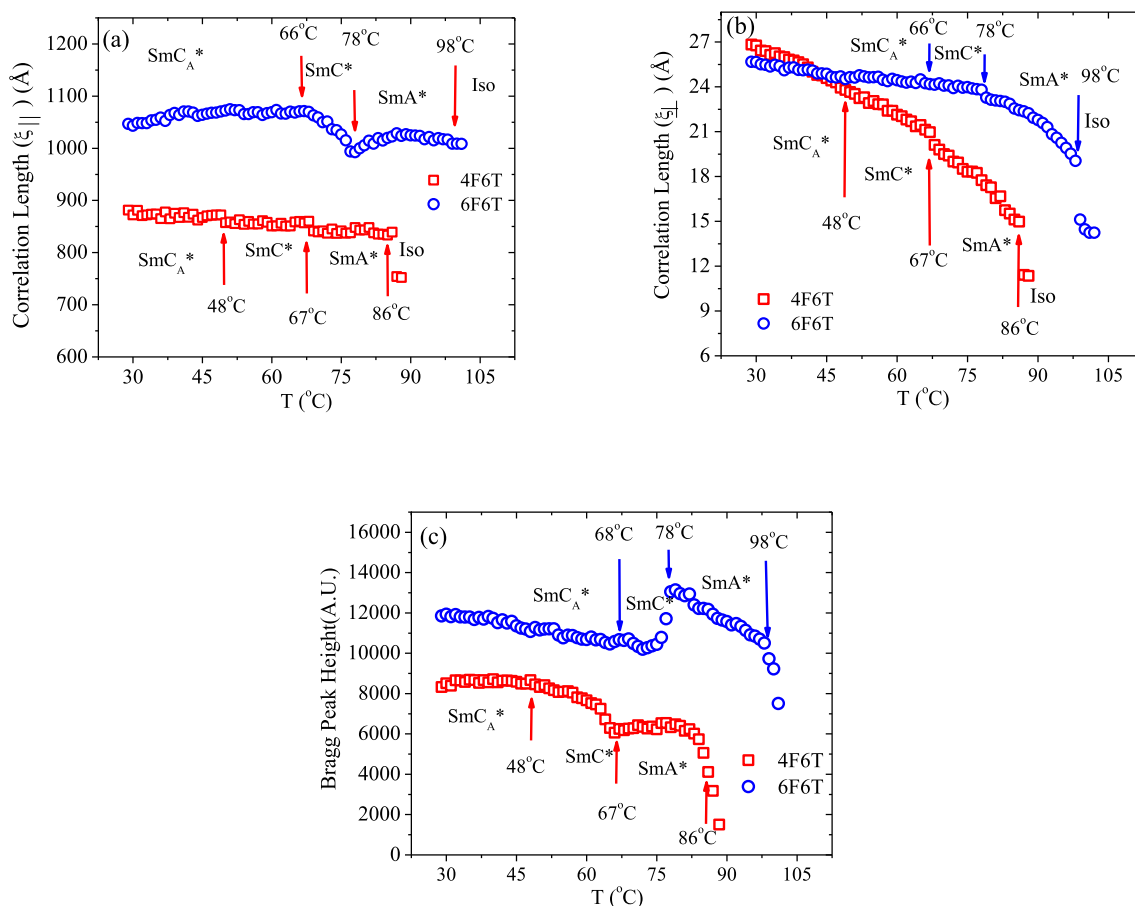


Fig. 6. Temperature evolution of (a) layer spacing, (b) intermolecular distance of 4F6T and 6F6T; fitted layer spacings in  $\text{SmC}^*$  phase of (c) 4F6T and (d) 6F6T (see text).



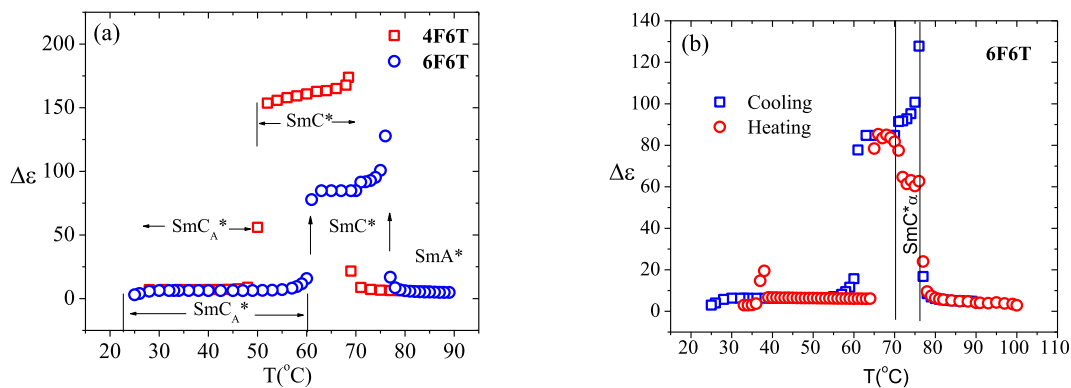
**Fig. 7.** Temperature evolution of correlation lengths (a) across the smectic layers ( $\xi_{||}$ ), (b) within the smectic layers ( $\xi_{\perp}$ ) and (c) intensity of the low angle Bragg peak (arbitrary unit) of 4F6T and 6F6T.

millisecond switching time and it increased with decrease of temperature from  $T_c$  (Fig. 14). A similar nature of temperature variation of  $\tau$  was found to be 744  $\mu$ s in 4F6T and 828  $\mu$ s in 6F6T at  $T_{AF}$ . Within  $SmC_A^*$  phase  $\tau$  increased sharply to 926  $\mu$ s in 6F6T, it could not be measured in 4F6T (Fig. 14). In a homologous series of ferroelectric liquid crystals with partially fluorinated biphenyl benzoate core and different number of fluorinated carbon and oligomethylene spacer in achiral chain (nFmR), Goswami et al. [10] reported the switching time as 80  $\mu$ s in 4F3R, 122.6  $\mu$ s in 5F3R and 158  $\mu$ s in 6F3R and observed that the  $\tau$

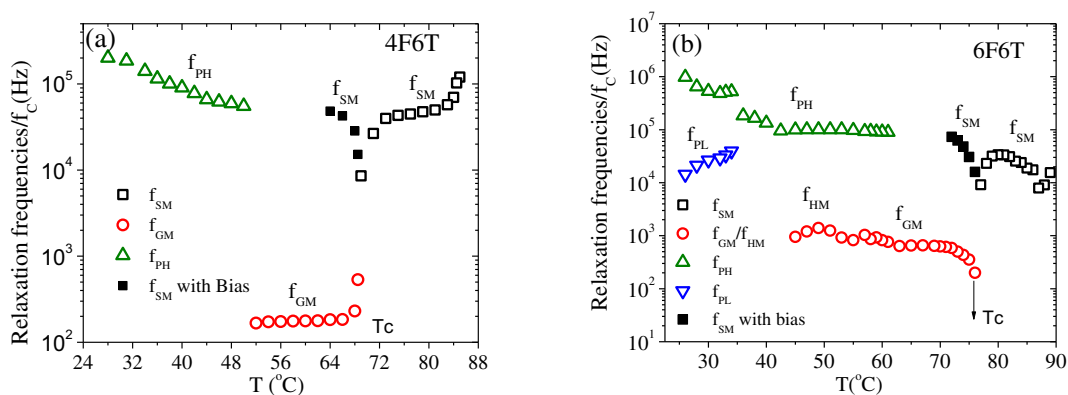
increased with increasing number of fluorinated carbon in achiral chain, thus with increasing achiral chain length. Same is true in the present compounds.

### 3.5.4. Effect of field on ferroelectric-antiferroelectric transition temperature ( $T_{AF}$ )

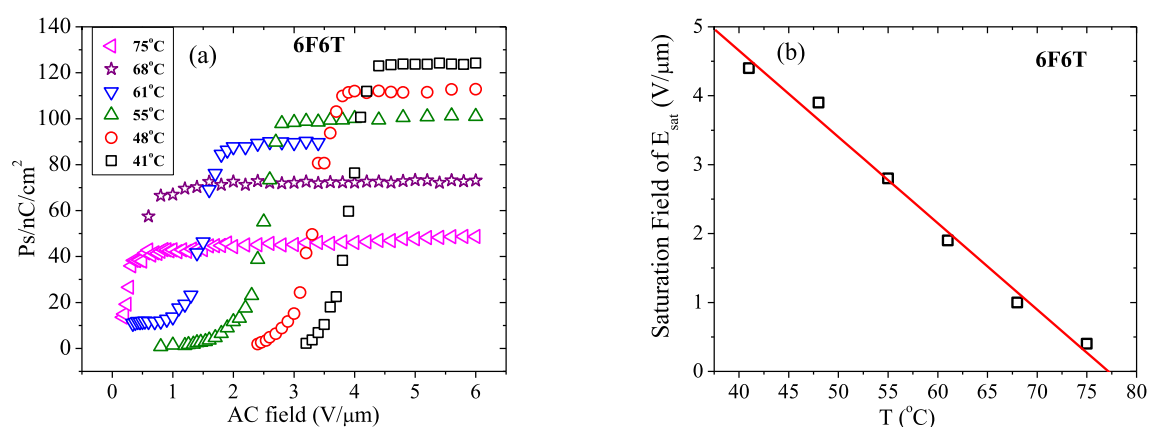
In order to study the effect of ac field on  $SmC^*$ – $SmC_A^*$  transition temperature ( $T_{AF}$ ), optical texture of the compounds were monitored with decreasing temperature under fixed low frequency ( $\sim 10$  Hz) ac fields and temperatures at which phase change takes



**Fig. 8.** Dielectric strength ( $\Delta\epsilon$ ) (a) of 4F6T and 6F6T during cooling, (b) of 6F6T during heating and cooling showing anomaly.



**Fig. 9.** Temperature dependence of relaxation frequencies ( $f_c$ ) of various relaxation modes in (a) 4F6T and (b) 6F6T. (For interpretation of the references to color in this figure, the reader is referred to the web version of this article.)



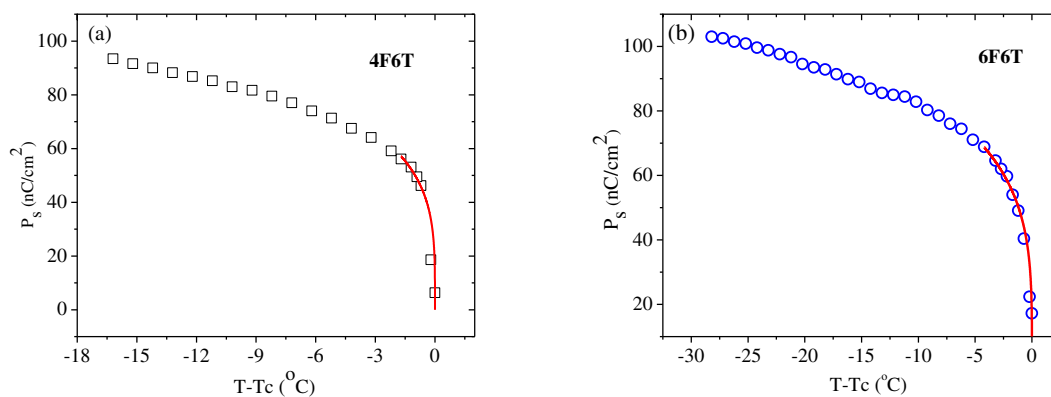
**Fig. 10.** (a) Polarization versus field in 6F6T at different temperatures and (b) linear increase of saturation field ( $E_{sat}$ ) with decreasing temperature.

place were noted.  $T_{AF}$  was observed to decrease linearly with increasing field ( $E_c$ ) in both the compounds as shown in Fig. 15. In 4F6T,  $T_{AF}$  was found to depress by 18.3 °C at 5.18 V/μm and in 6F6T it depressed by 35.5 °C at 4.4 V/μm. The gradient of depression of  $T_{AF}$  was higher in 6F6T (~8.19 °C/(V/μm)) than in 4F6T (~5.16 °C/(V/μm)).

A selected list of parameters of 4F6T, 5F6T, 6F6T are gathered in Table 3 for ease comparison.

#### 4. Conclusions

In order to investigate the correlation between structure and property, two terphenyl core based antiferroelectric liquid crystals – 4F6T and 6F6T – differing only in the number of fluorinated carbon at achiral chain have been studied using different experimental techniques and their properties have also been compared with the intermediate homologue 5F6T [24] wherever possible. Although all of them exhibited



**Fig. 11.** Fitted temperature variation of spontaneous polarization of (a) 4F6T and (b) 6F6T.

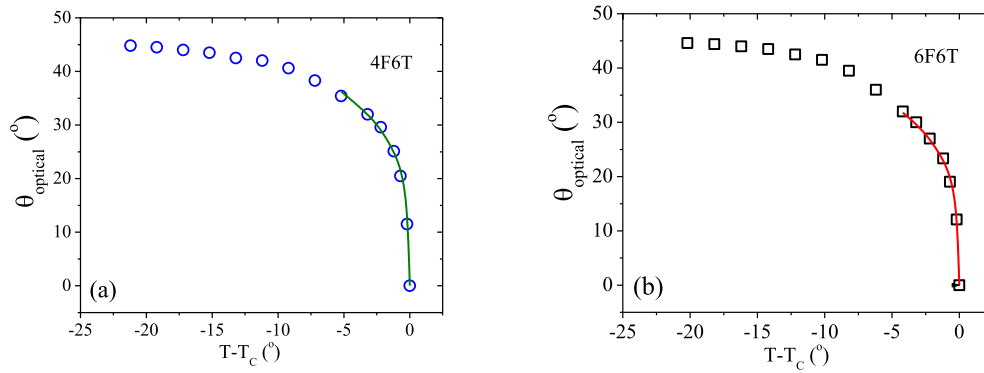


Fig. 12. Temperature variation of optical tilt of (a) 4F6T and (b) 6F6T, fitted curves near  $T_c$  are also shown.

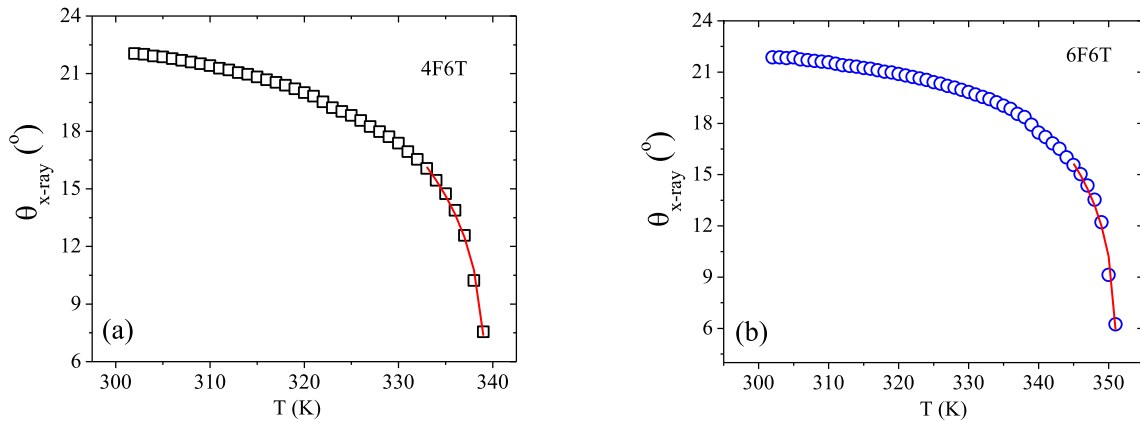


Fig. 13. Temperature variation of x-ray tilts of (a) 4F6T, (b) 6F6T.

antiferroelectric-ferroelectric-paraelectric ( $\text{SmC}_A^* - \text{SmC}^* - \text{SmA}^*$ ) phase sequence, melting point was observed to decrease with increasing achiral chain length but clearing point showed opposite trend. Thermal ranges of the antiferroelectric and ferroelectric phases were found to exhibit odd-even effect, so also the molecular dipole moments and spontaneous polarization. Layer spacings, average intermolecular distances and correlation lengths across the smectic planes were also observed to increase with achiral chain length. Temperature dependence of

layer spacings suggests tricritical nature of  $\text{SmC}^* - \text{SmA}^*$  transition which is also supported by temperature dependent x-ray tilt, optical tilt and spontaneous polarization. Dielectric increments decreased with increased achiral chain. Both soft mode and Goldstone mode critical frequencies were found to decrease with decreasing temperature in the lower derivative but opposite behaviour was observed in the higher derivative. Both the compounds, however, showed Curie-Weiss behaviour in soft mode near  $\text{SmC}^* - \text{SmA}^*$  transition temperature  $T_c$ . Goldstone

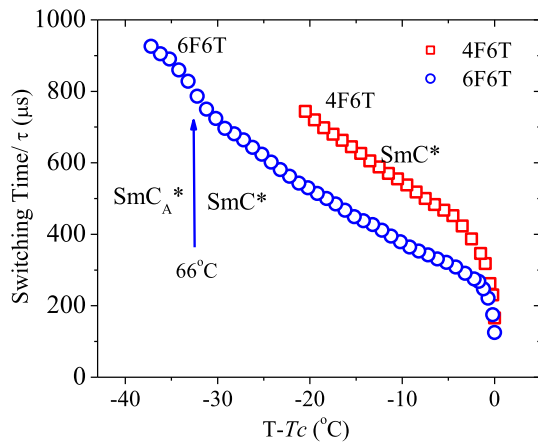


Fig. 14. Comparison of temperature dependence of switching time.

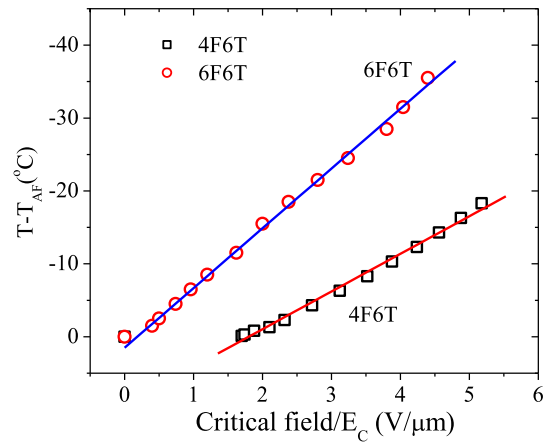


Fig. 15. AC field dependence of  $\text{SmC}^* - \text{SmC}_A^*$  transition temperature ( $T_{AF}$ ) of 4F6T and 6F6T.

**Table 3**  
Selected list of parameters of 4F6T, 5F6T, 6F6T.

Parameter	4F6T	5F6T	6F6T
D (Å) (max)	5.17		5.36
d (Å) (max)	34.64		37.16
$\xi_{  }$ (Å) (max)	870		1071
$\xi_{\perp}$ (Å) (max)	26.8		25.7
$\Delta\epsilon$ (max)	191.9	92.2	84.4
$f_{CM}$ (Hz)	167–540	590–1190	200–765
$f_{SM}$ (kHz)	8.5–120	2.5–65.8	7.9–33.6
$f_{PL}$ (kHz)	14.3–39.5		
$f_{PH}$ (kHz)	55.3–200		9–980
$P_s$ (nC/cm <sup>2</sup> ) (max)	93.6	118.7	103
$\tau$ (μs) (max)	744		926

mode critical frequency was much higher in 6F6T. Both  $P_L$  and  $P_H$  modes were observed in  $SmC_A^*$  phase but in 4F6T only  $P_H$  was observed and in 5F6T both modes were absent. Optical tilts exhibited orthoconic nature of the  $SmC_A^*$  phase in both the compounds. However, X-ray tilt was much less and the discrepancy was explained. Both the compounds showed sub-millisecond order switching time which was also found to increase with achiral chain length. Antiferroelectric-ferroelectric transition temperature ( $T_{AF}$ ) was observed to decrease with increasing ac field, effect was more in the higher derivative compared to the lower one.  $SmC_\alpha^*$  phase may be present within a small temperature range between  $SmA^*$  and  $SmC^*$  phases in 6F6T. It is thus concluded that the thermal range of different phases, smectic layer spacings, various dielectric and electro-optic properties of the two terphenyl based compounds are significantly influenced by the achiral chain length, whereas some others exhibit opposite trend, even there is an indication of presence of a new phase ( $SmC_\alpha^*$ ) in the higher derivative. Another important conclusion is that the ferroelectric to paraelectric phase transition is tricritical in nature and the ferroelectric-antiferroelectric transition temperature decreases with electric field in both the compounds. Moreover, because of the orthoconic nature of the  $SmC_A^*$  phase with sub-millisecond switching time and moderate spontaneous polarization these two compounds are expected to be suitable for preparation of mixtures suitable for display and other non-display applications [12–13,51–53,61–69].

## Declaration of competing interest

The authors declare that they have no known competing financial interests or personal relationships that could have appeared to influence the work reported in this paper.

## Acknowledgement

Portions of this research were carried out at the light source PETRA III of DESY, a member of the Helmholtz Association (HGF). We would like to thank Olof Gutowski and Abhisakh Sarma for assistance at beamline P07. Financial support by the Department of Science and Technology (Government of India) provided within the framework of the India@DESY collaboration is gratefully acknowledged.

## References

- [1] K. Dhare, P. Rudquist, M. Matuszczyk, S.T. Lagerwall, H. Pauwels, R.S. Dabrowski, Antiferroelectric liquid crystals with 45° tilt: new electro-optic effects in liquid crystals, in 'liquid crystal materials, devices, and flat panel displays', in: R. Shashidhar, B. Gnade (Eds.), Proceedings of SPIE, 3955, 2000, pp. 33–44.
- [2] G. Scalia, P. Rudquist, D.S. Hermann, K. Dhare, S.T. Lagerwall, Fully leaky guided mode study of an orthoconic antiferroelectric liquid crystal cell deviating from perfect horizontal surface stabilization, J. Appl. Phys. 91 (12) (2002) 9667–9675.
- [3] A. Bubnov, V. Novotna, V. Hamplova, M. Kaspar, M. Glogarova, Effect of multilactate chiral part of liquid crystalline molecule on mesomorphic behaviour, J. Mol. Struct. 892 (1–3) (2008) 151–157.

- [4] A. Poryvai, A. Bubnov, D. Pociecha, J. Svoboda, M. Kohout, The effect of the length of terminal n-alkyl carboxylate chain on self assembling and photosensitive properties of chiral lactic acid derivatives, J. Mol. Liq. 275 (2019) 829–838.
- [5] B. Barman, B. Das, M.K. Das, V. Hamplova, A. Bubnov, Effect of molecular structure on dielectric and electro-optic properties of chiral liquid crystals based on lactic acid derivatives, J. Mol. Liq. 283 (2019) 472–481.
- [6] M. Żurowska, J. Dziaduszek, M. Szala, P. Morawiak, A. Bubnov, Effect of lateral fluorine substitution far from the chiral center on mesomorphic behaviour of highly tilted antiferroelectric (S) and (R) enantiomers, J. Mol. Liq. 267 (2018) 504–510.
- [7] M. Kohout, A. Bubnov, J. Šturala, V. Novotna, J. Svoboda, Effect of alkyl chain length in the terminal ester group on mesomorphic properties of new chiral lactic acid derivatives, Liq. Cryst. 43 (2016) 1472–1485.
- [8] V. Hamplova, A. Bubnov, M. Kaspar, V. Novotna, M. Glogarova, New series of chiral ferroelectric liquid crystals with the keto group attached to the molecule core, Liq. Cryst. 30 (4) (2003) 493–497.
- [9] W.L. Tsai, T.C. Lu, H.W. Liu, M.Y. Tsai, C.M. Fu, A comparison of ferroelectric liquid crystals containing diastereomeric propionic acids derived from natural ethyl lactate, Liq. Cryst. 27 (2000) 1389.
- [10] D. Goswami, A. Debnath, P.K. Mandal, D. Węglowska, R. Dabrowski, K. Czuprynski, Effect of chain length and fluorination on the dielectric and electro-optic properties of three partially fluorinated biphenyl benzoate rigid core based ferroelectric liquid crystals, Liq. Cryst. 43 (11) (2016) 1–12.
- [11] K. Kunhnast, J. Sorubgerm, G. Scherowsky, F. Giebelmann, P. Zugenmaier, Ferroelectric liquid-crystalline side group polymers spacer length variation and comparison with the monomers, Liq. Cryst. 14 (3) (1993) 861–869.
- [12] A. Debnath, P.K. Mandal, Effect of fluorination on the phase sequence, dielectric and electro-optical properties of ferroelectric and antiferroelectric mixtures, Liq. Cryst. 44 (2017) 2192–2202.
- [13] A. Debnath, P.K. Mandal, Dielectric properties of four room temperature ferroelectric and antiferroelectric multi-component liquid crystalline mixtures, Liq. Cryst. 46 (2019) 234–248.
- [14] M. Żurowska, R. Dabrowski, J. Dziaduszek, K. Garbat, M. Filipowicz, M. Tykarska, W. Rejmer, K. Czuprynski, A. Spadło, N. Bennis, J.M. Oton, Influence of alkoxy spacer length and fluorosubstitution of benzene ring on mesogenic and spectral properties of high tilted antiferroelectric 4'-(S)-1-(methylheptyloxycarbonyl)biphenyl-4-yl-4-(2,2,3,3,4,4,4-heptafluorobutoxy)alkoxybenzoates, J. Mater. Chem. 21 (2011) 2144–2153.
- [15] R. Dabrowski, Liquid crystals with fluorinated terminal chains and antiferroelectric properties, Ferroelectrics 243 (2000) 1–11.
- [16] R. Dabrowski, J. Gąsowska, J.M. Oton, W. Piecek, J. Przedmojski, M. Tykarska, High tilted antiferroelectric liquid crystalline materials, Displays 25 (2004) 9–19.
- [17] E. Sokol, W. Drzewinski, J. Dziaduszek, R. Dabrowski, N. Bennis, J.M. Oton, The synthesis and properties of novel partially fluorinated ethers with high tilted anticlinic phase, Ferroelectrics 343 (2006) 41–48.
- [18] R. Dabrowski, W. Drzewinski, J. Dziaduszek, J. Gąsowska, P. Henderson, P. Kula, J.M. Oton, N. Bennis, Orthoconic antiferroelectric liquid crystals containing biphenyl, terphenyl, or naphthyl mesogenic unit, Opto-Electron. Rev. 15 (2007) 32–36.
- [19] M. Kaspar, V. Hamplova, V. Novotna, O. Pachrova, The effect of the alkyl chain length on the mesomorphic properties of new lactic acid derivatives, Liq. Cryst. 41 (08) (2014) 1179–1187.
- [20] R. Dabrowski, P. Kula, Z. Raszewski, W. Piecek, J.M. Oton, A. Spadło, New orthoconic antiferroelectrics useful for applications, Ferroelectrics 395 (2010) 116–132.
- [21] P.A. Henderson, W. Drzewinski, R. Dabrowski, Antiferroelectric liquid crystals containing a naphthoate mesogenic unit, Ferroelectrics 343 (2006) 11–18.
- [22] P. Kula, R. Dabrowski, K. Kenig, D. Chyczewska, New ferroelectric compounds from chiral terphenyls, Ferroelectrics 343 (2006) 19–26.
- [23] P. Kula, R. Dabrowski, M. Tykarska, Orthoconic antiferroelectric liquid crystals containing a terphenyl rigid core, Phase Trans 80 (6) (2007) 771–780.
- [24] S. Haldar, K.C. Dey, D. Sinha, P.K. Mandal, W. Haase, P. Kula, X-ray diffraction and dielectric spectroscopy studies on a partially fluorinated ferroelectric liquid crystal from the family of terphenyl esters, Liq. Cryst. 39 (10) (2012) 1196–1203.
- [25] K.C. Dey, P.K. Mandal, R. Dabrowski, Effect of lateral fluorination in antiferroelectric and ferroelectric mesophases: synchrotron X-ray diffraction, dielectric spectroscopy and electro-optic study, Journal of Phys. and Chem. of Solids. 88 (2016) 14–23.
- [26] A. de Vries, X-ray photographic studies of liquid crystals I. A cybotactic nematic phase, Mol. Cryst. Liq. Cryst. 10 (1970) 219–236.
- [27] J. Budai, R. Pindak, S.C. Davey, J.W. Goodby, Structural investigation of the liquid crystal phases of 4-(2'-methylbutyl)phenyl 4'-n-octylbiphenyl-4-carboxylate, J. Phys. Lett. 45 (1984) L1053–L1062.
- [28] E.B. Sirota, P.S. Pershan, L.B. Sorensen, J. Collett, X-ray studies of tilted hexatic phases in thin liquid-crystal films, Phys. Rev. Lett. 55 (19) (1985) 2039–2042.
- [29] K.S. Cole, R.H. Cole, Dispersion and absorption in dielectrics I. Alternating current characteristics, J. of Chem. Phys. 9 (1941) 341–351.
- [30] M. Buivydas, F. Gouda, G. Andersson, S.T. Lagerwall, B. Stebler, Collective and non-collective excitations in antiferroelectric and ferroelectric liquid crystals studied by dielectric relaxation spectroscopy and electro-optic measurements, Liq. Cryst. 23 (5) (1997) 723–739.
- [31] K. Miyasato, S. Abe, H. Takezoe, A. Fukuda, E. Kuze, Direct method with triangular waves for measuring spontaneous polarization in ferroelectric liquid crystals, Jpn. J. Appl. Phys. 22 (10) (1983) L661–L663.
- [32] K. Skarp, I. Dahl, S.T. Lagerwall, B. Stebler, Polarisation and viscosity measurements in a ferroelectric liquid crystal by the field reversal method, Mol. Cryst. Liq. Cryst. 114 (1984) 283–297.

- [33] M. Marzec, J. Popczyk, A. Fafara, S. Wróbel, R. Dąbrowski, Antiferroelectric liquid crystals studied by differential scanning calorimetry and electrooptic methods, *Ferroelectrics* 281 (2002) 123–134.
- [34] P. Sarkar, S. Paul, P. Mandal, The temperature dependence of static dielectric permittivities and dipole moments of two mesogens and their mixture, *Mol. Cryst. Liq. Cryst.* 330 (1999) 87–94.
- [35] Hyperchem 6.03, Hypercube Inc., Gainesville, FL, USA.
- [36] E. Megnassan, A. Proutiere, Dipole moments and Kerr constants of 4-*n* alkyl-4'-cyanobiphenyl molecules (from 1CB to 12CB) measured in cyclohexane solutions, *Mol. Cryst. Liq. Cryst.* 108 (1984) 245–254.
- [37] K.P. Gueu, E. Megnassan, A. Proutiere, Dipole moments of 4-*n* alkyl-4'-cyanobiphenyl molecules (from 0CB to 12CB) measurements in four solvents and theoretical calculations, *Mol. Cryst. Liq. Cryst.* 132 (1986) 303–323.
- [38] P. Sarkar, P.K. Mandal, S. Paul, X-ray diffraction, optical birefringence, dielectric and phase transition properties of the long homologous series of nematogens 4-(trans-4'-*n*-alkylcyclohexyl) isothiocyanatobenzenes, *Liq. Cryst.* 30 (2003) 507–527.
- [39] S. Marcelja, Chain ordering in liquid crystals, I. Even-odd effect, *The J. Chem. Phys.* 60 (9) (1974) 3599–3604.
- [40] B. Zeks, Landau free energy expansion for chiral ferroelectric smectic liquid crystal, *Mol. Cryst. Liq. Cryst.* 114 (1984) 259–270.
- [41] R. Shashidhar, B.R. Ratna, G.G. Nair, S.K. Prasad, C. Bahr, G. Heppke, Mean-field to tricritical crossover behaviour near the smectic-A-smectic-C\* tricritical point, *Phys. Rev. Lett.* 61 (5) (1988) 547–549.
- [42] C.S. Hartley, N. Kapernaum, J.C. Roberts, F. Giesselmann, R.P. Lemieux, Electroclinic effect in chiral SmA\* liquid crystals induced by atropisomeric biphenyl dopants: amplification of the electroclinic coefficient using achiral additives, *J. Mater. Chem.* 16 (2006) 2329–2337.
- [43] D. Sinha, A. Debnath, P.K. Mandal, Hexatic and blue phases in a chiral liquid crystal: optical polarizing microscopy, synchrotron radiation and dielectric study, *Mat. Research Exp.* 1 (2014) 1–13.
- [44] T. Carlsson, B. Zeks, C. Filipic, A. Levstik, Theoretical model of the frequency and temperature dependence of the complex dielectric constant of ferroelectric liquid crystals near the smectic-C\*–smectic-A phase transition, *Phys. Rev. A* 42 (2) (1990) 877–889.
- [45] D. Goswami, D. Sinha, A. Debnath, P.K. Mandal, S.K. Gupta, W. Haase, D. Ziobro, R. Dabrowski, Molecular and dynamical properties of a perfluorinated liquid crystal with direct transition from ferroelectric SmC\* phase to isotropic phase, *J. Mol. Liq.* 182 (2013) 95–101.
- [46] U. Manna, J.K. Song, G. Power, J.K. Vij, Effect of cell surfaces on the stability of chiral smectic-C phases, *Phys. Rev. E* 78 (2008) 021711–0217 (1–8).
- [47] C. Bahr, D. Flegner, C.J. Booth, J.W. Goodby, Experimental indication of a devil's staircase structure in a smectic liquid crystal, *Phys. Rev. E* 51 (5) (1995) R3823–R3826.
- [48] T. Isozaki, K. Hiraoka, Y. Takanishi, H. Takezoe, A. Fukuda, Y. Suzuki, I. Kawamura, Conoscopic study of the Sc $\alpha$ \* phase and the Devil's staircase in an antiferroelectric liquid crystal, *Liq. Cryst.* 12 (1992) 59–70.
- [49] Y. Takanishi, K. Hiraoka, V.K. Agarwal, H. Takezoe, A. Fukuda, M. Matsushita, Stability of antiferroelectricity and causes for its appearance in SmC\* $\alpha$  and SmC $\alpha$ \* phases of a chiral smectic liquid crystal, MHPOBC, *Jpn. J. Appl. Phys.* 30 (1991) 2023.
- [50] F. Gouda, K. Skarp, S.T. Lagerwall, Dielectric studies of the soft mode and goldstone mode in ferroelectric liquid crystals, *Ferroelectrics* 113 (1991) 165.
- [51] K.C. Dey, P.K. Mandal, Effect of multi-walled carbon nanotubes on dielectric and electro-optic properties of a high tilt antiferroelectric liquid crystal, *Phase Transit.* 92 (3) (2019) 302–315.
- [52] A. Debnath, P.K. Mandal, D. Wegłowska, R. Dabrowski, Induction of a room temperature ferroelectric SmC\* phase in binary mixtures with moderate spontaneous polarization and sub-millisecond switching time, *RSC Adv* 6 (2016) 84369–84378.
- [53] P.K. Mandal, S. Haldar, A. Lapanik, W. Haase, Induction and enhancement of ferroelectric smectic C\* phase in multi-component room temperature mixtures, *Jpn. J. Appl. Phys.* 48 (2009) 011501–011506.
- [54] W.N. Thurmes, M.D. Wand, R.T. Vohra, K.M. More, FLC materials for microdisplay applications, *SPIE Conf. Proc.* 3015, 1997, pp. 1–7.
- [55] D. Ziobro, R. Dąbrowski, M. Tykarska, W. Drzewiński, M. Filipowicz, W. Rejmer, K. Kuśmierek, P. Morowiak, W. Piecsek, Synthesis and properties of new ferroelectric and antiferroelectric liquid crystals with a biphenyl benzoate rigid core, *Liq. Cryst.* 39 (2012) 1011–1032.
- [56] R. Bartolino, J. Doucet, G. Durand, Molecular tilt in the smectic C phase: a zig-zag model, *Ann. de Phys.* 3 (1978) 389–395.
- [57] E.N. Keller, E. Nachaliel, D. Davidov, Evidence for the “zig-zag” model of the smectic-C phase in the liquid crystal 4'-butoxyphenylester 4-decyloxybenzoic acid (40P1008): a high resolution X-ray study, *Phys. Rev. A* 34 (5) (1986) 4363–4369.
- [58] M.S. Spector, P.A. Heiney, J. Naciri, B.T. Weslowski, D.B. Holt, R. Shashidhar, Electroclinic liquid crystals with large induced tilt angle and small layer contraction, *Phys. Rev. E* 61 (2) (2000) 1579–1584.
- [59] J.G. Meier, M. Nobili, T. Carlsson, P. Rudquist, A.S. Petrenko, J.W. Goodby, M. Brunet, S.T. Lagerwall, Possible model of an antiferroelectric twist grain boundary phase, *Phys. Rev. E* 76 (2007) 11704(1–9).
- [60] M. Wand, W. Thurmes, M. Meadows, FLC displays for high-resolution magnified view and projection applications, *Proc SPIE*, 3635, 1999, pp. 2–7.
- [61] A. Debnath, D. Sinha, P.K. Mandal, Formulation of a room temperature ferroelectric liquid crystal mixture with sub-millisecond switching time, *AIP Conf. Proc.* (59th DAE Solid State Symp.), 1665, 2015, 040004(1–3).
- [62] A. Debnath, P.K. Mandal, Wide range room temperature ferroelectric liquid crystal mixture with microsecond order switching, *J. Mol. Liq.* 221 (2016) 287–291.
- [63] J.P.F. Lagerwall, F. Giesselmann, Current topics in smectic liquid crystal research, *Chem Phys Chem* 7 (2006) 20–45.
- [64] S.T. Lagerwall, *Ferroelectric and Antiferroelectric Liquid Crystals*, WILEY-VCH Verlag GmbH, Weinheim, 2007 1–427.
- [65] J.P.F. Lagerwall, G. Scalia, A new era for liquid crystal research: applications of liquid crystals in soft matter nano-, bio- and microtechnology, *Curr. Appl. Phys.* 12 (2012) 1387–1412.
- [66] A. Dlubacz, M. Marzec, D. Dardas, M. Żurowska, New antiferroelectric liquid crystal for use in LCD, *Phase Trans* 89 (2016) 349–358.
- [67] A. Debnath, D. Sinha, P.K. Mandal, Wide range room temperature electroclinic liquid crystal mixture with large induced tilt and very small layer contraction, *J. Appl. Phys.* 119 (2016) 124103(1–4).
- [68] K.C. Dey, P.K. Mandal, Formulation of a binary eutectic antiferroelectric liquid crystal mixture: comparison of dielectric and electro-optic properties with the pure compounds, *J. Mol. Liq.* 243 (2017) 484–493.
- [69] A. Debnath, P.K. Mandal, Effect of non-mesogenic chiral terphenylate on the formulation of room temperature ferroelectric liquid crystal mixtures suitable for display applications, *J. Mol. Liq.* 292 (2019) 111317 (1–8).